HYBRID STRESS
FINITE ELEMENT METHOD

by

DAVID SUNG-SOO KANG

S.B., Massachusetts Institute of Technology (1981)
S.M., Massachusetts Institute of Technology (1982)

SUBMITTED TO THE DEPARTMENT OF AERONAUTICS AND ASTRONAUTICS
IN PARTIAL FULFILLMENT OF THE REQUIREMENTS FOR THE DEGREE OF

DOCTOR OF PHILOSOPHY

at the

MASSACHUSETTS INSTITUTE OF TECHNOLOGY

May 1986

Signature of Author _____
Department of Aeronautics and Astronautics
May 20, 1986

Certified by _____
Professor Theodore H. H. Pian
Thesis Supervisor

_____
Professor Emmett A. Witmer
Thesis Committee

_____
Professor David M. Parks
Thesis Committee

Accepted by _____
Professor Harold Y. Wachman
Chairman, Departmental Graduate Committee

To my parents

YOUNG-SUK and DOO-YOUNG

HYBRID STRESS

FINITE ELEMENT METHOD

by

DAVID SUNG-SOO KANG

Submitted to the
Department of Aeronautics and Astronautics
on May 20, 1986
in partial fulfillment of the requirements for the degree of
Doctor of Philosophy
in
Aeronautics and Astronautics

ABSTRACT

The development of the hybrid stress finite element method is presented and demonstrated through the construction of a wide range of finite elements. The family of hybrid stress elements considered are 8-node Solid, 4-node Plane, 4-node Plate, 2-node Arch, and 4-node General Shell. A systematic method for choosing the assumed stress fields is provided. For each class of elements, numerous benchmark examples are solved for comparison. The results are analyzed with emphasis on element distortion effects and accuracy for a crude mesh. The variational statements are restated to examine the equivalence conditions between the consistently derived hybrid stress elements and those based upon the reduced integration or the assumed strain methods. In sum, the hybrid elements, have been demonstrated to be very effective, and will serve as a standard of comparison for future finite element developments.

Thesis Commitee:

Theodore H. H. Pian
Professor of Aeronautics and Astronautics

Emmett A. Witmer
Professor of Aeronautics and Astronautics

David M. Parks
Professor of Mechanical Engineering

ACKNOWLEDGEMENTS

To begin with, I want to thank my family for their continuous encouragement and support.

I wish to express my gratitude to Professor Pian for his continuous interest and guidance. He first introduced me to the finite element method seven years ago. Also, I wish to thank Professor Witmer and Professor Parks for their frequent advice. Their concern for my overall education was invaluable. Discussions with Professor D.P. Chen helped to clarify my understanding of the finite elements in the early years of the research.

I am grateful to those people at Draper Laboratory who made my tenure a learning experience. They include F. Ayer, S. Fay, T. Henderson, S. Gates, J. Storch, and S. Hunziker.

I would also like to recognize D. Strnad, S. Silver, B. Agudelo, K. Sumihara, E. Jaselskis, R. Marshall, J. and T. Bussing, P. and A. Messac, M. and D. Boyce. They helped to create more enjoyable environment through the years at MIT. Finally, I would like to thank Jin-Soon for always being nearby and willing to listen.

The research reported herein was supported in part by NASA Lewis Research Center under NASA Grant No. NAG3-33 and by the Charles Stark Draper Laboratory under a Fellowship program. Publication of this thesis does not constitute approval by the Charles Stark Draper Laboratory of the findings and conclusions contained herein. It is published for the exchange and stimulation of ideas.

TABLE OF CONTENTS

APPENDIX

Appendix Page

LIST OF FIGURES

LIST OF TABLES

LIST OF SYMBOLS

Symbol	
$\underset{\sim}{a}$	Shell Surface Base Vector
$\underset{\sim}{B}$	Strain-Displacement Interpolation Matrix
$b_{\beta\zeta}$	Components of Second Fundamental Form
$\underset{\sim}{C}$	Stress-Strain Matrix
E	Young's Modulus
$\underset{\sim}{e}_i$	Rectangular Cartesian Base Vectors
$\underset{\sim}{g}_i$	Natural Base Vectors
h	Thickness
$\underset{\sim}{J}$	Jacobian Matrix
$\underset{\sim}{K}$	Stiffness Matrix
L	Length
$\mathcal{l}^{\alpha\beta}$	Membrane Stress Resultant
$m^{\alpha\beta}$	Bending Stress Resultant
$\underset{\sim}{N}$	Displacement Interpolation Matrix
$\underset{\sim}{n}$	Normal Vector
$\underset{\sim}{P}$	Stress Interpolation Matrix
$\underset{\sim}{Q}$	Nodal Load Vector
$\underset{\sim}{q}$	Nodal Degrees of Freedom
$\underset{\sim}{R}$	Position Vector
R	Radius

S	Surface
$\underset{\sim}{T}$	Traction Vector
$\underset{\sim}{t}_{\alpha}$	Surface Tangent Vectors
$\underset{\sim}{u}$	Displacement Vector
X,Y,Z	Rectangular Cartesian Coordinates (Global)
V	Domain (Volume)
β_i	Assumed Stress Constant Coefficients
$\underset{\sim}{\nabla}$	Linear Differential Operator
$\underset{\sim}{\epsilon}$	Strain Tensor
$\underset{\sim}{\gamma}^{\circ}$	Membrane Strain Tensor
$\underset{\sim}{\beta}$	Bending Strain Tensor
ν	Poisson's Ratio
$\underset{\sim}{\nu}$	Boundary Normal Vector
$\underset{\sim}{\sigma}$	Stress Tensor
θ_i	Rotation Components
$\underset{\sim}{\tau}$	Stress Tensor in Natural Bases
$\left.\begin{matrix}\xi,\eta,\zeta \\ \xi^i\end{matrix}\right\}$	Natural (Element) Coordinates
$\left\{\begin{matrix}\alpha \\ \beta\,\sigma\end{matrix}\right\}$	Components of Christoffel Symbol
$(\bar{\ })$	Prescribed Quantities

CHAPTER 1

INTRODUCTION

Because of tremendous economic motivation and backing, the method of finite elements enjoyed an explosive growth through the past thirty years. Correspondingly, abundant literature covers the method in much detail. In conjunction with this surge of knowledge, large commercial finite element codes were developed for practical application. Judging from years of industrial usage, noticeable differences in the types of application of the finite element method and the general philosophy of employing numerical methods became apparent.

In short, numerical methods deal with consistency, convergence, and stability of each method; each method is ranked and assessed with respect to truncation error [1-3]. Once the method is established, a sequence of solutions is obtained to a given problem using increasingly smaller spatial discretization. With such a sequence, corresponding accuracy of each analysis may be determined by a simple comparative norm.

In an application of the finite element method for industrial-type problems, the problem size is usually too

large to permit the generation, feasibly, of a sequence of solutions. Instead, the problems are analyzed by a single solution with spatial discretization made based upon "experience". Also, the spatial discretization sizes tend to vary significantly through the domain. In this context, the determination of "accuracy" depends on "experience"; it is often subjective. One aspect of finite element research in recent years may be described as a search for more definitive measures of accuracy and for finite elements of inherent superior accuracy. Two different elements with the same truncation error order are described and distinguished qualitatively by terms such as a "good" or "accurate" element. Qualitative features are based upon physical "feeling" and "experience". Various techniques attempt to satisfy a set of such qualitative features. As of yet, no general consensus has been reached on specific criteria to define an "accurate" element in more precise terms.

1.1 Justification of the Finite Element Method

The following discussion covers the arguments which justify the use of the finite element method for the solution of a boundary-value problem in elasticity. Although the method may be shown to converge in an abstract way, a judicious use of logical physical

modeling involved in solid mechanics is required to remedy the inadequacies often encountered in a so-called "direct" finite element method implementation.

The class of problems addressed comprises the linearized equations governing the mechanics of solids [4-6]. These are the governing equations of linear elasticity separated into four catagories:

Equilibrium Equations	$\vec{\nabla} \cdot \underset{\sim}{\sigma} + \underset{\sim}{F} = 0$
Strain-Displacement Relations	$\underset{\sim}{\varepsilon} = \frac{1}{2}\left(\vec{\nabla}\,\underset{\sim}{u} + \underset{\sim}{u}\,\vec{\nabla}\right)$
Linear Constitutive Relations	$\underset{\sim}{\sigma} = \underset{\sim}{L} : \underset{\sim}{\varepsilon}$
Compatibility Equations	$\vec{\nabla} \times \underset{\sim}{\varepsilon} \times \vec{\nabla} = 0$

(1.1)

These differential equations are to be satisfied pointwise within the domain. Together with the boundary conditions, they yield a unique solution to a specific problem of linear elasticity.

The general complexity of the governing equations demands that simplifications be made according to selected assumptions for a given class of problems. The arguments of dominant balance between similar terms allow certain terms to be neglected in comparison with others.

Within the framework of numerical analysis, such assumptions permit problem-size reduction through a reduction of the number of independent variables. Even more importantly, good numerical conditioning is required because of the need to use finite-precision calculations; this forces the elimination of variables that are negligible. A compendium of available "exact" solutions [7,8] provides comparative gages for numerical accuracy of finite element solutions; some of these solutions are exact but others represent only what is believed to be the most accurate known approximate solution.

1.1.1 Variational Principles

To provide a systematic variational basis for the finite element method, the governing equations with the boundary conditions must be recast into appropriate and useful integral forms. The variational principles may be obtained through the virtual work statement, energy principles, or the weighted residual method. However, for the equations of linear elasticity, all three methods yield equivalent forms.

The final forms of the integral expressions are categorized under the topic of variational principles of elasticity. As the name suggests, the Euler equations together with the a priori conditions generate the

governing equations. Since these variational principles form the basis of the finite element method, extensive compilations of various legitimate variational principles are available [9-13].

Although many statements of variational principles exist, they differ only in the assumptions made a priori. Such assumptions require that active variables satisfy one or more of the categories of conditions indicated in the equation (1.1). As an aside, the term "modified variational principles" concerns certain assumptions made about interelement continuity of certain quantities in the discretized domain. The four major variational principles are as follows:

Principle of Minimum Potential Energy - $\pi_p(\underset{\sim}{u})$

Hu-Washizu Principle - $\pi_G(\underset{\sim}{u},\underset{\sim}{\sigma},\underset{\sim}{\varepsilon})$

Hellinger-Reissner Principle - $\pi_R(\underset{\sim}{u},\underset{\sim}{\sigma})$

Principle of Minimum Complementary Energy - $\pi_C(\underset{\sim}{\sigma})$

The advantages of choosing one over any of the others for element formulation is not clear. Numerical experimentations have failed to provide a definitive illumination on the subject. The most popular choice, gaged upon current commercial codes, is the principle of minimum potential energy together with the use of assumed displacement fields. Although this chosen principle is cited in many finite element developments, sometimes it is not employed in rigorous and consistent fashion;

hence, certain "variational crimes" [2] are witnessed in the actual implementation.

1.1.2 Mathematical Aspects

Proceeding from the variational principles, the field variables (displacements, strains, and/or stresses) are discretized into piecewise polynomials through the domain. The stationary condition yields the algebraic equations which then leads to an approximate solution to a given boundary-value problem. The piecewise polynomials defined in the finite domain yield the name "finite element method". The method is also referred to as piecewise Rayleigh-Ritz-Galerkin technique.

The convergence of such piecewise construction to an exact solution has been assessed through examination of the truncation error made through polynomial approximation [14,15,2]. For multidimensional elements, the evaluation of the truncation errors rely only on the terms involving complete polynomial order. Polynomial order is called complete in the sense of Pascal's triangle for two-dimensional elements.

In general the assumed polynomials for finite elements do not come in nice packages of complete order of terms. For example, the bilinear element is complete to the linear term, and the truncation error is based

upon the linear order. Thus, the terms higher than the linear order are simply neglected.

The proofs of convergence generally require that the assumed piecewise polynomials be C^0 or C^1 continuous depending upon the order of the derivatives present. If only the values of the functions are continuous across boundaries, the function is said to be of class C^0. When the function and its first derivatives are continuous, it is of class C^1. In general, if the function and all its derivatives up to order α are continuous, it is said to be of class C^α. Furthermore, integrations carried out in the element domain should be exact. The number of sampling points for numerical integration should correspond to the number required for exact integration of the highest order term appearing in the integrand. Within the scope of these suppositions, the elements thus constructed will fulfill the convergence requirements.

1.1.3 Patch Test

Proposed by Irons [16,17], the patch test attempts to identify the elements that fail to meet the conditions of convergence and thereby commit "variational crimes". The patch test numerically examines the state of constant strain for an arbitrary mesh and proposes that this state

must be satisfied exactly for convergence to occur. As an engineering statement of consistency, the patch test was proposed without proof.

Later work of Stummel has shown that the patch test is neither necessary nor sufficient for convergence [18,19]. In reply, Irons stated that if the element shapes do not become "asymptotically" more eccentric in the limit, the pathological examples presented by Stummel as a counter-proof may be avoided [17]. Overall, whether the patch test provides a proof of consistency or not, the test may describe a desirable feature for practical elements.

1.2 Hybrid Method

For the present purpose, only the definition of the hybrid method shall be provided. Although the original concept was derived from the modified complementary energy principle which required that the stress assumption satisfy equilibrium exactly [11,20-28], the hybrid method has taken on a much broader definition. In the general definition, the hybrid formulation includes all methods employing Lagrange multipliers that are condensed out at the element level [29]. Element level condensation implies that the Lagrange multipliers are not restricted to be continuous across interelement

boundaries. As a point of clarification, with the advent of solvers such as the frontal solver, an element level condensation as the distinguishing factor for hybrid formulation may be insufficient. An additional definition to alleviate this confusion is to point out that the condensation required for the hybrid element may be carried out without further information from any other elements that make up the domain.

Using the broader definition, the hybrid formulation will be derived from the Hellinger-Reissner principle with displacement and stress as the assumed fields. The displacement field for C^0 elements will be the same as for the isoparametric elements and for C^1 elements will be incompatible. The assumed stress field will be defined for the local element coordinate system, and will satisfy equilibrium only approximately [30]. The present definition is summarized in Table 1-1.

1.3 Thesis Objectives and Overview

The basic research objective of this thesis is to establish a standard of comparison for the hybrid stress elements. Numerous choices available for the assumed stress fields introduce an inherent difficulty in the construction of hybrid stress elements. To compound the difficulty, the element performance is extremely

Table 1-1. Hybrid Method Definition Summary.

DEFINITION: "HYBRID" ELEMENT

- Hybrid element is derived from a functional with multiple assumed fields.

- Final resulting matrix equations must be a function of nodal displacements. All other field variables must be condensed at the element level.

$\underset{\sim}{K}\,\underset{\sim}{q} = \underset{\sim}{Q}$ Matrix-Displacement Method

- Original Idea: T.H.H. Pian (1964)

$$\pi_{mc}(\tilde{\underset{\sim}{u}}, \underset{\sim}{\sigma})$$

$\tilde{\underset{\sim}{u}}$ - Boundary Displacement
$\underset{\sim}{\sigma}$ - Equilibriating Stress

- Current Status:

$$\pi_R(\underset{\sim}{u}, \underset{\sim}{\sigma})$$

$\underset{\sim}{u}$ - Compatible Internal Displacement
$\underset{\sim}{\sigma}$ - Arbitrary Stress Field

or

$$\pi_{mR}(\tilde{\underset{\sim}{u}}, \underset{\sim}{\sigma}, \underset{\sim}{u})$$

$\underset{\sim}{u}$ - Incompatible Internal Displacement
$\underset{\sim}{\sigma}$ - Arbitrary Stress Field
$\tilde{\underset{\sim}{u}}$ - Boundary Displacement

sensitive to the choice of stress fields. In the following chapters, a systematic procedure used to select appropriate assumed stress fields for a wide range of elements is presented.

1.3.1 Definition of a "Good" Element

A "good" or "well-behaved" element is defined qualitatively as having the following three characteristics:

(1) Convergence to the Exact Solution.
(2) "Ball Park" Accuracy for a Crude Mesh.
(3) Ability to handle Practical Mesh Shape Distortion.

Regarding the first characteristic, a note of warning should be emphasized. Take an element with convergence rate

$$\epsilon(h) = O(h^p) \quad \text{as} \quad h \to 0$$

where

ϵ = Error
h = Steplength (Spatial Discretization)
p = Order depending on the complete polynomial represented in the field assumption.

It is important to guard against the temptation mentally to debase the notation $\epsilon(h) = O(h^p)$ to mean "$\epsilon(h)$ is roughly the same size as h^p, whatever the size of h".

Apparent discrepancies between theoretical estimates and numerical results frequently stem from a failure to realize that the notation $\epsilon(h) = O(h^p)$ carries with it the implication "as $h \to 0$".

In practical applications, the element size is definitely always finite. Thus, convergence alone cannot evaluate element performance. In another words, elements with the same rate of convergece may perform drastically differently for coarse mesh sizes. Due to differing opinions in the finite element community regarding the qualitative terminology used in characteristics (2) and (3), all numerical results in the present study are provided for various ranges of mesh discretization and distortion.

1.3.2 Overview of the Thesis Content

Chapter 2 presents the major techniques presently used to construct finite elements. These techniques offer various ways to obtain assumed fields required for element construction.

Chapter 3 contains the derivation of the equations and variational principles of linear elasticity. The derivation emphasizes the equivalence between the various techniques, and sheds new perspective on the variational principles used in the finite element method. As

indicated previously, the standard derivations are widely available.

Chapter 4 inter-relates the set of elements presented in the next five chapters. A unified treatment enforces consistency in the element developments presented.

Chapters 5 to 9 provide construction and assessment of a broad range of elements. Chapter 5 pertains to the three-dimensional solid elements, while Chapter 6 deals with the two-dimensional plane elements. Discussed in Chapter 7 are the plate elements. Next, the arch elements are described and evaluated in Chapter 8. Finally, Chapter 9 deals with the shell elements.

1.3.3 Brief Thesis Order-of-Development History

To form the background in the research with the assumed internal stress technique, the order of development shall be discussed briefly. During 1981, a methodical technique was developed to choose assumed stress fields such that zero-energy deformation modes, rank deficiency in the stiffness matrix, can be eliminated for C^0 elements [31]. Before this time, a selective trial procedure was used for obtaining the stress fields. The above technique allows one to evaluate the minimum number of stress modes needed to

eliminate the zero-energy deformation modes. However, the solution obtained is not unique. Using the method of group theory, the eight possible stress fields that contain the minimum number of stress modes and satisfy complete equilibrium may be obtained [32].

During the period of 1982, based upon experience, likely candidates for well-behaved stress fields were implemented and evaluated for solid and plane stress elements. Two other problems tackled in this period were invariance of the element stiffness matrix due to rigid-body rotation, and minimization of solution deterioration due to the shape distortion of the element. Both of these problems were handled by choosing a local skewed coordinate system having its origin at the element center. Again, selected problems were evaluated based upon the local coordinate system.

In the following year, attention turned to plate elements. The choices of assumed fields widened to include various possibilities for displacement assumptions. Plate elements of both C^0 and C^1 classes were proposed and evaluated. Remember at this point that suitable stress fields must also be chosen. These stress fields may satisfy the pointwise equilibrium equations completely or up to a designated polynomial order. The character of a hybrid element depends significantly on the choice of the stress field.

During the present year, the construction of an arch

element and a general shell element was considered. In order to consolidate the past years of work, each past element was reassessed in a unified manner by beginning with the three-dimensional continuum and proceeding to carry out the finite element modeling to a particular desired finite element model.

CHAPTER 2

TECHNIQUES OF ELEMENT MODIFICATION

A basic procedure for the finite element method such as numerical integration and the definitions of nodes, elements, connectivity, and assembly may be found in any of the introductory texts on the finite element method [33-38]. The major functional used involve the principle of minimum potential energy. The resulting finite element approximation yields a set of algebraic matrix displacement equations of the form:

$$\underset{\sim}{K}\ \underset{\sim}{q} = \underset{\sim}{Q} \qquad (2.1)$$

$\underset{\sim}{K}$ = Stiffness matrix

$\underset{\sim}{q}$ = Nodal point displacements

$\underset{\sim}{Q}$ = Applied generalized nodal loads

Equation (2.1) expresses the equilibrium equation with $\underset{\sim}{q}$ and $\underset{\sim}{Q}$ representing generalized conjugate variables. In the element level, when $|\underset{\sim}{K}| > |K|_{EXACT}$ the element is referred to as too stiff. The stability of the element may be checked through an Eigenvalue analysis of the stiffness matrix. The number of zero Eigenvalues must not be more than the number of the rigid-body modes.

Convergence, reduction of the error under mesh refinement, and consistency, valid approximate representation of the equations, together with stability provide validity of the numerical approximation.

Although the degrees of freedom may include a mixed set of variables, such as nodal point stress components as well as nodal displacements, the mixed formulations are rarely used due to increased bandwidth of the "stiffness" matrix. Many of the concepts underlying the matrix displacement method predate the development of the finite element method [39]. In the matrix displacement method, the stiffness matrix is calculated in a closed analytical form for a simple geometry. Even currently, such a method is advisable for one-dimensional beam or arch element construction where closed form solutions exist for the calculation of the stiffness matrix.

The techniques presented in the following form five categories:

(1) Isoparametric Formulation
(2) Reduced Integration
(3) Incompatible Element Formulation
(4) Assumed Strain Formulation
(5) Stress Element Technique

As mentioned previously, current finite element codes employ isoparametric elements with modifications involving "variational crimes"; techniques 2, 3, and 4

represent typical such examples. All five techniques employ only $\underset{\sim}{q}$ and $\underset{\sim}{Q}$ as the generalized conjugate variables for the final set of algebraic equations.

2.1 Isoparametric Formulation

Introduction of isoparametric formulation is the single most valuable contribution that enabled creation of codes for general use. This technique is straight forward to implement and satisfies all convergence requirements [2,14,15]. The following equations briefly summarize and define the notations to be used:

$$\underset{\sim}{u} = \sum_n \underset{\sim}{N}_n \underset{\sim}{u}^n$$

$$\underset{\sim}{R} = \sum_n \underset{\sim}{N}_n \underset{\sim}{R}^n \qquad (2.2)$$

where

$\underset{\sim}{u}$ = Displacement vector

$\underset{\sim}{R}$ = Position vector

$\underset{\sim}{u}^n$ = Nodal point displacements

$\underset{\sim}{R}^n$ = Nodal point position vector

$\underset{\sim}{N}_n$ = Interpolation function defined in the element domain and zero everywhere else

n = Ranges to the total number of nodes

The use of the same functions for interpolation of nodal

displacements and nodal position vectors rendered the name "isoparametric". The name isoparametric means that the same interpolation functions are used to represent both the displacement field and the position vector field in terms of relevant nodal quantities. The interpolation functions are defined as

$$\underset{\sim}{N}_n = \underset{\sim}{N}_n (\xi^i)$$

where

ξ^i = "natural" element coordinate system

The coordinate system is shown in Figure 2-1 for a two-dimensional element. This coordinate system arises "naturally" with element interpolation. The coordinates ξ^i range [-1,1] for implementation of numerical integration. Although Gaussian quadrature is popular, other alternative quadratures do exist, and may be more economical [40,41].

The evaluation of strain components, $\underset{\sim}{\varepsilon}$, requires the use of a transformation of the coordinate system from natural to Cartesian, as described in the following.

$$\underset{\sim}{\varepsilon} = \frac{1}{2} (\overset{\rightarrow}{\nabla} \underset{\sim}{u} + \underset{\sim}{u} \overset{\rightarrow}{\nabla})$$

$$\overset{\rightarrow}{\nabla} = \underset{\sim}{g}^i \frac{\partial}{\partial \xi^i} \qquad (2.3)$$

$$\overset{\rightarrow}{\nabla} = \frac{\partial}{\partial \xi^i} \underset{\sim}{g}^i$$

The natural base vectors for the undeformed confuguration

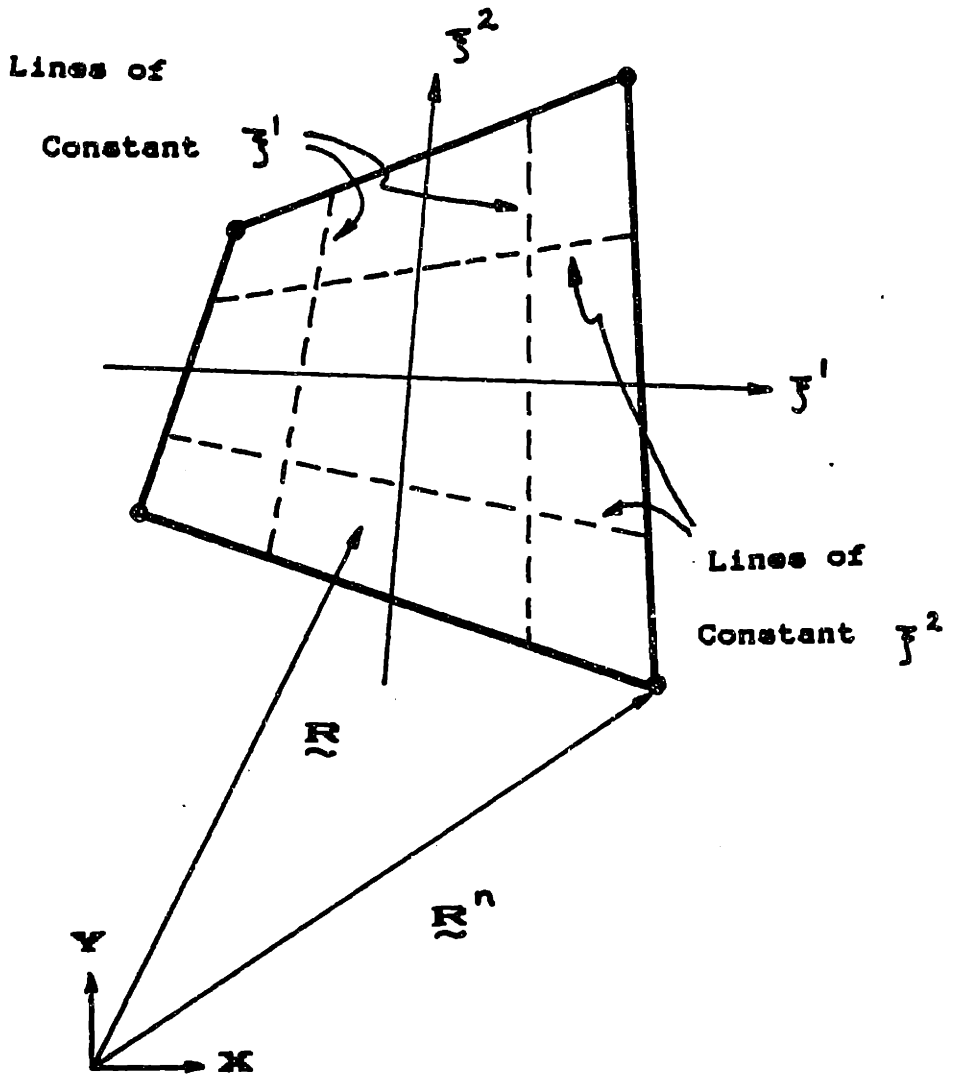

Figure 2-1. "Natural" Element Coordinate System.

are defined as

$$\underset{\sim}{g}_i = \frac{\partial \underset{\sim}{R}}{\partial \xi^i} = \frac{\partial}{\partial \xi^i} \sum_n \underset{\sim}{N}_n \underset{\sim}{R}^n$$

$$g_{ij} = \underset{\sim}{g}_i \cdot \underset{\sim}{g}_j \qquad (2.4)$$

$$[g^{ij}] = [g_{ij}]^{-1}$$

$$\underset{\sim}{g}^i = g^{ij} \underset{\sim}{g}_j$$

Usually, all strain components are expressed in the Cartesian system for global analysis.

$$\underset{\sim}{\varepsilon} = \frac{1}{2} \left(u_{j,i} \; \underset{\sim}{g}^i \underset{\sim}{e}_j + u_{j,i} \; \underset{\sim}{e}_j \underset{\sim}{g}^i \right)$$

$$= \varepsilon^*_{rs}(\xi^i) \; \underset{\sim}{e}_r \underset{\sim}{e}_s \qquad (2.5)$$

where

ε^*_{rs} = Cartesian components

$\underset{\sim}{e}_r$ = Cartesian base vectors

2.2 Reduced Integration

In the element stiffness construction, the integration is performed through the application of Gaussian quadrature. The stiffness matrix is calculated from the term involving the integration of the strain energy density. For now denote the numerical integration

schematically as

$$\int_V \underset{\sim}{\xi} : \underset{\sim}{L} : \underset{\sim}{\xi}\, dV = \sum_{\ell} (\underset{\sim}{\xi} : \underset{\sim}{L} : \underset{\sim}{\xi})_{\ell} |J|_{\ell} W_{\ell} \qquad (2.6)$$

where

ℓ = range of total no. of integration points

$(\underset{\sim}{\xi} : \underset{\sim}{L} : \underset{\sim}{\xi})_{\ell}$ = evaluated at integration point

$|J|_{\ell}$ = determinant of Jacobian matrix

W_{ℓ} = weighting factors

Define

ℓ_E = number of integration points needed for exact integration

ℓ_R = number of integration points used in the reduced integration technique

Thus

$$\ell_R < \ell_E$$

For "uniform reduced integration", all the terms in the integrand are evaluated using reduced number of integration points, ℓ_R. When the integrand is expanded out into separate components, "selective reduced integration" chooses only a particular group for application of reduced integration.

From a mechanical viewpoint, reduced integration plays the role of truncating polynomials as exemplified by the following example. Suppose the integrand is

$$\varepsilon_x = \alpha_1 + \alpha_2 \xi + \alpha_3 \eta + \alpha_4 \zeta \qquad (2.7)$$

An evaluation at a single point yields

$$(\varepsilon_x)_{\xi=\eta=\zeta=0} = \alpha_1 \qquad (2.8)$$

By using only the value evaluated at the origin, the effect of α_2, α_3, and α_4 have been eliminated. Overall, the reduced integration forms a numerical surgical tool for shaping the strain field assumptions. This process is denoted as

$$\underset{\sim}{\varepsilon}^S = \underset{\sim}{\varepsilon}^* - \underset{\sim}{\varepsilon}^B$$

where

$\underset{\sim}{\varepsilon}^S$ = Selectively integrated strain
$\underset{\sim}{\varepsilon}^*$ = Isoparametric formulation strain
$\underset{\sim}{\varepsilon}^B$ = Truncated strain

In practice, reduced integration is applied only to the strain assumption. The displacement interpolations are kept the same.

When too few integration points are used, the stiffness matrix becomes rank deficient [33,38]. A stability test for the reduced integration may be used [42] or a simple Eigenvalue analysis may be done to assess stability. Now consider a case when the stiffness matrix is rank deficient at the element level but stable when assembled with one or more elements. Some claim that these elements are acceptable on the grounds of stability [43]. However, from a viewpoint of an

efficient use of all degrees of freedom, rank deficiency at the element level demonstrates that the proposed element is not numerically efficient in employing all possible independent combinations of the given degrees of freedom.

To place the technique of reduced integration in a more legitimate framework, the equivalence of reduced integration to a logically constructed mixed formulation for particular cases has been provided [44-50]. The proof consists of demonstrating the role of the Lagrange multiplier in constraining the strain-displacement relations, as follows:

$$\underset{\sim}{\lambda}^{T} \left(\underset{\sim}{\varepsilon} - \underset{\sim}{\underset{\sim}{D}}\,\underset{\sim}{u} \right) = 0 \qquad (2.10)$$

If equation (2.10) is satisfied exactly, the stiffness matrix resulting from the mixed formulation will be identical to the one obtained from reduced integration. Such an equivalence demonstrates only an existence without providing insight on why the particular choice of strain might be well-behaved. In summary, there are only limited combinations of stable reduced integration schemes for each element. Once a combination is chosen, the strain field is fixed for all element configurations. Due to this lack of control, the element constructed using reduced integration is well-behaved only for the rectangular element geometry.

2.3 Incompatible Element Formulation

The basic idea behind an incompatible element formulation is to improve element performance by adding incompatible displacement terms to complete higher polynomial order [51-53]. For example, a four node isoparametric plane element contains an incomplete quadratic order assumed displacement field. This formulation simply includes additional terms required to complete the quadratic order. For C^0 elements

$$\underset{\sim}{u}^{W} = \underset{\sim}{u}^{*} + \underset{\sim}{u}^{A} \qquad (2.11)$$

where

$\underset{\sim}{u}^{*}$ = Compatible displacement assumption

$\underset{\sim}{u}^{A}$ = Added incompatible displacement modes

Upon construction of the element stiffness matrix, the added degrees of freedom are statically condensed. Static condensation requires an inversion of a matrix of order of the number of added degrees of freedom.

To validate the element, series of patch tests was performed. Initial results indicated that the element failed the patch test for distorted element configurations. Later modification of local element coordinate system for the added displacement modes remedied the problem. The local element coordinate is located at the center of the element. As a result, the

incompatible element formulation offers a viable technique. Presently, the implementation of this technique mainly involves directly completing a higher order polynomial by adding incompatible displacement terms.

2.4 Assumed Strain Formulation

The development of the assumed strain formulation is motivated by seeking a remedy to element deterioration under distorted geometry using selective integration. Using the strain modes obtained from reduced integration technique for the undistorted geometry, the assumed strain formulation solves the inverse problem of relating the strain modes to displacement degrees of freedom for general geometry [54-56]. The key to this technique is to relate the degrees of freedom in a manner that reduces sensitivity to distortion. Although not generally applicable, the assumed strain formulation for C^0 plate element shows most promise. The basic assumption for the assumed strain formulation is the knowledge of a well-behaved strain field. Since the strains are assumed independently of and inconsistently with the displacements, the assumed strain formulation yields non-conforming elements, ie. they are the possessors of and victims of "variational crimes".

2.5 Stress Element Technique

The stress element technique is derived under the principle of minimum complementary energy. As the name suggests, the starting point for this technique is to assume a stress field that satisfies the equilibrium equations. This may be done by the use of a stress function expressed in the local element coordinate system. The next step consists of relating the stress modes to nodal point forces through an equivalent work description along the element boundary [57-59].

The nodal point displacements may be obtained through virtual work principle expressed in a manner similar to Castigliano's method. The nodal displacements are energetic conjugates to the calculated nodal force relations. Since the calculation of equivalent work along the boundary require an assumption of boundary displacements, the stress element technique is similar (and often identical) to the hybrid element technique derived from the modified complementary energy principle. The main drawback for the stress technique is the need to calculate the equilibriating stress field.

2.6 Summary

A possibility of the existence of equivalence

amongst these various techniques presented is apparent from the previous discussion. The key to unraveling the confusion that arises from claims that one technique is superior to another involves the use of a consistent derivation that admits all features through the assumed distribution of the field variables. This may be achieved only through a strict adherence to the variational proper statements. Patching of or remedying the inadequacies of the displacement formulation through various techniques may be understood through an examination of alternate formulations which provide solutions without committing "variational crimes".

The equivalence between the various techniques may be obtained through the use of exact relations provided by the virtual work statement. The derivations presented in the next chapter are carried out in this spirit.

CHAPTER 3

EQUATIONS AND VARIATIONAL PRINCIPLES IN LINEAR ELASTICITY

The integral expressions of linear elasticity may be derived through construction of weighted residual upon the governing equations or through the definition of internal and external work. In the following discussion, the derivation following these two approaches will be presented with special emphasis on quantification of approximations based on polynomial expansions.

The first section will briefly present the variational principles as related through the Lagrange multipliers. The second section recasts the variational principles as measures of approximation deviating from the exact solution using work interpretation. For completeness, the third section covers the derivation through the weighted residual method.

Throughout the discussion the reciprocity, linearity, positive-definiteness, and duality [dependent properties known by different names] imbedded in the quality of linear elasticity shall be exploited to flush out redundant assumptions made in the integral expressions with multiple assumed independent fields.

The constitutive relations shall be assumed to hold and to be invertible. Thus, an assumed stress field implies a corresponding strain field but not necessary the displacement field.

The motivation for the following derivation involves the separation of (1) the concept of accuracy and (2) the rate of convergence employed for the judgment of finite element performance. The rate of convergence distinction is much too blunt to assess the accuracy of the analysis involving finite discretization. The regularity-of-convergence argument is valid only under limiting point of discretization. In another words, the reduction in error after mesh refinement correlate with the rate of convergence only as element size vanish. Such correlation is referred to as "regularity". Practical usage involve relatively crude discretization of the domain where the fluctuation about the regularity is significant.

In addition, various techniques of element modifications are casted into equivalent variational forms. Comparison of these equivalent variational forms yields the specific conditions of equivalence.

3.1 Assumed Field Notation and Definition

For the multiple field functionals, the present

notation recognizes that for each field the governing equations hold to the assigned degree of admissibility. For example, if a stress field is assumed, the constitutive relations implicitly assigns an associated strain field. First define the following:

V = Domain

S = Boundary Surface

$$S = S_\sigma + S_u$$

S_σ - Traction Prescribed Surface Boundary

S_u - Displacement Prescribed Surface Boundary

Statically Admissible Field:

This is a field that satisfies the following equilibrium equations and traction boundary conditions:

$$\sigma_{ij,i} + F_j = 0 \qquad \text{in } V$$

$$T_i = n_j \sigma_{ji} = \bar{T}_i \qquad \text{on } S_\sigma$$

Kinematically Admissible Field:

This is a field that satisfies the following strain-displacement equations and the displacement boundary conditions:

$$\varepsilon_{ij} = \frac{1}{2}\left(u_{i,j} + u_{j,i}\right) \qquad \text{in } V$$

$$u_i = \bar{u}_i \qquad \text{on } S_u$$

Table 3-1 provides a list of fields for future reference. The effort taken to change the notation may be illustrated by following examples of 4-node plane stress hybrid element derived from the Hellinger-Reissner principle, $\pi_R\left(u_i^*, \hat{\sigma}_{ij}\right)$. For pure bending of a cantilever beam, the numerical result obtained by a single element gave

$$\hat{\sigma}_{ij} = \text{Exact}$$

$$\varepsilon_{ij}^*\left(u_i^*\right) = \text{Not Exact}$$

In the notation provided, however,

$$\hat{\varepsilon}_{ij}\left(\hat{\sigma}_{ij}\right) = \text{Exact} \neq \varepsilon_{ij}^*\left(u_i^*\right)$$

Verbally, in a two field functional with assumed displacement and assumed stress, the strain calculated from the displacement field may not be equal to the strain calculated from the stress field through the constitutive relations. This example provided the initial motivation. The following sections will demonstrate a novel approach to understanding such examples and more importantly the difference between the variational principles.

TABLE 3-1. Assumed Field Notation.

$(\sigma_{ij}, \varepsilon_{ij}, u_i)$	-	Exact Field
$(\sigma_{ij}^{*}, \varepsilon_{ij}^{*}, u_i^{*})$	-	Kinematically Admissible Field
$(\sigma_{ij}^{o}, \varepsilon_{ij}^{o})$	-	Statically Admissible Field
$(\tilde{\sigma}_{ij}, \tilde{\varepsilon}_{ij}, \tilde{u}_i)$	-	Field Satisfying Strain-Displacement Relations (Does not satisfy displacement boundary conditions)
$(\hat{\sigma}_{ij}, \hat{\varepsilon}_{ij})$	-	Arbitrary Field
$(\hat{\hat{\sigma}}_{ij}, \hat{\hat{\varepsilon}}_{ij})$	-	Arbitrary Field

3.2 Variational Principles

Since the following variational principles are used by later sections, the functional for the principle of minimum potential energy is stated without further explanation.

$$\pi_P = \int_V \left[\tfrac{1}{2} \sigma_{ij}^* \varepsilon_{ij}^* - F_i u_i^* \right] dV - \int_{S_\sigma} \bar{T}_i u_i^* \, ds \qquad (3.1)$$
$$= \text{MIN.}$$

where $(\sigma_{ij}^*, \varepsilon_{ij}^*, u_i^*)$ - Kinematically Admissible Field
Setting $\delta\pi_p = 0$ leads to

$$\sigma_{ij,i}^* + F_j = 0 \qquad \text{in } V$$
$$n_i \sigma_{ij}^* = \bar{T}_j \qquad \text{on } S_\sigma \qquad (3.2)$$

The kinematically admissible condition can be relaxed through the Lagrange multiplier method which simultaneously separates strain and displacement as independent fields. This results in a three-field generalized variational principle known as the Hu-Washizu principle:

$$\pi_G = \int_V \left[\tfrac{1}{2} \hat{\sigma}_{ij} \hat{\varepsilon}_{ij} - F_i \tilde{u}_i \right] dV - \int_{S_\sigma} \bar{T}_i \tilde{u}_i \, ds$$
$$- \int_V \hat{\hat{\sigma}}_{ij} \left[\hat{\varepsilon}_{ij} - \tilde{\varepsilon}_{ij} \right] dV - \int_{S_u} n_j \hat{\hat{\sigma}}_{ji} (\tilde{u}_i - \bar{u}_i) \, ds \qquad (3.3)$$

where

$(\tilde{\sigma}_{ij}, \tilde{\varepsilon}_{ij}, \tilde{u}_i)$ - Field satisfying strain-displacement relation

$(\hat{\sigma}_{ij}, \hat{\varepsilon}_{ij})$ - Arbitrary

$(\hat{\hat{\sigma}}_{ij}, \hat{\hat{\varepsilon}}_{ij})$ - Arbitrary

Comparing Eq. (3.3) with Eq. (3.1), $\hat{\hat{\sigma}}_{ij}$ can be identified as the Lagrange multiplier. Since both $\hat{\hat{\sigma}}_{ij}$ and $\hat{\sigma}_{ij}$ are completely arbitrary fields, they are redundant.

Setting $\delta\pi_G = 0$ leads to

$$\hat{\hat{\sigma}}_{ij} = \hat{\sigma}_{ij} = L_{ijkl} \hat{\varepsilon}_{kl}$$
$$\hat{\varepsilon}_{ij} = \tilde{\varepsilon}_{ij} = \tfrac{1}{2} (\tilde{u}_{i,j} + \tilde{u}_{j,i}) \qquad \text{in } V$$
$$\hat{\hat{\sigma}}_{ij,i} + F_j = 0 \qquad (3.4)$$

$$n_i \hat{\hat{\sigma}}_{ij} = \bar{T}_j \qquad \text{on } S_\sigma$$

$$\tilde{u}_i = \bar{u}_i \qquad \text{on } S_u$$

The Hellinger-Reissner principle can be obtained by equating the two completely arbitray fields, and thus removing the redundancy:

$$(\hat{\sigma}_{ij}, \hat{\varepsilon}_{ij}) = (\hat{\hat{\sigma}}_{ij}, \hat{\hat{\varepsilon}}_{ij})$$

$$\pi_R = \int_V \left[-\tfrac{1}{2}\hat{\sigma}_{ij}\hat{\varepsilon}_{ij} + \hat{\sigma}_{ij}\tilde{\varepsilon}_{ij} - F_i\tilde{u}_i\right] dV \qquad (3.5)$$

$$- \int_{S_\sigma} \bar{T}_i \tilde{u}_i \, ds - \int_{S_u} n_j \hat{\sigma}_{ji}(\tilde{u}_i - \bar{u}_i)\, ds$$

where

$(\tilde{\sigma}_{ij}, \tilde{\varepsilon}_{ij}, \tilde{u}_i)$ - Field satisfying strain-displacement relation

$(\hat{\sigma}_{ij}, \hat{\varepsilon}_{ij})$ - Arbitrary

Setting $\delta\pi_R = 0$ leads to

$$\hat{\sigma}_{ij,i} + F_j = 0 \qquad \text{in } V$$

$$\hat{\varepsilon}_{ij} = \tilde{\varepsilon}_{ij} = \tfrac{1}{2}(\tilde{u}_{i,j} + \tilde{u}_{j,i}) \qquad (3.6)$$

$$n_i \hat{\sigma}_{ij} = \bar{T}_j \qquad \text{on } S_\sigma$$

$$\tilde{u}_i = \bar{u}_i \qquad \text{on } S_u$$

The principle of minimum complementary energy can be obtained by constraining the arbitrary field $(\hat{\sigma}_{ij}, \hat{\varepsilon}_{ij})$ in π_R to be the Statically Admissible Field:

$$(\hat{\sigma}_{ij}, \hat{\varepsilon}_{ij}) = (\sigma^o_{ij}, \varepsilon^o_{ij}) \tag{3.1}$$

$$-\pi_c = \int_V -\tfrac{1}{2}\sigma^o_{ij}\varepsilon^o_{ij}\,dV + \int_{S_u} n_j \sigma^o_{ji}\bar{u}_i\,dS$$

The Euler equations for π_c can be obtained by using stress functions and thus establishing the integrability condition for ε^o_{ij}. The rigid body motion under integration is suppressed through prescribed displacements.

3.3 Work Principles

3.3.1 Virtual Work Principle

The external work done by the external forces acting through the displacements u_i from the unstressed state to the state of equilibrium is

$$W_{ext} = \int_V F_i u_i \, dV + \int_S T_i u_i \, dS$$

$$= \int_V F_i u_i \, dV + \int_V (\sigma_{ij} u_i)_{,j} \, dV \qquad (3.8)$$

$$= \int_V \sigma_{ij} \varepsilon_{ij} \, dV = W_{int}$$

where $(\sigma_{ij}, \varepsilon_{ij}, u_i)$ - Exact Field.

Now consider a Kinematically Admissible Field $(\sigma_{ij}^*, \varepsilon_{ij}^*, u_i^*)$ with the actual force variable working through ε_{ij}^*.

$$W_{int}^* = \int_V \sigma_{ij} \varepsilon_{ij}^* \, dV \qquad (3.9)$$

The extremum principle can be derived through construction of:

$$W_{int}^* - W_{int} = \int_V \sigma_{ij} (\varepsilon_{ij}^* - \varepsilon_{ij}) \, dV \qquad (3.10)$$

$$= \int_V (\sigma_{ij} u_i^* - \sigma_{ij} u_i)_{,j} \, dV - \int_V \sigma_{ij,j} (u_i^* - u_i) \, dV$$

$$= \int_{S_\sigma} \bar{T}_i (u_i^* - u_i) \, dS + \int_V F_i (u_i^* - u_i) \, dV$$

Where

$$\sigma_{ij,j} = -F_i \qquad \text{in } V$$

$$u_i^* = u_i = \bar{u}_i \qquad \text{on } S_u$$

has been used.

In the notation for virtual quantities as the quantities deviating from the exact field, the principle of virtual work states

$$\delta W_{int} = \int_V \sigma_{ij} \, \delta \varepsilon_{ij} \, dV \qquad (3.10')$$

$$= \int_{S_\sigma} \bar{T}_i \, \delta u_i \, dS + \int_V F_i \, \delta u_i \, dV = \delta W_{ext}$$

with

$$\delta \varepsilon_{ij} = \frac{1}{2} (\delta u_{i,j} + \delta u_{j,i}) \qquad \text{in } V$$

$$\delta u_i = 0 \qquad \text{on } S_u$$

(σ_{ij} is the Exact Field)

Although the two statements (3.10) and (3.10′) are identical, Eq. (3.10) emphasize that σ_{ij} is the hypothetical exact solution and $\delta \varepsilon_{ij}$ is the difference in strain from the exact solution. The principle of virtual work is an equality statement regarding the behavior of the exact solution.

3.3.2 Extremum Principle

The integrand in the internal work term may be reorganized as

$$\sigma_{ij}(\varepsilon_{ij}^{*} - \varepsilon_{ij}) = \tfrac{1}{2}\left\{ (\sigma_{ij}^{*}\varepsilon_{ij}^{*} - \sigma_{ij}\varepsilon_{ij}) - (\sigma_{ij}^{*}\varepsilon_{ij}^{*} - 2\sigma_{ij}\varepsilon_{ij}^{*} + \sigma_{ij}\varepsilon_{ij}) \right\}$$

$$= \tfrac{1}{2}\left\{ (\sigma_{ij}^{*}\varepsilon_{ij}^{*} - \sigma_{ij}\varepsilon_{ij}) - (\sigma_{ij}^{*} - \sigma_{ij})(\varepsilon_{ij}^{*} - \varepsilon_{ij}) \right\} \qquad (3.11)$$

where reciprocity

$$\sigma_{ij}\varepsilon_{ij}^{*} = \sigma_{ij}^{*}\varepsilon_{ij}$$ has been used.

Reciprocity and positive definiteness of the quadratic

$$(\sigma_{ij}^{*} - \sigma_{ij})(\varepsilon_{ij}^{*} - \varepsilon_{ij}) \geq 0 \qquad (3.12)$$

is valid for the linear material under consideration. Thus the inequality

$$\tfrac{1}{2}(\sigma_{ij}^{*}\varepsilon_{ij}^{*} - \varepsilon_{ij}\sigma_{ij}) \geq \sigma_{ij}(\varepsilon_{ij}^{*} - \varepsilon_{ij}) \qquad (3.13)$$

substituted into Eq. (3.10) yield the extremum principle:

$$\pi = \tfrac{1}{2}\int_{v} \sigma_{ij}\varepsilon_{ij}\,dV - \int_{v} F_i u_i\,dV - \int_{S_\sigma} \bar{T}_i u_i\,ds \qquad (3.14)$$

$$\leq \tfrac{1}{2}\int_{v} \sigma_{ij}^{*}\varepsilon_{ij}^{*}\,dV - \int_{v} F_i u_i^{*}\,dV - \int_{S_\sigma} \bar{T}_i u_i^{*}\,ds = \pi_p$$

Adding the quadratic term, Eq. (3.14) may be rewritten as the following equality:

$$\pi = \pi_p - \int_V \tfrac{1}{2}(\sigma_{ij}^* - \sigma_{ij})(\varepsilon_{ij}^* - \varepsilon_{ij})\, dV \qquad (3.15)$$

Similarly, for a Statically admissible field

$$W_{int}^{o} - W_{int} = \int_V (\sigma_{ij}^{o} - \sigma_{ij})\,\varepsilon_{ij}\, dV = \int_{S_u} (T_i^{o} - T_i)\,\bar{u}_i\, dS \qquad (3.16)$$

In the notation for virtual quantities, the complementary virtual work principle states

$$\delta W_{int}^{c} = \int_V \delta\sigma_{ij}\,\varepsilon_{ij}\, dV = \int_{S_u} \delta T_i\,\bar{u}_i\, dS = \delta W_{ext}^{c} \qquad (3.16')$$

with

$$\delta\sigma_{ij,j} = 0 \quad \text{in } V$$

$$\delta T_i = 0 \quad \text{on } S_\sigma$$

(ε_{ij} is Exact Field)

The resulting extremum principle is

$$-\pi \leq \tfrac{1}{2}\int_V -\sigma_{ij}^{o}\,\varepsilon_{ij}^{o}\, dV - \int_{S_u} T_i^{o}\,\bar{u}_i\, dS = -\pi_c \qquad (3.17)$$

Rewriting Eq. (3.17) into an equality relation

$$\pi = \pi_c + \int_V \tfrac{1}{2}(\sigma_{ij}^0 - \sigma_{ij})(\varepsilon_{ij}^0 - \varepsilon_{ij})\, dV \qquad (3.18)$$

3.3.3 Stationary Principles

The expression (3.15) and (3.18) reveal an explicit "distance" measure for gaging the accuracy of the approximation for any admissible fields. In a similar fashion, the Hu-Washzu and the Hellinger-Reissner principle may be factored into quadratic forms:

$$\pi_G = \int_V (\tfrac{1}{2}\tilde{\sigma}_{ij}\tilde{\varepsilon}_{ij} - F_i\tilde{u}_i)\,dV - \int_{S_\sigma} \bar{T}_i\tilde{u}_i\,ds - \int_{S_u} n_j\hat{\hat{\sigma}}_{ji}(\tilde{u}_i - \bar{u}_i)\,ds$$
$$- \int_V \tfrac{1}{2}(\hat{\sigma}_{ij} - \hat{\hat{\sigma}}_{ij})(\tilde{\varepsilon}_{ij} - \hat{\hat{\varepsilon}}_{ij})\,dV + \int_V \tfrac{1}{2}(\hat{\hat{\sigma}}_{ij} - \hat{\sigma}_{ij})(\hat{\hat{\varepsilon}}_{ij} - \hat{\varepsilon}_{ij})\,dV \qquad (3.19)$$

$$\pi_R = \int_V (\tfrac{1}{2}\tilde{\sigma}_{ij}\tilde{\varepsilon}_{ij} - F_i\tilde{u}_i)\,dV - \int_{S_\sigma} \bar{T}_i\hat{u}_i\,ds \qquad (3.20)$$
$$- \int_{S_u} n_j\hat{\sigma}_{ji}(\tilde{u}_i - \bar{u}_i)\,ds - \int_V \tfrac{1}{2}(\tilde{\sigma}_{ij} - \hat{\sigma}_{ij})(\tilde{\varepsilon}_{ij} - \hat{\varepsilon}_{ij})\,dV$$

The explicit relation between π_G and π_R may be obtained by comparing Eqs. (3.19) and (3.20).

$$\pi_G = \pi_R + \int_V \tfrac{1}{2}(\hat{\hat{\sigma}}_{ij} - \hat{\sigma}_{ij})(\hat{\hat{\varepsilon}}_{ij} - \hat{\varepsilon}_{ij})\,dV \qquad (3.21)$$

The observation noted based upon explicit representation of the integral expressions indicates that the relation between these equations can be obtained through the integral difference of the field quantities assumed.

3.3.4 Comparative Case Studies

As a first case study, examine the relation between π_P and π_R with the $(\tilde{\ })$ field limited to be a kinematically admissible field:

$$(\tilde{\sigma}_{ij}, \tilde{\varepsilon}_{ij}, \tilde{u}_i) = (\sigma_{ij}^*, \varepsilon_{ij}^*, u_i^*) \qquad (3.22)$$

Then these two functionals are related as

$$\pi_P = \pi_R + \int_V \tfrac{1}{2}(\sigma_{ij}^* - \hat{\sigma}_{ij})(\varepsilon_{ij}^* - \hat{\varepsilon}_{ij})\,dV \qquad (3.23)$$

Note the inequalities

$$\pi \leq \pi_P$$
$$\pi_R \leq \pi_P \qquad (3.24)$$

and

$$\pi = \pi_P - \int_V \tfrac{1}{2}(\sigma_{ij}^* - \sigma_{ij})(\varepsilon_{ij}^* - \varepsilon_{ij})\,dV$$

$$= \pi_R - \int_V \tfrac{1}{2}(\sigma_{ij}^* - \sigma_{ij})(\varepsilon_{ij}^* - \varepsilon_{ij})\,dV \qquad (3.25)$$

$$+ \int_V \tfrac{1}{2}(\sigma_{ij}^* - \hat{\sigma}_{ij})(\varepsilon_{ij}^* - \hat{\varepsilon}_{ij})\,dV$$

Equations (3.24) and (3.25) state that a second order correction to the assumed potential can be made through appropriate choices of stress in π_R. Thus in a strict sense, π_R is more accurate then π_P if and only if

$$\int_V \tfrac{1}{2}(\sigma_{ij}^* - \hat{\sigma}_{ij})(\varepsilon_{ij}^* - \hat{\varepsilon}_{ij})\,dV \leq 2\int_V \tfrac{1}{2}(\sigma_{ij}^* - \sigma_{ij})(\varepsilon_{ij}^* - \varepsilon_{ij})\,dV$$

(3.26)

Further, if

$$\int_V \tfrac{1}{2}(\sigma_{ij}^* - \hat{\sigma}_{ij})(\varepsilon_{ij}^* - \hat{\varepsilon}_{ij})\,dV = \int_V \tfrac{1}{2}(\sigma_{ij}^* - \sigma_{ij})(\varepsilon_{ij}^* - \varepsilon_{ij})\,dV$$

(3.27)

the solution attains optimal accuracy. In addition, if the external work terms

$$\int_V F_i u_i^*\,dV + \int_{S_\sigma} \bar{T}_i u_i^*\,dS = \int_V F_i u_i\,dV + \int_{S_\sigma} \bar{T}_i u_i\,ds$$

(3.28)

the solution is exact due to uniqueness.

As a second case study, consider Wilson's incompatible element [51-53] and the corresponding functional. The basic idea behind the element is to add an additional field to the kinematically admissible field:

$$(\sigma_{ij}^{W}, \varepsilon_{ij}^{W}, u_i^{W}) = (\sigma_{ij}^{*}, \varepsilon_{ij}^{*}, u_i^{*}) + (\sigma_{ij}^{A}, \varepsilon_{ij}^{A}, u_i^{A}) \tag{3.29}$$

where

$(\,^{*}\,)$ = kinematically admissible field

$(\,^{A}\,)$ = added field

$$\pi_W = \int_V \tfrac{1}{2}\, \sigma_{ij}^{W} \varepsilon_{ij}^{W} dV - \int_V F_i u_i^{*} dV - \int_{S_\sigma} \bar{T}_i u_i^{*} dS \tag{3.30}$$

The added field denotes additional polynomial terms required to complete the order of the displacement field. The added displacement field is incompatible. Equation (3.29) states this process in a functional group form. Equation (3.30) describes the variational principle used to construct the incompatible element. Substituting Eq. (3.29) into Eq. (3.30)

$$\pi_W = \pi_P + \int_V \frac{1}{2}\left(2\sigma_{ij}^{A}\varepsilon_{ij}^{*} + \sigma_{ij}^{A}\varepsilon_{ij}^{A}\right) dV \tag{3.31}$$

Comparing Eqs. (3.31) and (3.23), the equivalence condition between π_R and π_W is

$$\int_V \frac{1}{2}\left(2\sigma_{ij}^{A}\varepsilon_{ij}^{*} - \sigma_{ij}^{A}\varepsilon_{ij}^{A}\right) dV = -\int_V \frac{1}{2}\left(\sigma_{ij}^{*} - \hat{\sigma}_{ij}\right)\left(\varepsilon_{ij}^{*} - \hat{\varepsilon}_{ij}\right) dV \tag{3.32}$$

By recognizing that any added field may be expressed as difference from Eq. (3.29), set

$$(\hat{}) = (^{W}) \tag{3.33}$$

Hence,

$$(^{A}) = (\hat{}) - (^{*})$$

Thus, the equivalence condition may be simplified as

$$\int_V \sigma_{ij}^{A}\varepsilon_{ij}^{*}\, dV = -\int_V \left(\sigma_{ij}^{*} - \hat{\sigma}_{ij}\right)\left(\varepsilon_{ij}^{*} - \hat{\varepsilon}_{ij}\right) dV \tag{3.34}$$

As the final case study, examine the following selective

integration functional:

$$\pi_S = \int_V \frac{1}{2} \sigma_{ij}^S \varepsilon_{ij}^S dV - \int_V F_i u_i^* dV - \int_{S_\sigma} \bar{T}_i u_i^* dS \tag{3.35}$$

π_S is in the same form as π_W with subtracting a field instead of adding one:

$$(\sigma_{ij}^S, \varepsilon_{ij}^S) = (\sigma_{ij}^*, \varepsilon_{ij}^*, u_i^*) - (\sigma_{ij}^B - \varepsilon_{ij}^B) \tag{3.36}$$

$$\pi_S = \pi_P + \int_V \frac{1}{2} (-2\sigma_{ij}^* \varepsilon_{ij}^B + \sigma_{ij}^B \varepsilon_{ij}^B) \tag{3.37}$$

where

$(^B)$ = Subtracted field

Recall that the selective integration trucates the assumed strain field by under-integration of selected strain components. The resulting field does not necessarily satisfy strain-displacement relation. In another words, the resulting strain may not be integrable. Since the displacement field may not exist, the left-hand-side of Eq. (3.36) does not contain a displacement field. A similar argument leads to the equivalence condition:

$$\int_V \sigma_{ij}^B \varepsilon_{ij}^* dV = \int_V (\sigma_{ij}^* - \hat{\sigma}_{ij})(\varepsilon_{ij}^* - \hat{\varepsilon}_{ij}) dV \qquad (3.38)$$

The equivalence conditions of π_s and π_w to π_R may be viewed as sufficient requirement for convergence for π_s and π_w, or alternate formulations for π_R. As an added bonus, the equivalence condition between π_s and π_w is

$$\int_V \sigma_{ij}^A \varepsilon_{ij}^* dV = - \int_V \sigma_{ij}^B \varepsilon_{ij}^* dV \qquad (3.39)$$

3.3.5 Summary

The derivations presented in the previous sections are collected here for future reference. At this time, these results shall be used for a concise summary. First using the virtual work principle, the extremum principles are used to bound the true potential, π.

$$\pi_c \leqslant \pi \leqslant \pi_p \qquad (3.14) \quad (3.17)$$

To study various conditions of equivalence, the inequalities are eliminated using "distance" measure.

$$\pi = \pi_P - \int_V \tfrac{1}{2} (\sigma_{ij}^* - \sigma_{ij})(\varepsilon_{ij}^* - \varepsilon_{ij}) dV \qquad (3.15)$$

$$\pi = \pi_C + \int_V \tfrac{1}{2} (\sigma_{ij}^0 - \sigma_{ij})(\varepsilon_{ij}^0 - \varepsilon_{ij}) dV \qquad (3.18)$$

An examination of stationary principles yielded an important relation:

$$\pi_G = \pi_R + \int_V \tfrac{1}{2} (\hat{\hat{\sigma}}_{ij} - \hat{\sigma}_{ij})(\hat{\hat{\varepsilon}}_{ij} - \hat{\varepsilon}_{ij}) dV \qquad (3.21)$$

As shown, the only difference between the two principles are gaged by completely arbitrary fields! The accuracy is not affected by equating the two fields.

In the comparative case studies, two element modifications are presented in a variational form. Now compare

$$\pi_R = \pi_P - \int_V \tfrac{1}{2} (\sigma_{ij}^* - \hat{\sigma}_{ij})(\varepsilon_{ij}^* - \hat{\varepsilon}_{ij}) dV \qquad (3.23)$$

$$\pi_W = \pi_P + \int_V \tfrac{1}{2} (2\sigma_{ij}^A \varepsilon_{ij}^* + \sigma_{ij}^A \varepsilon_{ij}^A) dV \qquad (3.31)$$

$$\pi_S = \pi_P + \int_V \tfrac{1}{2} (-2\sigma_{ij}^* \varepsilon_{ij}^B + \sigma_{ij}^B \varepsilon_{ij}^B) dV \qquad (3.37)$$

Presented in this form, the Hellinger-Reissner principle, π_R, the incompatible formulation, π_W, and the selective integration, π_S may be considered as modifications of the assumed displacement formulation, π_P. Since, $(\hat{\sigma}_{ij}, \hat{\varepsilon}_{ij})$ used in π_R is completely arbitrary, π_R can duplicate modifications made by π_S

and π_w.

3.4 Weighted Residuals

The virtual work principles and the corresponding conditions of admissibility are the dual integral statements of the governing equations. In the previous section the approximate solution methods are obtained through the consideration of extremum principles. The weighted residual method presented below provides an alternate solution scheme without resorting to inequality arguments. Although the results will be the same for linear elasticity, the weighted residual method is a more general statement.

The principle of virtual work states

$$\int_V \sigma_{ij}\, \delta\varepsilon_{ij}\, dV - \int_{S_\sigma} \bar{T}_i\, \delta u_i\, dS - \int_V F_i\, \delta u_i\, dV = 0 \qquad (3.40)$$

where

$$\begin{aligned} &\sigma_{ij} = \text{EXACT FIELD} && (3.41)\\ &\delta\varepsilon_{ij} = \tfrac{1}{2}\left(\delta u_{i,j} + \delta u_{j,i}\right) && \text{in } V\\ &\delta u_i = 0 && \text{on } S_u \end{aligned}$$

Construct the residual

$$R = \int_V \tilde{\sigma}_{ij}\, \delta\varepsilon_{ij}\, dV - \int_{S_\sigma} \bar{T}_i\, \delta u_i\, dS - \int_V F_i\, \delta u_i\, dV \tag{3.42}$$

where

$(\tilde{\sigma}_{ij}, \tilde{\varepsilon}_{ij}, \tilde{u}_i)$ = Kinematically Admissible Field

Since the virtual fields are arbitrary, choose

$$\begin{aligned} \delta\varepsilon_{ij} &= \delta\tilde{\varepsilon}_{ij} \\ \delta u_i &= \delta\tilde{u}_i \end{aligned} \tag{3.43}$$

$$R = \int_V \tilde{\sigma}_{ij}\, \delta\tilde{\varepsilon}_{ij}\, dV - \int_{S_\sigma} \bar{T}_i\, \delta\tilde{u}_i\, dS - \int_V F_i\, \delta\tilde{u}_i\, dV \tag{3.44}$$

At this time, the virtual fields are interpreted as the weighting functions needed to set

$$R = 0$$

The approximation field must be kinematically admissible in order to satisfy the condition on the virtual field. The admissibility conditions may be relaxed through the construction of further residuals on the conditions, and adding to Eq. (3.44). The results are the same as the previous section. Overall validity of the residual argument from the virtual work statement is derived through an integral representation of the differential equation. The virtual work principle is the

statement of the equilibrium equation and the complementary virtual work principle is the statement of compatibility.

CHAPTER 4

FINITE ELEMENT FAMILY

In the present chapter the job of systematically constraining the three dimensional continuum element to reduce the dimension in a consistent manner to obtain the necessary stress fields for the hybrid element construction is undertaken. Consistency implies that the actual assumptions used in plane stress, plate, and shell theories will be applied directly to the chosen three dimensional element. A flowchart for the element constraint process is shown in Figure 4-1.

As demonstrated later, the main differences between the present development and the direct application of pre-constrained governing partial differential equations are twofold. First, the parallel constraints in the kinematic and force variable field assumptions can be derived and observed as natural consequences of the modeling process. Secondly, through association, past work in finite element developments can be correlated and interpretated within the framework of the present "family" of elements. More generally, whether the technique used was reduced integration, assumed strain, or the hybrid method, every member of the family of

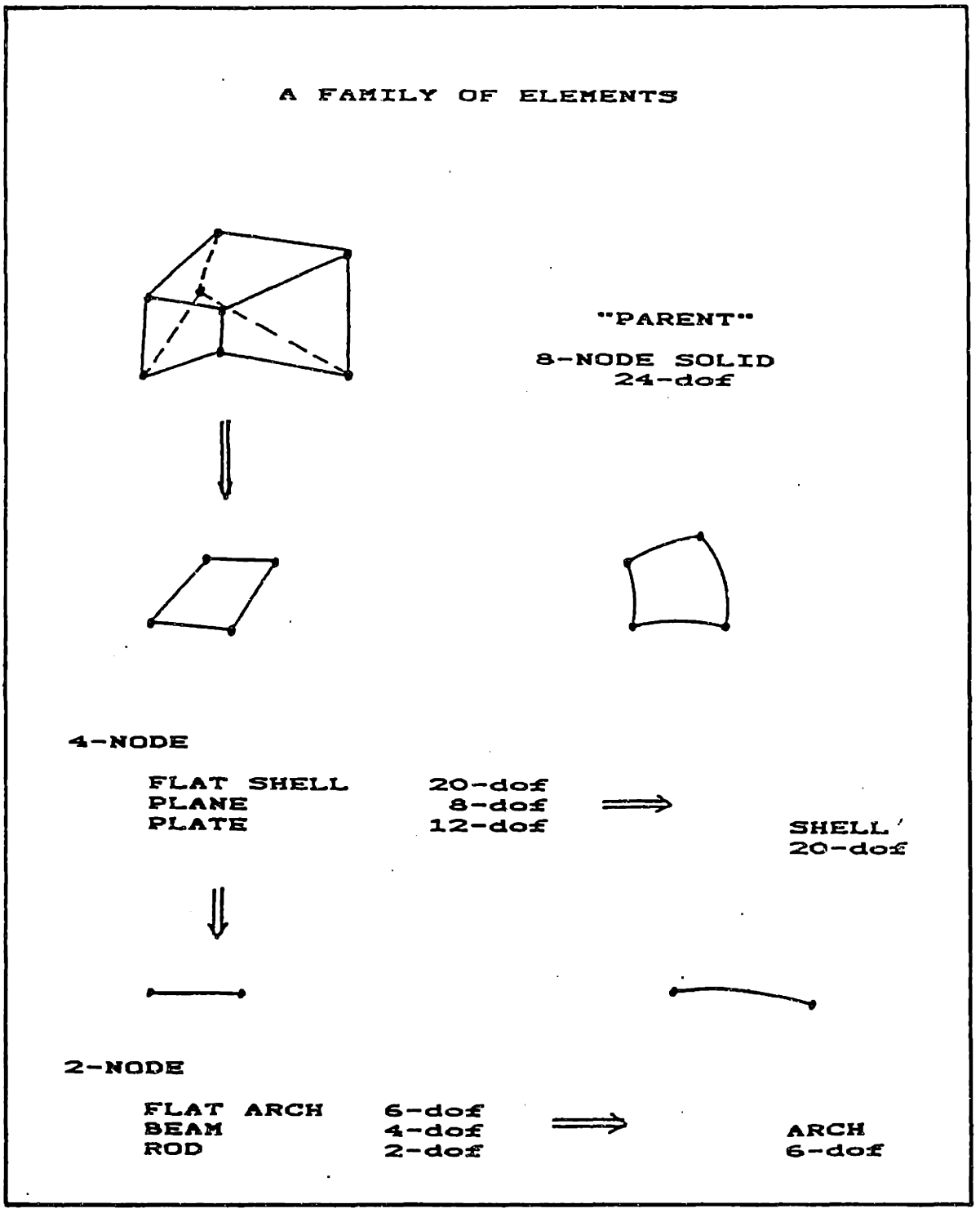

Figure 4-1. Flowchart for a Family of Elements.

elements should employ the same technique.

4.1 Solid Element

The starting point for the application of modeling constraints shall be a three-dimensional continuum element. This constraint application is in the same spirit with reduction of partial differential equations of continuum. The following stress field presented for the solid hybrid element provides a well-behaved element [30,53,60]. From this field, a systematic method will be outlined to reduce the stress assumption to be appropriate for plane, plate, and shell elements.

$$\begin{aligned}
\sigma_x &= \beta_1 + \beta_2 y + z[\beta_3 + \beta_4 y] \\
\sigma_y &= \beta_5 + \beta_6 x + z[\beta_7 + \beta_8 x] \\
\sigma_z &= \beta_9 + \beta_{10} x + \beta_{11} y + \beta_{12} xy \qquad (4.1) \\
\sigma_{xy} &= \beta_{13} + z[\beta_{14}] \\
\sigma_{yz} &= \beta_{15} + \beta_{16} x \\
\sigma_{xz} &= \beta_{17} + \beta_{18} y
\end{aligned}$$

Although the above stress assumption is expressed in terms of the rectangular Cartesian system, the actual element will employ a local "isoparametric" coordinate system. The present coordinate system, however, is adequate for stress field reduction purposes. Further

discussion regarding the above stress assumption is reserved for Chapter 5.

4.2 Plane Stress Model

The constraints used for arriving at the plane stress model consist of averaging the stress through the thickness with the condition on the applied loading that top and bottom surfaces are traction free with boundary traction being symmetric with the midplane, Figure 4-2. Together with $h/L << 1$, the σ_z , σ_{xz} , and σ_{yz} contributions can be neglected as compared with the other stress components. Furthermore, the in-plane stress components σ_x , σ_y , and σ_{xy} are constant through thickness. Thus

$$\sigma_z = \sigma_{xz} = \sigma_{yz} = 0$$
$$\beta_3 = \beta_4 = \beta_7 = \beta_8 = \beta_{14} = 0 \qquad (4.2)$$

Applying the constraint (4.2) to (4.1), the resulting strain field for the plane stress model is

$$\sigma_x = \beta_1 + \beta_2 y$$
$$\sigma_y = \beta_5 + \beta_6 x \qquad (4.3)$$
$$\sigma_{xy} = \beta_{13}$$

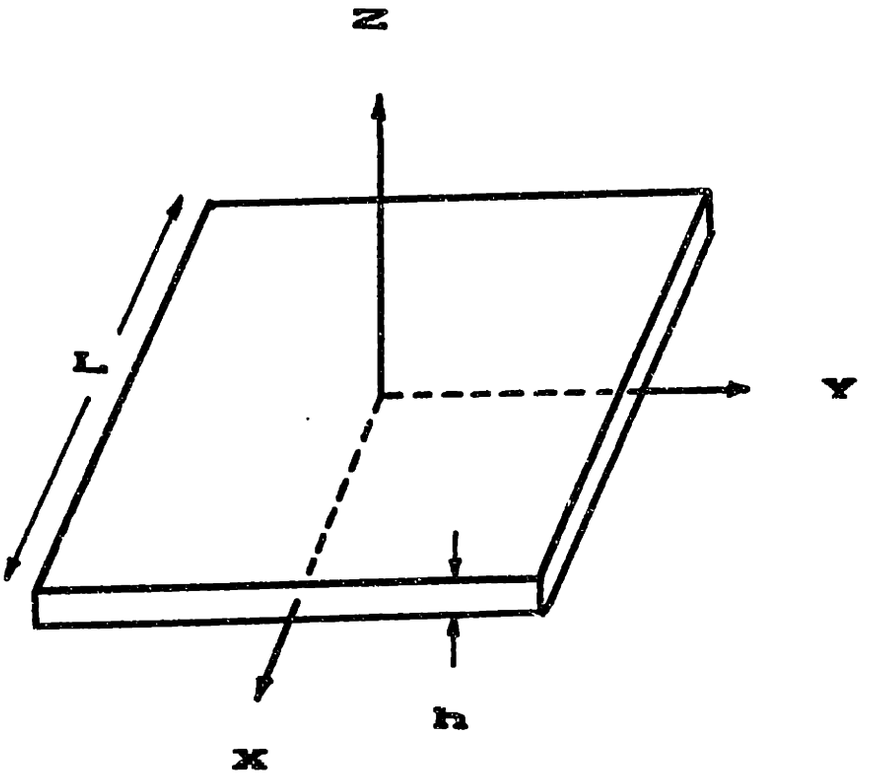

Figure 4-2. Plane Geometry.

4.3 Plate Models

Three different plate models are considered for the hybrid stress method. These are denoted as the degenerate solid, the Reissner/Mindlin plate, and the Kirchhoff plate. They are distinguished by the choice of kinematic constraints and transverse shear stress distribution. Other treatments of the hybrid plate element with transverse shear effect are reported by Spilker et al. [68-72] and Pian and Tong [21].

4.3.1 Degenerate Solid

The degenerate solid element, as the name suggests, collapses a solid element to allow only bending action. Such degeneration imposes kinematic constraints on the displacement field of form

$$\begin{aligned} u &= -z\,\theta_x(x,y) \\ v &= -z\,\theta_y(x,y) \\ w &= w(x,y) \end{aligned} \qquad (4.4)$$

Since the rotations, θ_x and θ_y, are assumed independently of the out-of-plane displacement, w, the degenerate solid element is of class C^0 continuity.

Similarly for the stress field, in-plane stresses are constrained to be linear through the thickness to

take on bending action. Furthermore, σ_z is neglected in comparison with other components of stress. Application of these constraints to Eq. (4.1) yield

$$\sigma_z = 0$$
$$\beta_1 = \beta_2 = \beta_5 = \beta_6 = \beta_{13} = 0 \qquad (4.5)$$

The resulting stress field for the degenerate solid element is

$$\begin{aligned} \sigma_x &= z\,[\,\beta_3 + \beta_4 y\,] \\ \sigma_y &= z\,[\,\beta_7 + \beta_8 x\,] \\ \sigma_{xy} &= z\,[\,\beta_{14}\,] \\ \sigma_{yz} &= \beta_{15} + \beta_{16} x \\ \sigma_{xz} &= \beta_{17} + \beta_{18} y \end{aligned} \qquad (4.6)$$

The field assumptions (4.4) and (4.6) represent physical degeneration of the solid to eliminate degrees of freedom not pertaining to bending action.

4.3.2 Reissner/Mindlin Plate

The Reissner/Mindlin plate takes on the same kinematic constraints, Eq. (4.4), as the degenerate solid element. Therefore, this element is of class C^0 continuity.

For the stress assumption, a functional form of the dominant stress distribution through the thickness derived through asymtotic power series expansion is imposed [61-63]. The method consists of substituting stress components expressed as a power series in plate thickness into the continuum equations of elasticity and equating coefficients of like powers of thickness.

Functionally, the result requires that the transverse shear stress components to assume parabolic form.

$$\sigma_{yz} = \left(\frac{h^2}{4} - z^2\right)\left[\beta_{15} + \beta_{16} x\right]$$
$$\sigma_{xz} = \left(\frac{h^2}{4} - z^2\right)\left[\beta_{17} + \beta_{18} y\right] \qquad (4.7)$$

The equilibrium equations require that

$$\frac{\partial \sigma_x}{\partial x} + \frac{\partial \sigma_{xy}}{\partial y} = -\frac{\partial \sigma_{xz}}{\partial z} = 2z\left[\beta_{17} + \beta_{18} y\right]$$
$$\frac{\partial \sigma_{xy}}{\partial x} + \frac{\partial \sigma_y}{\partial y} = -\frac{\partial \sigma_{yz}}{\partial z} = 2z\left[\beta_{15} + \beta_{16} x\right] \qquad (4.8)$$

Integrating Eq. (4.8) and adding the in-plane stress field in Eq. (4.6) gives:

$$\sigma_x = z\left[\beta_1 + \beta_2 x + \beta_3 y + \beta_4 xy\right]$$
$$\sigma_y = z\left[\beta_5 + \beta_6 x + \beta_7 y + \beta_8 xy\right] \qquad (4.9a)$$
$$\sigma_{xy} = z\left[\beta_9 + \beta_{10} x + \beta_{11} y + \beta_{12} \frac{x^2}{2} + \beta_{13} \frac{y^2}{2}\right]$$

$$\sigma_{yz} = \left(\frac{h^2}{4} - z^2\right)\left[\frac{1}{2}(\beta_{10} + \beta_7) + \frac{1}{2}(\beta_{12} + \beta_8)x\right]$$

$$\sigma_{xz} = \left(\frac{h^2}{4} - z^2\right)\left[\frac{1}{2}(\beta_2 + \beta_{11}) + \frac{1}{2}(\beta_4 + \beta_{13})y\right] \qquad (4.9b)$$

The coefficients are renumbered for convenience.

4.3.3 Kirchhoff Plate

The Kirchhoff plate theory, also known as "thin" plate theory, imposes further kinematic constraints by assuming that the transverse shear strain vanishes. In terms of displacements, the constraints impose the following:

$$\begin{aligned} u &= -z\, w_{,x}(x,y) \\ v &= -z\, w_{,y}(x,y) \\ w &= w(x,y) \end{aligned} \qquad (4.10)$$

Due to the presence of the derivatives of w in Eq. (4.10), the Kirchhoff plate is of class C^1 continuity. The stress field for this plate is the same as Eq. (4.9) without the transverse shear components, σ_{yz} and σ_{xz}.

Alternate derivation of the assumed stress field for the Kirchhoff plate element may be obtained by a

"balanced formulation" [64]. In this formulation, the internal displacements are added to serve as Lagrange multipliers to introduce the equilibrium constraints in each element. In a balanced formulation the assumed stresses are initially unconstrained and are complete polynomials. The internal displacements are added to make the total displacements also complete and the corresponding strains are of the same order as the assumed stresses.

4.4 General Shell

The general shell element will be considered as a distorted flat shell. A flat shell consists simply of a combination of plate and plane stress elements. One of the major tasks involved in the construction of the shell element is the definition of the geometry. Once the geometry is defined, obtaining the strain is only matter of the application of the strain-displacement relations in shell bases. However, due to the complexity of the equilibrium equations, transforming the stresses is a demanding task. To allow approximate satisfaction of the equilibrium equations, the Reissner principle will be used. Preliminary analysis with a circular arch indicates that the equilibrium approximation is adequate. Aspects of the shell geometry and approximations will be covered in a later chapter.

CHAPTER 5

SOLID ELEMENTS

For practical problems, three-dimensional finite element analyses are costly. In present general finite element codes, the 27-node solid elements developed based on the assumed displacement method are usually recommended for three-dimensional analysis. This higher order element is used to prevent overly rigid behavior under bending deformation. Since each element has 81 degrees of freedom, they are expensive to use. In the present chapter, the details required to construct a well-behaved hybrid stress 8-node solid element with 24 degrees of freedom as an alternate are outlined.

5.1 Element Construction

For the 8-node hybrid stress solid element, the Hellinger-Reissner principle, π_R , will be used. The actual construction of this element is simple and does not deviate much from the traditional element construction procedure based on the assumed displacement method. The functional form of the Hellinger-Reissner

principle is stated concisely in matrix form for the general solid element domain as follows:

$$\pi_R(\underset{\sim}{u},\underset{\sim}{\sigma}) = \int_V \left[-\tfrac{1}{2}\underset{\sim}{\sigma}^T\underset{\sim}{S}\underset{\sim}{\sigma} + \underset{\sim}{\sigma}^T(\underset{\sim}{D}\underset{\sim}{u}) - \underset{\sim}{F}^T\underset{\sim}{u}\right]dV - \int_{S_\sigma}\underset{\sim}{\bar{T}}^T\underset{\sim}{u}\,ds \qquad (5.1)$$

where

$\underset{\sim}{\sigma}$ = Six stress components

$\underset{\sim}{u}$ = Three displacement components

$\underset{\sim}{D}$ = Differential operator for strain calculation

$\underset{\sim}{F}$ = Body force

$\underset{\sim}{T}$ = Prescribed traction

Since equation (5.1) defines a two field principle, two independent field assumptions are to be chosen. Denoting these choices as

$$\underset{\sim}{u} = \underset{\sim}{N}\,\underset{\sim}{q} \qquad (5.2)$$
$$\underset{\sim}{\sigma} = \underset{\sim}{P}\,\underset{\sim}{\beta}$$

where

$\underset{\sim}{q}$ = Nodal degrees of freedom

$\underset{\sim}{\beta}$ = Set of stress coefficients

the process of element construction may resume.

Substituting Eq. (5.2) into Eq. (5.1), the following concise statement may be obtained:

$$\pi_R = -\tfrac{1}{2}\underset{\sim}{\beta}^T\underset{\sim}{H}\,\underset{\sim}{\beta} + \underset{\sim}{\beta}^T\underset{\sim}{G}\,\underset{\sim}{q} - \underset{\sim}{Q}^T\underset{\sim}{q} \qquad (5.3)$$

where

$$\underset{\sim}{H} = \int_V \underset{\sim}{P}^T \underset{\sim}{S} \underset{\sim}{P} \, dV$$

$$\underset{\sim}{G} = \int_V \underset{\sim}{P}^T \underset{\sim}{B} \, dV \qquad (5.4)$$

$\underset{\sim}{B} = \underset{\sim}{D}\,\underset{\sim}{N}$ = Same strain-displacement matrix as in the assumed displacement method

$$Q = \int_V \underset{\sim}{N}^T \underset{\sim}{F} \, dV + \int_{S_\sigma} \underset{\sim}{N}^T \underset{\sim}{\bar{T}} \, dS$$

Applying the stationary condition, $\delta\pi_R = 0$, one obtains

$$\underset{\sim}{K}\,\underset{\sim}{\beta} = \underset{\sim}{Q}$$

where

$$\underset{\sim}{K} = \underset{\sim}{G}^T \underset{\sim}{H}^{-1} \underset{\sim}{G} \qquad (5.5)$$

$$\underset{\sim}{\beta} = \underset{\sim}{H}^{-1} \underset{\sim}{G}\,\underset{\sim}{q}$$

As a side note, the definition of the matrices used above are standard in most literature concerning hybrid elements. Maybe with the exception of the shell elements, a choice of a suitable stress field is the major obstacle for hybrid element construction rather than the programming of the above algorithm.

5.2 Examination of Assumed Fields

5.2.1 Assumed Displacement Field

The assumed displacement field for the present solid element is the following standard linear Lagrangian interpolation:

$$N_i = \frac{1}{2}(1+\xi_i\xi)(1+\eta_i\eta)(1+\zeta_i\zeta) \qquad (5.6)$$

$i = 1\text{-}8$

(ξ_i, η_i, ζ_i) = Node i values of the natural coordinates (see Figure 2-1)

5.2.2 Assumed Stress Field

In order to account for element rotation and to reduce its sensitivity to distortion, the stress components are defined in local skew coordinate bases emanating from the center of the element. The local skew coordinate bases are defined as

$$\underset{\sim}{g}_i = \left(\sum_{r=1}^{8} \frac{\partial N_r}{\partial \xi^i}\, \underset{\sim}{R}_r\right)_{\xi^1=\xi^2=\xi^3=0} \qquad (5.7)$$

where

$\underset{\sim}{R}_r$ = Nodal position vector

ξ^1 =

ξ^2 = Natural (element) coordinates

ξ^3 =

The rectangular Cartesian components of stress σ^{rs} are

obtained through the following change of bases:

$$\tau^{ij}\, \underset{\sim}{g}_i \underset{\sim}{g}_j = \sigma^{rs}\, \underset{\sim}{e}_r \underset{\sim}{e}_s$$

$$\sigma^{rs} = \tau^{ij}\, (\underset{\sim}{g}_i \cdot \underset{\sim}{e}_r)(\underset{\sim}{g}_j \cdot \underset{\sim}{e}_s) \qquad (5.8)$$

where

$\underset{\sim}{e}_r$ = Rectangular Cartesian base vectors

Computationally, components of $(\underset{\sim}{g}_j \cdot \underset{\sim}{e}_s)$ are the Jacobian matrix determined at the center of the element. Thus

$$[\sigma^{rs}] = [\hat{J}]^T [\tau^{ij}] [\hat{J}] \qquad (5.9)$$

where

$[\hat{J}]$ = Jacobian Matrix at $\xi = \eta = \zeta = 0$

Since the Christoffel symbols vanish for the skew coordinate system, the stress equilibrium equations reduce to

$$\frac{\partial \tau^{ij}}{\partial \hat{\xi}^i} = 0 \qquad (5.10)$$

where

$\hat{\xi}^i$ = Skew coordinates

The skew coordinates, $\hat{\xi}^i$, coincide with the natural (element) coordinates, ξ^i, only for elements with parallel sides.

For the present solid element, the assumed stress field given by Eq. (5.11) is used to satisfy the equilibrium equations exactly only for elements with

parallel sides:

$$\tau^{11} = \beta_1 + \beta_2 \eta + \beta_3 \zeta + \beta_4 \eta\zeta$$
$$\tau^{22} = \beta_5 + \beta_6 \xi + \beta_7 \zeta + \beta_8 \xi\zeta$$
$$\tau^{22} = \beta_9 + \beta_{10} \xi + \beta_{11} \eta + \beta_{12} \xi\eta$$

$$\tau^{12} = \beta_{13} + \beta_{14} \zeta \qquad (5.11)$$
$$\tau^{23} = \beta_{15} + \beta_{16} \xi$$
$$\tau^{13} = \beta_{17} + \beta_{18} \eta$$

The number of stress terms used, 18 β's, represent the minimum number of terms required to eliminate any rank deficiency in the stiffness matrix other than that for the six proper rigid body modes. The stress terms represented in Eq. (5.11) were selected initially to eliminate the rank deficiency and to minimize the coupling between the stress components. Essentially, the technique employed matches a stress term for every independent strain term [30,31]. Starting with the assumed displacement field given by Eq. (5.6), the strain field for a rectangular element geometry may be expressed as

$$\varepsilon_x = \alpha_2 + \alpha_5 \eta + \alpha_7 \zeta + \alpha_8 \eta\zeta$$
$$\varepsilon_y = \alpha_{11} + \alpha_{13} \xi + \alpha_{14} \zeta + \alpha_{16} \xi\zeta \qquad (5.12a)$$
$$\varepsilon_z = \alpha_{20} + \alpha_{22} \eta + \alpha_{23} \xi + \alpha_{24} \xi\eta$$

$$\gamma_{xy} = (\alpha_3 + \alpha_{10}) + \alpha_5 \xi + \alpha_{13} \eta + (\alpha_6 + \alpha_{15}) \zeta + \alpha_8 \xi\zeta + \alpha_{16} \eta\zeta$$

$$\gamma_{yz} = (\alpha_{12} + \alpha_{19}) + (\alpha_{15} + \alpha_{21}) \xi + \alpha_{14} \eta + \alpha_{22} \zeta + \alpha_{16} \xi\eta + \alpha_{24} \xi\zeta \qquad (5.12b)$$

$$\gamma_{xz} = (\alpha_4 + \alpha_{18}) + \alpha_7 \xi + (\alpha_6 + \alpha_{21}) \eta + \alpha_{23} \zeta + \alpha_8 \xi\eta + \alpha_{24} \eta\zeta$$

where the α's are function of the nodal displacement degrees of freedom. Matching the strain terms in Eq. (5.12) with the stress terms in Eq. (5.11), note that every independent α_i is accounted for. Another available selection is to choose more shear stress terms for matching, however, the equilibrium equation will start to couple the stress components.

The assumed stress field given by Eq. (5.11) may be derived, alternately, by starting with complete polynomial order of the stress and the displacement field. The added incompatible displacement field yields constraints required to eliminate the extraneous stress terms [65,66]. The same stress distribution was obtained by Irons and Loikkanen using physical reasoning and

insight [53,60]. Yang, Rubinstein, and Atluri [32] using group theory also arrived at the same stress distribution as a possibility for a well-behaved element. Overall, various techniques used to arrive the stress distribution expressed in Eq. (5.11) tend to agree that this stress field is well-behaved.

5.3 Numerical Examples

In the following examples, three types of elements are compared, and are denoted as as

HYBRID = 8-node hybrid solid with 18 β's.
Stress assumed in local skew coordinates.
[Equation (5.11)]

HYBRID-XYZ = 8-node hybrid solid with 18 β's.
Stress assumed in rectangular
Cartesian coordinates.

COMPATIBLE = 8-node solid using the assumed
displacement method. Compatible
displacement field.

5.3.1 Solid Cantilever Beam with Element Distortion

For the cantilever beam under pure bending, a single

hybrid solid element provides (that is, duplicates) the analytical solution. To demonstrate the effect of element distortion, two elements are used to model the beam. Figure 5-1 defines the two distortion cases and the distortion parameter, a. Full triangularization occurs for 2a=10 (i.e. a=5).

The tip displacement error versus distortion are plotted in Figures 5-2 and 5-3. These results clearly indicate that the use of stresses defined in the local skew coordinates are superior to the use of those defined in terms of the rectangular Cartesian coordinates. The maximum error over the complete range of distortion is under 40% for the HYBRID element.

The assumed displacement element (COMPATIBLE) and the HYBRID element have the same rate of convergence. Both elements employ the same assumed displacement field. Yet, the accuracy of these elements for this problem differs dramatically.

5.3.2 Thermal Loading in a Sphere with a Cavity

A thermal loading problem involving a sphere with a cavity is used to study the convergence behavior of the solid elements. Figure 5-4 defines the geometry, material, and temperature profile used. Only a single row of elements is used with symmetry conditions applied.

DISTORTION A

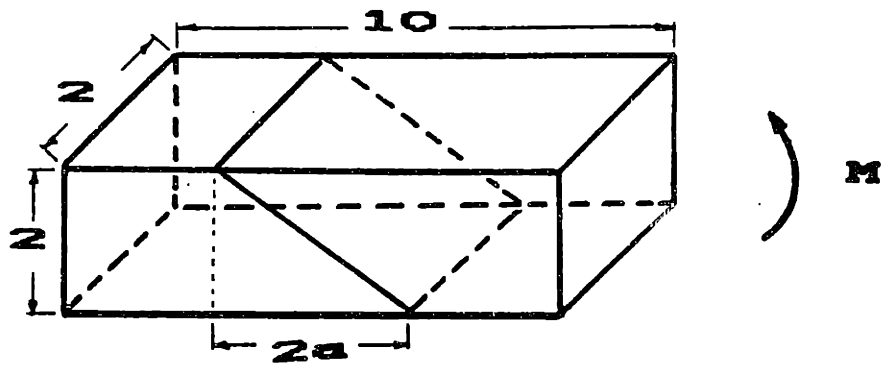

DISTORTION B

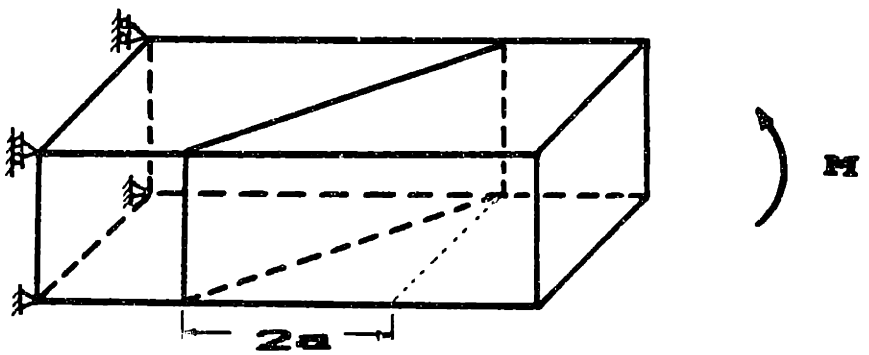

Figure 5-1. Distortion of Solid Cantilevered Beam under Pure Bending.

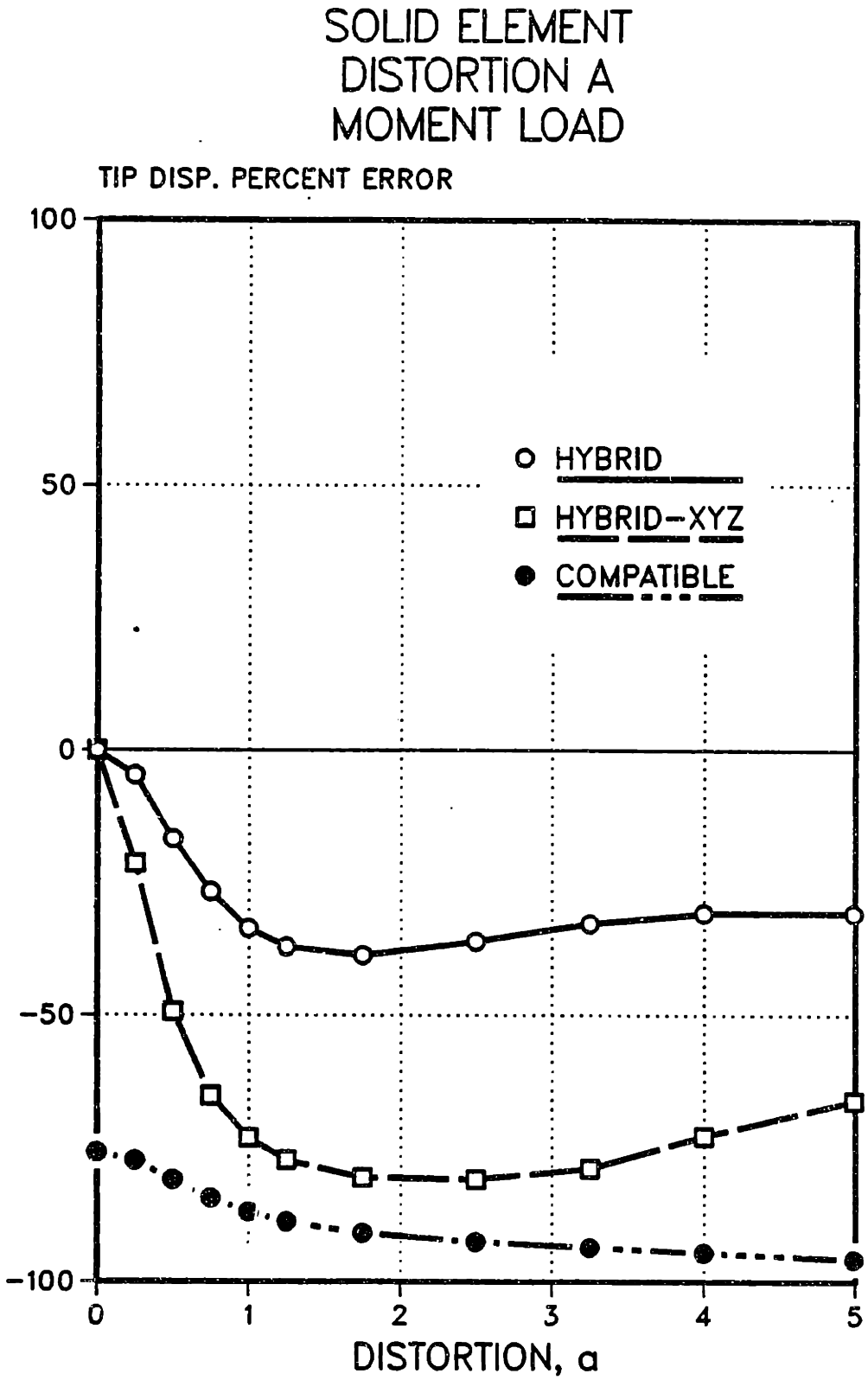

Figure 5-2. Effect of Solid Element Distortion on Tip Displacement under Pure Bending. [Distortion A]

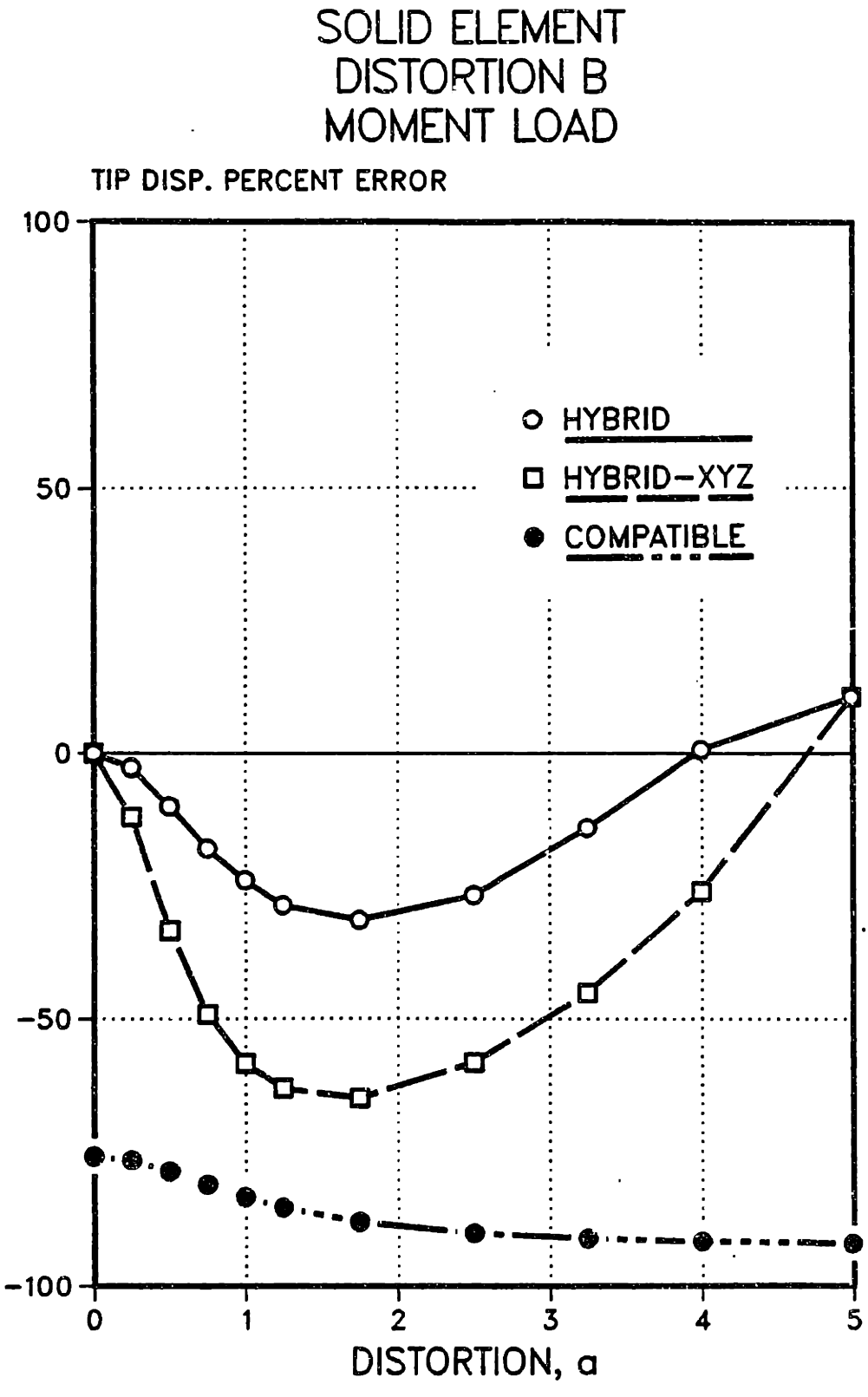

Figure 5-3. Effect of Solid Element Distortion on Tip Displacement under Pure Bending. [Distortion B]

Figures 5-5 to 5-8 provide radial and tangental stress results at the element centroid for HYBRID and for COMPATIBLE solid elements. Even for the radial stress which exhibits a sharp stress gradient, the HYBRID element provides a remarkably good result even for a crude mesh of only two elements. The COMPATIBLE element requires six elements to capture the radial stress gradient with reasonable accuracy (Figure 5-6).

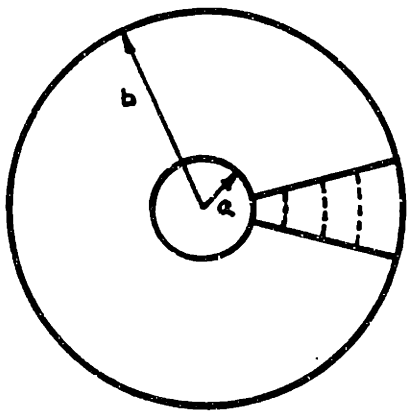

Temperature Profile:

$$T = \frac{T_o \; a}{b - a} \left(\frac{b}{R} - 1 \right)$$

$T_o = 100$ C

$a = 2$

$b = 8$

$\alpha = 1.22 \times 10^{-5}$ /°C

$\nu = .3$

$E = 2.1 \times 10^{7}$

Figure 5-4. Thermal Loading in Sphere with Cavity.

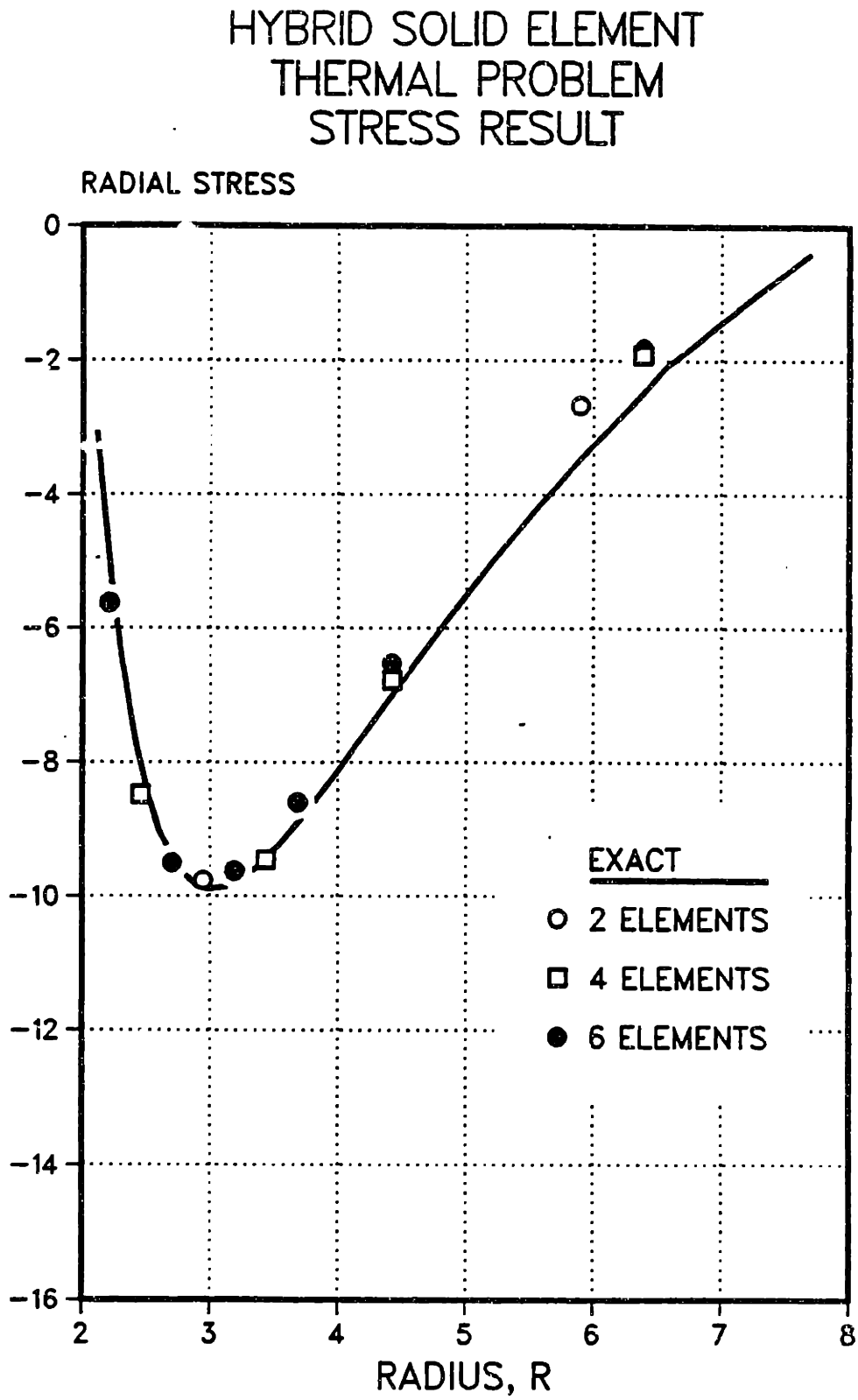

Figure 5-5. Radial Stress results for Sphere with Cavity problem [HYBRID Solid].

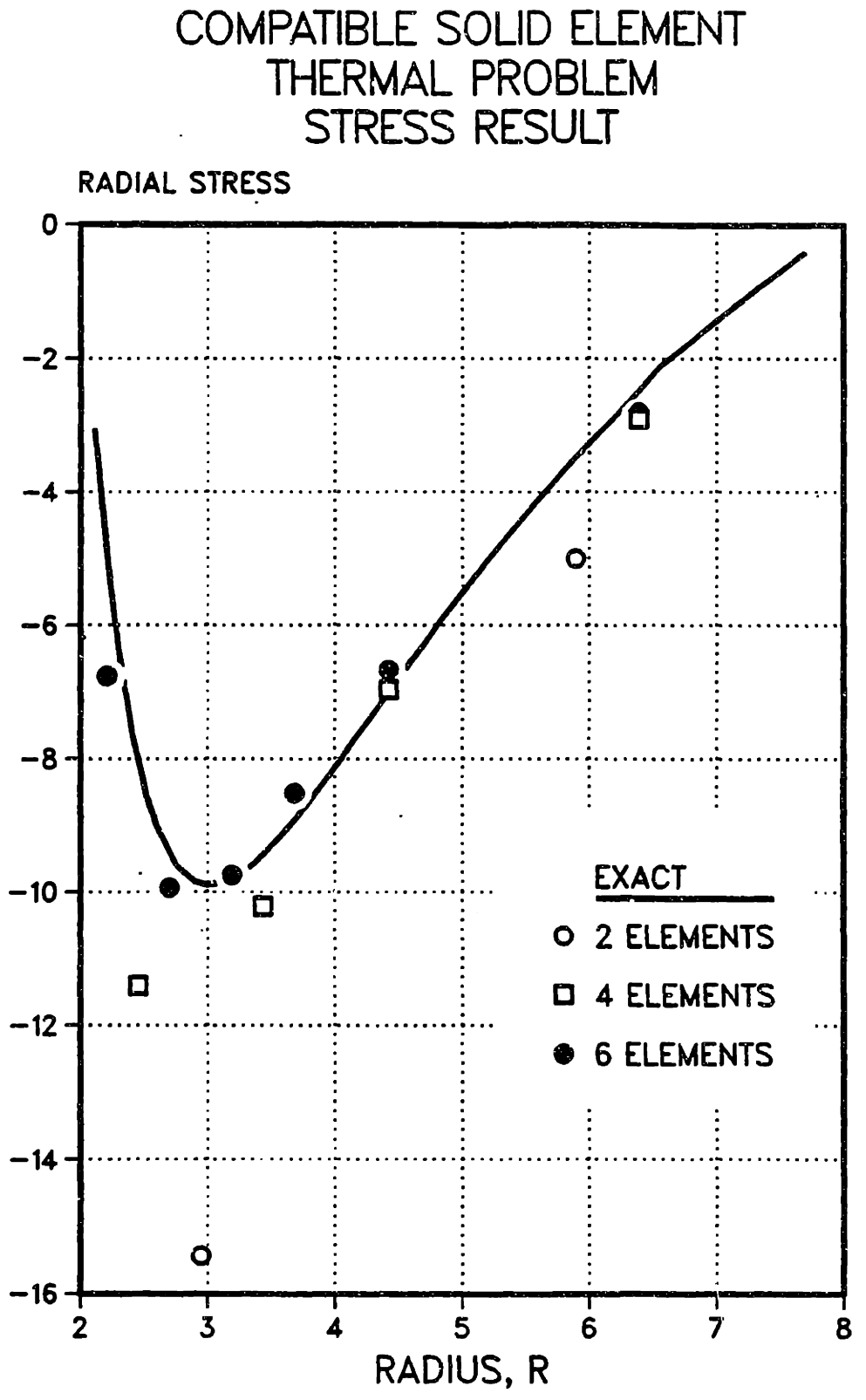

Figure 5-6. Radial Stress results for Sphere with Cavity problem [COMPATIBLE Solid].

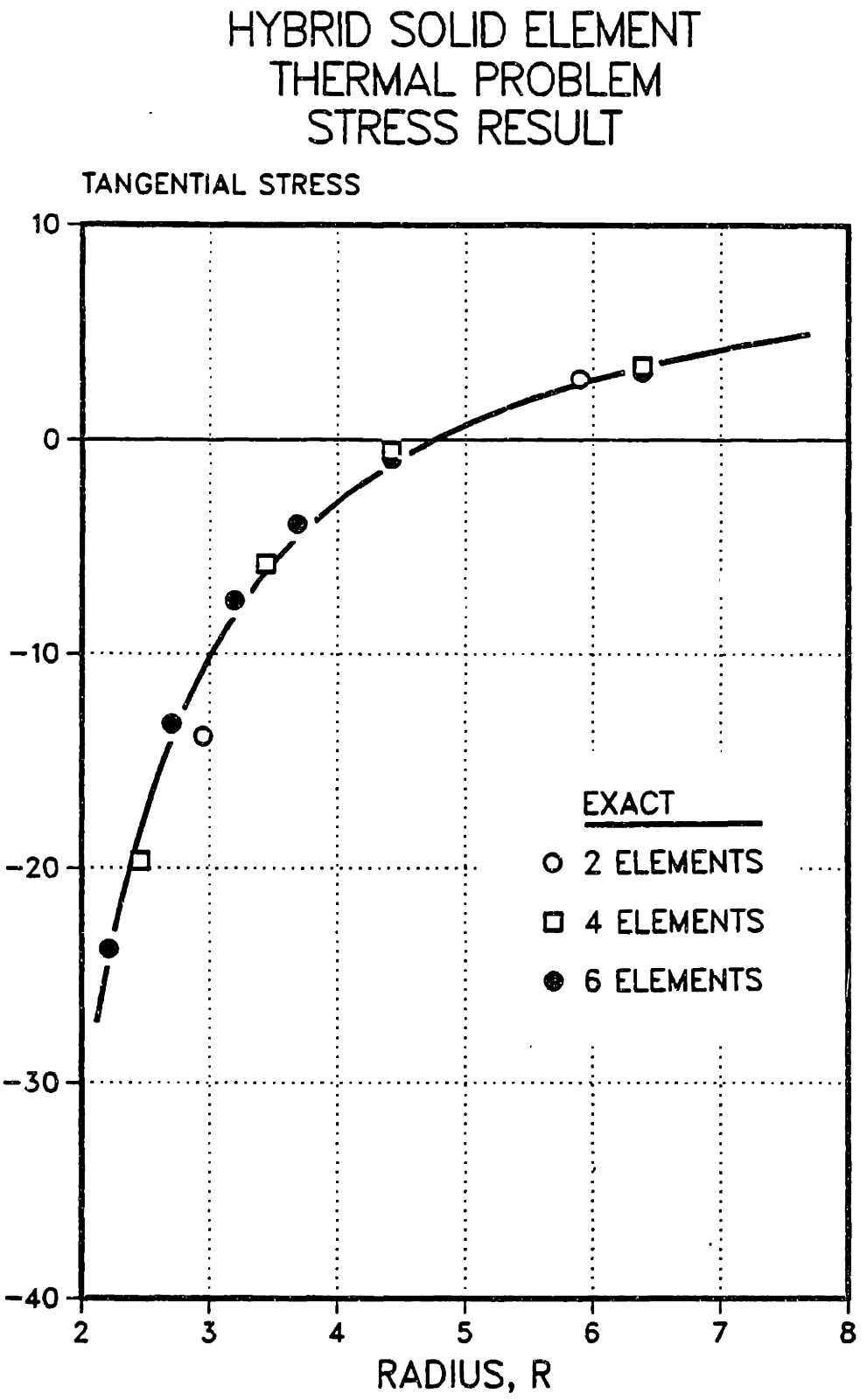

Figure 5-7. Tangential Stress results for Sphere with Cavity Problem [HYBRID Solid].

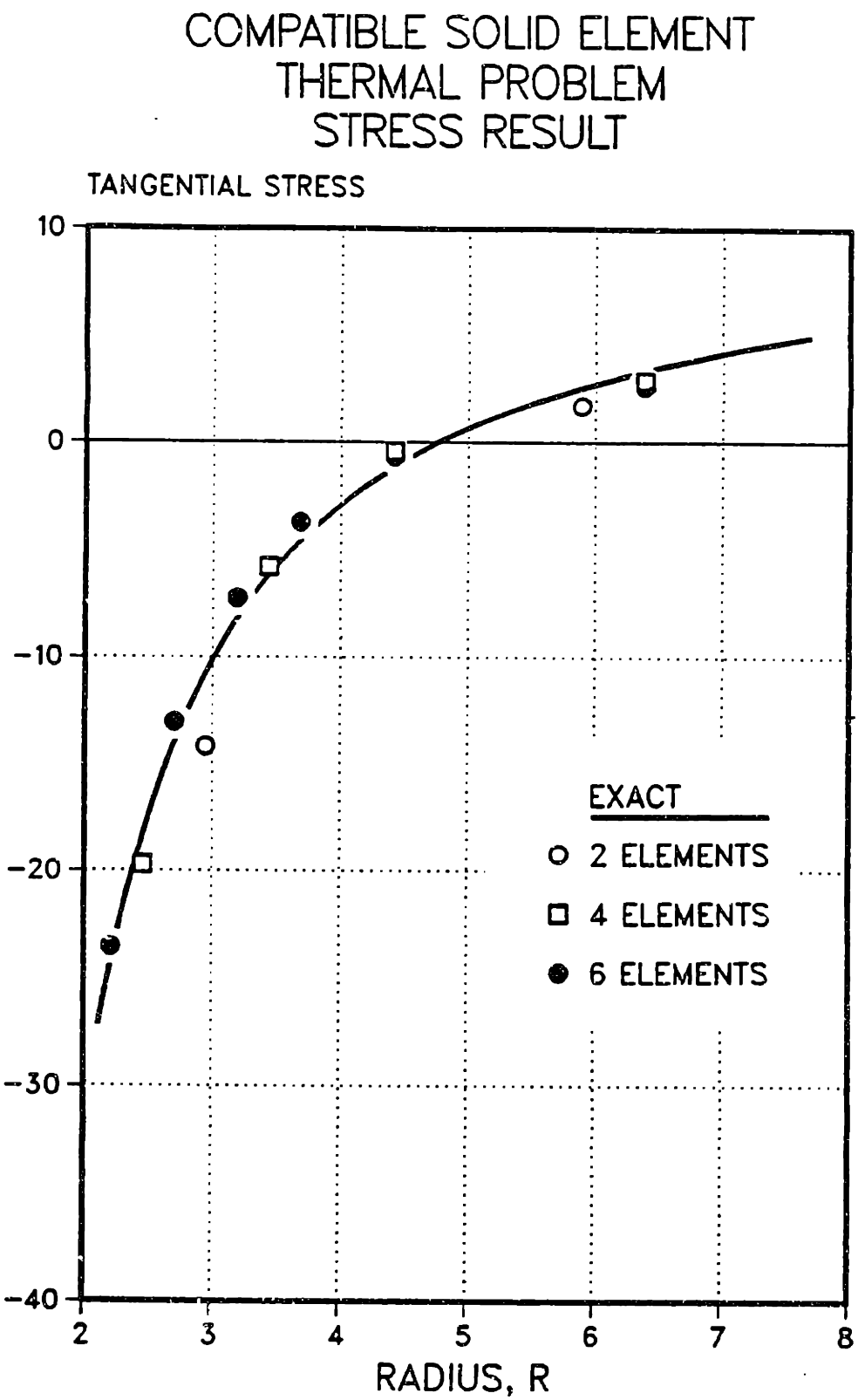

Figure 5-8. Tangential Stress results for Sphere with Cavity Problem [COMPATIBLE Solid].

CHAPTER 6

PLANE ELEMENTS

The hybrid stress 4-node plane element represent a clear case study for comparison with other element modification methods. To study the details of the assumed fields, the algebra required is minimal. After a brief presentation of element construction in the first section, the second section provides an explicit comparison of the assumed fields.

6.1 Element Construction

For the 4-node hybrid stress plane element, the Hellinger-Reissner principle, π_R , shall be used. The equations required are identical to those presented for the solid element in Chapter 5. The plane assumption in X-Y plane reduces the required displacement and stress components into

$$\underset{\sim}{u} = \begin{Bmatrix} u \\ v \end{Bmatrix} \tag{6.1}$$

and

$$\underset{\sim}{\sigma} = \begin{Bmatrix} \sigma_x \\ \sigma_y \\ \sigma_{xy} \end{Bmatrix}$$

The assumptions appropriate for the plane stress and the plane strain models are implemented through the constitutive equations.

6.2 Examination of Assumed Fields

6.2.1 Assumed Fields for the Hybrid Element

The assumed displacement field for the present plane element is a standard linear Lagrangian interpolation, as follows:

$$N_i = \frac{1}{4}(1+\xi_i\xi)(1+\eta_i\eta) \qquad (6.2)$$

$i = 1\text{-}4$

(ξ_i, η_i) = Node i values

Again the stress components are defined in the local skew coordinate bases.

$$\tau^{\alpha\beta}\,\underset{\sim}{g}_\alpha\,\underset{\sim}{g}_\beta = \sigma^{\lambda\mu}\,\underset{\sim}{e}_\lambda\,\underset{\sim}{e}_\mu$$

$$\sigma^{\lambda\mu} = \tau^{\alpha\beta}(\underset{\sim}{g}_\alpha \cdot \underset{\sim}{e}_\lambda)(\underset{\sim}{g}_\beta \cdot \underset{\sim}{e}_\mu) \qquad (6.3)$$

where

$\underset{\sim}{e}_\lambda$ = Rectangular Cartesian Base Vectors

The 5 β stress field presently employed is

$$\begin{aligned} \tau^{11} &= \beta_1 + \beta_2 \eta \\ \tau^{22} &= \beta_3 + \beta_4 \xi \\ \tau^{12} &= \beta_5 \end{aligned} \tag{6.4}$$

The number of stress terms used, 5 β's, represent a minimum number of terms required to eliminate rank deficiency in the stiffness matrix other than for the three rigid body modes.

Performing the required algebra to extract the Cartesian components of the stress measure gives

$$\begin{aligned} \sigma_x &= \beta_1 + (a_1)^2 \beta_2 \eta + (a_3)^2 \beta_4 \xi \\ \sigma_y &= \beta_3 + (b_1)^2 \beta_2 \eta + (b_3)^2 \beta_4 \xi \\ \sigma_{xy} &= \beta_5 + (a_1 b_1) \beta_2 \eta + (a_3 b_3) \beta_4 \xi \end{aligned} \tag{6.5}$$

where

$$\begin{aligned} a_1 &= (-x_1 + x_2 + x_3 - x_4) \\ a_3 &= (-x_1 - x_2 + x_3 + x_4) \end{aligned} \tag{6.6a}$$

$$b_1 = (-y_1 + y_2 + y_3 - y_4)$$
$$b_3 = (-y_1 - y_2 + y_3 + y_4) \qquad (6.6b)$$

x_i and y_i = Values at Node i

The coefficients, a_i and b_i, are the components of the Jacobian matrix evaluated at $\xi = \eta = 0$ [65]. For a rectangular element geometry, a =b =0, and Eq. (6.5) may be rewritten as

$$\sigma_x = \beta_1 + \beta_2 y$$
$$\sigma_y = \beta_3 + \beta_4 x \qquad (6.7)$$
$$\sigma_{xy} = \beta_5$$

6.2.2 Comparison with Other Models

For the sake of uniformity, only the strain fields are compared. The chosen element geometry is rectangular and the material property is isotropic plane stress.

HYBRID

To set the benchmark of comparison, the strain field

associated with the hybrid stress field in Eq. (6.7) may be expressed as

$$\varepsilon_x = \alpha_2 + \alpha_4 y - \nu \alpha_8 x$$
$$\varepsilon_y = \alpha_7 + \alpha_8 x - \nu \alpha_4 y \qquad (6.8)$$
$$\gamma_{xy} = (\alpha_3 + \alpha_6)$$
$$\alpha_i = \alpha_i (\beta_i)$$

A pronounced feature of this hybrid element is that one obtains an exact representation of the pure bending mode.

ISOPARAMETRIC

The strain field for the isoparametric element is derived from the bi-linear displacement field.

$$u = \alpha_1 + \alpha_2 x + \alpha_3 y + \alpha_4 xy$$
$$v = \alpha_5 + \alpha_6 x + \alpha_7 y + \alpha_8 xy \qquad (6.9)$$

$$\varepsilon_x = \alpha_2 + \alpha_4 y$$
$$\varepsilon_y = \alpha_7 + \alpha_8 x \qquad (6.10)$$
$$\gamma_{xy} = (\alpha_3 + \alpha_6) + \alpha_4 x + \alpha_8 y$$

This element is found to be an overly rigid element with respect to its bending behavior. Since the pure bending mode is the lowest energy mode, the most flexible mode, for a square domain using ordinary isotropic material

properties, this element exhibit a serious shortcoming. The basic reason for the overly rigid behavior is the inherent coupling of shear to normal modes represented by the coefficients α_4 and α_8 .

REDUCED INTEGRATION

Through reduced integration of the shear strain component in Eq. (6.10), the inherent coupling may be eliminated. The resulting strain field is

$$\begin{aligned} \varepsilon_x &= \alpha_2 + \alpha_4 y \\ \varepsilon_y &= \alpha_7 + \alpha_8 x \\ \gamma_{xy} &= (\alpha_3 + \alpha_6) \end{aligned} \qquad (6.11)$$

For a rectangular configuration, the above strain field provides a good approximation of the pure bending mode. However, the element deteriorates rapidly for distorted geometry.

INCOMPATIBLE (DISPLACEMENTS)

The motivation behind the incompatible displacement method is to add enough additional incompatible displacement modes to complete the polynomial order represented. For a plane element,

$$u = \alpha_1 + \alpha_2 x + \alpha_3 y + \alpha_4 xy + \lambda_1 (1-x^2) + \lambda_2 (1-y^2)$$
$$v = \alpha_5 + \alpha_6 x + \alpha_7 y + \alpha_8 xy + \lambda_3 (1-x^2) + \lambda_4 (1-y^2) \qquad (6.12)$$

The resulting strain field is

$$\begin{aligned} \varepsilon_x &= \alpha_2 + \alpha_4 y - 2\lambda_1 x \\ \varepsilon_y &= \alpha_7 + \alpha_8 x - 2\lambda_4 y \\ \gamma_{xy} &= (\alpha_3 + \alpha_6) + (\alpha_4 - 2\lambda_3) x + (\alpha_8 - 2\lambda_2) y \end{aligned} \qquad (6.13)$$

The role of the added incompatible modes may be clarified by performing the static condesation in closed form. After some tedious algebra, one obtains

$$\begin{aligned} \lambda_1 &= \frac{\nu}{2} \alpha_8 \\ \lambda_2 &= \frac{1}{2} \alpha_8 \\ \lambda_3 &= \frac{1}{2} \alpha_4 \\ \lambda_4 &= \frac{\nu}{2} \alpha_4 \end{aligned} \qquad (6.14)$$

Substituting Eq. (6.14) into Eq. (6.13):

$$\begin{aligned} \varepsilon_x &= \alpha_2 + \alpha_4 y - \nu \alpha_8 x \\ \varepsilon_y &= \alpha_7 + \alpha_8 x - \nu \alpha_4 y \\ \gamma_{xy} &= (\alpha_3 + \alpha_6) \end{aligned} \qquad (6.15)$$

The result is identical to the hybrid strain field given by Eq. (6.8).

The reduced integration and the added incompatible displacement modes represent two examples of "variational crimes". The hybrid element is constructed with a strict adherence to the variational statement. Yet an inescapable puzzle remaining is the similarity of the strain fields for these three methods.

To resolve this puzzle, the material model is changed to plane strain with the limiting incompressibility constraint included. The details are outlined in Appendix A. Once again, the incompatible displacement method turns out to be identical to the hybrid method with 5 β stress terms. However, the reduced integration modification failed to provide a rational results for the limiting incompressibility condition (see Appendix A).

In summary, the above results indicate that the changes introduced through the reduced integration method is material dependent. Furthermore, the comparison with incompatible element demonstrates that the hybrid element may inherently include incompatible modes through stress field assumption.

6.3 Numerical Examples

In the following examples, four types of elements are compared, and are denoted as

HYBRID = 4-node hybrid plane element; assumed stresses with 5 β's (Equation (6.4)) satisfy the equilibrium equations for elements with parallel sides.

HYBRID-SKEW = Same as HYBRID except that coordinates changed to skew coordinates.

$$\xi - \hat{\xi}$$
$$\eta - \hat{\eta}$$

The assumed stresses satisfy the equilibrium equations for all element geometries.

COMPATIBLE = 4-node plane element using the assumed displacement method; compatible displacement field.

CQUAD 4 = 4-node plane element from a general finite element code, MSC-NASTRAN; this is an assumed displacement element which uses reduced integration.

6.3.1 Plane Cantilevered Beam with Element Distortion

To demonstrate the effects of element distortion, two elements are used to model a cantilevered beam under pure bending. Figure 6-1 defines the distortion

parameter, a. Full triangularization occurs for a=5.

The tip displacement versus distortion is plotted in Figure 6-2. Results from the two hybrid elements are similar. However, the HYBRID element with relaxed equilibrium provided a little more accurate result. As mentioned previously, the compatible element is overly rigid in bending. The CQUAD4 element demonstrates that the reduced integration method deteriorates rapidly under distortion.

6.3.2 Circular Hole in an Infinite Strip

This "circular hole problem", shown in Figure 6-3, is used to study the convergence behavior of the hybrid plane element. The error in stress concentration at (x,y) = (0,R) is plotted inf Figure 6-4 and indicates that the hybrid 4-node element converges slowly for this problem. Similar results were obtained for other elements. For better accuracy, a more specialized element [67] to handle the stress concentration would be appropriate for this type of example.

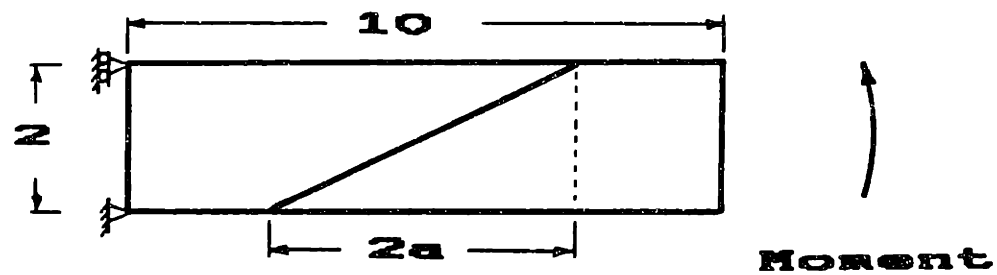

Figure 6-1. Distortion of Plane Cantilevered Beam under pure Bending.

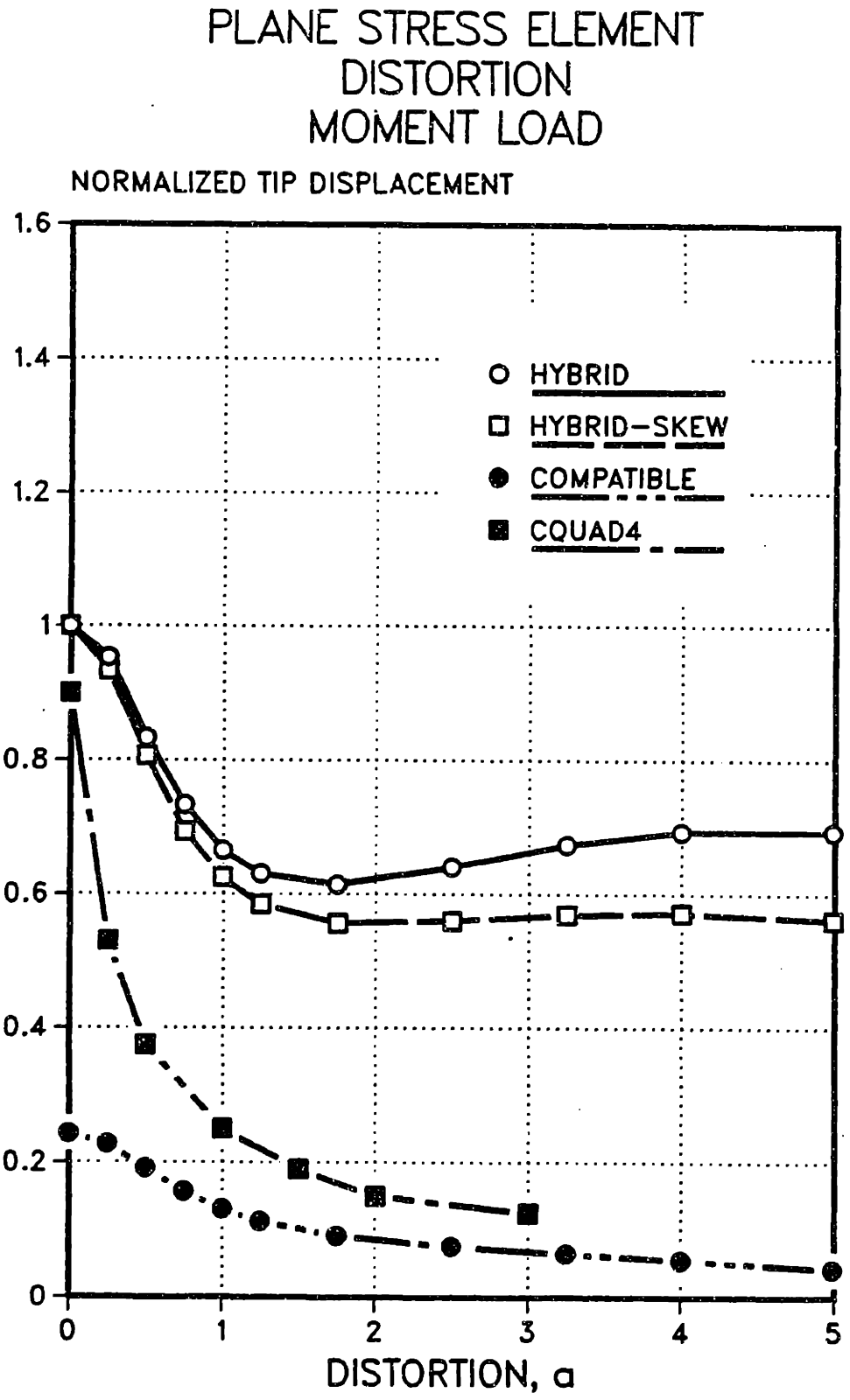

Figure 6-2. Effect of Plane Element Distortion on Tip Displacement under Pure Bending.

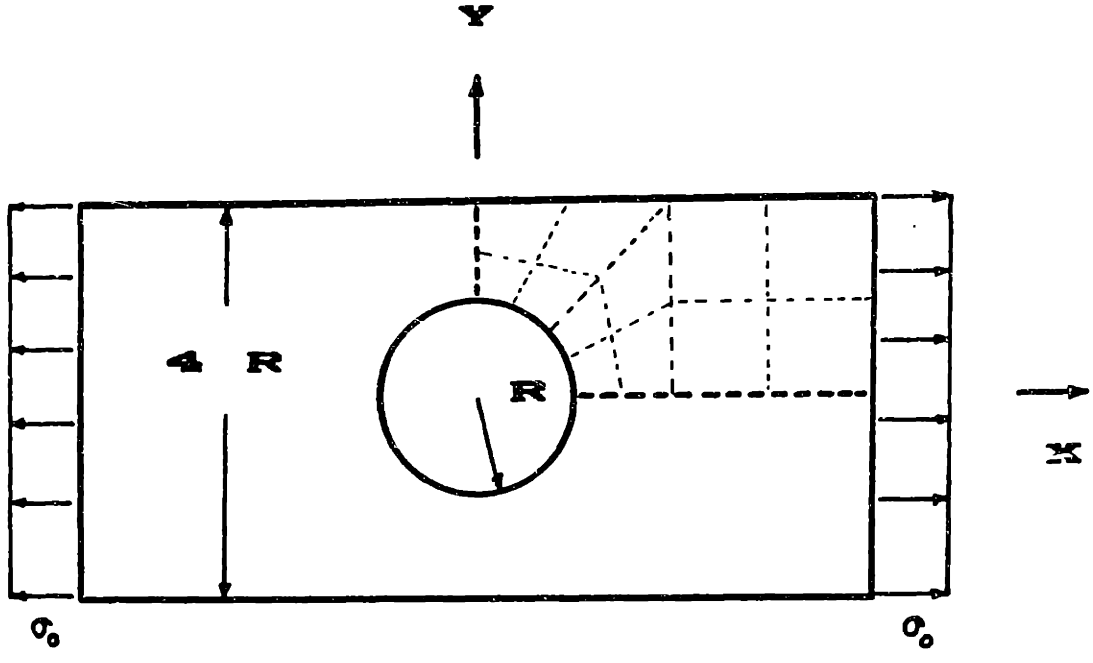

Figure 6-3. Circular Hole in an Infinite Strip.

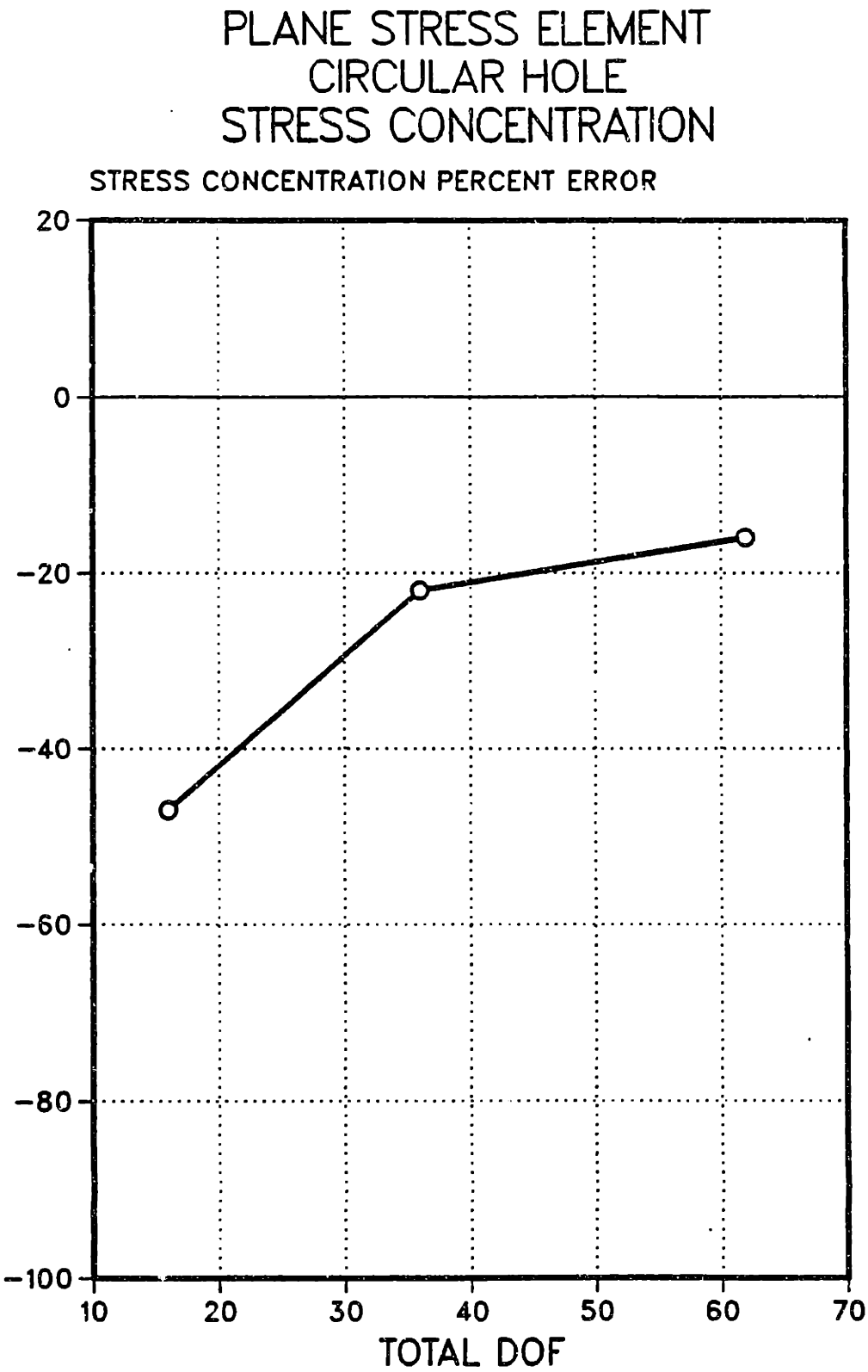

Figure 6-4. Stress Concentration Results for Circular Hole in an Infinite Strip Problem.

CHAPTER 7

PLATE ELEMENTS

Within the context of the present development, a plate is a structural member bounded by two parallel planes called its faces. The distance h between the plane faces is called the thickness of the plate, and it is assumed that the thickness is small compared with the characteristic dimensions of the faces. Concerning the coordinate system employed, the X-Y axes are taken to coincide with the middle surface, and the z axis is in the direction of the normal to the middle surface.

In the following discussion, three plate models will be developed. The three models consist of the degenerate solid, the Reissner/Mindlin plate, and the Kirchhoff plate. The Hellinger-Reissner principle, π_R , shall be used to develop hybrid stress plate elements for each of these three cases. For the sake of a uniform development of these three plate models, the stress and strain measures are left in continuum components instead of using the (integrated) stress and strain resultants. Thus, the equations required for the construction of the matrices are identical to those presented for the solid element in Chapter 5 with exception of a slight

modification for the Kirchhoff plate element. Another source of the hybrid plate derivations and results available for comparison is the extensive list of possible assumed stress fields compiled by Spilker et al.[68-72].

7.1 Assumed Fields for C^0 Plates

Both the degenerate solid and the Reissner/Mindlin plates are of C^0 class. For the assumed displacement method, these two models are the same. However, for the hybrid method, the additional independent stress assumption allows two distinct possibilities. Since both models employ the same kinematic assumptions, only the stress assumptions lead to distinct differences.

7.1.1 Kinematic Assumptions

The kinematic constraints of the Reissner/Mindlin plate model and the degenerate solid are identical. With the following three assumptions, a solid continuum is constrained for bending action:

(1) Straight material line elements which are perpendicular to the midplane of the plate in the undeformed state remain straight in

the deformed state.

(2) All points on any straight material line element which is perpendicular to the midplane before deformation experience the same transverse displacement, that is, there is no "thickness stretch".

(3) There is no stretching of the midplane.

These assumptions may be implemented functionally as

$$\begin{aligned} u &= -z\,\theta_x(x,y) \\ v &= -z\,\theta_y(x,y) \\ w &= w(x,y) \end{aligned} \tag{7.1}$$

Substitution into the strain-displacement relations gives

$$\begin{aligned} \varepsilon_x &= -z\,\frac{\partial \theta_x}{\partial x} \\ \varepsilon_y &= -z\,\frac{\partial \theta_y}{\partial y} \\ \gamma_{xy} &= -z\left(\frac{\partial \theta_x}{\partial y} + \frac{\partial \theta_y}{\partial x}\right) \\ \gamma_{yz} &= \frac{\partial w}{\partial y} - \theta_y \\ \gamma_{xz} &= \frac{\partial w}{\partial x} - \theta_x \\ \varepsilon_z &= 0 \end{aligned} \tag{7.2}$$

Notice from Eq. (7.2) that the bending strain, ε_x, ε_y, and γ_{xy}, are linear in z and the transverse shear strains, γ_{yz} and γ_{xz}, are constant in z. For linear materials, the transverse stress components calculated

corresponding to these strains must also be constant through the thickness. However, since the plate faces are traction-free, the transverse shear stress components must exhibit a parabolic distribution. The plates constructed using the assumed displacement method include a factor of 5/6 into the transverse shear strain energy to compensate for this discrepency.

The nodal degrees of freedom are interpolated using a linear Lagrangian interpolation.

$$\begin{Bmatrix} w \\ \theta_x \\ \theta_y \end{Bmatrix}_i \quad \text{Nodal Degrees of Freedom}$$

$$\begin{Bmatrix} w \\ \theta_x \\ \theta_y \end{Bmatrix} = \sum_{i=1}^{4} N_i \begin{Bmatrix} w \\ \theta_x \\ \theta_y \end{Bmatrix}_i \tag{7.3}$$

where

$$N_i = \frac{1}{4}(1+\xi_i\xi)(1+\eta_i\eta) \tag{7.4}$$

$i = 1\text{-}4$

(ξ_i, η_i) = Node i values

7.1.2 Degenerate Solid

Previously derived in Chapter 4, the stress assumption for the degenerate solid model may be

expressed in terms of the components defined in local skew coordinate bases emanating from the center of the element, as follows:

$$\begin{aligned} \tau^{11} &= z\,[\beta_1 + \beta_2 \eta] \\ \tau^{22} &= z\,[\beta_3 + \beta_4 \xi] \\ \tau^{12} &= z\,[\beta_5] \\ \tau^{23} &= \beta_6 + \beta_7 \xi \\ \tau^{13} &= \beta_8 + \beta_9 \eta \end{aligned} \qquad (7.5)$$

The base vectors required for transformation are

$$\underset{\sim}{g}_i = \left(\sum_{r=1}^{4} \frac{\partial N_r}{\partial \xi^i} \underset{\sim}{R}_r \right)_{\xi^1 = \xi^2 = 0} \qquad (7.6)$$

(i = 1,2)

where

$\underset{\sim}{R}_r$ = Nodal Position Vector

$\xi^1 = \xi$, $\xi^2 = \eta$ } Natural (element) Coordinates

Also,

$\underset{\sim}{g}_3 = \underset{\sim}{n} = \underset{\sim}{e}_3$ Unit Normal (Defined along z-axis)

The base vectors, $\underset{\sim}{g}_1$ and $\underset{\sim}{g}_2$, lie on the midplane of the plate. The rectangular Cartesian components are obtained through a change of bases:

$$\tau^{\alpha\beta}\, \underset{\sim}{g}_\alpha\, \underset{\sim}{g}_\beta = \sigma^{\lambda\gamma}\, \underset{\sim}{e}_\lambda\, \underset{\sim}{e}_\gamma$$

$$\sigma^{\lambda\gamma} = \tau^{\alpha\beta} (\underset{\sim}{g}_\alpha \cdot \underset{\sim}{e}_\lambda)(\underset{\sim}{g}_\beta \cdot \underset{\sim}{e}_\gamma) \qquad (7.8)$$

$$(\alpha, \beta, \gamma, \lambda = 1, 2)$$

For out-of-plane components,

$$\sigma^{\alpha z} = \tau^{\lambda 3} (\underset{\sim}{g}_\lambda \cdot \underset{\sim}{e}_\alpha) \qquad (7.9)$$

These equations required for transformation shall be used for all three models.

As a final note, the number of stress terms used, 9 β's, represents a minimum number of terms required to eliminate rank deficiency in the stiffness matrix, other than that for the three rigid body modes.

7.1.3 Reissner/Mindlin Plate

The stress assumptions for the Reissner/Mindlin plates introduce a parabolic distribution of the transverse shear components through the thickness.

$$\tau^{11} = z\left[\beta_1 + \beta_2\xi + \beta_3\eta + \beta_4\xi\eta\right]$$
$$\tau^{22} = z\left[\beta_5 + \beta_6\xi + \beta_7\eta + \beta_8\xi\eta\right]$$
$$\tau^{12} = z\left[\beta_9 + \beta_{10}\xi + \beta_{11}\eta + \beta_{12}\frac{\xi^2}{2} + \beta_{13}\frac{\eta^2}{2}\right] \qquad (7.10)$$
$$\tau^{23} = \left(\frac{h^2}{4} - z^2\right)\left[\frac{1}{2}(\beta_{10}+\beta_7) + \frac{1}{2}(\beta_{12}+\beta_8)\xi\right]$$
$$\tau^{13} = \left(\frac{h^2}{4} - z^2\right)\left[\frac{1}{2}(\beta_2+\beta_{11}) + \frac{1}{2}(\beta_4+\beta_{13})\eta\right]$$

Only 9 β's are required to eliminate rank deficiency. Yet, the above 13 β stress field resulted from a systematic reduction of hybrid stress solid element. Since the hybrid element construction requires an inversion of a matrix of order of the number of stress terms used, a minimum number, 9 β's, is more efficient. To gage the difference in accuracy, two other assumptions are investigated.

First, 2 β's are eliminated from Eq. (7.10) to result in an 11 β field:

$$\beta_{12} = \beta_{13} = 0 \qquad (7.11)$$

Second, 4 β's are eliminated from Eq. (7.10) to result in a 9 β field:

$$\beta_{10} = \beta_{11} = \beta_{12} = \beta_{13} = 0 \qquad (7.12)$$

These are the two cases available to eliminate rank deficiency.

7.2 Assumed Fields for C^1 Plates

The 4-node Kirchhoff plate with an incompatible displacement field presents an element that must be formulated by using the hybrid method. Along the element boundary, the assumed stress plays the role of a Lagrange multiplier enforcing the compatibility of displacement field across the boundary. The modified Hellinger-Reissner principle, π_{mR} , required for this element is

$$\pi_{mR}(\underset{\sim}{u}, \underset{\sim}{\sigma}, \tilde{w}_{,\nu}) = \int_V \left[-\tfrac{1}{2}\,\underset{\sim}{\sigma}^T \underset{\sim}{S}\,\underset{\sim}{\sigma} + \underset{\sim}{\sigma}^T(\underset{\sim}{D}\underset{\sim}{u}) - \underset{\sim}{F}^T\underset{\sim}{u}\right] dV$$
$$- \int_{S_B} \sigma_{\nu\nu}(w_{,\nu} - \tilde{w}_{,\nu})\,ds - \int_{S_\sigma} \underset{\sim}{\bar{T}}^T \underset{\sim}{u}\,ds \qquad (7.13)$$

where

S_B = Surface defined at plate edge

$\underset{\sim}{\nu}$ = Boundary normal

$\sigma_{\nu\nu} = \underset{\sim}{\nu}^T \underset{\sim}{\sigma}\,\underset{\sim}{\nu}$ = Boundary normal stress component (Lagrange multiplier)

$w_{,\nu}$ = Boundary normal derivative

$\tilde{w}_{,\nu}$ = Compatible boundary normal derivative

The assumed fields are denoted by

$$\underset{\sim}{u} = \underset{\sim}{N}\,\underset{\sim}{\delta}$$

$$\underset{\sim}{\sigma} = \underset{\sim}{P}\,\underset{\sim}{\beta} \qquad (7.14)$$

$$\tilde{w}_{,\nu} = \tilde{\underset{\sim}{N}}_{\nu}\,\underset{\sim}{\delta}$$

The compatible boundary interpolation function $\tilde{\underset{\sim}{N}}_{\nu}$ is a standard linear interpolation function. The boundary components are

$$w_{,\nu} = \underset{\sim}{N}_{\nu}\,\underset{\sim}{\delta} \qquad (7.15)$$

$$\sigma_{\nu\nu} = \underset{\sim}{P}_{\nu}\,\underset{\sim}{\beta}$$

Substituting Eqs. (7.14) and (7.15) into Eq. (7.13), one obtains

$$\pi_{mR} = -\tfrac{1}{2}\,\underset{\sim}{\beta}^{T}\underset{\sim}{H}\,\underset{\sim}{\beta} + \underset{\sim}{\beta}^{T}\underset{\sim}{G}\,\underset{\sim}{\delta} - \underset{\sim}{Q}^{T}\,\underset{\sim}{\delta} \qquad (7.16)$$

where

$$\underset{\sim}{H} = \int_{V} \underset{\sim}{P}^{T}\underset{\sim}{S}\,\underset{\sim}{P}\,dV$$

$$\underset{\sim}{G} = \int_{V} \underset{\sim}{P}^{T}\underset{\sim}{B}\,dV - \int_{S_B} \underset{\sim}{P}^{T}_{\nu}\left(\underset{\sim}{N}_{\nu} - \tilde{\underset{\sim}{N}}_{\nu}\right) dS \qquad (7.17)$$

$$\underset{\sim}{Q} = \int_{V} \underset{\sim}{N}^{T}\underset{\sim}{F}\,dV + \int_{S_\sigma} \underset{\sim}{N}^{T}\underset{\sim}{\bar{T}}\,dS$$

Applying the stationary condition, $\delta\pi_{mR}=0$, one obtains

$$\underset{\sim}{K}\,\underset{\sim}{\delta} = \underset{\sim}{Q} \qquad (7.18)$$

where

$$\underset{\sim}{K} = \underset{\sim}{G}^T \underset{\sim}{H}^{-1} \underset{\sim}{G}$$

$$\underset{\sim}{\beta} = \underset{\sim}{H}^{-1} \underset{\sim}{G} \underset{\sim}{\delta}$$

With exception of the G-matrix, the element construction algorithm is identical to other elements presented thus far.

7.2.1 Kinematic Assumption

An added constraint imposed by the Kirchhoff plate model may be stated as:

> Material line elements which are originally straight and normal to the plate's midplane in the undeformed state remain straight and normal to this plane during deformation.

This implies the neglect of transverse shear deformation in the plate. In terms of displacements,

$$\begin{aligned} u &= -z\, w_{,x} \\ v &= -z\, w_{,y} \\ w &= w(x,y) \end{aligned} \qquad (7.19)$$

The resulting strain field is

$$\varepsilon_x = -z\, w_{,xx}$$
$$\varepsilon_y = -z\, w_{,yy}$$
$$\gamma_{xy} = -2z\, w_{,xy} \qquad (7.20)$$

$$\varepsilon_z = \gamma_{yz} = \gamma_{xz} = 0$$

The nodal degrees of freedom:

$$\begin{Bmatrix} w \\ w_{,x} \\ w_{,y} \end{Bmatrix}_i \quad \text{Nodal Degrees of Freedom} \qquad (7.21)$$

are interpolated using a twelve parameter polynomial expansion; the twelve parameter field for w may be expressed as

$$\begin{aligned} w = {} & \alpha_1 + \alpha_2 \xi + \alpha_3 \eta + \alpha_4 \xi\eta + \alpha_5 \xi^2 + \alpha_6 \eta^2 \\ & + \alpha_7 \xi^2\eta + \alpha_8 \xi\eta^2 + \alpha_9 \xi^3 + \alpha_{10} \eta^3 \\ & + \alpha_{11} \xi^3\eta + \alpha_{12} \xi\eta^3 \end{aligned} \qquad (7.22)$$

In terms of the nodal degrees of freedom

$$\begin{aligned} w = \sum_{i=1}^{4} \Big[& \tfrac{1}{8}\{(\xi_i\xi+1)(\eta_i\eta+1)(2+\xi_i\xi+\eta_i\eta-\xi^2-\eta^2)\} \\ & \tfrac{1}{8}\{\xi_i(\xi_i\xi+1)^2(\xi_i\xi-1)(\eta_i\eta+1)\} \\ & \tfrac{1}{8}\{\eta_i(\xi_i\xi+1)(\eta_i\eta+1)^2(\eta_i\eta-1)\}\Big] \begin{Bmatrix} w \\ w_{,\xi} \\ w_{,\eta} \end{Bmatrix}_i \end{aligned} \qquad (7.23)$$

where

$$\begin{Bmatrix} w_{,\xi} \\ w_{,\eta} \end{Bmatrix}_i = \begin{bmatrix} \frac{\partial x}{\partial \xi} & \frac{\partial y}{\partial \xi} \\ \frac{\partial x}{\partial \eta} & \frac{\partial y}{\partial \eta} \end{bmatrix} \begin{Bmatrix} w_{,x} \\ w_{,y} \end{Bmatrix}_i \qquad (7.24)$$

Note that the transformation matrix in Eq. (7.24) is just a Jacobian matrix evaluated at node i.

7.2.2 Stress Field Assumptions

The stress assumptions for the Kirchhoff plates are similar to the Reissner/Mindlin plate:

$$\begin{aligned} \tau^{11} &= z\left[\beta_1 + \beta_2\xi + \beta_3\eta + \beta_4\xi\eta\right] \\ \tau^{22} &= z\left[\beta_5 + \beta_6\xi + \beta_7\eta + \beta_8\xi\eta\right] \\ \tau^{12} &= z\left[\beta_9 + \beta_{10}\xi + \beta_{11}\eta + \beta_{12}\frac{\xi^2}{2} + \beta_{13}\frac{\eta^2}{2}\right] \end{aligned} \qquad (7.25)$$

To reduce the number of β's, two other cases are examined. First, the 11 β field with

$$\beta_{12} = \beta_{13} = 0 \qquad (7.26)$$

Secondly, the 9 β field with

$$\beta_{10} = \beta_{11} = \beta_{12} = \beta_{13} = 0 \qquad (7.27)$$

7.3 Numerical Examples

In the numerical examples, the following titles are used for the elements compared:

DEGENERATE = 4-node hybrid degenerate solid plate with 9 β's. [Equation (7.5)]

REISSNER13 = 4-node hybrid Reissner/Mindlin plate with 13 β's. [Equation (7.10)]

REISSNER11 = 4-node hybrid Reissner/Mindlin plate with 11 β's. [Equation (7.11)]

REISSNER9 = 4-node hybrid Reissner/Mindlin plate with 9 β's. [Equation (7.12)]

KIRCHHOFF13 = 4-node hybrid C^1 plate with 13 β's. [Equation (7.25)]

KIRCHHOFF11 = 4-node hybrid C^1 plate with 11 β's. [Equation (7.26)]

KIRCHHOFF9 = 4-node hybrid C^1 plate with 9 β's. [Equation (7.27)]

WOLF = 4-node hybrid plate with 17 β's. (Complete quadratic) [73]

DVORKIN = 4-node assumed displacement C^0 plate. (Assumed strain method) [56]

HUGHES = 4-node assumed displacement C^0 plate. (Selective integration method) [74]

Of the hybrid plate elements, only the elements DEGENERATE, REISSNER13, and KIRCHHOFF13 contain consistently derived stress fields. All other hybrid elements contain a reduced set of stress terms, 11 β's and 9 β's.

7.3.1 Cantilevered Beam using a Single Plate Element

To examine one dimensional behavior of the three classes of hybrid plate elements, a single plate element is used to model a cantilevered beam (Figure 7-1). By setting Poisson's ratio to zero, a plate may emulate a beam. With such a constraint, the resulting plate has two degrees of freedom per node, w and θ. For the thin beam limit, the rotation angle θ must approximate the gradient of w. Within this limit, the four degrees of freedom along the length of the beam should approximate a cubic polynomial representation of w.

Two load cases are examined; applied are tip moment and tip force. The exact solution for tip moment loading results in a quadratic polynomial for w, and for tip force results in a cubic polynomial for w.

The element results are provided in Table 7-1. Each category of plate models represent all hybrid elements with different number of β's for the respective models. The "exact" result refers to the analytical solution obtained in the "thin" plate limit. The error of -25% in tip deflection for the Degenerate Solid under tip force indicates a need for the quadratic transverse shear stress distribution along the thickness direction.

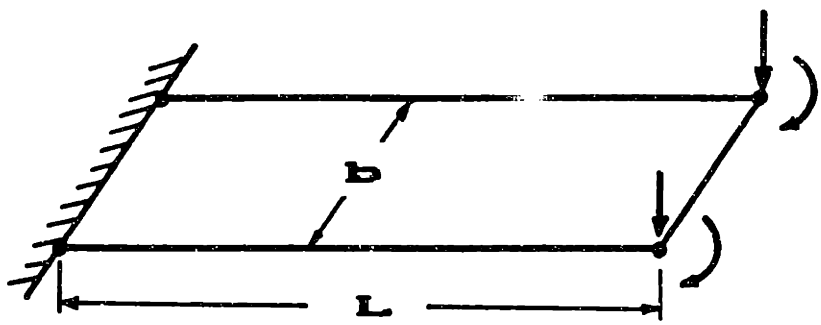

$$\frac{L}{h} = 100$$

$$b = 1$$

$$E = 10^{7}$$

$$\nu = 0$$

Figure 7-1. Cantilevered Beam using a Single Plate.

Table 7-1. Results for the Cantilevered Beam using a Single Plate Element.

Plate Models	Tip Moment		Tip Force	
	Tip Deflection	Tip Rotation	Tip Deflection	Tip Rotation
Degenerate Solid	Exact	Exact	-25% Error	Exact
Reissner/ Mindlin Plate	Exact	Exact	Exact	Exact
Kirchhoff Plate	Exact	Exact	Exact	Exact

7.3.2 Square Plate Problem

For the square plate problem depicted in Figure 7-2, the following boundary conditions and load cases are examined.

(1) Clamped boundary condition along all edges with a concentrated load at center.
(2) Clamped boundary condition along all edges with a uniformly distributed load.
(3) Simply-supported boundary condition along all edges with a concentrated load at center.
(4) Simply-supported boundary condition along all edges with a uniformly distributed load.

With symmetry conditions employed, only 1/4 of the plate needs to be and is modeled. To present a practical perspective on accuracy, all results are presented with +/- 20% error as a cutoff point for "ball-park" accuracy (denoted as "cutoff accuracy"). These figures may be used to assess (1) the level of mesh discretization required to fall under the +/- 20% error bound and (2) the convergence behavior under mesh refinement. Since the cutoff accuracy is somewhat arbitrary, the reader may wish to set a similar bound for personal preference.

To begin, Figures 7-3 to 7-6 provide the center displacement results for C^0 hybrid plates for all four cases. Generally, a (2X2) mesh for the quarter plate is

required to keep within cutoff accuracy for all elements, with the exception of the REISSNER9 element. The results obtained for the REISSNER11 and the REISSNER13 element are similar. For clamped boundary conditions, the DEGENERATE element gives an overly rigid result for a single element mesh.

The center displacement results for C^1 hybrid elements are provided in Figures 7-7 to 7-10. Only (1X1) mesh is required to achieve cutoff accuracy for all elements. Even more dramatically, the KIRCHHOFF11 and the KIRCHHOFF13 element have less than 10% error for all single element mesh cases. Furthermore, these two elements give similar results.

Figures 7-11 and 7-12 provide center X-moment results for the simply-supported uniform load case. All elements required a (2X2) mesh for cutoff accuracy.

The displacement results for DEGENERATE, MIDLIN13, and KIRCHHOFF13 elements are plotted together with the HUGHES element in Figures 7-13 and 7-14. For the square plate problem, the HUGHES and the DVORKIN element provide almost identical results [56,74]. A comparison with the hybrid elements indicates that the DEGENERATE element is virtually the same as the elements constructed by using the assumed strain method (DVORKIN) and the selective integration method (HUGHES). Overall, the KIRCHHOFF13 element provides the most accurate results. A (1X1) mesh of KIRCHHOFF13 elements gives just as accurate results as does a (2X2) mesh of other elements.

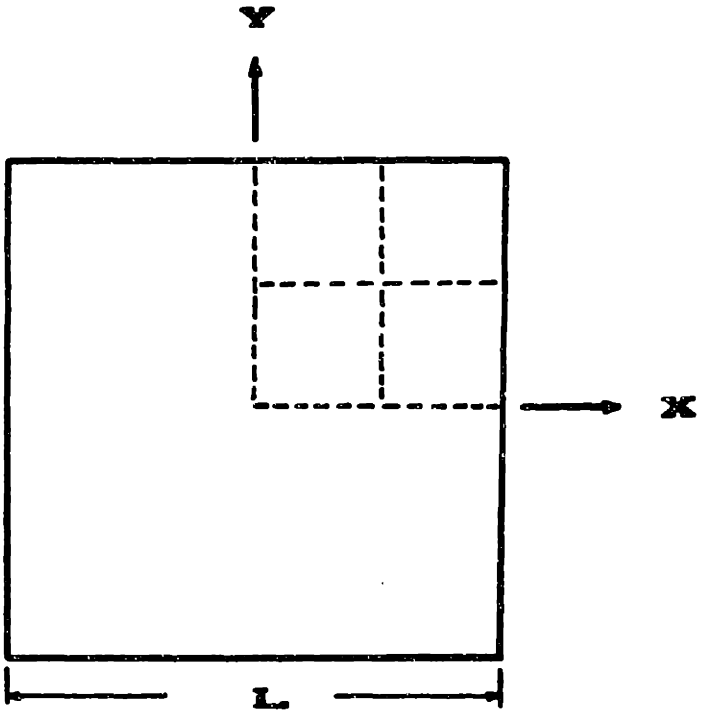

$$\frac{L}{h} = 200 \qquad L = 20$$

$$E = 10^{7} \qquad \nu = .3$$

Figure 7-2. Square Plate Problem.

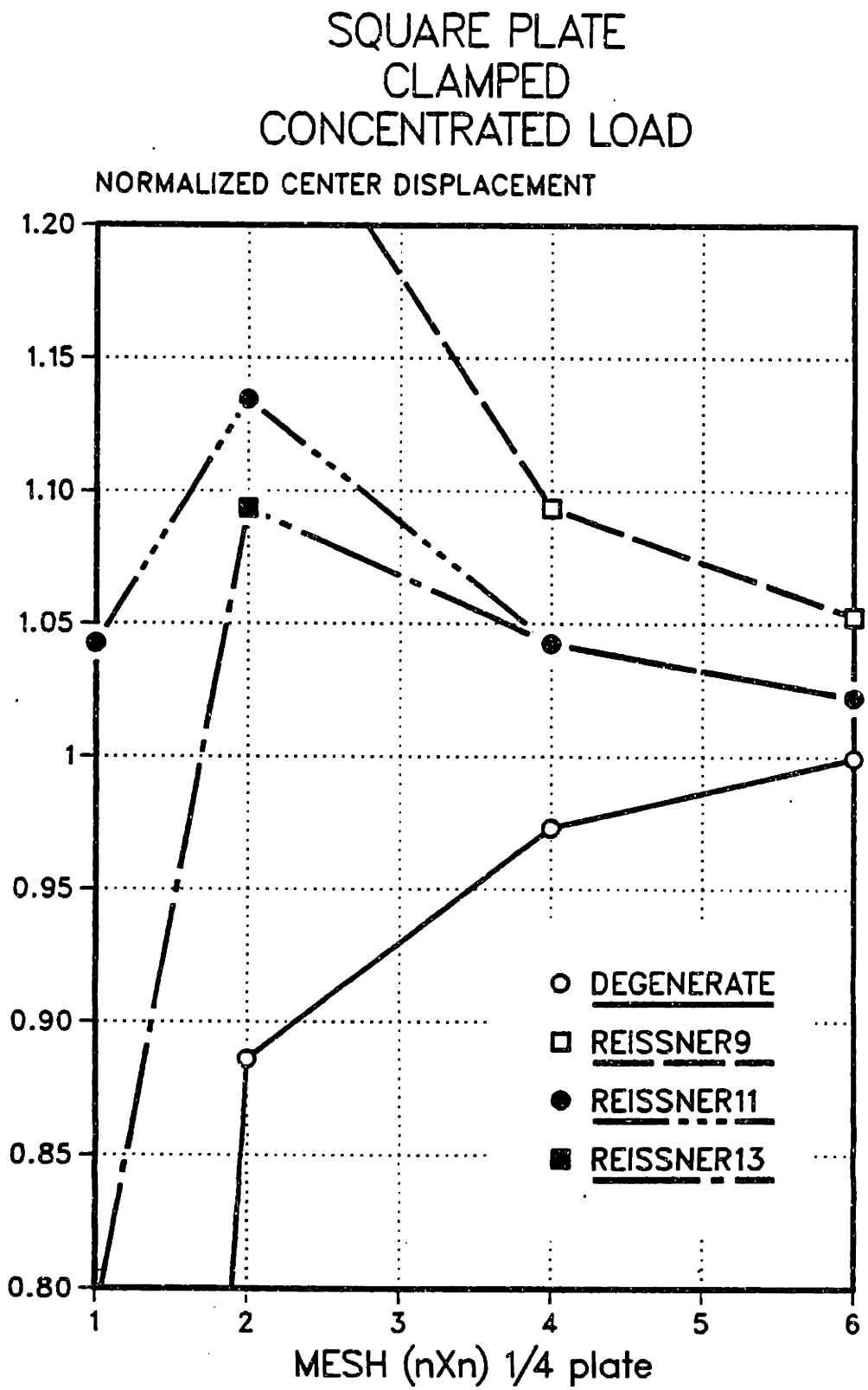

Figure 7-3. **C^0 Plate Center Displacement Results for Square Plate with Clamped Boundary and Central Concentrated Load.**

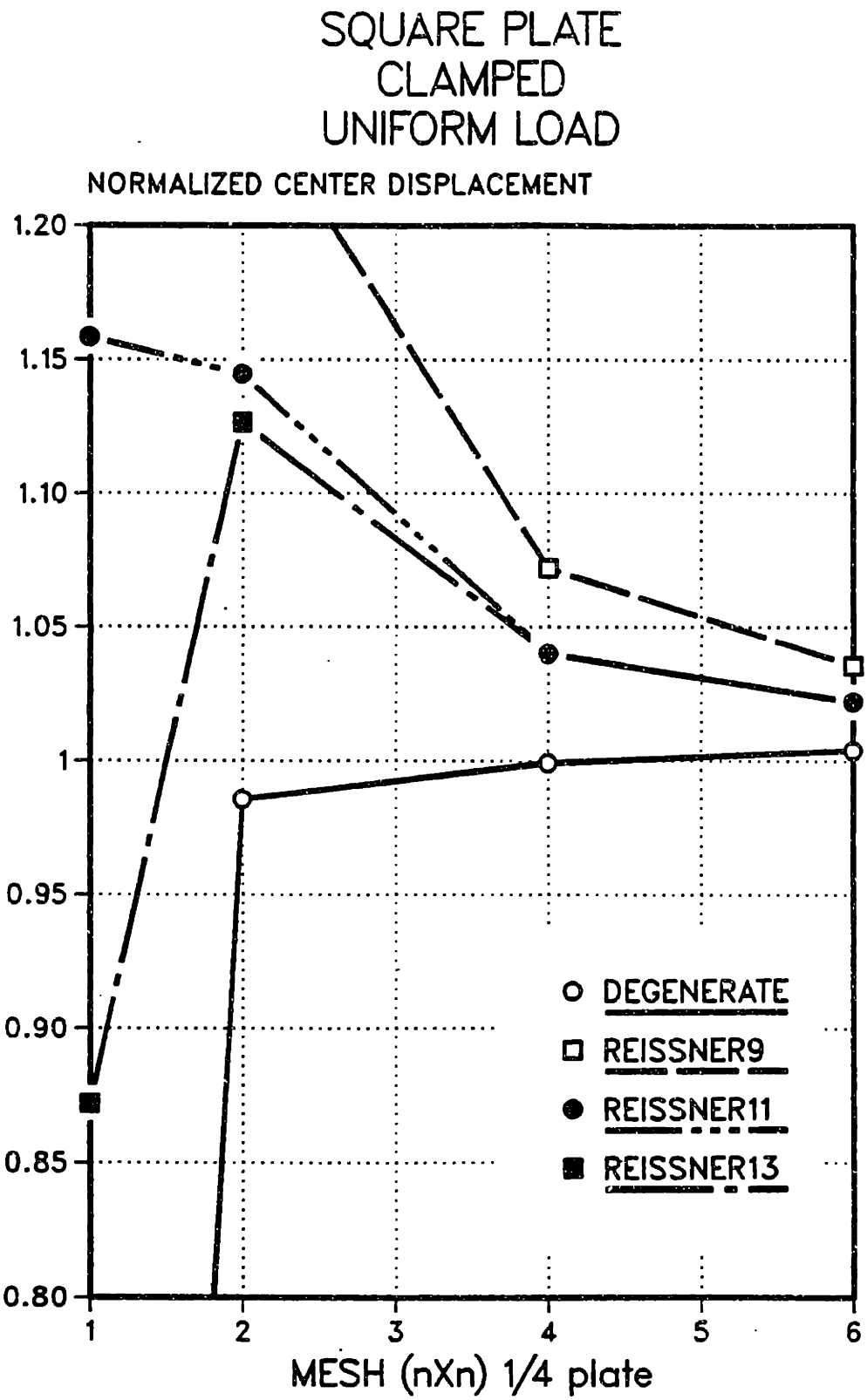

Figure 7-4. **C^0 Plate Center Displacement Results for Square Plate with Clamped Boundary and Uniformly Distributed Load.**

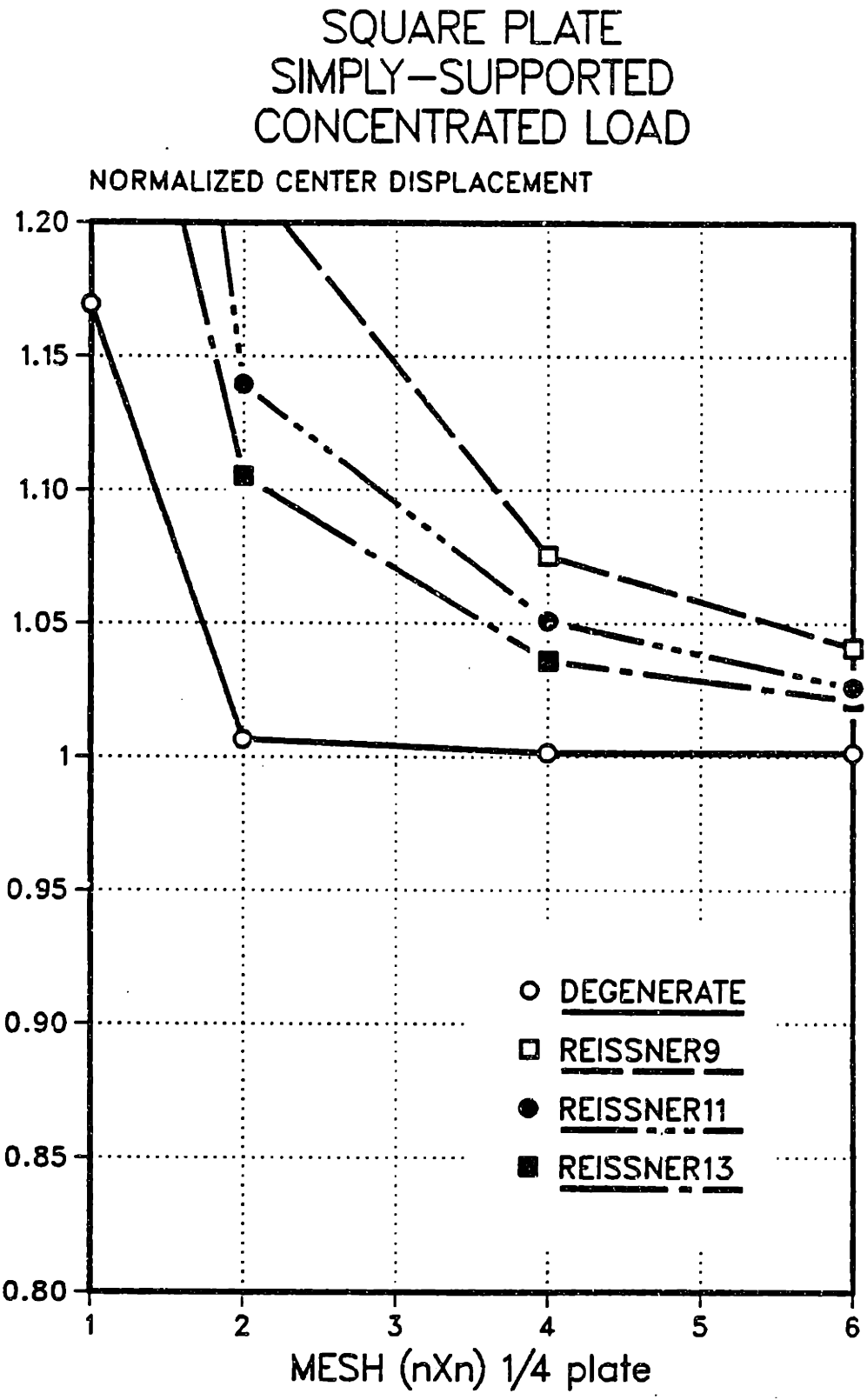

Figure 7-5. C^0 **Plate Center Displacement Results for Square Plate with Simply-Supported Boundary and Central Concentrated Load.**

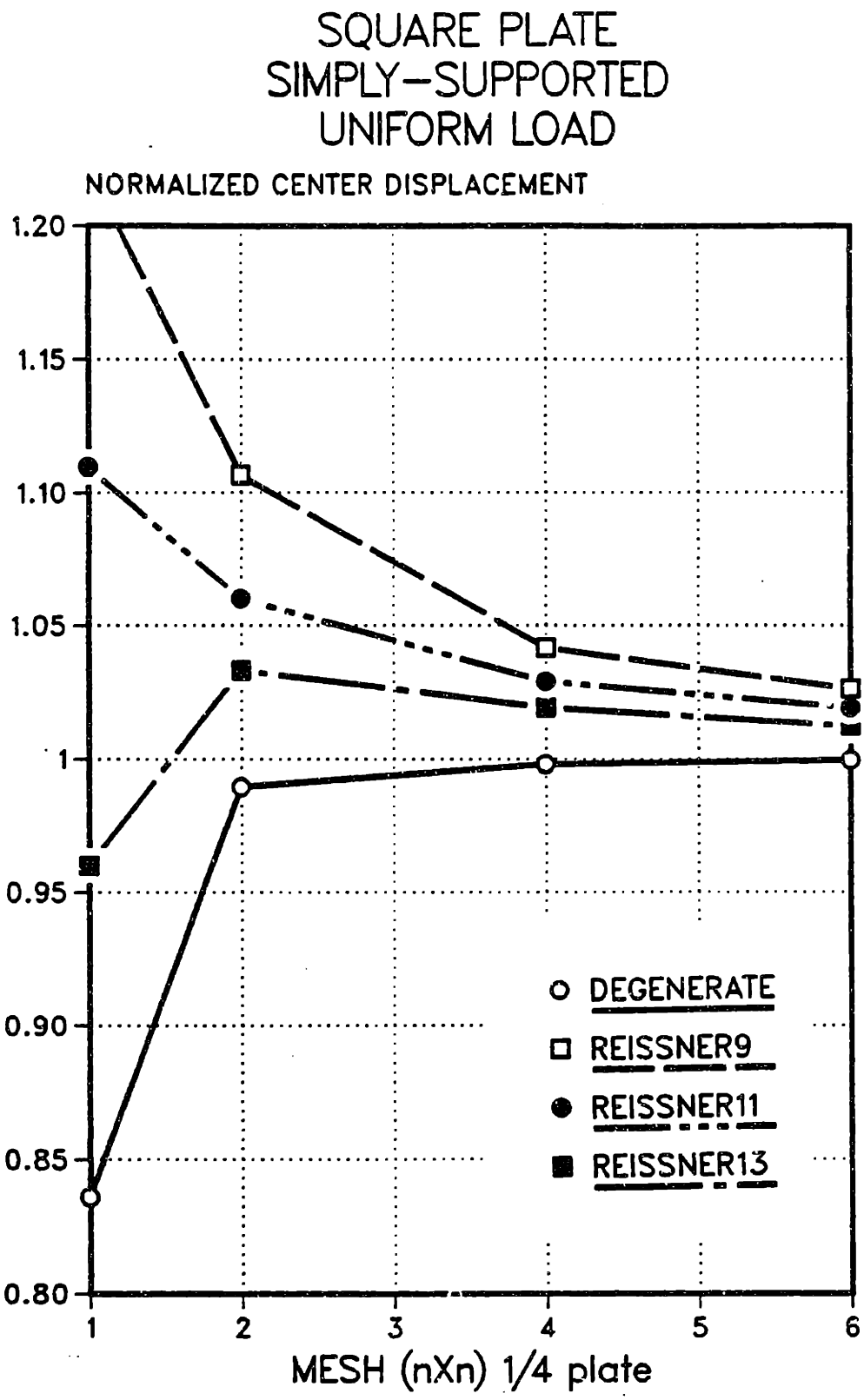

Figure 7-6. C^0 **Plate Center Displacement Results for Square Plate with Simply-Supported Boundary and Uniformly Distributed Load.**

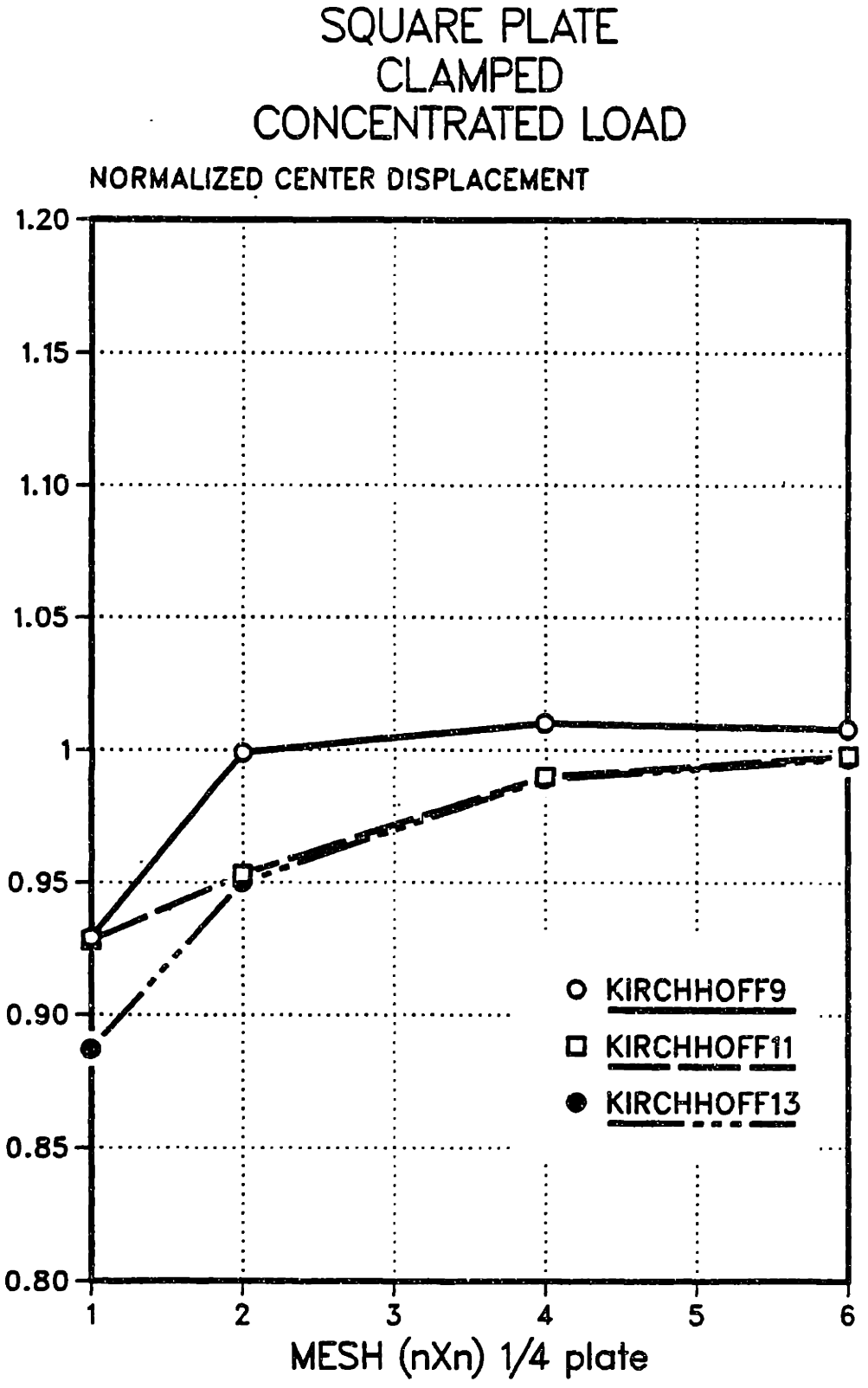

Figure 7-7. **C^1 Plate Center Displacement Results for Square Plate with Clamped Boundary and Central Concentrated Load.**

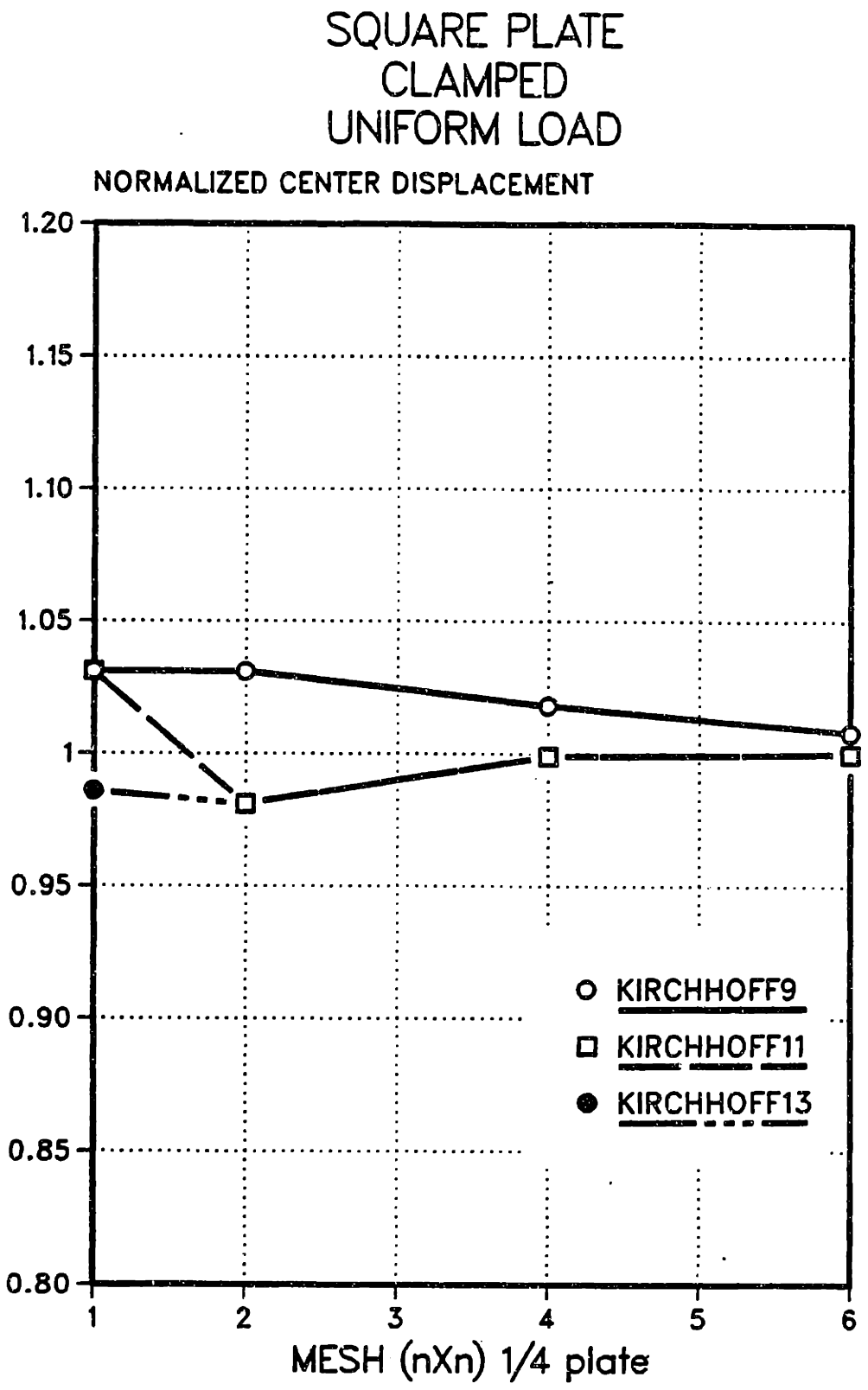

Figure 7-8. C^1 **Plate Center Displacement Results for Square Plate with Clamped Boundary and Uniformly Distributed Load.**

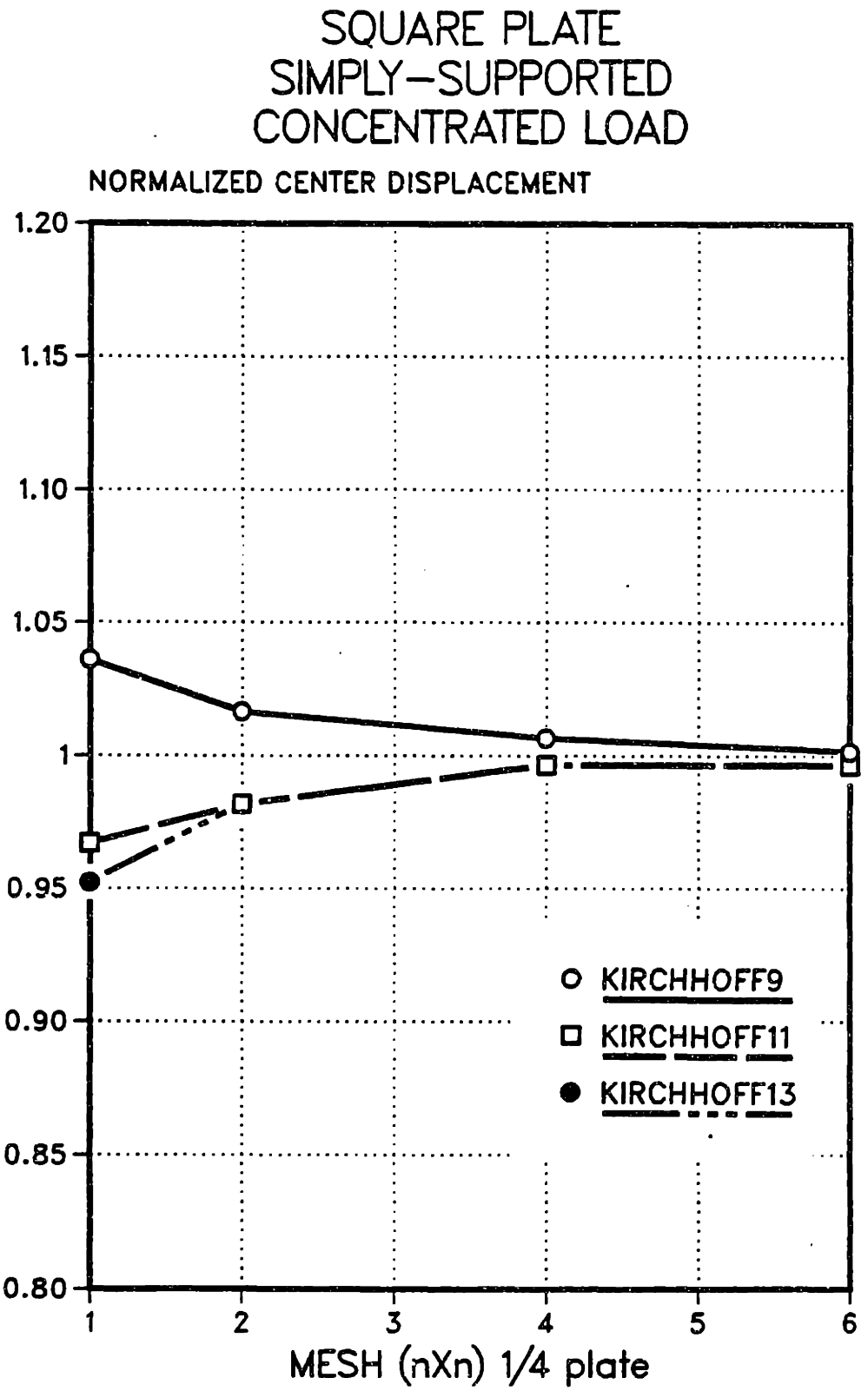

Figure 7-9. C^1 **Plate Center Displacement Results for Square Plate with Simply-Supported Boundary and Central Concentrated Load.**

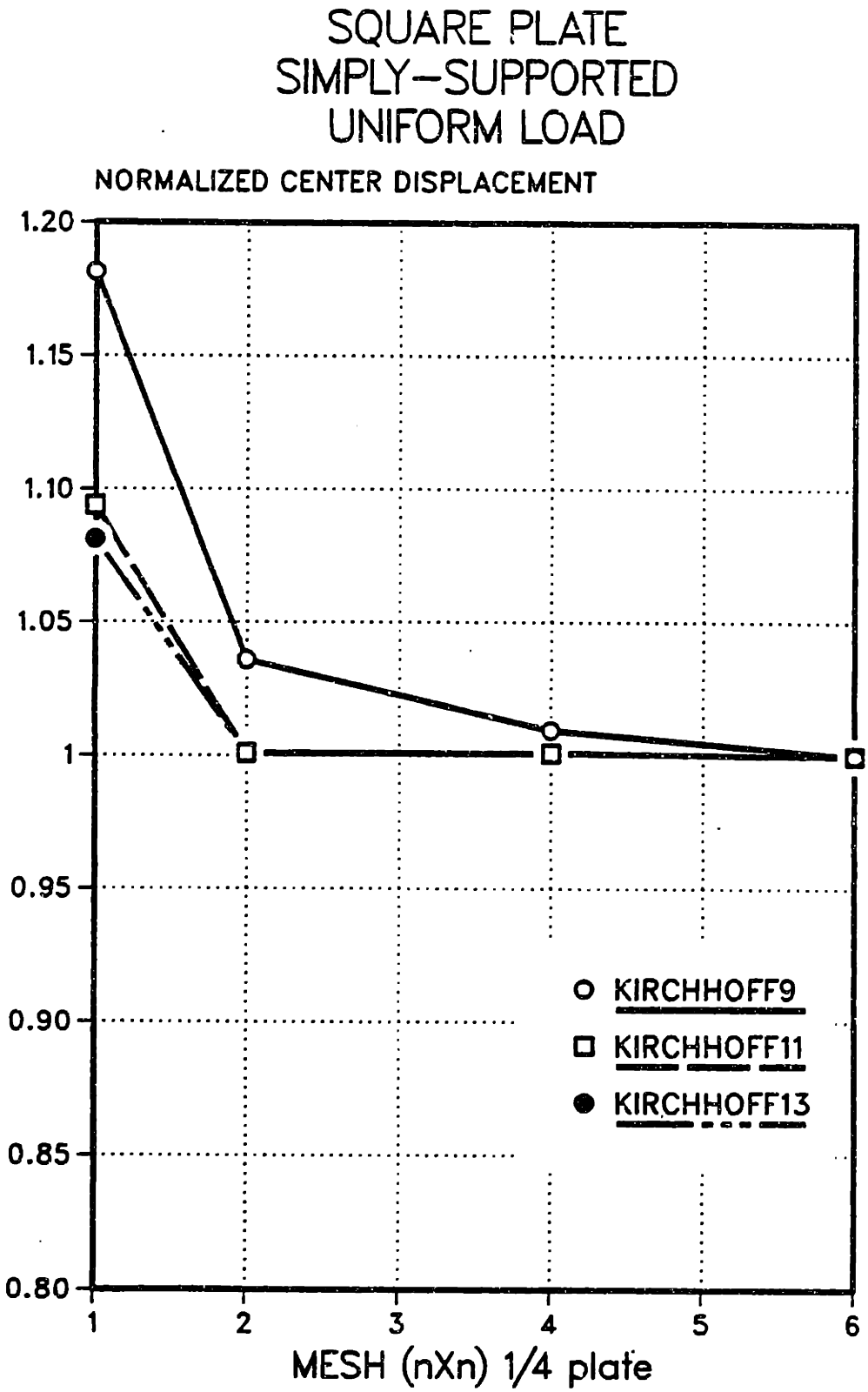

Figure 7-10. C^1 **Plate Center Displacement Results for Square Plate with Simply-Supported Boundary and Uniformly Distributed Load.**

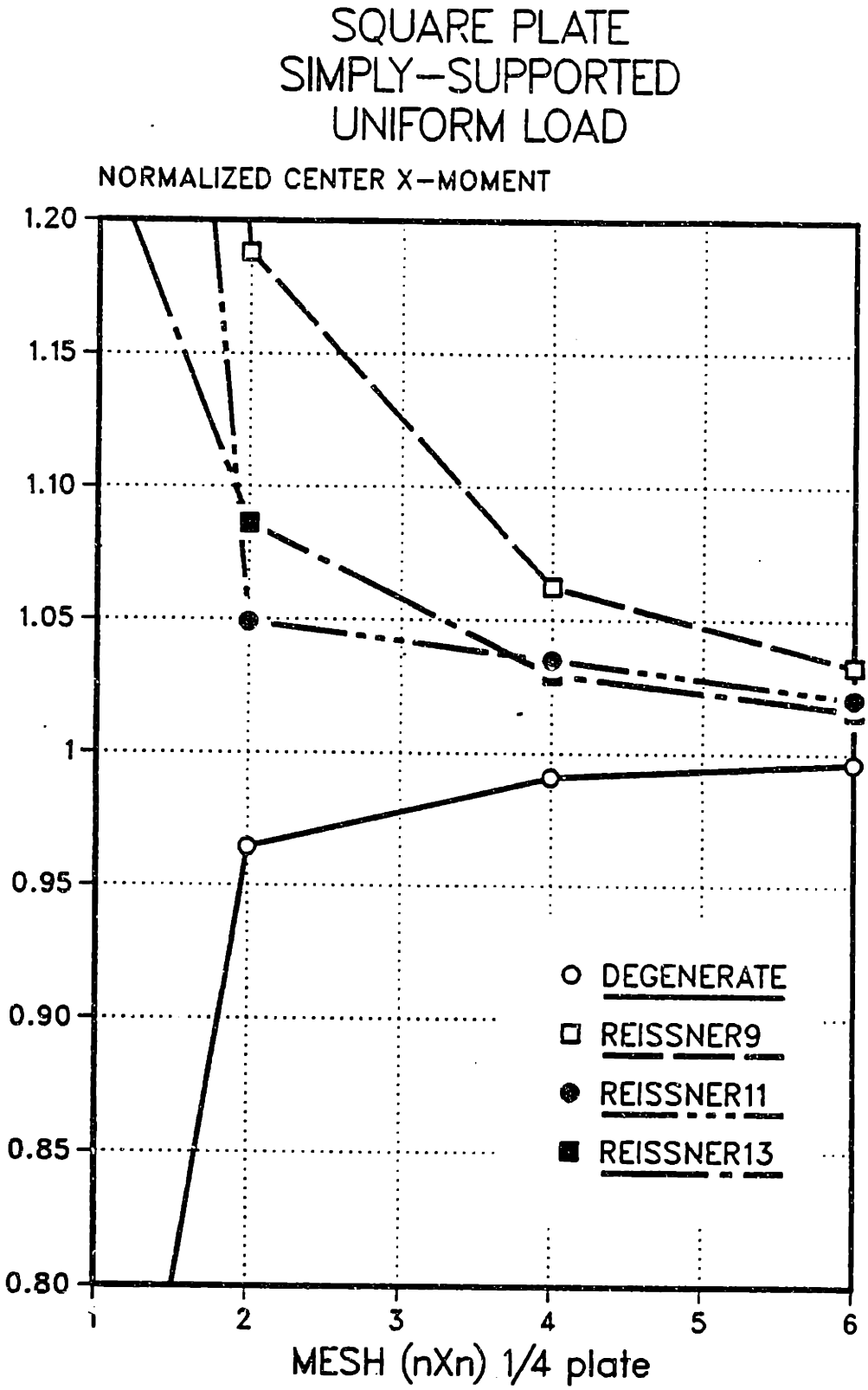

Figure 7-11. C^0 **Plate Center X-Moment Results for Square Plate with Simply-Supported Boundary and Uniformly Distributed Load.**

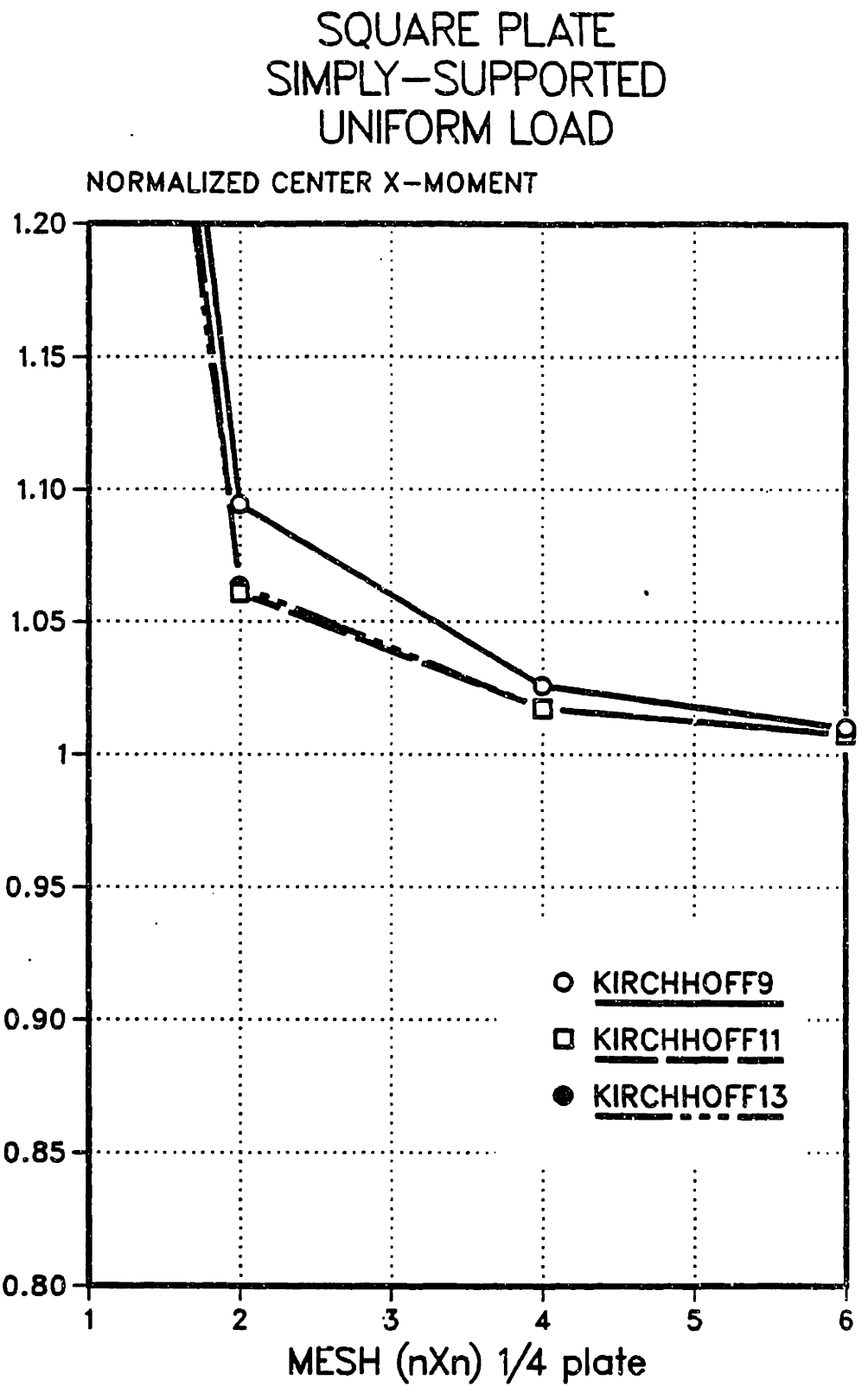

Figure 7-12. **C^1 Plate Center X-Moment Results for Square Plate with Simply-Supported Boundary and Uniformly Distributed Load.**

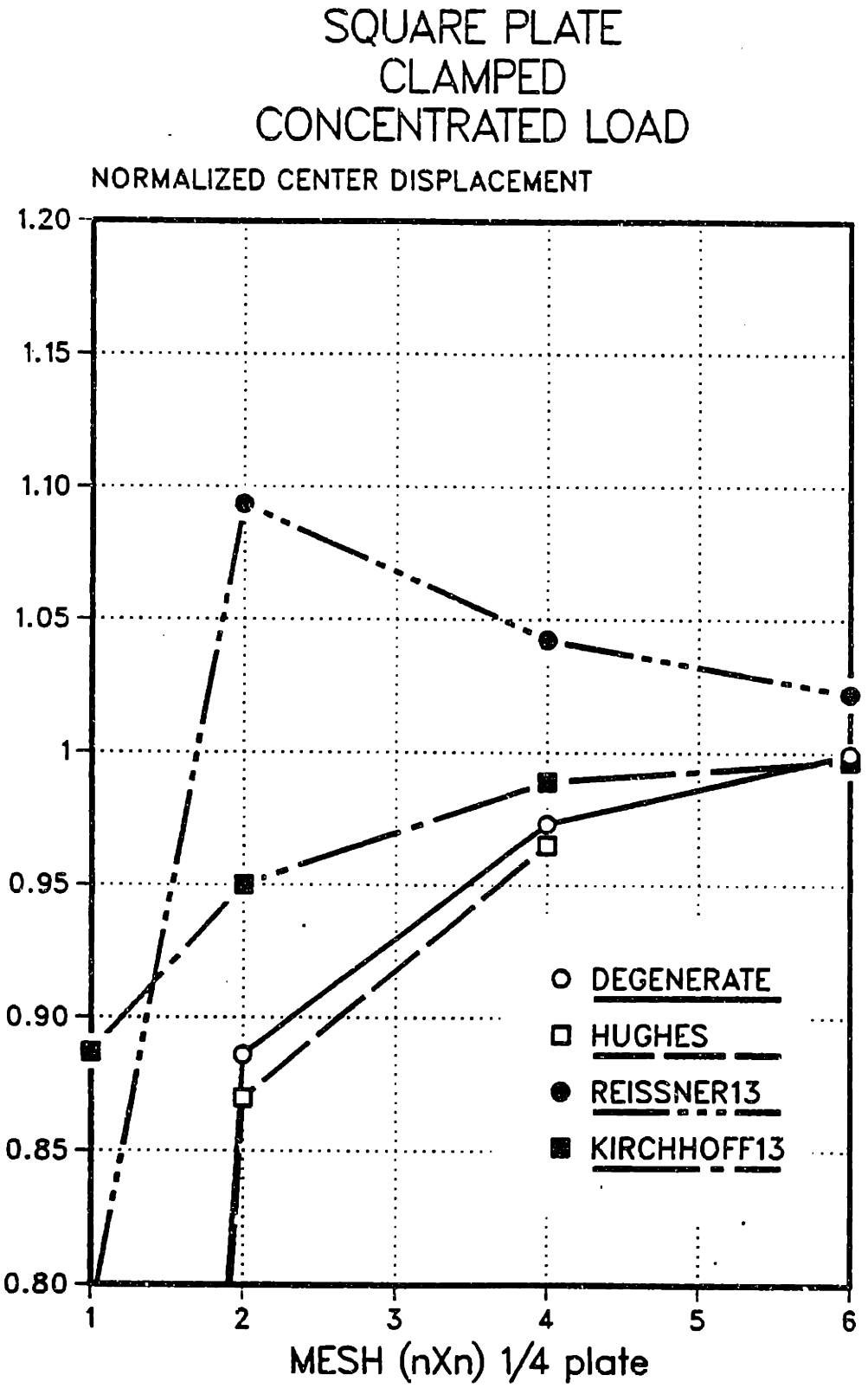

Figure 7-13. Comparison of Center Displacement Results Square Plate with Clamped Boundary and Central Concentrated Load.

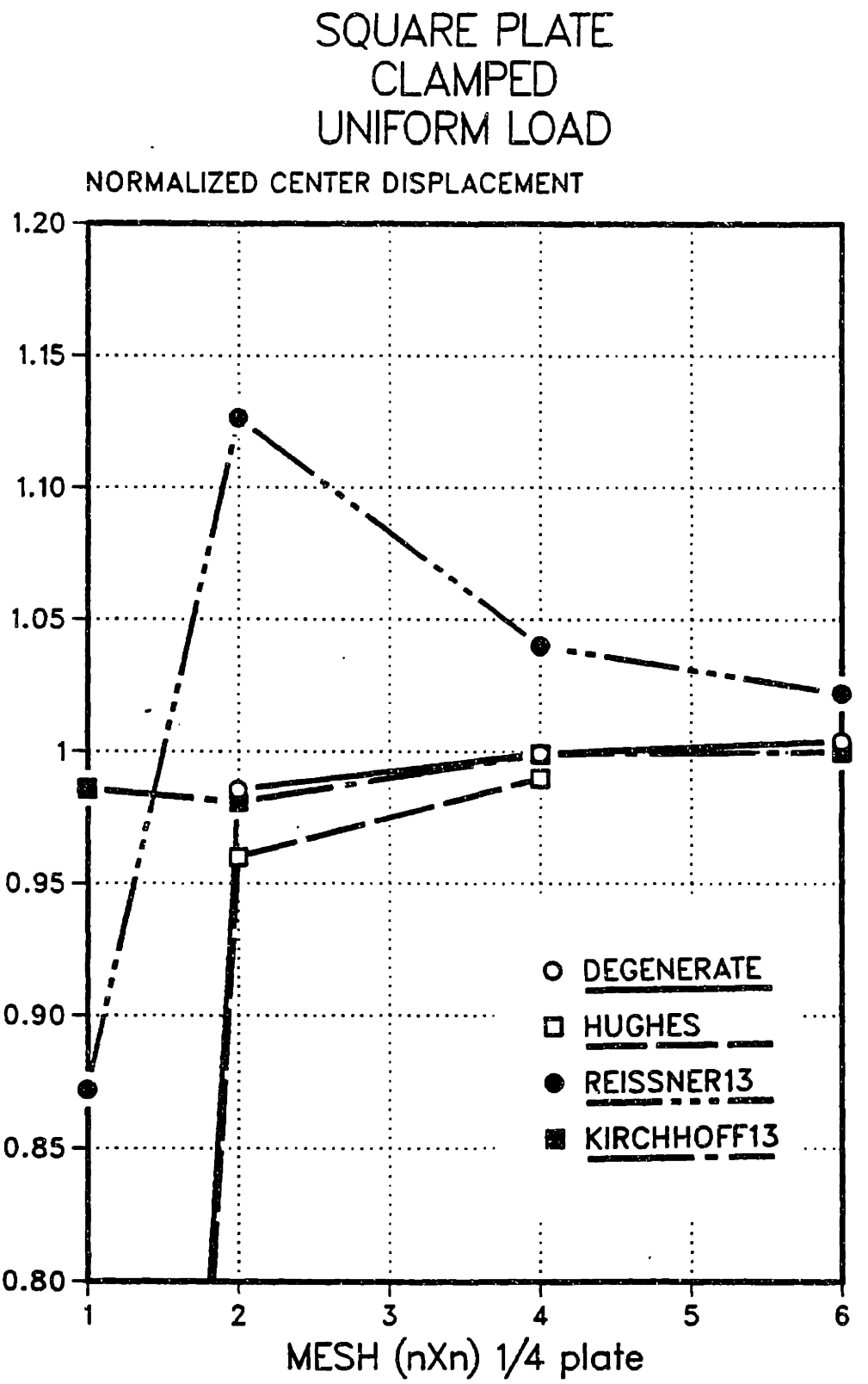

Figure 7-14. Comparison of Center Displacement Results Square Plate with Clamped Boundary and Uniformly Distributed Load.

7.3.3 Square Plate with Element Distortion

To demonstrate the effect of element distortion, a (2X2) mesh of elements is used. The case chosen is the simply-supported square plate under concentrated center load. Figure 7-15 defines the distortion parameter, a. Full triangularization occurs for a=5.

The center displacement versus distortion is plotted in Figures 7-16 and 7-17 for hybrid plates. The results indicate a severe deterioration for the DEGENERATE (solid) element. The distortion study for C^0 elements, indicates a much superior performance of REISSNER plate elements over DEGENERATE plate elements; this provides a key feature necessary to distinguish these two elements. The KIRCHHOFF plates are basically insensitive to distortion up to a=4.

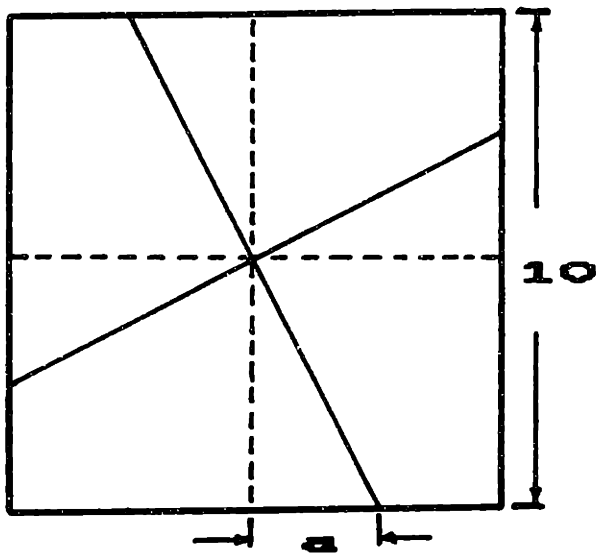

Figure 7-15. Distortion Study of Simply-Supported Square Plate under Concentrated Load.

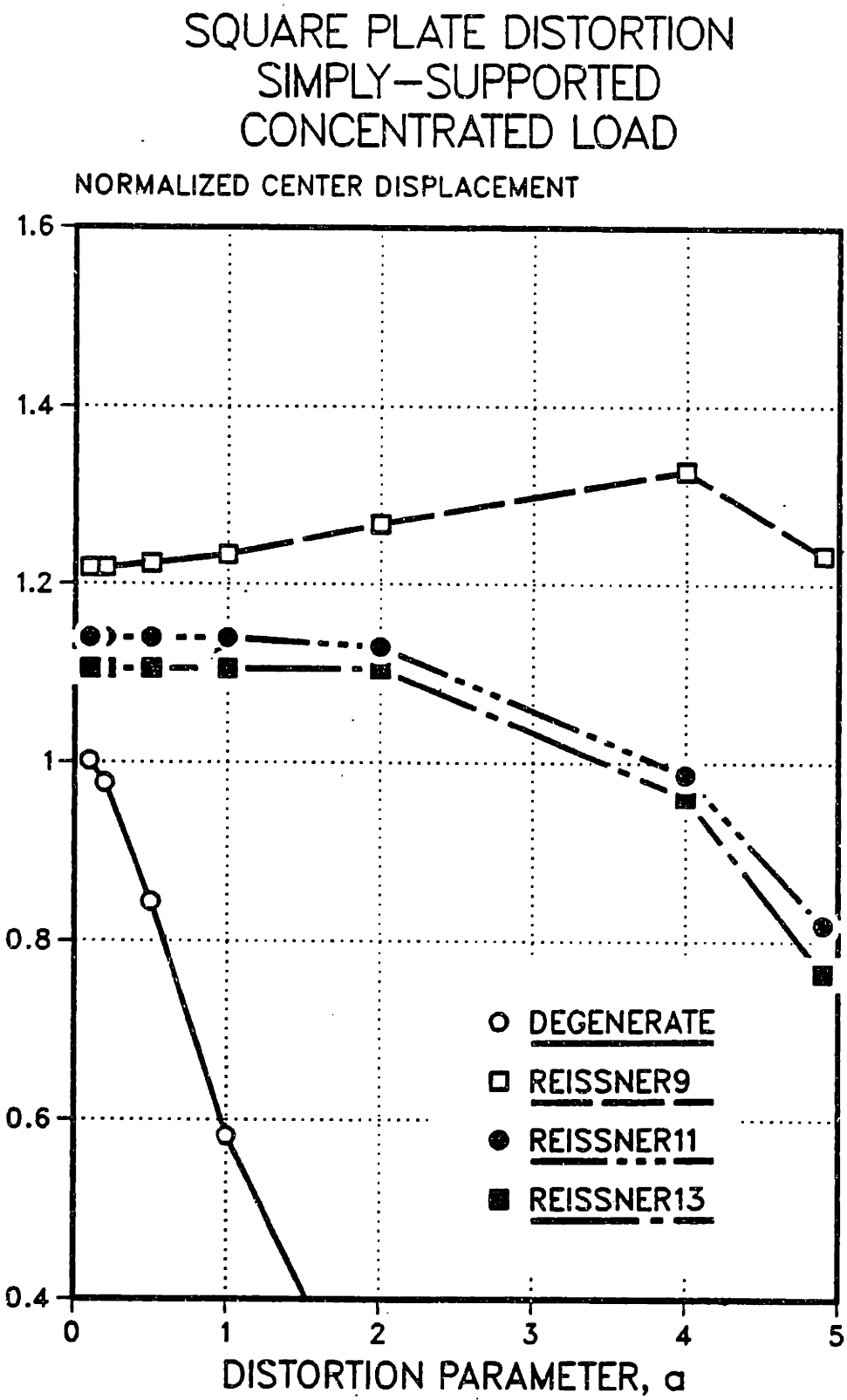

Figure 7-16. C^0 **Plate Distortion Study Center Displacement Results.**

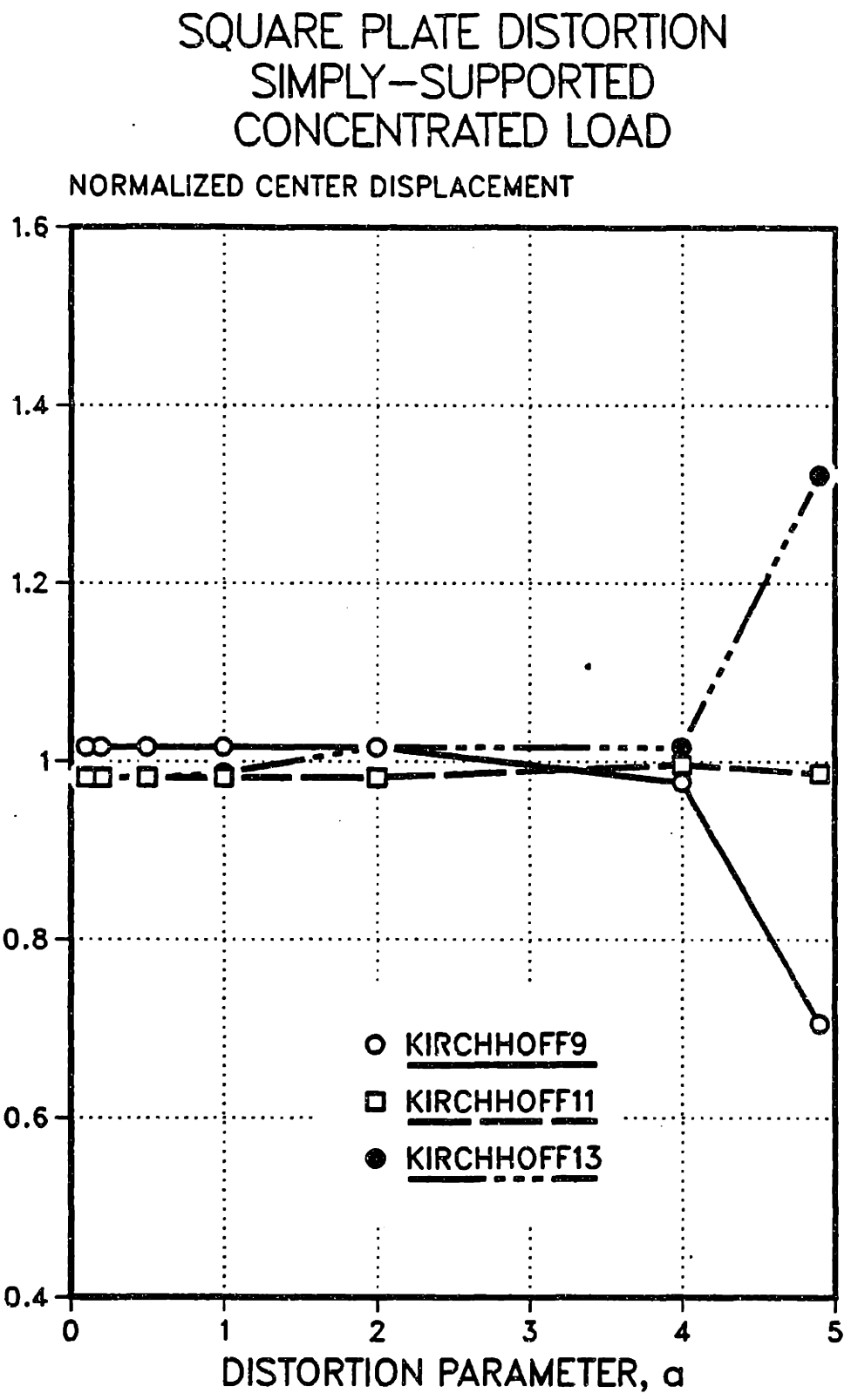

Figure 7-17. C' Plate Distortion Study Center Displacement Results.

7.3.4 30^0 Rhombic Plate Problem

A benchmark problem widely used to assess and rank plate elements is the 30^0 rhombic plate problem, also known as the Morley's skew plate problem [75]. Shown in Figure 7-18, the rhombic plate exhibits a uniform distortion. The angles of each element are maintained as mesh is refined. The results from large number of elements, compiled by Robinson [76], indicate that this problem is a severe test for the performance of plate elements.

To begin with, Figures 7-19 and 7-20 provide the center displacement results for hybrid plates. The results clearly indicate that 9 β elements for both REISSNER and KIRCHHOFF elements give poor results compared with almost identical results obtained by 11 β and 13 β elements of REISSNER and KIRCHHOFF types. For 11 β and 13 β elements, only a (2X2) mesh is required for cutoff accuracy of +/- 20% error.

Figures 7-21 and 7-22 provide the maximum and minimum moments at the center of the plate. For cutoff accuracy, a (4X4) mesh is required for the maximum moment and an (8X8) mesh is required for the minimum moment.

A comparative plot is shown in Figure 7-23 for the center displacements. In overall performance, the REISSNER13 and the KIRCHHOFF13 elements give superior accuracy. The most dramatic and telling differences are

provided by the crude mesh, (2X2), result. The sensitivity of the hybrid elements to a particular stress field assumption is demonstrated by the WOLF element with its 17 β stress assumption [73]. The result is a much-too-rigid behavior. Clearly that stress assumption is not a "best choice".

As a final point, examine the moment distribution results for a (16X16) KIRCHHOFF13 element mesh. The analytical solution for moments includes a singular moment at the obtuse corner. Although the KIRCHHOFF13 element results are accurate for most of the domain, the singularity at the obtuse corner is not captured well. The only way to capture the singular behavior efficiently by using finite elements is to employ specialized elements with an appropriate embeded singularity [73], as has been also done for crack-tip elements [77].

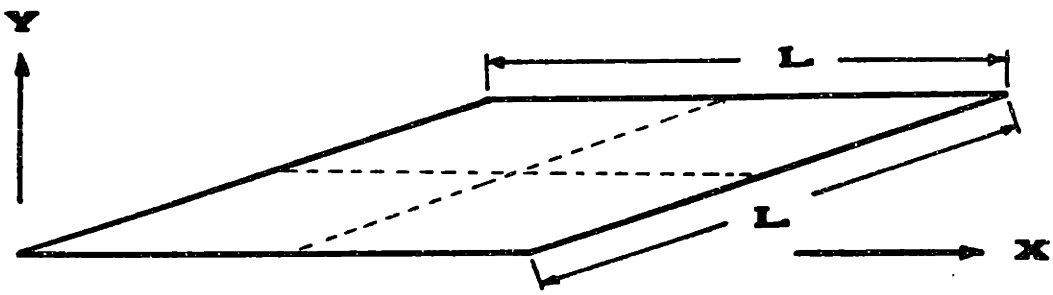

$$\frac{L}{h} = 100$$

$$E = 3 \times 10^{7}$$

$$\nu = .3$$

Figure 7-18. 30^{0} Rhombic Plate (Morley's Skew Plate) with Simply-Supported Boundary (w=0) under Uniform Load.

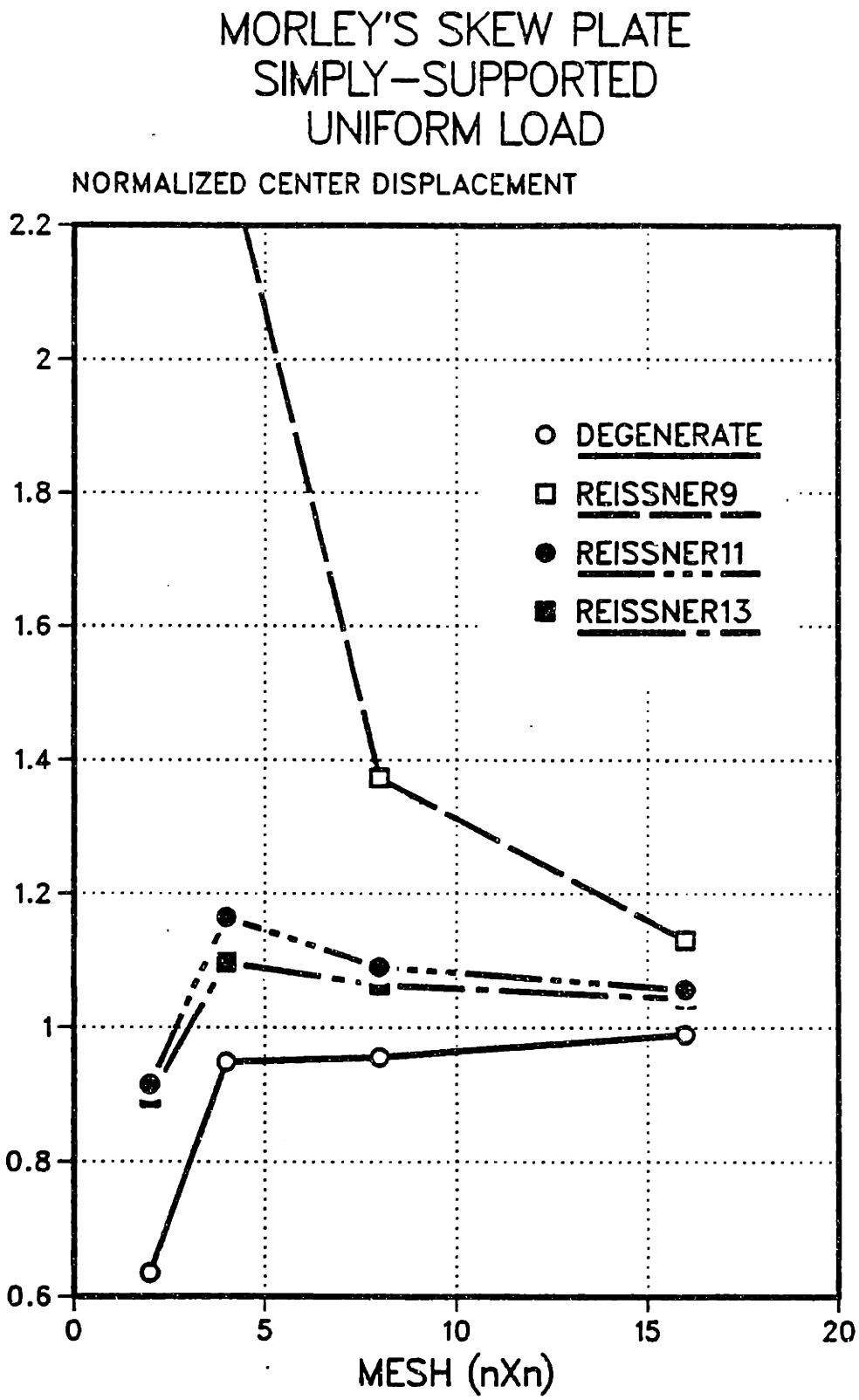

Figure 7-19. C^0 Plate Center Displacement Results for Morley's Skew Plate.

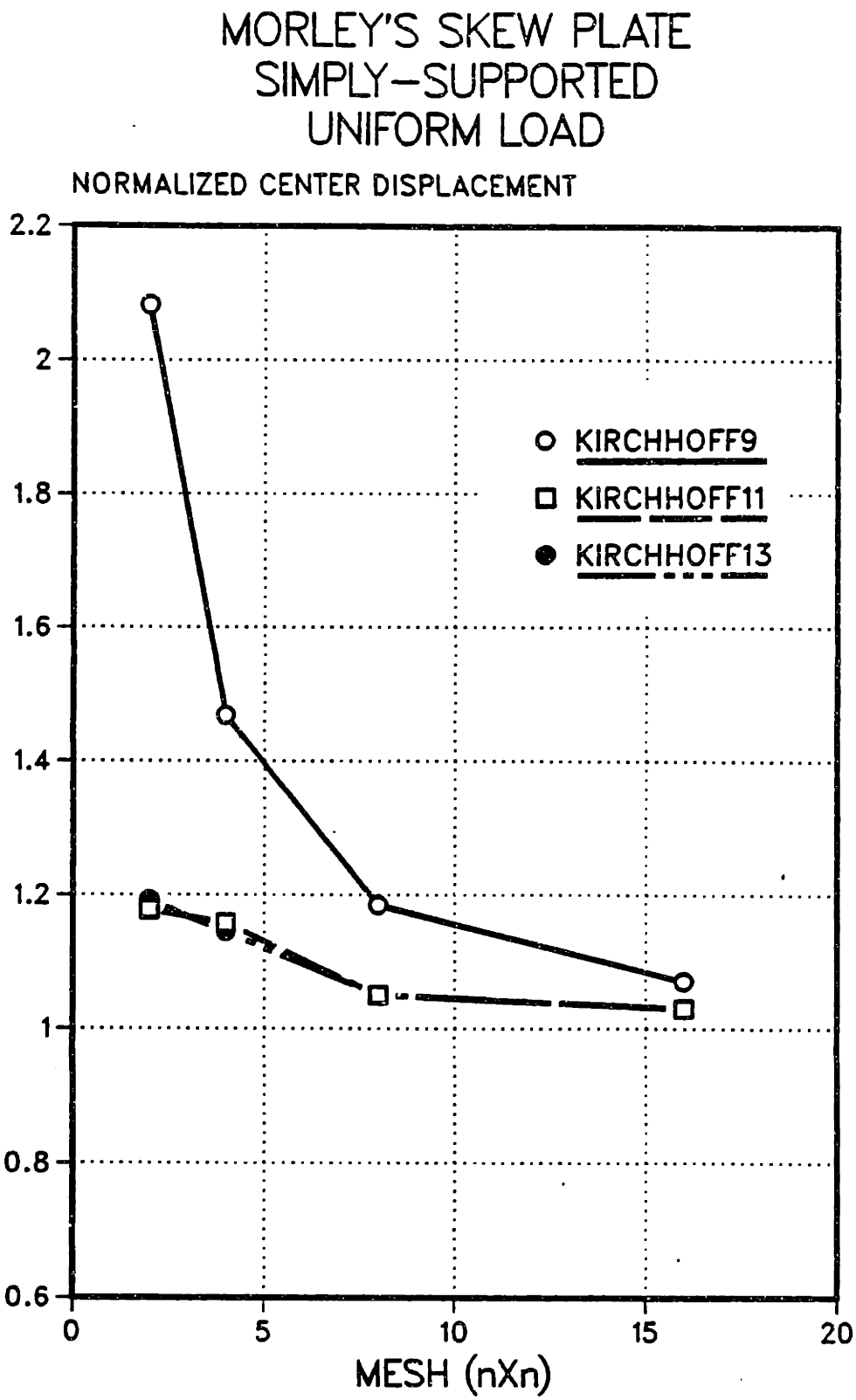

Figure 7-20. C^1 **Plate Center Displacement Results for Morley's Skew Plate.**

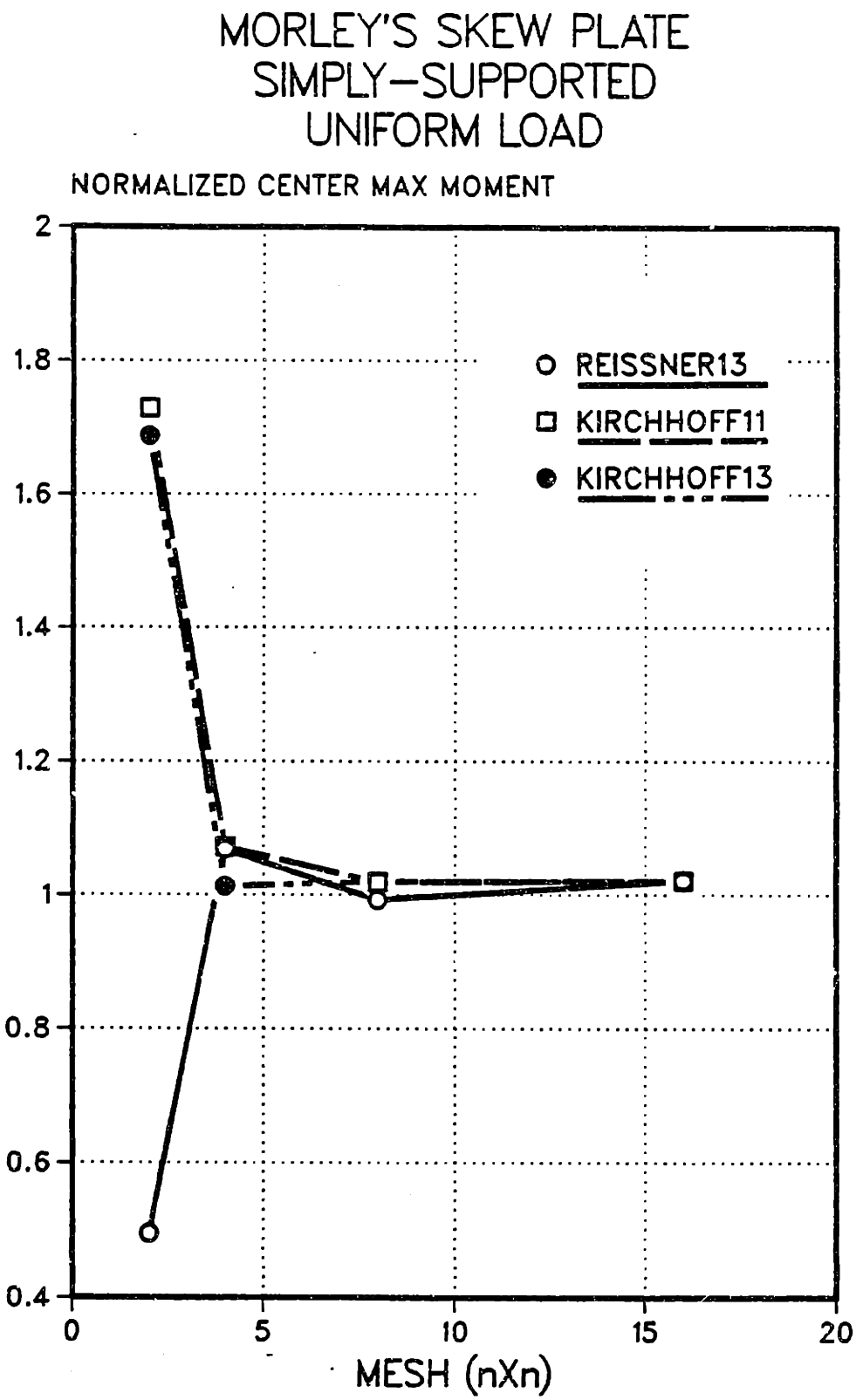

Figure 7-21. Maximum Moment at Center for Morley's Skew Plate.

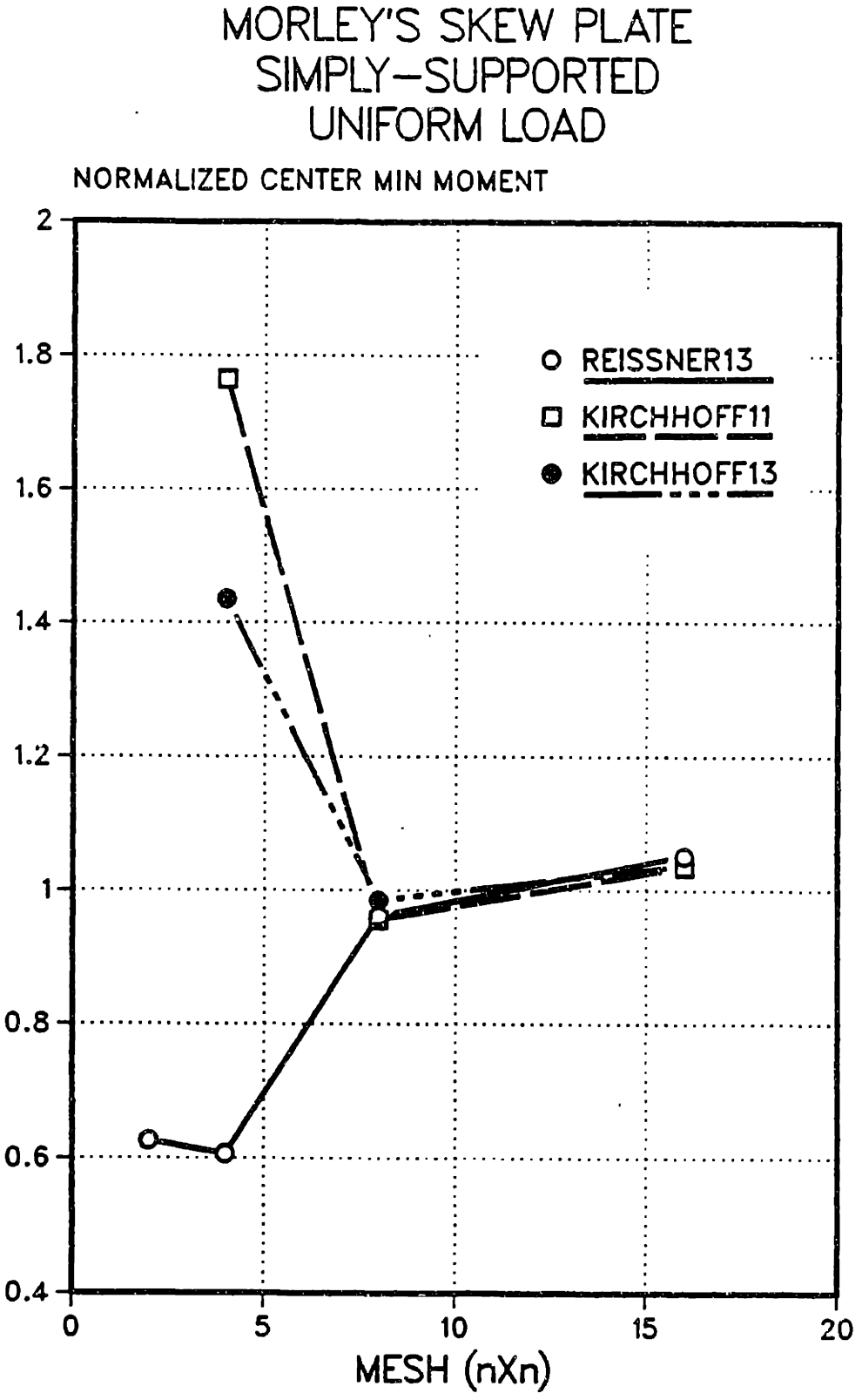

Figure 7-22. Minimum Moment at Center for Morley's Skew Plate.

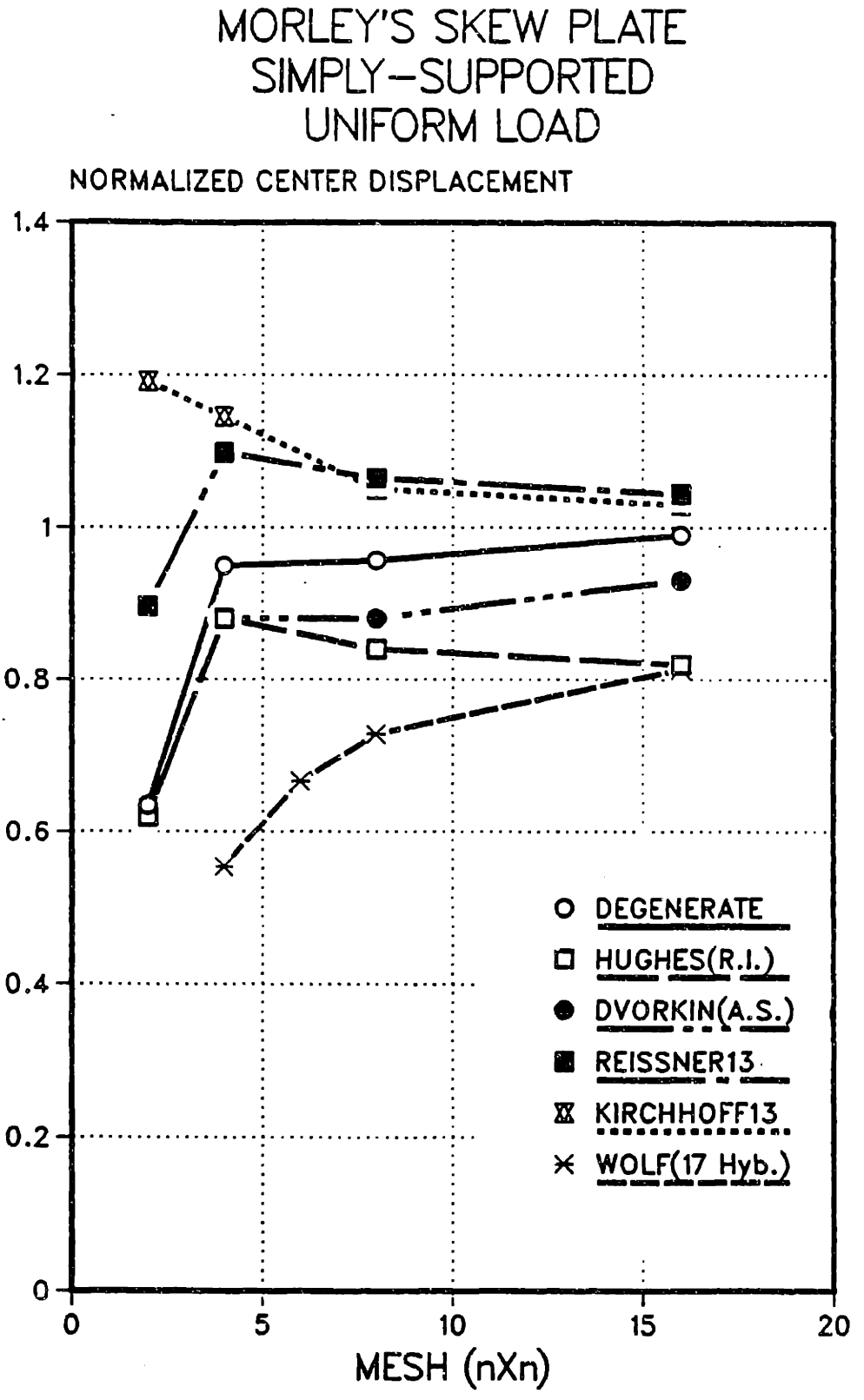

Figure 7-23. Comparison of Center Displacement Results for Morley's Skew Plate.

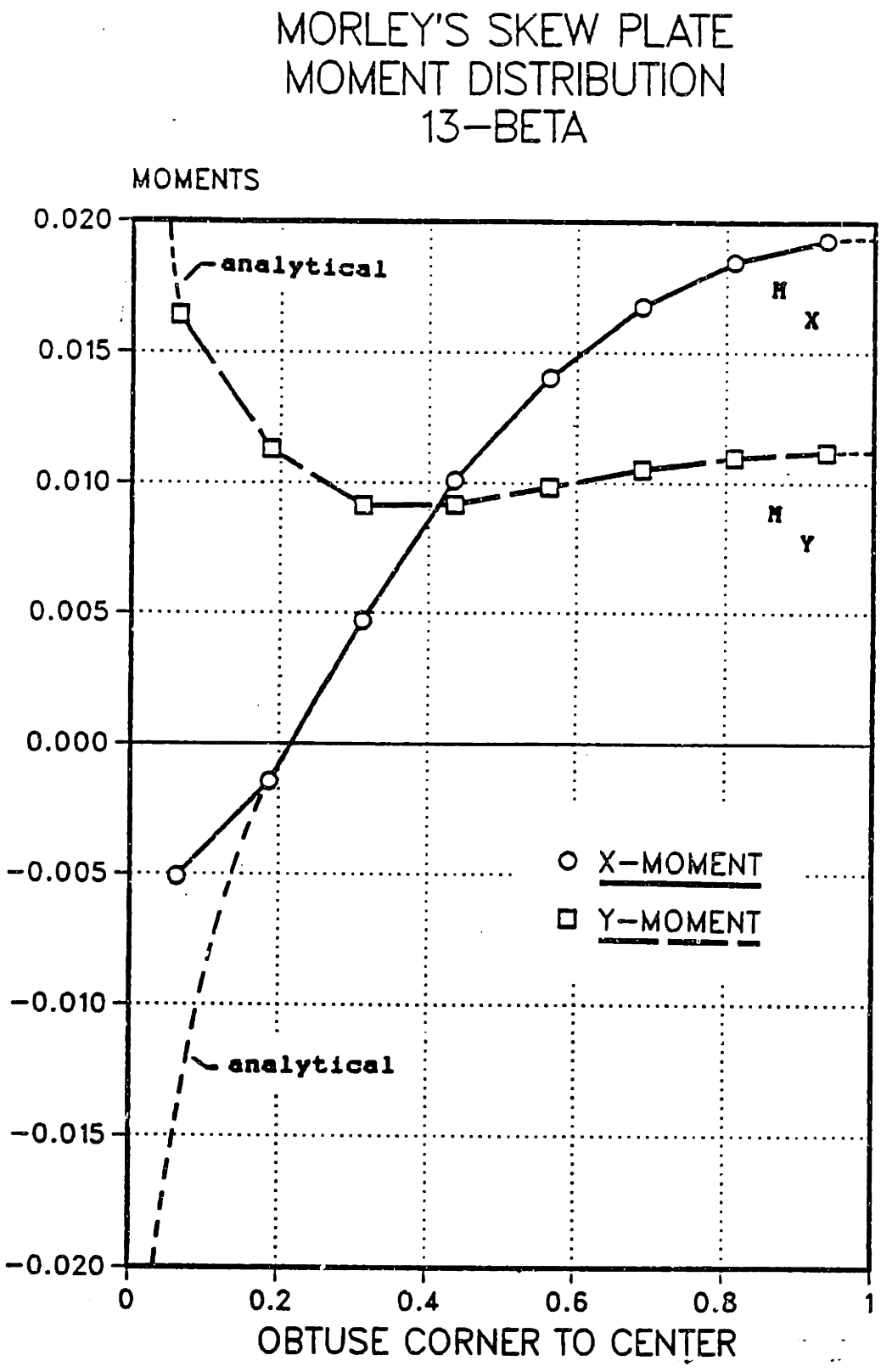

Figure 7-24. KIRCHHOFF13 (16X16) Mesh X and Y Moment Distribution Results for Morley's Skew Plate.

7.3.5 Summary

Overall, the numerical examples presented demonstrate the superior performance of the KIRCHHOFF13 hybrid element. Since the results for the KIRCHHOFF11 hybrid element is virtually identical to those for the KIRCHHOFF13 element, the KIRCHHOFF11 element is the recommended choice amongst these plate elements.

In the distortion example, the DEGENERATE element is shown to be too sensitive to element distortion. REISSNER elements are clearly less accurate than KIRCHHOFF elements for the square plate examples.

CHAPTER 8

ARCH ELEMENTS

In this chapter, as a prelude to discussing shell elements, a technique necessary to map a field distribution from the flat to a curved configuration will be studied. To allow a detailed study, the mapping process is limited to a one dimensional element: an arch. Recall that the main motivation in introducing the mapping technique is to eliminate multiple possibilities in the selection of a proper field assumption.

The arch element is introduced in the first section through the presentation of past developments. The second section provides the details for constructing an arch element by collapsing a two dimensional element described in terms of the polar coordinate system. The third section illustrates a simple procedure for developing a C^1 element by simply starting with a corresponding flat configuration field assumption and mapping this to a curved geometry. Two numerical examples are illustrated to provide a comparison between two different chosen stress assumptions.

8.1 Assumed Displacement/Strain Arch Elements

In the catagory of a two node C^1 arch element, there are four major types of assumed displacement/strain fields, as follows:

A. Compatible Displacement Field

B. Exact Rigid Body Motion Included

C. Assumed Strain

D. Equal Polynomial Order for Both Displacement Components

Qualitatively, the same categories hold for the shell element. Exhaustive trials of assumed fields for the circular arch element have been made by Ashwell et al.[78-81] and Dawe [82-84]. Although both groups covered the four major types mentioned above, Dawe also included higher order elements.

Before proceeding to the circular configuration, a review of the flat configuration is worthwhile. The strain-displacement relation for a flat arch (that is a straight beam under axial and bending action) may be written as

$$\varepsilon = \frac{du}{ds}$$
$$K = -\frac{d^2w}{ds^2} \qquad (8.1)$$

where and represent the membrane and bending

strain measures, respectively. For the two node element with three degrees of freedom at each node, the only possible compatible displacement assumption is

$$w = \alpha_1 + \alpha_2 s + \alpha_3 s^2 + \alpha_4 s^3$$
$$u = \alpha_5 + \alpha_6 s \qquad (8.2)$$

The displacement field w is formed from the Hermite functions and u from the linear Lagrangian function. The corresponding strain field is

$$\varepsilon = \alpha_6$$
$$K = -2\alpha_3 - 6\alpha_4 s \qquad (8.3)$$

The assumed displacement flat arch element represented by Eq. (8.3) is a well-behaved element when it is used for flat-geometry problems. Some traits of the flat arch element to be emulated by the circular arch element may be stated as:

(A) Assumed displacements are compatible.

(B) Rigid body motions are satisfied.

(C) Membrane and Bending strains are decoupled.

The circular arch element geometry is defined in Figure 8-1. The strain-displacement relation is

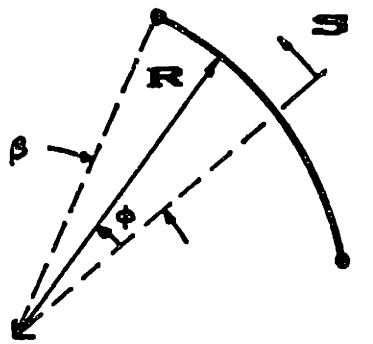

$$s = \phi R$$

Figure 8-1. Circular Arch Element Geometry.

$$\varepsilon = \frac{du}{ds} + \frac{w}{R}$$

$$\kappa = \frac{d}{ds}\left(\frac{u}{R} - \frac{dw}{ds}\right) \qquad (8.4)$$

Four types of assumed displacements can be applied for the arch element [81]. The first type consists of assuming a compatible displacement field without regard to rigid body motion or decoupled strains:

TYPE A Field

$$w = \alpha_1 + \alpha_2 s + \alpha_3 s^2 + \alpha_4 s^3$$
$$u = \alpha_5 + \alpha_6 s \qquad (8.5)$$

$$\varepsilon = \alpha_6 + \frac{1}{R}\left[\alpha_1 + \alpha_2 s + \alpha_3 s^2 + \alpha_4 s^3\right]$$
$$\kappa = \frac{\alpha_6}{R} - 2\alpha_3 - 6\alpha_4 s$$

The second type includes the field corresponding to the exact rigid body motion for a circular arch:

TYPE B Field

$$w = \alpha_1 \sin\phi + \alpha_2 \cos\phi + \alpha_3 R \sin\phi \cos\beta + \alpha_5 s^2 + \alpha_6 s^3$$
$$u = \alpha_1 \cos\phi - \alpha_2 \sin\phi - \alpha_3 R (1 - \cos\beta\cos\phi) + \alpha_4 s$$

(8.6a)

$$\varepsilon = \alpha_4 + \frac{1}{R}[\alpha_5 s^2 + \alpha_6 s^3]$$

$$K = \frac{\alpha_4}{R} - 2\alpha_5 - 6\alpha_6 s$$

(8.6b)

The above field does not satisfy compatibility because of the trigonometric functions which are present. However, the incompatible portion contributes only to the rigid-body motion. Interestingly, energy cannot distinguish incompatible modes represented in the rigid-body modes.

The third type is the assumed strain element. A strain field is assumed and then integrated to deduce the displacement field. The resulting displacement field is not compatible. One such strain assumption is

TYPE C Field

$$\varepsilon = \alpha_5 + \frac{\alpha_4}{R} \qquad (8.7)$$

$$K = \frac{\alpha_5}{R} + \frac{\alpha_6}{R} y$$

with the corresponding displacement field

$$W = \alpha_1 \cos\phi + \alpha_2 \sin\phi + \alpha_4 - \alpha_6 R s \qquad (8.7')$$
$$u = -\alpha_1 \sin\phi + \alpha_2 \cos\phi + \alpha_3 + \alpha_5 s + \tfrac{1}{2}\alpha_6 s^2$$

Since the α's are arbitrary coefficients, the strain field is decoupled. Further, the coefficients α_1, α_2, α_3 represent the rigid body motion.

The last type consists of using the same assumed polynomial order for each of the displacements:

TYPE D Field

$$w = \alpha_1 + \alpha_2 s + \alpha_3 s^2 + \alpha_4 s^3$$
$$u = \alpha_5 + \alpha_6 s + \alpha_7 s^2 + \alpha_8 s^3$$

$$\varepsilon = \alpha_6 + 2\alpha_7 s + 3\alpha_8 s^2 + \frac{1}{R}\left[\alpha_1 + \alpha_2 s + \alpha_3 s^2 + \alpha_4 s^3\right]$$
$$\kappa = \frac{1}{R}\left[\alpha_6 + 2\alpha_7 s + 3\alpha_8 s^2\right] - 2\alpha_3 - 6\alpha_4 s$$

Subsequently, the two additional dof's are condensed at element level. The main reason for field (8.8) is to establish a polynomial field that may have a well behaved performance.

Numerical results from an example problem consisting of a centrally-loaded clamped-clamped arch, Figure 8-2, are presented in Figure 8-3. The dramatic superiority of the assumed strain element, TYPE C, is firmly demonstrated. However a major difficulty exists with the

CLAMPED-FREE

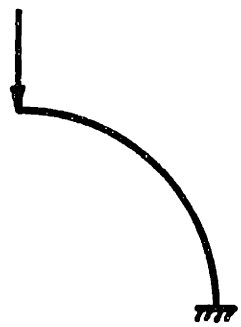

CLAMPED-CLAMPED

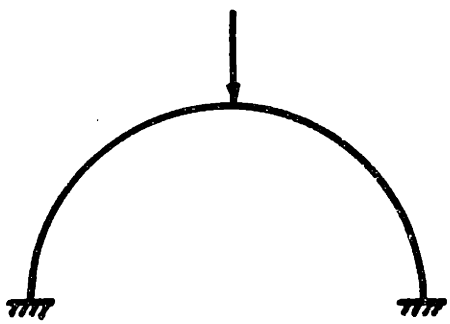

$\frac{R}{h} = 100 \qquad E = 10^7$

Figure 8-2. Circular Arch Problems.

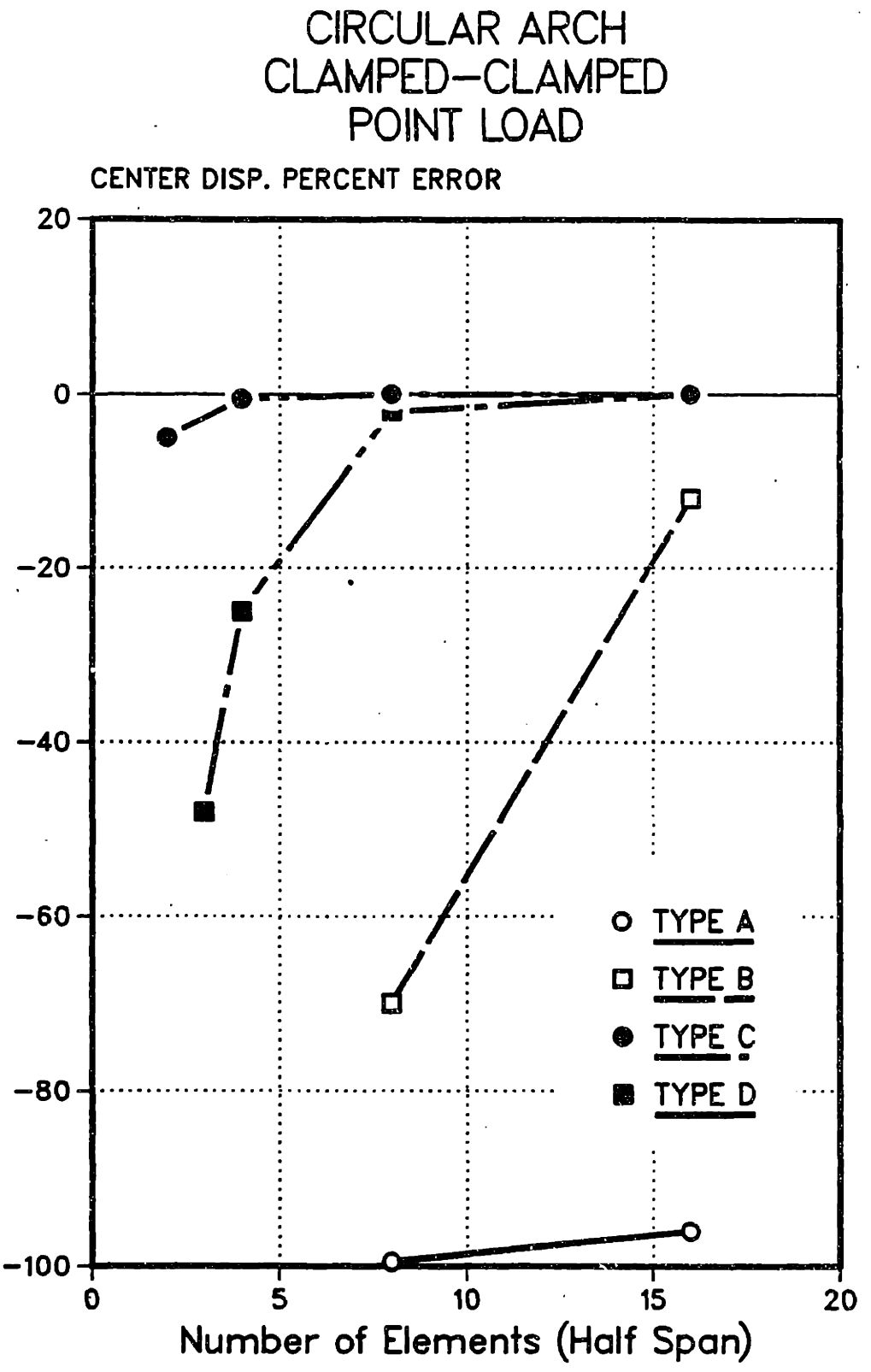

Figure 8-3. Error in Deflection under the Load for Clamped-Clamped Circular Arch Problem [67].

assumed strain element method when an attempt is made to extend to an arbitrary shell geometry. The questions that arise involve the choice of strain fields, and their integration to obtain the displacement field. Furthermore, the manner and proof of convergence of such element is unclear.

8.2 2/D Plane to Arch

In order to establish the validity of extracting the stress field for the curved members from the flat member field, the following derivation is provided to reduce the two dimensional stress field systematically to an arch element field. To start with, consider the following plane stress field in a rectangular Cartesian system:

$$\begin{aligned} \sigma_x &= \beta_1 + \beta_4 y \\ \sigma_y &= \beta_2 + \beta_5 x \\ \sigma_{xy} &= \beta_3 \end{aligned} \qquad (8.9)$$

In the previous chapter, the stress field given by Eq. (8.9) was shown to be well behaved for a rectangular geometry. Now the question is whether an equally well behaved stress field may be obtained through the direct application of the arch assumptions on the two dimensional field.

Limiting the current discussion to a constant

curvature arch, the necessary stress field must be expressed in a polar coordinate system (Figure 8-4). Dealing with stress components that must be valid in both flat and constant curvature configurations, the resulting stress field must be in the form

$$\sigma_s = \beta_1 + \beta_4 r + \frac{\Sigma_s(s,r)}{r}$$
$$\sigma_r = \beta_2 + \beta_5 s + \frac{\Sigma_r(s,r)}{r} \qquad (8.10)$$
$$\sigma_{sr} = \beta_3 + \frac{\Sigma_{sr}(s,r)}{r}$$

For the flat configuration, with $1/r \to 0$, Eq. (8.10) reduces to Eq. (8.9). Σ_s , Σ_r , Σ_{sr} can be determined through an application of the equilibrium equations in the polar coordinate system:

$$\frac{\partial \sigma_r}{\partial r} + \frac{\partial \sigma_{sr}}{\partial s} + \frac{\sigma_r - \sigma_s}{r} = 0$$
$$\frac{\partial \sigma_s}{\partial s} + \frac{\partial \sigma_{sr}}{\partial r} + \frac{2\sigma_{sr}}{r} = 0 \qquad (8.11)$$

An exact satisfaction of the equilibrium equation above is rather difficult. However, the application of the following two assumptions reduces Eq. (8.11) to a more manageable form:

(A) Truncate the stress field to include only the linear terms.

[Consistent with (8.9)]

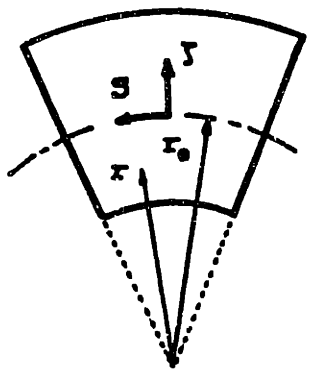

Figure 8-4. Polar Coordinate System Definition.

(B) Impose the thin arch condition.

$$\frac{\zeta}{r_o} \ll 1 \qquad \frac{1}{r} = \frac{1}{r_o}\left[1 - \frac{\zeta}{r_o} + \left(\frac{\zeta}{r_o}\right)^2 - \cdots\right]$$

$$\approx \frac{1}{r_o} \tag{8.12}$$

Implementing assumption B into Eq. (8.11) yields:

$$\begin{aligned} \frac{\partial \Sigma_\zeta}{\partial \zeta} + \frac{\partial \Sigma_{s\zeta}}{\partial s} + \sigma_\zeta - \sigma_s &= 0 \\ \frac{\partial \Sigma_s}{\partial s} + \frac{\partial \Sigma_{s\zeta}}{\partial \zeta} + 2\sigma_{s\zeta} &= 0 \end{aligned} \tag{8.13}$$

Assumption A together with Eq. (8.10) substituted into Eq. (8.13) yields

$$\begin{aligned} \frac{\partial \Sigma_\zeta}{\partial \zeta} + \frac{\partial \Sigma_{s\zeta}}{\partial s} + \beta_2 - \beta_1 &= 0 \\ \frac{\partial \Sigma_s}{\partial s} + \frac{\partial \Sigma_{s\zeta}}{\partial \zeta} + 2\beta_3 &= 0 \end{aligned} \tag{8.14}$$

The solution of Eq. (8.14) involves adding two additional β's. Note that there are four differential quantities with only two equations. The resulting stress field is

$$\sigma_s = \beta_1 + \beta_4 \zeta + \frac{\beta_7}{r_o} s$$

$$\sigma_\zeta = \beta_2 + \beta_5 s + \frac{\beta_1 - \beta_2 - \beta_6}{r_o} \zeta \qquad (8.15)$$

$$\sigma_{s\zeta} = \beta_3 + \frac{\beta_6}{r_o} s - \frac{2\beta_3 + \beta_7}{r_o} \zeta$$

The stress field for the arch may be obtained by imposing the stress constraints on Eq. (8.15), as follows:

From $\sigma_\zeta = 0$ obtain

$$\beta_2 = \beta_5 = 0$$

$$\beta_1 - \beta_6 = 0 \qquad (8.16)$$

For $\sigma_{s\zeta}$ being an even function in ζ obtain

$$2\beta_3 + \beta_7 = 0$$

Thus, Eq. (8.15) is reduced to

$$\sigma_s = \beta_1 - \frac{2\beta_3}{r_o} s + \zeta[\beta_4]$$

$$\sigma_{s\zeta} = \beta_3 + \frac{\beta_1}{r_o} s \qquad (8.17)$$

Notice that as $1/r \to 0$, Eq. (8.17) reduces to

$$\sigma_s = \beta_1 + \beta_4 \zeta$$

$$\sigma_{s\zeta} = \beta_3 \qquad (8.18)$$

which is identical to Eq. (8.10) with $\sigma_r = 0$ in the flat configuration. Furthermore, by starting with Eq. (8.18) and applying the reduced form of the equilibrium equation, Eq. (8.17) may be derived with much less effort.

In summary, the previous derivation demonstrates that an arch stress assumption may be obtained by mapping a flat beam to a curved configuration. To collapse a solid element stress field in a general curved three-dimensional domain to a general shell domain in the same manner is a difficult task. This brief coverage of an arch element provides a procedure which may be used to bypass such a technique. The starting point for a general shell stress assumption may be taken directly from a flat plate/plane stress combination. The sequence of steps required is:

(a) Start with a flat configuration stress field.

(b) Use equilibrium in the curved system to identify additional terms required.

(c) Truncate beyond some chosen order.

8.3 Flat to Curved Configuration

The present section deals with the stress resultants for a C^1 circular arch element, following the guidelines described in the previous section. First, starting with

the N and M distributions for a flat "circular" arch:

[FLAT ARCH]

$$N = \beta_1$$
$$M = \beta_2 + \beta_3 s \qquad (8.19)$$

the equilibrium equations for the circular arch may be applied.

$$\frac{dN}{ds} + \frac{1}{r_o}\frac{dM}{ds} = 0$$
$$\frac{d^2M}{ds^2} - \frac{1}{r_o} N = 0 \qquad (8.20)$$

Truncating beyond the linear terms, the stress field becomes

[LINEAR ARCH]

$$N = \beta_1 - \frac{\beta_3}{r_o} s$$
$$M = \beta_2 + \beta_3 s \qquad (8.21)$$

The above field represents a consistently derived assumed stress field for an arch element. The expansion is in polynomial form in s to model the arbitrary stress distribution. In the limit of vanishing curvature, the distribution reduces to the flat arch case which in turn may be related to the plate and solid element stress

fields.

For the two node C^1 arch element with three degrees of freedom at each node, the only consistent displacement field available is the TYPE A field presented in the first section:

$$w = \alpha_1 + \alpha_2 s + \alpha_3 s^2 + \alpha_4 s^3$$
$$u = \alpha_5 + \alpha_6 s \qquad (8.22)$$

Recall that for the assumed displacement formulation, the TYPE A field exhibited an extremely rigid behavior for the circular arch problem presented in Figure 8-3.

With the same displacement/strain field, TYPE A, two hybrid elements now are constructed using the flat and linear arch stress fields. The solutions to example problems are given in Figures 8-5 and 8-6.

Comparing the results shown in Figures 8-3, 8-5, and 8-6, several observations can be made:

(i) Both of the present hybrid elements with the TYPE A field give results similar to those of the assumed strain element, TYPE C. They are all much more accurate than the TYPE A, B, and D elements [81].

(ii) Both hybrid elements give the correct number of rigid body modes.

(iii) The accuracy of the linear arch stress

field is dramatic for a crude mesh. However, beyond a number of elements equal to 4, the results for the flat arch stress field are comparable to the other predictions shown.

Overall, the results indicate that a general shell element may be constructed by using an appropriate polynomial expansion for the displacement field in conjunction with a stress distribution based on constant curvature geometry. In another words, since both the flat and linear cases of arch elements are comparable, there should be close correspondence with linear and general cases. An accurate element may be constructed even with a geometric approximation included in the equilibrium equations used to constrain the stress field.

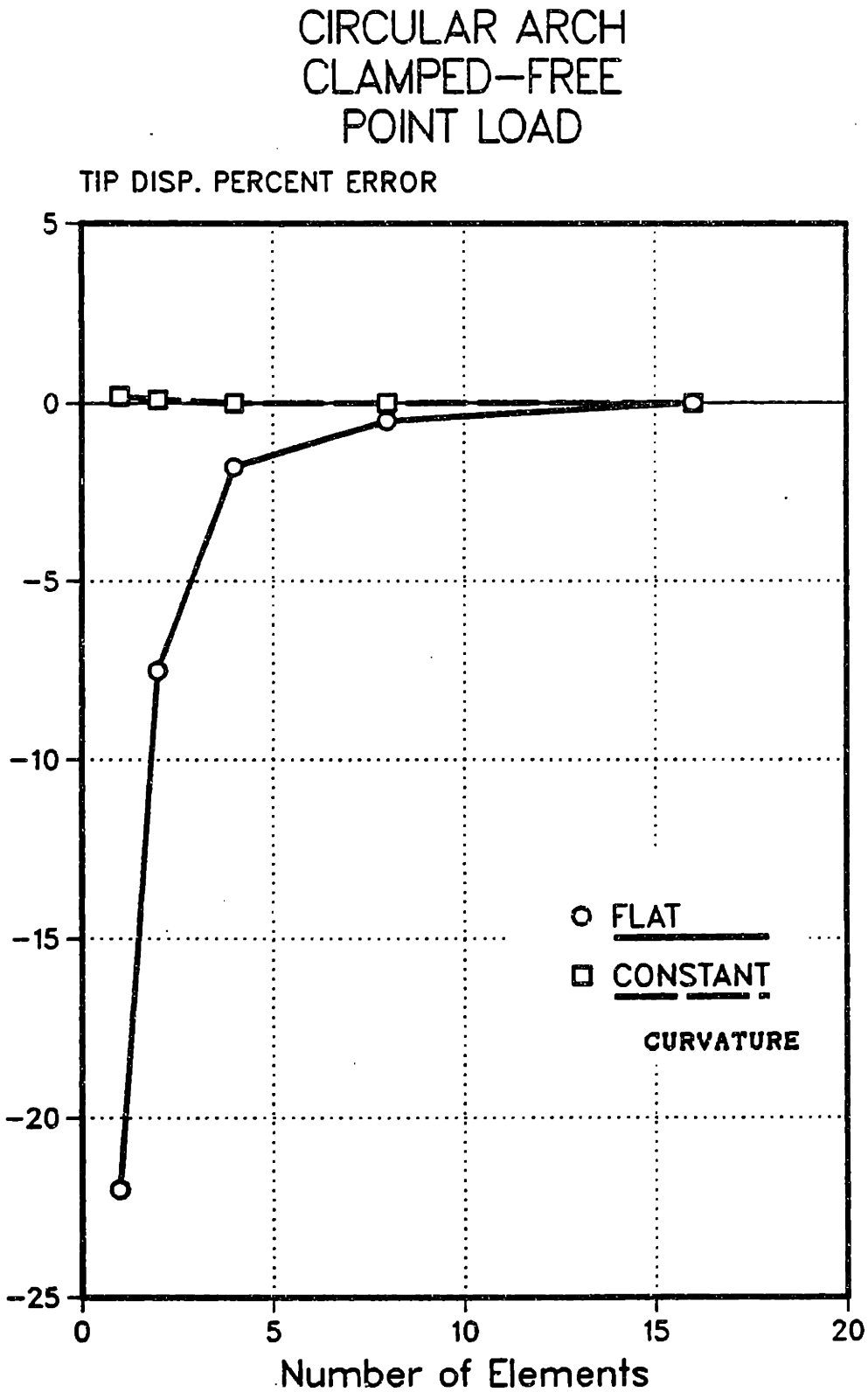

Figure 8-5. Error in Deflection under the Load for Clamped-Free Circular Arch Problem.

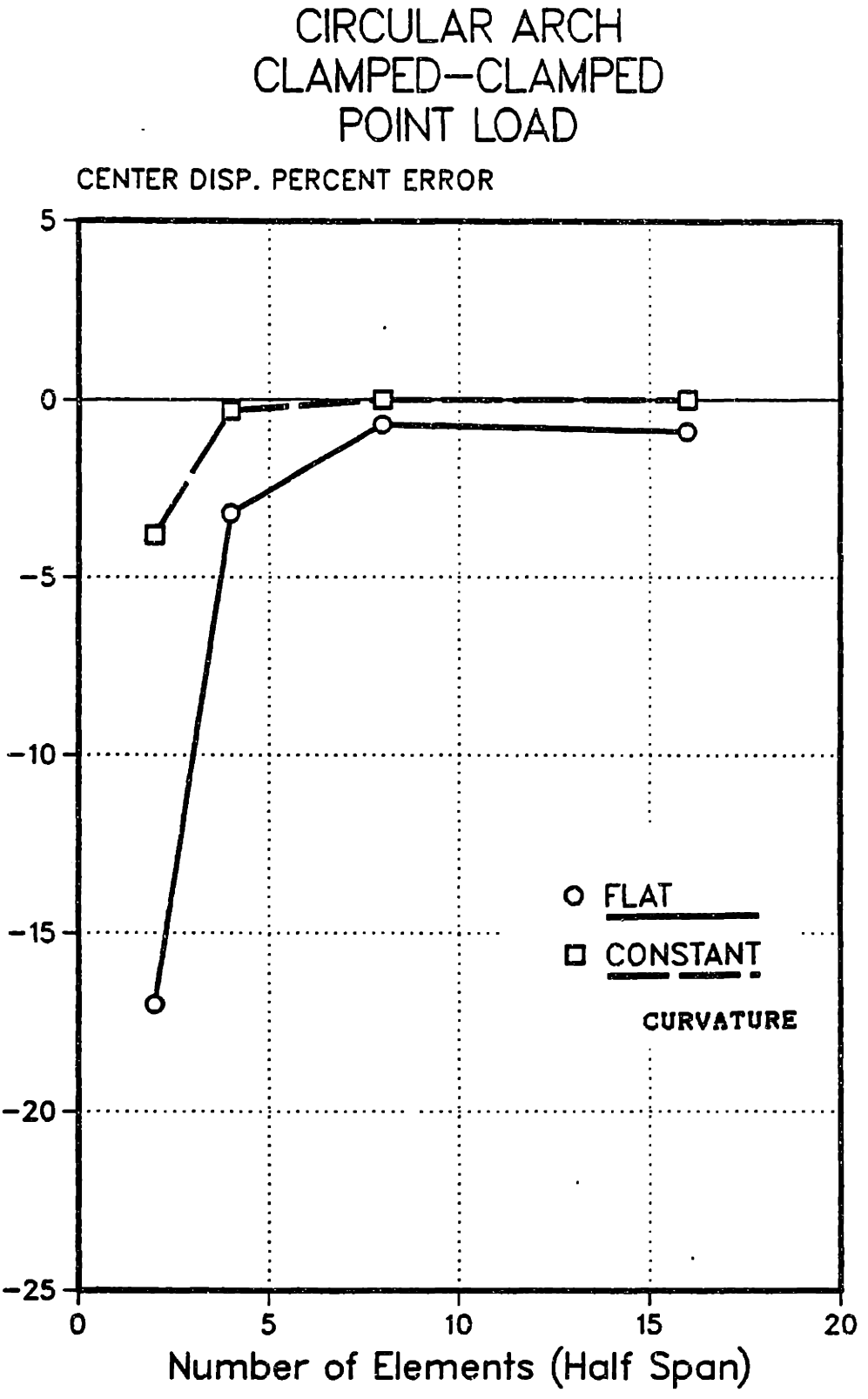

Figure 8-6. Error in Deflection under the Load for Clamped-Clamped Circular Arch Problem.

CHAPTER 9

SHELL ELEMENTS

The descriptive term "shell" refers to a thin, curved, three-dimensional solid domain which is relatively flexible in bending as compared with its stretching behavior. Such a contrast in stiffness introduces an extreme sensitivity to variations in geometry. In simplified terms, the difficulties of dealing with a shell domain may be summarized by the following two points:

* Complex thin curved domain.
* Discrepancy in bending and stretching behavior introducing sensitivity to geometry.

To deal with a shell domain, two types of 4-node shell elements are presently available:

(1) **FLAT SHELL** element

(2) **EXACT GEOMETRY SHELL** element

The flat shell element may be constructed by merging a C^0 plate element and a plane stress element. For practical general shell problems, the flat shell element is widely accepted due to its versatility to approximate

an arbitrary geometry. However, to reduce the severity of the geometric approximation of the shell domain, one is required to use a fine mesh discretization. For the problems sensitive to geometric approximation effects, the flat shell element solutions tend to converge much too slowly for practical applications [85].

In the other extreme, the exact geometry shell elements exchange versatility of the flat shell elements for an exact representation of a particular geometry. Under this category, the elements constructed with compatible displacement assumption exhibit overly rigid behavior. Furthermore, the polynomial expansion of the compatible displacements can only approximate the transcendental functions required to satisfy rigid body motion correctly. These inadequacies are suppressed only when the element dimensions approach the thickness dimension of the shell [86-90].

In a manner similar to the arch elements developed and discussed in the previous chapter, modifications to the polynomial approximation for the assumed fields can be carried out to include an exact representation of rigid body modes [91,92]. An immediate consequence of this modification is an acceptance of non-conforming assumed displacements. Within the scope of such a restriction on the geometry, this modification is regarded as being successful [85]. Yet, due to the non-conforming nature and the lack of versatility, these

types of elements have not commanded confidence nor achieved popularity.

In the present chapter, a general shell element that combines versatility with more accurate approximation of the geometry is developed. This achievement is made possible through an application of the hybrid stress method by using the Hellinger-Reissner principle. The first section of Chapter 9 briefly presents the Koiter-Sander shell theory and the corresponding variational principles. The second section describes the details of the element construction. The final section provides a set of numerical examples to demonstrate the effectiveness of this shell element. The examples are carefully chosen to cover a broad range of geometrically sensitive shell problems.

9.1 Shell Formulation

A shell in a reference configuration may be described by a middle surface and a set of normals defined pointwise on the surface. Material filaments aligned with the normals establish the bounding surfaces to form a three-dimensional body. The length of the filaments, called thickness, is assumed to be much smaller than any characteristic length of the reference surface. Although the description may sound artificial, it provides a lucid mechanical model of the shell continuum.

Historically, the major motivating factor for the development of a general shell theory stems from the reduction of three-dimensional problems to one characterized by two-dimensional equations. However, in the regime of the finite element method, further motivations arise from a need to eliminate relatively small terms to preserve numerical accuracy in finite digit arithmatic.

The linear equations of shell theory have been derived by many authors [7,93-95]. Because of variations in rigor concerning the reduction to first approximation equations (i.e., linearization), a variety of equations occurs in the literature. A widely accepted form for a first approximation to shells is known as the

Koiter-Sanders theory [96-99]. In the Koiter-Sanders theory, the stress and strain resultants are defined as work conjugates through the virtual work principle and the use of symmetric tensors.

In order to construct the shell theory in a manner convenient for and consistent with the intended finite element domain discretization, the natural element coordinate system will be used as general shell coordinates. As a result, only two coordinate systems, reference and natural, are required. In contrast, past endeavors have required the use of a third system of coordinates. The usual approach involves mapping shell coordinates, such as cylindrical or spherical, to natural coordinates for numerical integration. As described in later discussion, the major difference arise in the treatment of the element distortion. The element distortion directly effects the shell coordinate system.

9.1.1 Definition of Shell Coordinates

A position vector to a general point in the shell continuum may be expressed as a vector sum of a position vector to the middle surface and a vector along the normal to the middle surface.

$$\underset{\sim}{r}(\xi^1, \xi^2, \zeta) = \underset{\sim}{r}_0(\xi^1, \xi^2) + \zeta\, \underset{\sim}{n}(\xi^1, \xi^2) \qquad (9.1)$$

where

$\underset{\sim}{r}$ = position vector

$\underset{\sim}{r}_o$ = position vector to the middle surface

$\underset{\sim}{n}$ = unit normal vector to the middle surface

ζ = coordinate defined along the normal $\underset{\sim}{n}$

ξ^1, ξ^2 = the middle surface coordinates

To re-emphasize, the coordinates are defined strictly within the discretized domain of a single element.

$$\begin{aligned} \xi^1 &: [\ -1\ ,\ 1\ ] \\ \xi^2 &: [\ -1\ ,\ 1\ ] \\ \xi^3 \equiv \zeta &: [\ -h/2\ ,\ h/2\ ] \end{aligned} \qquad (9.2)$$

where

h = thickness

As provided, ξ^1, ξ^2, and ζ serve as both element and shell coordinates. Information regarding element distortion remains preserved through the definition of a general shell theory in a discrete domain. The coordinates are graphically displayed in Figure 9-1.

The base vectors are defined by the following convention:

$\underset{\sim}{e}_i$ = Rectangular Cartesian Base Vectors

For the shell system, the base vectors are

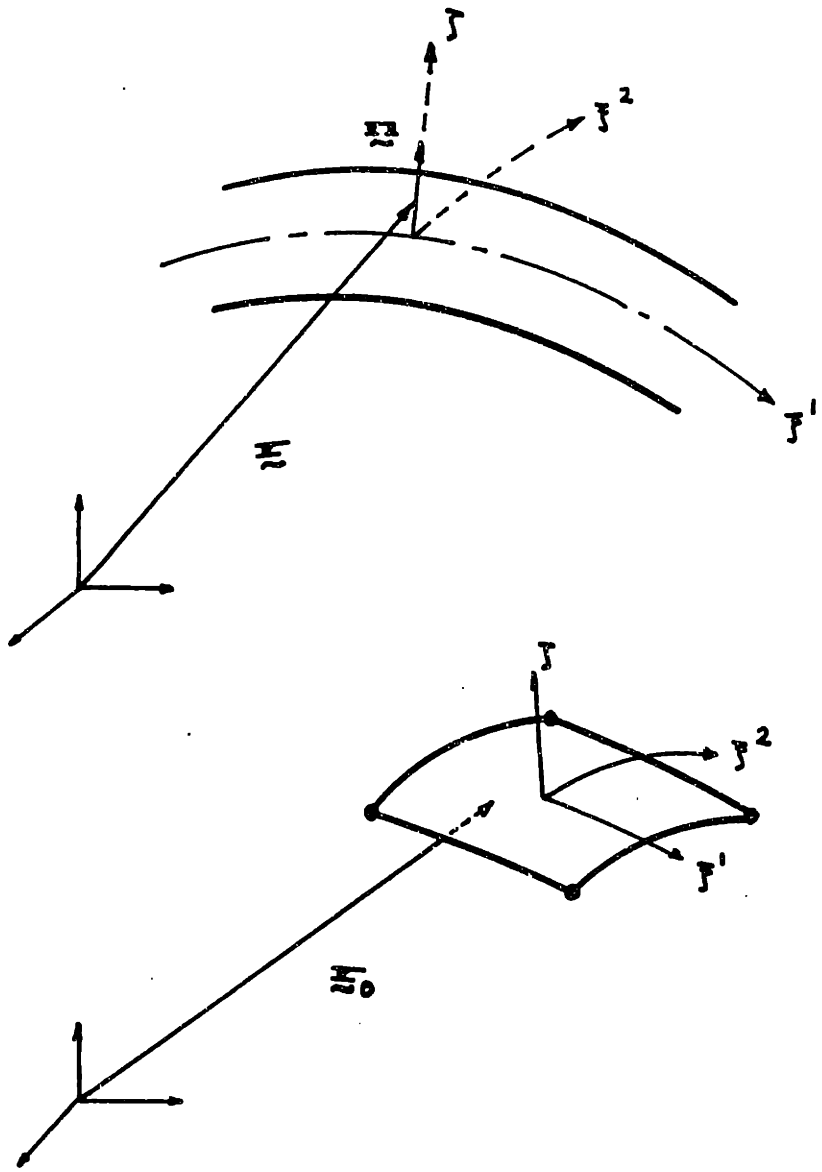

Figure 9-1. Shell Coordinate System.

$$\underset{\sim}{g}_\alpha = \frac{\partial \underset{\sim}{r}}{\partial \xi^\alpha} = \frac{\partial \underset{\sim}{r}_0}{\partial \xi^\alpha} + \zeta \frac{\partial \underset{\sim}{n}}{\partial \xi^\alpha}$$

$$\underset{\sim}{g}_3 = \frac{\partial \underset{\sim}{r}}{\partial \zeta} = \underset{\sim}{n} \qquad (9.3)$$

On the middle surface,

$$\underset{\sim}{a}_\alpha = \frac{\partial \underset{\sim}{r}_0}{\partial \xi^\alpha} \qquad (9.4)$$

The Greek indicies range (1,2). Throughout this section the summation convention of repeated indicies is implied unless noted otherwise.

9.1.2 Koiter-Sanders Theory

Since the derivation of the Koiter-Sanders theory is widely available in the literature, only the results are presented for the sake of uniform notation and conciseness. Starting with kinematic quantities, the displacements are separated into components tangent and normal to the middle surface, and rotation of the normal vector.

$$\underset{\sim}{V}(\xi^\alpha, \zeta) = \underset{\sim}{V}^0(\xi^\alpha) + \zeta(\underset{\sim}{N} - \underset{\sim}{n}) \qquad (9.5)$$

where

$$\underset{\sim}{V}^{\circ} = V^{\circ\gamma}\,\underset{\sim}{a}_{\gamma} + w\,\underset{\sim}{n}$$

$$\underset{\sim}{N} - \underset{\sim}{n} = -\theta_{\gamma}\,\underset{\sim}{a}^{\gamma} = -\theta^{\gamma}\,\underset{\sim}{a}_{\gamma}$$

$$\theta_{\sigma} = w_{,\sigma} + V^{\circ}_{\gamma}\, b^{\gamma}_{\sigma}$$

$V^{\circ\gamma}$ = Tangential components of displacement

w = Normal component of displacement

θ^{γ} = Components describing the rotation of the normal under deformation

b^{γ}_{σ} = Mixed components of second fundamental form

In component form, strains are separated into membrane and bending components:

$$\gamma_{\alpha\beta} = \gamma^{\circ}_{\alpha\beta} + \zeta\, k_{\alpha\beta} \qquad (9.6)$$

where

$$\gamma^{\circ}_{\alpha\beta} = \tfrac{1}{2}\left(V^{\circ}_{\alpha,\beta} + V^{\circ}_{\beta,\alpha}\right) - w\, b_{\alpha\beta}$$

$$k_{\alpha\beta} = -\tfrac{1}{2}\left(\theta_{\alpha,\beta} + \theta_{\beta,\alpha}\right) - \tfrac{1}{2}\left(b^{\sigma}_{\alpha}\omega_{\beta\sigma} + b^{\sigma}_{\beta}\omega_{\alpha\sigma}\right)$$

$$\theta_{\alpha} = w_{,\alpha} + V^{\circ}_{\sigma}\, b^{\sigma}_{\alpha}$$

$$\omega_{\alpha\beta} = \tfrac{1}{2}\left(V^{\circ}_{\beta,\alpha} - V^{\circ}_{\alpha,\beta}\right)$$

In the first approximation of the linear constitutive relation, the stress resultants turn out to be decoupled,

as follows:

$$\ell^{\alpha\beta} = h\,\Omega^{\alpha\beta\sigma\tau}\,\gamma^{0}_{\sigma\tau}$$
$$m^{\alpha\beta} = \frac{h^3}{12}\,\Omega^{\alpha\beta\sigma\tau}\,k_{\sigma\tau} \qquad (9.7)$$

where

$$\Omega^{\alpha\beta\sigma\tau} = \frac{E}{2(1+\nu)}\left\{a^{\alpha\sigma}a^{\beta\tau} + a^{\alpha\tau}a^{\beta\sigma} + \frac{2\nu}{1-\nu}\,a^{\alpha\beta}a^{\sigma\tau}\right\}$$

The Principle of Virtual Work provides a most direct approach for the derivation of the equilibrium equations and the boundary conditions:

$$\delta W_{int} = \delta W_{ext} \qquad (9.8)$$

where

$$\begin{aligned}\delta W_{int} &= \int_A \left[\ell^{\alpha\beta}\,\delta\gamma^{0}_{\alpha\beta} + m^{\alpha\beta}\,\delta k_{\alpha\beta}\right] dA \\ &= \int_A \Big\{\Big[-\ell^{\alpha\beta}{}_{,\alpha} + m^{\alpha\sigma}{}_{,\alpha}\,b^{\beta}_{\sigma} + \tfrac{1}{2}\left(m^{\alpha\sigma}b^{\beta}_{\sigma}\right)_{,\alpha} \\ &\qquad - \tfrac{1}{2}\left(m^{\beta\alpha}b^{\sigma}_{\alpha}\right)_{,\sigma}\Big]\delta v^{0}_{\beta} \\ &\qquad + \left[-\ell^{\alpha\beta}b_{\alpha\beta} - m^{\alpha\beta}{}_{,\beta\alpha}\right]\delta w\Big\}\,dA \\ &\quad + \int_{\partial A}\Big\{\left[\ell^{\alpha\beta} - \tfrac{1}{2}\,m^{\alpha\sigma}b^{\beta}_{\sigma} + \tfrac{1}{2}\,m^{\beta\sigma}b^{\alpha}_{\sigma}\right]\nu_{\alpha}\,\delta v^{0}_{\beta} \\ &\qquad - \nu_{\alpha}\,m^{\alpha\beta}\,\delta\theta_{\beta} + \nu_{\alpha}\,m^{\alpha\beta}{}_{,\beta}\,\delta w\Big\}\,ds\end{aligned}$$

and

$$\delta W_{ext} = \int_{\partial A_\sigma} \{ \bar{\ell}^{\alpha\beta} \nu_\alpha \delta r^0_\beta - \nu_\alpha \bar{m}^{\alpha\beta} \delta\theta_\beta + \nu_\alpha \bar{g}^\alpha \delta w \} ds - \int_A \{ F^\alpha \delta r_\alpha + F^3 \delta w \} dA$$

where

ν_α = Components of the Boundary Normal

$(\bar{\ })$ = Prescribed Quantities

F^i = Contribution from the Body Forces

The surface integral terms provide the equilibrium equations, and the boundary integral terms provide the boundary conditions as shown in Eqs. (9.9) and (9.10).

$$\ell^{\alpha\beta}{}_{,\alpha} - m^{\alpha\sigma}{}_{,\alpha} b^\beta_\sigma + \tfrac{1}{2}\left(m^{\beta\sigma} b^\alpha_\sigma - m^{\alpha\sigma} b^\beta_\sigma\right)_{,\alpha} + F^\beta = 0$$

$$m^{\alpha\beta}{}_{,\beta\alpha} + \ell^{\alpha\beta} b_{\alpha\beta} + F^3 = 0 \qquad \text{in } A \qquad (9.9)$$

$$\bar{\ell}^{\alpha\beta}\nu_\alpha = \left[\ell^{\alpha\beta} - \tfrac{1}{2} m^{\alpha\sigma} b^\beta_\sigma + \tfrac{1}{2} m^{\beta\sigma} b^\alpha_\sigma\right]\nu_\alpha$$

$$\bar{m}^{\alpha\beta}\nu_\alpha = m^{\alpha\beta}\nu_\alpha \qquad \text{on } \partial A_\sigma$$

$$\nu_\alpha \bar{g}^\alpha = \nu_\alpha m^{\alpha\beta}{}_{,\beta} \qquad (9.10)$$

Equations (9.5) to (9.10) provide the governing equations of the general shell theory outlined by Koiter and Sanders [96-99].

9.1.3 Variational Principles

Conceptually, the variational principles for the shell theory correspond to the functionals derived for a general solid continuum. The components, in the functionals for the shell theory, are separated into membrane and bending contributions. Otherwise, the admissibility conditions and the resulting Euler equations are the same. To emphasize the correspondence, the functionals are shown in Eqs. (9.11), (9.12), and (9.13), and are left in recognizable form.

The condition of kinematic admissibility and the constitutive relations applied to the statement of virtual work Eq. (9.8) yield the principle of minimum potential energy, π_p :

$$
\begin{aligned}
-\pi_p(v_\beta^\circ, w) = \int_A \Big\{ \tfrac{1}{2}\Big[h\,\Omega^{\alpha\beta\sigma\tau}\,\gamma^{\circ}_{\sigma\tau}\,\gamma^{\circ}_{\alpha\beta} + \frac{h^3}{12}\,\Omega^{\alpha\beta\sigma\tau}\,k_{\sigma\tau}\,k_{\alpha\beta}\Big] \\
- F^\alpha v_\alpha - F^3 w \Big\}\, dA \\
- \int_{S_\sigma} \big[\bar{l}^{\alpha\beta}\,\nu_\alpha\,v_\beta - \nu_\alpha\,\bar{m}^{\alpha\beta}\,\theta_\beta \qquad (9.11) \\
+ \nu_\alpha\,\bar{q}^\alpha\,w \big]\, ds
\end{aligned}
$$

The Hu-Washizu principle, π_G , may be obtained by relaxing the strain-displacement relations:

$$\pi_G(v_\beta, w, \gamma^\circ_{\sigma\tau}, k_{\sigma\tau}, l^{\alpha\beta}, m^{\alpha\beta}) =$$

$$\int_A \Big\{ \tfrac{1}{2}\Big[h\,\Omega^{\alpha\beta\sigma\tau}\gamma^\circ_{\sigma\tau}\gamma^\circ_{\alpha\beta} + \tfrac{h^3}{12}\Omega^{\alpha\beta\sigma\tau}k_{\sigma\tau}k_{\alpha\beta}\Big]$$
$$- l^{\alpha\beta}\Big[\gamma^\circ_{\alpha\beta} - \tfrac{1}{2}\big(v_{\alpha,\beta} + v_{\beta,\alpha} - 2w\,b_{\alpha\beta}\big)\Big]$$
$$- m^{\alpha\beta}\Big[k_{\alpha\beta} - \tfrac{1}{2}\big((\theta_{\alpha,\beta}+\theta_{\beta,\alpha}) + (b^\sigma_\alpha\omega_{\beta\sigma} + b^\sigma_\beta\omega_{\alpha\sigma})\big)\Big]$$
$$- F^\alpha v_\alpha - F^3 w\Big\}\,dA$$
$$- \int_{S_\sigma}\big[\bar{l}^{\alpha\beta}\nu_\alpha v_\beta - \nu_\alpha\bar{m}^{\alpha\beta}\theta_\beta + \nu_\alpha\bar{g}^\alpha w\big]\,ds$$

(9.12)

The Hellinger-Reissner principle, π_R , results with application of the constitutive relations:

$$\pi_R(v_\beta, w, l^{\alpha\beta}, m^{\alpha\beta}) =$$

$$\int_A \Big\{ -\tfrac{1}{2}\Big[\tfrac{1}{2}\Sigma_{\alpha\beta\sigma\tau}\,l^{\sigma\tau}l^{\alpha\beta} + \tfrac{12}{h^3}\Sigma_{\alpha\beta\sigma\tau}\,m^{\alpha\beta}m^{\sigma\tau}\Big]$$
$$+ l^{\alpha\beta}\gamma_{\alpha\beta} + m^{\alpha\beta}k_{\alpha\beta} - F^\alpha v_\alpha - F^3 w\Big\}\,dA$$
$$- \int_{S_\sigma}\big[\bar{l}^{\alpha\beta}\nu_\alpha v_\beta - \nu_\alpha\bar{m}^{\alpha\beta}\theta_\beta + \nu_\alpha\bar{g}^\alpha w\big]\,ds$$

(9.13)

Derived via the virtual work statement, the functionals in Eqs. (9.11), (9.12), and (9.13) are consistent with the first-order-approximation shell behavior governed by the Koiter-Sanders theory.

9.2 General Shell Element

The construction of a general shell element imposes difficulties not readily solved by standard modifications used for isoparametric elements. Presently, the geometrically complex domain inherent in general shell problems requires some gross geometric simplifications or other strict limitations. In fact, flat shell elements are the most popular element for shell problems. Such popularity stems from the ease with which such elements can be applied to approximate general shells.

In the following derivation of a general shell element, the set of geometric information required for element definition is minimized. The geometric information consists of a position vector and a normal vector at each node. Additional information required to fix the bi-normal of a three-dimensional space curve is obtained from the position vector to the midpoint of the boundary. By the construction of two surface tangents at each node, the element curvature may be approximated using a bi-cubic shape interpolation function.

The resulting 4-node, 20 degrees of freedom shell element falls under the catagory of C^1 continuity; this general shell element is constructed by using the Hellinger-Reissner principle. The internal displacement field is incompatible, and the stress field does not

satisfy the pointwise equilibrium. The development, however, is rigorous and consistent with the Hellinger-Reissner variational principle.

9.2.1 Element Geometry

In the following construction, the element geometry is defined completely by the position vector and the normal provided at the corner nodes and the position vector to the midside nodes. This is the minimum amount of information needed for shell element geometry definition. The corresponding surface tangents are calculated from these nodal information. Figure 9-2 illustrates graphically the element geometry, and Figure 9-3 provides additional details for unique tangent vectors. As shown, a plane of tangent vectors is defined by a directed vector to the mid-node and a directed vector to an adjacent corner node, $\underset{\sim}{s}$. Within this plane, a tangent vector, $\underset{\sim}{t}$, is positioned orthogonally to the normal.

The element middle surface may be obtained through interpolation of the nodal quantities

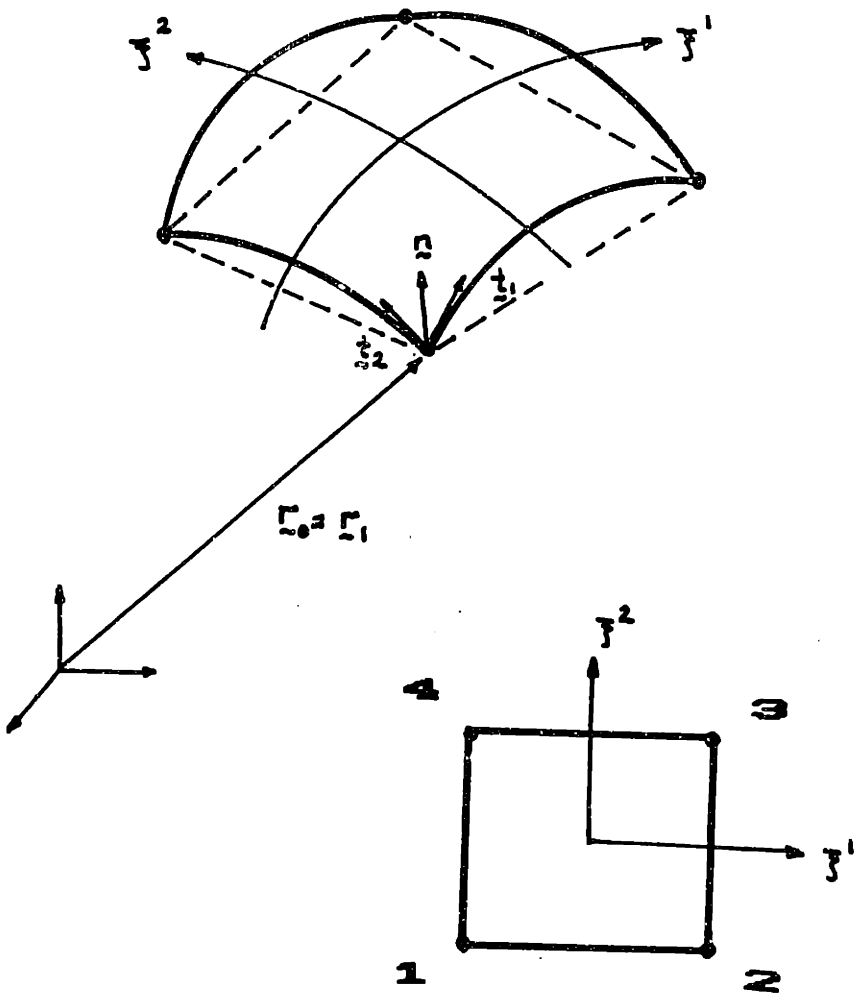

Figure 9-2. Element Geometry.

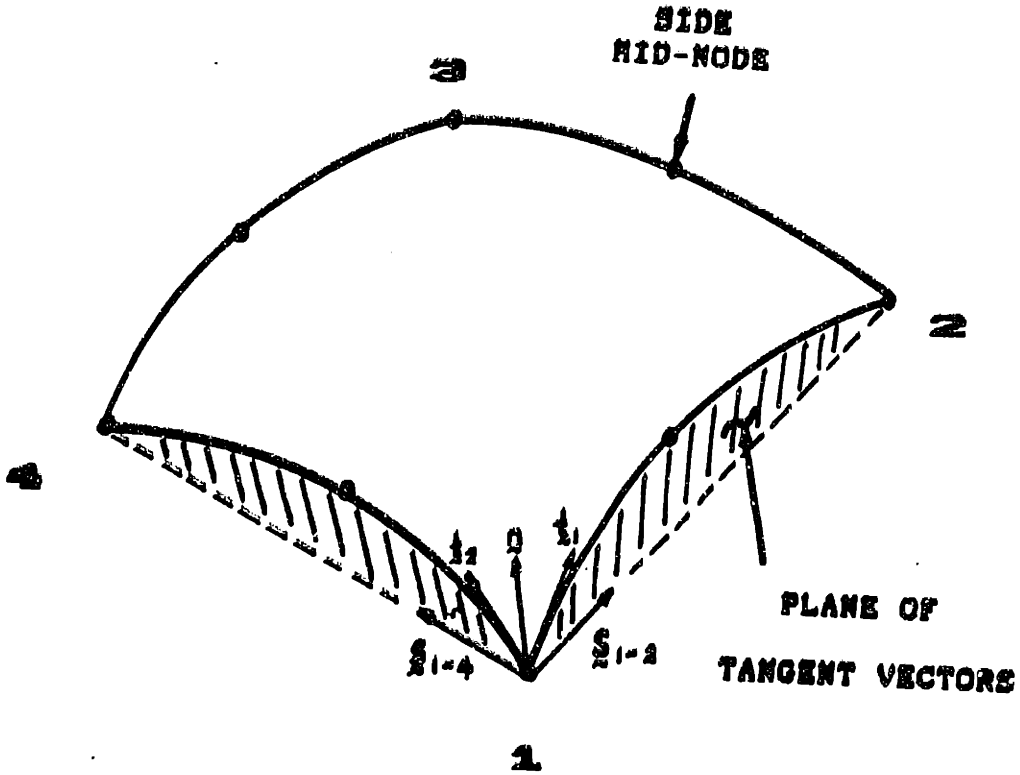

Figure 9-3. Tangent Vectors.

$$\underset{\sim}{r}_o(\xi^1,\xi^2) = \underset{\sim}{N}(\xi^1,\xi^2) \begin{Bmatrix} (\underset{\sim}{r})_1 \\ (\frac{\partial \underset{\sim}{r}}{\partial \xi^1})_1 \\ (\frac{\partial \underset{\sim}{r}}{\partial \xi^2})_2 \\ (\underset{\sim}{r})_2 \\ \vdots \end{Bmatrix} = \underset{\sim}{N}\ \underset{\sim}{R} \qquad (9.14)$$

where

$(\underset{\sim}{r})_i$ = Position vector to node i

$\frac{\partial \underset{\sim}{r}}{\partial \xi^1} = \Lambda_1\ \underset{\sim}{t}_1$

$\frac{\partial \underset{\sim}{r}}{\partial \xi^2} = \Lambda_2\ \underset{\sim}{t}_2$

$\underset{\sim}{N}$ = 12-parameter bi-cubic interpolation function (7.23)

Λ_i = Stretch factor

For the present element, the Adini functions [38] are chosen as the interpolation functions. Since the same functions will be used for the displacement interpolation, the nature of this element is isoparametric. The stretch factor, Λ_i, may be obtained from the following linear surface approximation:

$$\Lambda_i = \frac{|\underset{\sim}{r}_k - \underset{\sim}{r}_l|}{2} \qquad (9.16)$$

Nodes k and l define the natural coordinate, ξ^i, direction. Alternately, a constant curvature

approximation may be used to calculate the stretch factors:

$$\Lambda_i = \frac{\bar{\theta}}{2 \sin \bar{\theta}} \left| \underset{\sim}{r}_k - \underset{\sim}{r}_\ell \right| \qquad (9.17)$$

where

θ_ℓ = Angle between the tangent at node ℓ and the vector from node ℓ to k.

$$\bar{\theta} = \tfrac{1}{2} \left\{ |\theta_\ell| + |\theta_{k_2}| \right\}$$

In the flat plate limit, $\bar{\theta} \to 0$; hence, Eq. (9.17) reduces to Eq. (9.16). Since the difference in computational effort between the above two approximations is negligible, Eq. (9.17) should be used for the calculation of the stretch factors.

The relevant formulae of the theory of surfaces in connection with the element derivation are summarized below. These equations are displayed in a form suitable for numerical computation. To begin with, the covariant base vectors of the middle surface are defined by

$$\underset{\sim}{a}_\alpha = \frac{\partial \underset{\sim}{r}_o}{\partial \xi^\alpha} = \frac{\partial \underset{\sim}{N}}{\partial \xi^\alpha} \underset{\sim}{R} \qquad (9.18)$$

The resulting vectors are used to calculate the metric tensors and the contravariant base vectors.

$$a_{\alpha\beta} = \underset{\sim}{a}_\alpha \cdot \underset{\sim}{a}_\beta$$

$$[a^{\alpha\beta}] = [a_{\alpha\beta}]^{-1} \qquad (9.19)$$

$$\underset{\sim}{a}^\alpha = a^{\alpha\beta}\, \underset{\sim}{a}_\beta \qquad (9.20)$$

The element of surface area is then given by

$$dA = \sqrt{a}\; d\xi^1 d\xi^2 \qquad (9.21)$$

where

$$a = \det [a_{\alpha\beta}]$$

The unit normal vector of the surface is given by

$$\underset{\sim}{n} = \frac{\underset{\sim}{a}_1 \times \underset{\sim}{a}_2}{\sqrt{a}} \qquad (9.22)$$

The formulae of Weingarten and Gauss

$$\frac{\partial \underset{\sim}{a}_\alpha}{\partial \xi^\beta} = \left\{ \begin{matrix} \lambda \\ \alpha\beta \end{matrix} \right\} \underset{\sim}{a}_\lambda + b_{\alpha\beta}\, \underset{\sim}{n}$$

$$\frac{\partial \underset{\sim}{a}^\alpha}{\partial \xi^\beta} = - \left\{ \begin{matrix} \alpha \\ \lambda\beta \end{matrix} \right\} \underset{\sim}{a}^\lambda + b^\alpha_\beta\, \underset{\sim}{n} \qquad (9.23)$$

$$\frac{\partial \underset{\sim}{n}}{\partial \xi^\alpha} = - b^\beta_\alpha\, \underset{\sim}{a}_\beta$$

provide the coefficients of the second fundamental form and the Christoffel symbols of the second kind.

$$b_{\alpha\beta} = \frac{\partial \underset{\sim}{a}_\alpha}{\partial \xi_\beta} \cdot \underset{\sim}{n}$$

$$= \left(\frac{\partial^2 \underset{\sim}{N}}{\partial \xi_\alpha \partial \xi_\beta} \underset{\sim}{R} \right) \cdot \underset{\sim}{n} \qquad (9.24)$$

$$\left\{ \begin{matrix} \lambda \\ \alpha\beta \end{matrix} \right\} = \frac{\partial \underset{\sim}{a}_\alpha}{\partial \xi_\beta} \cdot \underset{\sim}{a}^\lambda \qquad (9.25)$$

The above equations provide necessary information regarding element geometry, with a generality matching that for flat shells. In the present shell surface interpolation, note that the element geometry information has been fully utilized.

9.2.2 Assumed Displacement/Strain

In a sense, a shell element is an extension of plane stress and plate elements combined to capture membrane and bending behavior (Figure 9-4). To define the nodal degrees of freedom, re-examine these elements. An implied direction associated with each degrees of freedom corresponds to global directions. Such a definition serves two purposes. First, the element assembly requires a unique set and, secondly, the continuity of displacements may be addressed. A basic question regarding continuity involves the selection of appropriate interpolation functions in conjunction with nodal the degrees of freedom. The quantities

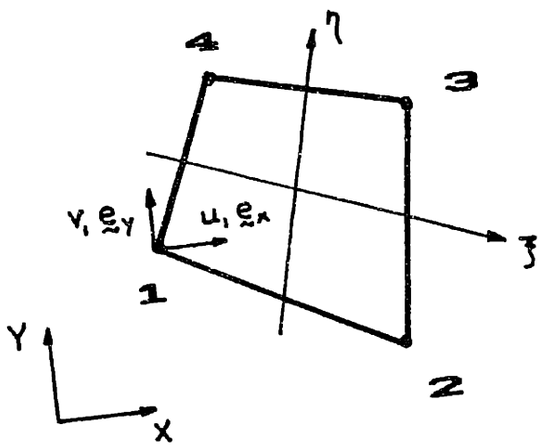

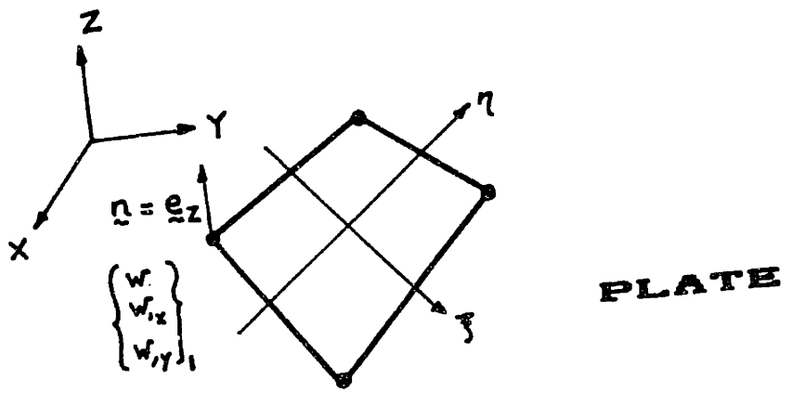

Figure 9-4. Nodal Degrees of Freedom for Plane and Plate Elements.

interpolated must be associated with the global directions. For example, in a plane-stress element:

$$u = \sum_i N_i(\xi,\eta)\, u_i$$
$$v = \sum_i N_i(\xi,\eta)\, v_i \qquad (9.26)$$

where

u_i, v_i = Nodal degrees of freedom

In more precise notation, the above expression may be rewritten as

$$u\,\underset{\sim}{e}_1 = \sum_i N_i\,(u\,\underset{\sim}{e}_1)_i$$
$$v\,\underset{\sim}{e}_2 = \sum_i N_i\,(v\,\underset{\sim}{e}_2)_i \qquad (9.27)$$

where

$\underset{\sim}{e}_i$ = Cartesian base vectors

$(u\,\underset{\sim}{e}_1)_i$, $(v\,\underset{\sim}{e}_2)_i$ = Nodal degrees of freedom

The associated directions, $\underset{\sim}{e}_1$, and $\underset{\sim}{e}_2$, are explicitly included in the nodal degrees of freedom. Since these directions are Cartesian base vectors of the reference coordinate system, the degrees of freedom at each node are defined a priori for all elements associated with that node. Thus, along the boundary, continuity of such a pre-defined quantity is meaningful. The difference in

the two notations (9.26) and (9.27) is much more dramatic for general shell elements.

In order to be consistent with previous analysis of plane stress and plate displacement interpolations, the present shell element should contain compatible in-plane displacement interpolations, and incompatible out-of-plane displacement interpolations. For the out-of-plane displacement, only the normal derivative is incompatible. With such consistency, the shell element will degenerate into the plane stress and plate combination for the flat configuration.

Upon closer examination of a distorted shell element in arbitrary free space (Figure 9-5), a problem concerning such a choice of interpolations is apparent. To be unique globally, nodal degrees of freedom with corresponding directions must be clearly defined. Without providing tangents at each node, directed tangents, obtained through the technique described previously, from A-B and B-C in Figure 9-5 are not parallel at B. Because of multiplicity, covariant or contravariant components of in-plane displacements cannot be interpolated. The only option is to interpolate the Cartesian components linearly to achieve compatibility, and then to extract the in-plane contribution. For the out-of- plane displacements, the assigned normals enable one to use direct interpolation of the normal components.

Specific details necessary for this computation are

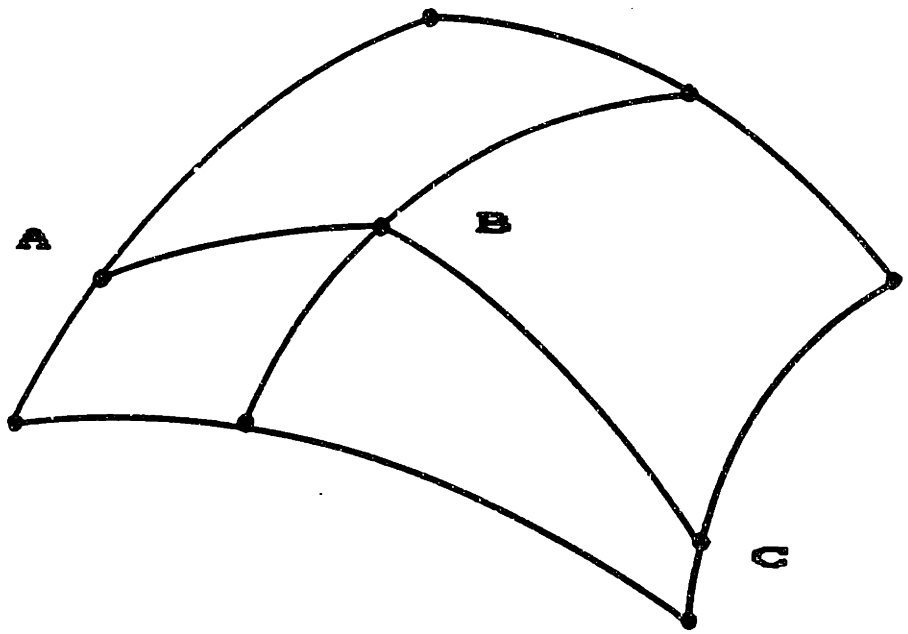

Figure 9-5. Distorted Shell Elements.

outlined below. First, the global degrees of freedom are defined at each node as

$$\begin{Bmatrix} u_1 \ \underset{\sim}{e}_1 \\ u_2 \ \underset{\sim}{e}_2 \\ u_3 \ \underset{\sim}{e}_3 \\ \hat{\theta}_1 \ \underset{\sim}{f}^1 \\ \hat{\theta}_2 \ \underset{\sim}{f}^2 \end{Bmatrix} \tag{9.28}$$

where

$u_i \ \underset{\sim}{e}_i$ = Cartesian components

$\hat{\theta}_i$ = Rotation

$\underset{\sim}{f}^i$ = Vectors in the tangent plane defined uniquely

These global degrees of freedom may be expressed in terms of other nodal components through local basis change. Two sets used for the present element are

$$\begin{Bmatrix} V^{o1} \ \underset{\sim}{a}_1 \\ V^{o2} \ \underset{\sim}{a}_2 \\ w \ \underset{\sim}{n} \\ \theta_1 \ \underset{\sim}{a}^1 \\ \theta_2 \ \underset{\sim}{a}^2 \end{Bmatrix} \tag{9.29}$$

where

$\underset{\sim}{a}_i$ = Surface base vectors

$\underset{\sim}{n}$ = Normal to the surface

$\underset{\sim}{a}^i$ = Contravariant surface base vectors

and

$$\begin{Bmatrix} v^{01} & \underset{\sim}{a}_1 \\ v^{02} & \underset{\sim}{a}_2 \\ w & \underset{\sim}{n} \\ w_{,1} & \underset{\sim}{a}^1 \\ w_{,2} & \underset{\sim}{a}^2 \end{Bmatrix} \qquad (9.30)$$

The relations used for transformations are

$$\begin{aligned} v^{0i} &= u^i \left(\underset{\sim}{e}_i \cdot \underset{\sim}{a}^i \right) \\ \theta_\beta &= \hat{\theta}_\alpha \left(\underset{\sim}{f}^\alpha \cdot \underset{\sim}{a}_\beta \right) \\ \theta_\sigma &= w_{,\sigma} + v^{0\gamma} b_{\gamma\sigma} \end{aligned} \qquad (9.31)$$

Functionally, as result of the compatibility requirement stated, one obtains

$$\begin{aligned} v^{0\alpha} &= v^{0\alpha} (u_1, u_2, u_3) \\ w &= w (w, w_{,1}, w_{,2}) \end{aligned} \qquad (9.32)$$

Before proceeding further, recall the following strain-displacement relations for the Koiter-Sanders theory:

$$\begin{aligned} \gamma^0_{\alpha\beta} &= \tfrac{1}{2} \left(v^0_{\alpha,\beta} + v^0_{\beta,\alpha} \right) - w b_{\alpha\beta} \\ k_{\alpha\beta} &= -\tfrac{1}{2} \left(\theta_{\alpha,\beta} + \theta_{\beta,\alpha} \right) - \tfrac{1}{2} \left(b^\sigma_\alpha \omega_{\beta\sigma} + b^\sigma_\beta \omega_{\alpha\sigma} \right) \end{aligned} \qquad (9.33)$$

where

$$\theta_\alpha = w_{,\alpha} + v^0_\sigma b^\sigma_\alpha$$

$$\omega_{\alpha\beta} = \frac{1}{2}\left(v^0_{\beta,\alpha} - v^0_{\alpha,\beta} \right)$$

To obtain the covariant derivative of the in-plane displacement, start with interpolation of the Cartesian components of displacements:

$$\underset{\sim}{u} = \sum_m \hat{N}_m (\xi^1, \xi^2)\, \underset{\sim}{u}_m \qquad (9.34)$$

where

m = Nodes

$\hat{N}_m$ = Linear interpolation function

$$\underset{\sim}{u}_m = \begin{Bmatrix} u_1 \underset{\sim}{e}_1 \\ u_2 \underset{\sim}{e}_2 \\ u_3 \underset{\sim}{e}_3 \end{Bmatrix}$$

Next, take the derivative of the displacement vector,

$$\vec{\nabla}\, \underset{\sim}{u} = v_{\beta,\alpha}\, \underset{\sim}{a}^\alpha \underset{\sim}{a}^\beta$$

$$= \underset{\sim}{a}^\alpha \sum_m \frac{\partial \hat{N}_m}{\partial \xi^\alpha}\, \underset{\sim}{u}_m \qquad (9.35)$$

Equation (9.35) provides a needed relation

$$v_{\beta,\alpha} = \sum_m \frac{\partial \hat{N}_m}{\partial \xi^\alpha} \left(\underset{\sim}{u}_m \cdot \underset{\sim}{a}_\beta \right) \qquad (9.36)$$

For the bending part of the strain measure, the covariant derivative of the rotation requires an additional relation derived as follows.

$$w = \sum_m \underset{\sim}{N}_m (\xi^1, \xi^2)\, \underset{\sim}{w}_m \qquad (9.37)$$

where

$\underset{\sim}{N}_m$ = 12-parameter bi-cubic interpolation function

$$\underset{\sim}{w}_m = \begin{Bmatrix} w\,\underset{\sim}{a} \\ w_{,1}\,\underset{\sim}{a}^1 \\ w_{,2}\,\underset{\sim}{a}^2 \end{Bmatrix}$$

Taking the derivatives, one obtains

$$w_{,\alpha} = \sum_m \frac{\partial \underset{\sim}{N}_m}{\partial \xi^\alpha}\, \underset{\sim}{w}_m \qquad (9.38)$$

$$w_{,\alpha\beta} = \sum_m \frac{\partial^2 \underset{\sim}{N}_m}{\partial \xi^\alpha \partial \xi^\beta}\, \underset{\sim}{w}_m \qquad (9.39)$$

$$- \sum_m \frac{\partial \underset{\sim}{N}_m}{\partial \xi^\gamma}\, \underset{\sim}{w}_m \begin{Bmatrix} \gamma \\ \alpha\beta \end{Bmatrix}$$

All other expressions needed are geometric in nature and have been dealt with in the previous section.

After calculation and placement of each of the terms, the strain components may be expressed as

$$\underset{\sim}{\gamma}^0 = \underset{\sim}{B}\,\underset{\sim}{q} \qquad (9.40)$$

$$\underset{\sim}{k} = \underset{\sim}{D}\,\underset{\sim}{q}$$

where

$\underset{\sim}{q}$ = 20 global degrees of freedom

$\underset{\sim}{\gamma}^0$ $\underset{\sim}{k}$ = Deflated strain tensor components into vector form using symmetry

9.2.3 Assumed Stress

For the present shell element, the stress assumption shall be constructed such that in the flat configuration the stress assumption reduces to the previous expressions for plane stress and C^1 plate elements. Furthermore, since the functional chosen for the shell element is the Hellinger-Reissner principle, the selected stress assumption does not have to satisfy equilibrium in a pointwise manner. The complexity of the general shell equilibrium equations demands such a relaxation. Thus, the main objective for the present section results in a description of a systematic relaxation procedure with respect to the equilibrium equations.

To begin with, the equilibrium equations for the general shells are

$$\ell^{\alpha\beta}{}_{,\alpha} - m^{\alpha\sigma}{}_{,\alpha}\, b^{\beta}_{\sigma} + \frac{1}{2}\left(m^{\beta\sigma} b^{\alpha}_{\sigma} - m^{\alpha\sigma} b^{\beta}_{\sigma}\right)_{,\alpha} = 0$$

$$m^{\alpha\beta}{}_{,\beta\alpha} + \ell^{\alpha\beta} b_{\alpha\beta} = 0 \qquad (9.41)$$

Using a local coordinate system defined at the center of the element, all of the geometric quantities are set to the corresponding constants evaluated at the center. In relation to the element developed in the previous chapters, this process is the same as evaluating the Jacobian matrix at the center of the element to transform the stress components. The equilibrium equations in this

local coordinate system are

$$\mathcal{Q}^{\alpha\beta}{}_{,\alpha} - \frac{3}{2} m^{\alpha\sigma}{}_{,\alpha} b^{\beta}_{\sigma} + \frac{1}{2} m^{\beta\sigma}{}_{,\alpha} b^{\alpha}_{\sigma} = 0$$

$$m^{\alpha\beta}{}_{,\beta\alpha} + \mathcal{Q}^{\alpha\beta} b_{\alpha\beta} = 0 \qquad (9.4\text{-}2)$$

To relax these equations in an orderly manner, consider the following list of the magnitudes of the geometric parameters:

$$\begin{aligned} |\underset{\sim}{a}_{\alpha}| &= O\left(\tfrac{L}{2}\right) \\ |a_{\alpha\beta}| &= O\left(\tfrac{L^2}{4}\right) \\ |b_{\alpha\beta}| &= O\left(\tfrac{L^2}{4R}\right) \\ |b^{\alpha}_{\beta}| &= O\left(\tfrac{1}{R}\right) \\ \left|\left\{\begin{matrix}\lambda \\ \alpha\beta\end{matrix}\right\}\right| &= O\left(\tfrac{L}{2R}\right) \end{aligned} \qquad (9.43)$$

where

L = Characteristic Length of the Element

R = Characteristic Radius of Curvature

Implicit in the definition of the characteristic scales, both L and R are non-dimensional parameters normalized by a characteristic length of the problem domain. As the element size vanish, $L \to 0$. The magnitude of R remains

constant throughout the mesh refinement. Using these parameters, four sets of relaxed equilibrium equations may be obtained. They are summarized below:

terms of order	set to zero	
SET 1 :	$\left(\frac{1}{R}\right) = 0$	All Curvature Terms Vanish (Flat Shell Assumption)
SET 2 :	$\left(\frac{L}{R}\right) = 0$	
SET 3 :	$\left(\frac{L}{R}\right)^2 = 0$	$\left(\frac{L}{R^2}\right) = 0$
SET 4 :	All terms in (9.42) retained	

The corresponding equilibrium equations are

SET 1 :

$$\frac{\partial \ell^{\alpha\beta}}{\partial \xi^{\alpha}} = 0$$

$$\frac{\partial m^{\alpha\beta}}{\partial \xi^{\alpha} \partial \xi^{\beta}} = 0 \qquad (9.44)$$

SET 2 :

$$\frac{\partial \ell^{\alpha\beta}}{\partial \xi^{\alpha}} - \frac{3}{2} \frac{\partial m^{\alpha\sigma}}{\partial \xi^{\alpha}} b_{\sigma}^{\beta} + \frac{1}{2} \frac{\partial m^{\beta\sigma}}{\partial \xi^{\alpha}} b_{\sigma}^{\alpha} = 0$$

$$\frac{\partial m^{\alpha\beta}}{\partial \xi^{\alpha} \partial \xi^{\beta}} = 0 \qquad (9.45)$$

SET 3 :

$$\frac{\partial l^{\alpha\beta}}{\partial \xi^{\alpha}} + \left\{ {\alpha \atop \sigma\alpha} \right\} l^{\sigma\beta} + \left\{ {\beta \atop \sigma\alpha} \right\} l^{\alpha\sigma}$$

$$- \frac{3}{2} \frac{\partial m^{\alpha\sigma}}{\partial \xi^{\alpha}} b^{\beta}_{\sigma} + \frac{1}{2} \frac{\partial m^{\beta\sigma}}{\partial \xi^{\alpha}} b^{\alpha}_{\sigma} = 0 \qquad (9.46)$$

$$\frac{\partial m^{\alpha\beta}}{\partial \xi^{\alpha} \partial \xi^{\beta}} + \left\{ {\alpha \atop \lambda\beta} \right\} \frac{\partial m^{\lambda\beta}}{\partial \xi^{\alpha}} + 2 \left\{ {\beta \atop \lambda\beta} \right\} \frac{\partial m^{\alpha\lambda}}{\partial \xi^{\alpha}} + l^{\alpha\beta} b_{\alpha\beta} = 0$$

SET 4 :

$$l^{\alpha\beta}{}_{,\alpha} - \frac{3}{2} m^{\alpha\sigma}{}_{,\alpha} b^{\beta}_{\sigma} + \frac{1}{2} m^{\beta\sigma}{}_{,\alpha} b^{\alpha}_{\sigma} = 0$$

$$m^{\alpha\beta}{}_{,\beta\alpha} + l^{\alpha\beta} b_{\alpha\beta} = 0 \qquad (9.47)$$

Starting with SET 1 where the stress terms are decoupled, the assumed stress field is simply a combination of the plane stress field and the C^1 plate stress field derived previously:

SET 1 :

$$\begin{aligned} l^{11} &= \beta_1 + \beta_4 \xi^2 \\ l^{22} &= \beta_2 + \beta_5 \xi^1 \\ l^{12} &= \beta_3 \end{aligned} \qquad (9.48)$$

$$\begin{aligned} m^{11} &= \beta_6 + \beta_9 \xi^1 + \beta_{12} \xi^2 + \beta_{15} \xi^1 \xi^2 \\ m^{22} &= \beta_7 + \beta_{10} \xi^1 + \beta_{13} \xi^2 + \beta_{16} \xi^1 \xi^2 \\ m^{12} &= \beta_8 + \beta_{11} \xi^1 + \beta_{14} \xi^2 + \beta_{17} (\xi^1)^2 + \beta_{18} (\xi^2)^2 \end{aligned}$$

Progressively, further equilibrium terms in SET 2 to 4 involve adding more terms into Eq. (9.48):

SET 2 : SET 1 +

$$\ell^{11} = b_1^1 \beta_9 \bar{\xi}^1 - \tfrac{1}{2} \beta_{12} b_1^2 \bar{\xi}^1$$

$$\ell^{22} = b_2^2 \beta_{13} \bar{\xi}^2 - \tfrac{1}{2} \beta_{10} b_2^1 \bar{\xi}^2 \qquad (9.49)$$

$$\ell^{12} = b_2^1 \beta_{11} \bar{\xi}^2 - \left(\tfrac{1}{2} b_2^2 - \tfrac{3}{2} b_1^1\right) \beta_{14} \bar{\xi}^2 - \left(\tfrac{1}{2} b_1^1 - \tfrac{3}{2} b_2^2\right) \beta_{11} \bar{\xi}^1 + b_1^2 \beta_{14} \bar{\xi}^1$$

SET 3 : SET 2 +

$$\ell^{11} = -\left[2 \left\{ {1 \atop 1\,1} \right\} + \left\{ {2 \atop 1\,2} \right\}\right] \beta_1 \bar{\xi}^1$$

$$\ell^{22} = -\left[2 \left\{ {2 \atop 2\,2} \right\} + \left\{ {1 \atop 2\,1} \right\}\right] \beta_2 \bar{\xi}^2 \qquad (9.50a)$$

$$\ell^{12} = -\left[3 \left\{ {1 \atop 2\,1} \right\} + \left\{ {2 \atop 2\,2} \right\}\right] \beta_3 \bar{\xi}^2 - \left[\left\{ {1 \atop 1\,1} \right\} + 3 \left\{ {2 \atop 1\,2} \right\}\right] \beta_3 \bar{\xi}^1$$

$$m^{11} = -\frac{b_{11}}{2}\beta_1(\bar{\xi}^1)^2 - \frac{1}{2}\left[3\left\{{1\atop 11}\right\} + 2\left\{{2\atop 12}\right\}\right]\beta_9(\bar{\xi}^1)^2 - \frac{1}{2}\left\{{2\atop 11}\right\}\beta_{12}(\bar{\xi}^1)^2$$

$$m^{22} = -\frac{b_{22}}{2}\beta_2(\bar{\xi}^2)^2 - \frac{1}{2}\left\{{1\atop 22}\right\}\beta_{10}(\bar{\xi}^2)^2 - \frac{1}{2}\left[2\left\{{1\atop 21}\right\} + 3\left\{{2\atop 22}\right\}\right]\beta_{13}(\bar{\xi}^2)^2$$

$$m^{12} = -b_{12}\beta_3\bar{\xi}^1\bar{\xi}^2 - \frac{1}{2}\left[4\left\{{1\atop 21}\right\} + 2\left\{{2\atop 22}\right\}\right]\beta_{11}\bar{\xi}^1\bar{\xi}^2$$
$$- \frac{1}{2}\left[2\left\{{1\atop 11}\right\} + 4\left\{{2\atop 12}\right\}\right]\beta_{14}\bar{\xi}^1\bar{\xi}^2 \qquad (9.50b)$$

SET 4 : SET 3 +

$$\ell^{11} = a\beta_6\bar{\xi}^1$$
$$\ell^{22} = e\beta_7\bar{\xi}^2$$
$$\ell^{12} = c\beta_8\bar{\xi}^2 + f\beta_8\bar{\xi}^1 \qquad (9.51)$$
$$m^{11} = -\frac{g}{2}\beta_6(\bar{\xi}^1)^2$$
$$m^{22} = -\frac{h}{2}\beta_7(\bar{\xi}^2)^2$$
$$m^{12} = -\frac{i}{2}\beta_8\bar{\xi}^1\bar{\xi}^2$$

where

$$a = 2\left\{{1\atop 11}\right\}b_1^1 + \frac{3}{2}\left\{{2\atop 12}\right\}b_1^1 + \left\{{2\atop 11}\right\}b_2^1 - \left\{{1\atop 12}\right\}b_1^2 - \frac{1}{2}\left\{{2\atop 12}\right\}b_2^2$$

$$c = \frac{7}{2}\left\{{1\atop 21}\right\}b_1^1 + \left\{{1\atop 11}\right\}b_2^1 + 4\left\{{2\atop 12}\right\}b_2^1 + \frac{3}{2}\left\{{2\atop 22}\right\}b_1^1$$
$$- \frac{1}{2}\left\{{1\atop 12}\right\}b_2^2 - \frac{1}{2}\left\{{1\atop 22}\right\}b_1^2 - \frac{1}{2}\left\{{2\atop 22}\right\}b_1^2 - \frac{1}{2}\left\{{2\atop 22}\right\}b_2^2$$

$$e = 2\left\{{2\atop 22}\right\}b_2^2 - \left\{{2\atop 21}\right\}b_2^1 + \frac{3}{2}\left\{{1\atop 21}\right\}b_2^2 + \left\{{1\atop 22}\right\}b_1^2 - \frac{1}{2}\left\{{1\atop 21}\right\}b_1^1$$

$$f = -\frac{7}{2}\left\{{}^{2}_{12}\right\} b_2^2 + \left\{{}^{2}_{22}\right\} b_1^2 + 4\left\{{}^{1}_{12}\right\} b_1^2 - \frac{3}{2}\left\{{}^{1}_{11}\right\} b_2^2$$
$$- \frac{1}{2}\left\{{}^{2}_{11}\right\} b_1^2 - \frac{1}{2}\left\{{}^{2}_{21}\right\} b_1^1 - \frac{1}{2}\left\{{}^{1}_{11}\right\} b_1^1 - \frac{1}{2}\left\{{}^{2}_{11}\right\} b_2^1$$

$$g = 2\left\{{}^{1}_{11}\right\}^2 + 3\left\{{}^{2}_{12}\right\}\left\{{}^{1}_{11}\right\} + \left\{{}^{1}_{21}\right\}\left\{{}^{2}_{11}\right\}$$
$$+ \left\{{}^{2}_{22}\right\}\left\{{}^{2}_{11}\right\} + \left\{{}^{2}_{12}\right\}^2$$

$$h = 2\left\{{}^{2}_{22}\right\}^2 + 3\left\{{}^{2}_{22}\right\}\left\{{}^{1}_{21}\right\} + \left\{{}^{1}_{11}\right\}\left\{{}^{1}_{22}\right\}$$
$$+ \left\{{}^{2}_{12}\right\}\left\{{}^{1}_{22}\right\} + \left\{{}^{1}_{21}\right\}^2$$

$$i = 4\left\{{}^{1}_{11}\right\}\left\{{}^{1}_{12}\right\} + 6\left\{{}^{1}_{21}\right\}\left\{{}^{2}_{12}\right\}$$
$$+ 4\left\{{}^{2}_{22}\right\}\left\{{}^{2}_{12}\right\} + 2\left\{{}^{1}_{11}\right\}\left\{{}^{2}_{22}\right\}$$

The four sets of relaxed equilibrium equations are presented to gage to what extent the assumed stress field satisfies the pointwise equilibrium equations for a well-behaved shell element. The order of magnitude analysis on the geometrical parameters determine which terms tend to vanish faster under mesh refinement. This leads to a systematic breakdown of the terms represented in the equilibrium equations.

Symbolically, for the purpose of outlining the stiffness matrix construction, denote

$$\underset{\sim}{\ell} = \underset{\sim}{P}_{\ell}\,\underset{\sim}{\beta}$$
$$\underset{\sim}{m} = \underset{\sim}{P}_{m}\,\underset{\sim}{\beta} \qquad (9.52)$$

$\underset{\sim}{\ell}$, $\underset{\sim}{m}$ = Deflated stress tensor components into vector form using symmetry

9.2.4 Element Matrices

In the present section, the Hellinger-Reissner principle shall be tailored to accommodate the field assumptions in the previous sections. In short, the Hellinger-Reissner principle is chosen since the stress assumption does not need to satisfy equilibrium in an exact pointwise manner. Further modification is needed since the boundary normal derivative of w is incompatible. For programming convenience, the tensor component notation is changed to matrix notation.

Recall that the Hellinger-Reissner principle may be written for general shell theory as

$$\pi_R = \int_A \{-\tfrac{1}{2}[\tfrac{1}{h}\Sigma_{\alpha\beta\sigma\tau}\, l^{\sigma\tau} l^{\alpha\beta} + \tfrac{12}{h^3}\Sigma_{\alpha\beta\sigma\tau}\, m^{\alpha\beta} m^{\sigma\tau}]$$
$$+ l^{\alpha\beta}\gamma_{\alpha\beta} + m^{\alpha\beta} k_{\alpha\beta} - F^{\alpha} v_{\alpha} - F^{3} w\}\, dA$$
$$- \int_{S_\sigma} [\bar{l}^{\alpha\beta} \nu_\alpha v_\beta - \nu_\alpha \bar{m}^{\alpha\beta}\theta_\beta + \nu_\alpha \bar{q}^{\alpha} w]\, ds$$

(9.53)

In matrix notation,

$$\pi_R = \int_A \{-\tfrac{1}{2}[\tfrac{1}{h}\, \underset{\sim}{l}^T \underset{\sim}{\Sigma}\, \underset{\sim}{l} + \tfrac{12}{h^3}\, \underset{\sim}{m}^T \underset{\sim}{\Sigma}\, \underset{\sim}{m}]$$
$$\underset{\sim}{l}^T \underset{\sim}{\gamma} + \underset{\sim}{m}^T \underset{\sim}{k} - \underset{\sim}{F}^T \underset{\sim}{v} - F^3 w\}\, dA$$
$$- \int_{S_\sigma} [(\underset{\sim}{\nu}^T \underset{\sim}{\bar{l}})^T \underset{\sim}{v} - (\underset{\sim}{\nu}^T \underset{\sim}{\bar{m}})^T \underset{\sim}{\theta} + \underset{\sim}{\nu}^T \underset{\sim}{\bar{q}} w]\, ds$$

(9.54)

where

$$\underset{\sim}{l} = \begin{Bmatrix} l_{11} \\ l_{22} \\ l_{12} \end{Bmatrix} \qquad \underset{\sim}{m} = \begin{Bmatrix} m_{11} \\ m_{22} \\ m_{12} \end{Bmatrix}$$

$$\underset{\sim}{\Sigma} = \underset{\sim}{\Omega}^{-1} = \begin{bmatrix} \Omega^{1111} & & \\ \Omega^{2211} & \Omega^{2222} & \\ \Omega^{1211} & \Omega^{1222} & \Omega^{1212} \end{bmatrix}^{-1}$$

$$\underset{\sim}{\gamma} = \begin{Bmatrix} \gamma_{11} \\ \gamma_{22} \\ 2\gamma_{12} \end{Bmatrix} \qquad \underset{\sim}{k} = \begin{Bmatrix} k_{11} \\ k_{22} \\ 2k_{12} \end{Bmatrix}$$

The entries of the material matrix are defined in Eq. (9.7) for an isotropic material. Substituting the assumed stress and strain fields,

$$\Pi_R = -\frac{1}{2}\underset{\sim}{\beta}^T \underset{\sim}{H}\underset{\sim}{\beta} + \underset{\sim}{\beta}^T \underset{\sim}{G}\underset{\sim}{q} - \underset{\sim}{Q}^T \underset{\sim}{q} \qquad (9.55)$$

where

$$\underset{\sim}{H} = \int_A \frac{1}{h} \underset{\sim}{P}_l^T \underset{\sim}{\Sigma} \underset{\sim}{P}_l + \frac{12}{h^3} \underset{\sim}{P}_m^T \underset{\sim}{\Sigma} \underset{\sim}{P}_m \, dA$$

$$\underset{\sim}{G} = \int_A \underset{\sim}{P}_l^T \underset{\sim}{B} + \underset{\sim}{P}_m^T \underset{\sim}{D} \, dA \qquad (9.56)$$

$$\underset{\sim}{Q}^T = \int_A \underset{\sim}{F}^T \underset{\sim}{N}_r + F^3 \underset{\sim}{N}_w \, dA$$

$$- \int_{S_\sigma} (\underset{\sim}{\nu}^T \underset{\sim}{\bar{l}})^T \underset{\sim}{N}_r - (\underset{\sim}{\nu}^T \underset{\sim}{\bar{m}})^T \underset{\sim}{N}_\theta + \underset{\sim}{\nu}^T \underset{\sim}{\bar{q}} \underset{\sim}{N}_w \, ds$$

To compensate for the incompatible boundary normal displacement, following term must be included in Eq. (9.53):

$$- \int_{\partial A} m^{\alpha\beta} \nu_\alpha \nu_\beta (\tilde{w}_{,\nu} - w_{,\nu}) \, ds \qquad (9.57)$$

where

$\underset{\sim}{\nu} = \nu_\alpha \underset{\sim}{a}^\alpha$ = Unit normal to the boundary curve

$\tilde{w}_{,\nu}$ = Compatible normal derivative

$w_{,\nu}$ = Incompatible normal derivative

Defining

$$\tilde{w}_{,\nu} - w_{,\nu} \equiv \underset{\sim}{N}_\nu \underset{\sim}{q} \qquad (9.58)$$

Equation (9.57) yields

$$- \underset{\sim}{\beta}^T \underset{\sim}{G}_\nu \underset{\sim}{q} \qquad (9.59)$$

where

$$\underset{\sim}{G}_\nu = \int_{\partial A} \underset{\sim}{P}^T_\nu \underset{\sim}{N}_\nu \, ds \qquad (9.60)$$

Combining with Eq. (9.55)

$$\pi_R = -\frac{1}{2} \underset{\sim}{\beta}^T \underset{\sim}{H} \underset{\sim}{\beta} + \underset{\sim}{\beta}^T (\underset{\sim}{G} - \underset{\sim}{G}_\nu) \underset{\sim}{q} - \underset{\sim}{Q}^T \underset{\sim}{q} \qquad (9.61)$$

$$\underset{\sim}{\beta} = \underset{\sim}{H}^{-1} (\underset{\sim}{G} - \underset{\sim}{G}_\nu) \underset{\sim}{q}$$

$$\underset{\sim}{K} = (\underset{\sim}{G} - \underset{\sim}{G}_\nu)^T \underset{\sim}{H}^{-1} (\underset{\sim}{G} - \underset{\sim}{G}_\nu) \qquad (9.62)$$

Finally,

$$\underset{\sim}{K} \underset{\sim}{q} = \underset{\sim}{Q} \qquad (9.63)$$

9.3 Numerical Examples

In the numerical examples, the following titles are used for the elements compared. The "SETs" correspond to the relaxed equilibrium equations presented in the previous section.

SET1(18) = 4-node hybrid shell with 18 β's.
[Equation (9.48)] Flat Shell Case

SET2(18) = 4-node hybrid shell with 18 β's.
[Equation (9.49)]

SET3(18) = 4-node hybrid shell with 18 β's.
[Equation (9.50)]

SET4(18) = 4-node hybrid shell with 18 β's.
[Equation (9.51)]

SET1(16)
SET2(16)
SET3(16)
SET4(16) = Corresponds to the above notation but with 16 β's. $\beta_{17} = \beta_{18} = 0$

MORRIS-24 = 4-Node 24 DOF Exact Geometry Shell using assumed displacement method [85].

MORRIS-48 = 4-Node 48 DOF Exact Geometry Shell using assumed displacement method [85].

DVORKIN = 4-node Assumed Displacement flat shell [56].

LINDBERG = Exact Geometry Shell using assumed displacement method with 48 degrees of freedom [100].

STANLEY = 4-Node Assumed Displacement Flat Shell using Selective Reduced Integration [101].

HEPPLER = 16-Node Assumed Displacement C^0 Shell with Full Integration [102].

BOLOURCHI(F) = 8-Node Assumed Displacement C^0 Shell with Full Integration [103].

BOLOURCHI(R) = 8-Node Assumed Displacement C^0 Shell with Reduced Integration [103].

As a final note, the hybrid shell elements are denoted as SETn with the pointwise equilibrium condition enforced increasingly with increasing number.

9.3.1 Rigid Body Motion

The representation of the rigid body motion of a finite element may be studied by an Eigenvalue analysis of the stiffness matrix. For the hybrid shell elements, the cylindrical panel geometry shown in Figure 9-6 is used for the Eigenvalue analysis. By keeping the chord, c, constant and varying the radius, the curvature of the element may be varied. For $\theta = 0^{\circ}$ the geometry takes on a limiting flat configuration and for $\theta = 90^{\circ}$ the geometry results in a quarter of a full cylinder. Although the latter case is extreme for a single shell element, the overall spectrum of results provide a complete range of Eigenvalues. The cylindrical panel geometry is chosen to isolate a single rigid body mode as affected by curvature change. This mode is denoted as Eigenvalue 6. The most flexible mode is denoted as Eigenvalue 7. The ratio of these two Eigenvalues will parameterize the effect of curvature change on the rigid body motion.

The results are provided in Figure 9-7. Since the energy of the structure under deformation is represented by an Eigenvector and is proportional to the square of the corresponding Eigenvalue, all elements provide an adequate representation of the rigid body motion throughout the complete range of curvature values examined.

For both 16 β and 18 β hybrid elements, the SET2 clearly demonstrated a superior representation of the rigid body motion over the SET1 element behavior. In another words, satisfaction of equilibrium equations, even approximately, has a direct effect on the representation of the rigid body motion. The SET3 and SET4 elements provide the same results as the SET2 elements. Note that most of the added equilibrium terms in the SET3 and SET4 element stress fields are a function of the Christoffel symbols which vanish for cylindrical geometry. This behavior will be seen repeatedly for other examples with undistorted elements in the cylindrical geometry.

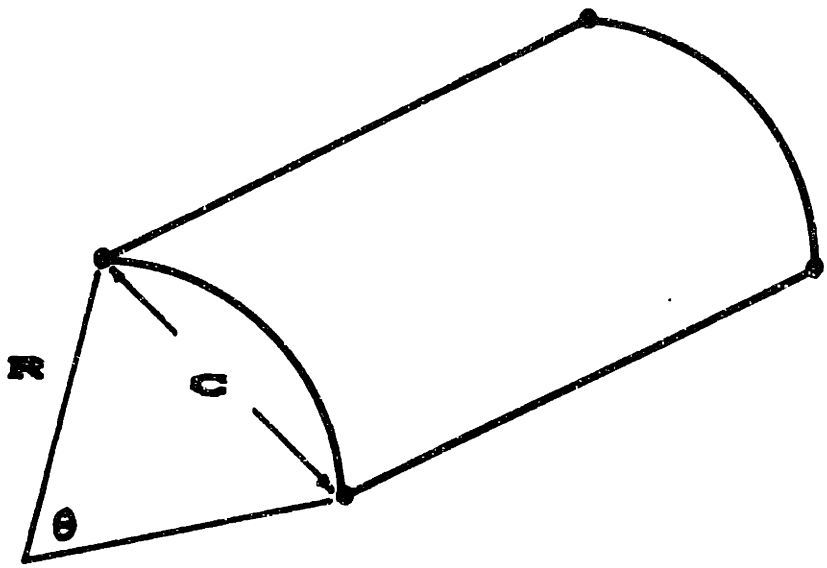

C = CONSTANT

Figure 9-6. Cylindrical Panel used for Rigid Body Motion Study.

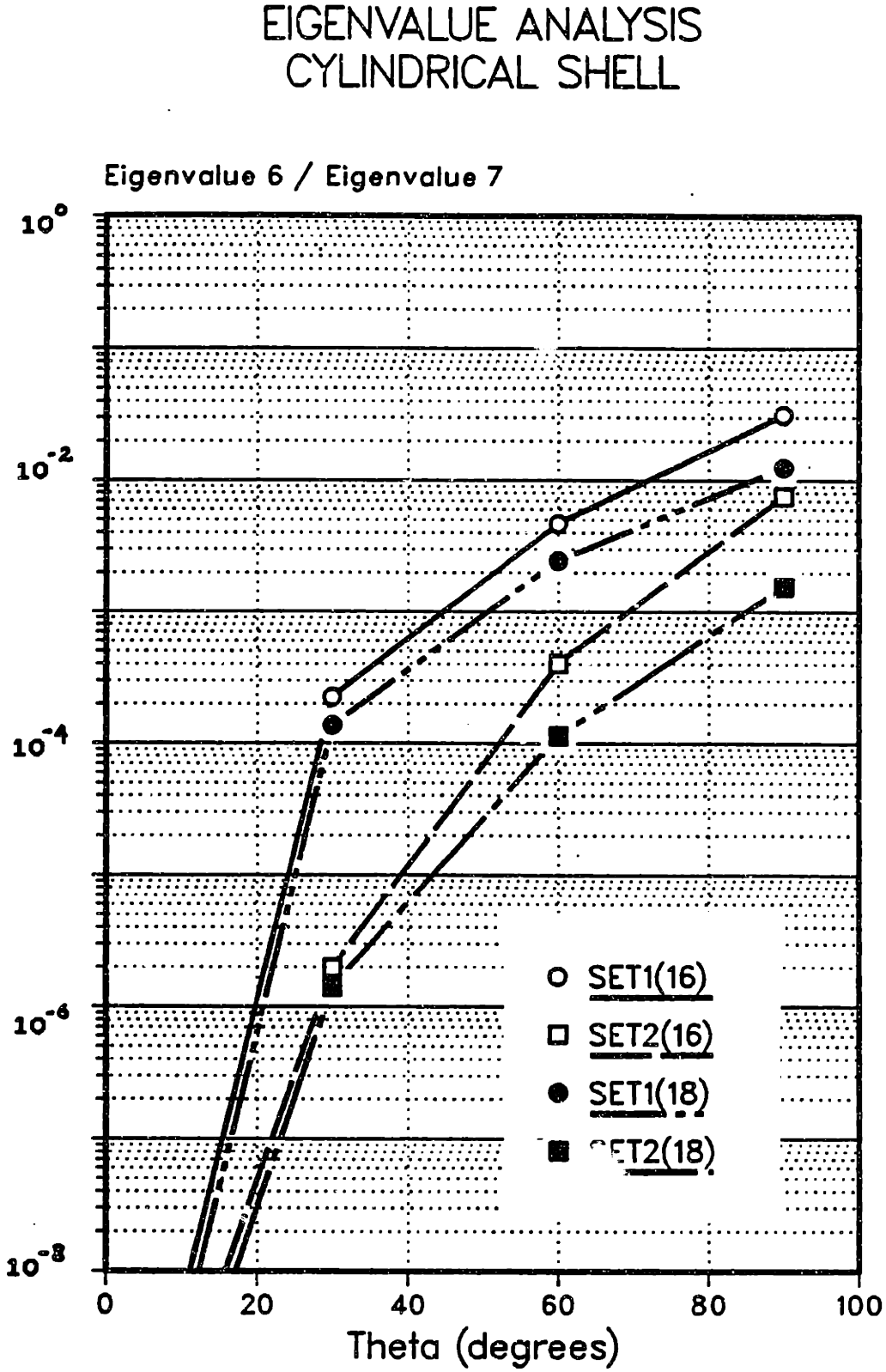

Figure 9-7. Stiffness Matrix Eigenvalue Analysis Results for Cylindrical Panel.

9.3.2 Slit Cylinder

The torsion-loaded slit cylinder problem provides a superb example for studying the effect of the polynomial representation of the assumed fields for a curved shell. The problem, shown in Figure 9-8, has a simple solution, the only significant contribution to the stress field being a constant torsional couple. The rigid body modes are secured so that the normal displacement occurs, as outlined by Morris [85]. This problem may be carried out by using only one element. Considering the equilibrium of the whole shell, the equivalent nodal forces, F_1 and F_2, are assigned to each node.

The results from the hybrid 20 degrees of freedom general shell elements are compared with those from 4-node cylindrical shell elements with 24 and 48 degrees of freedom constructed using assumed displacement method [85]. In the present notation, the latter results are denoted by MORRIS-24 and by MORRIS-48. The degrees of freedom represented at each node for these elements are

MORRIS-24 u

v

$w,\ w_{,x},\ w_{,y},\ w_{,xy}$

and

MORRIS-48 $u,\ u_{,x},\ u_{,y},\ u_{,xy}$

$v,\ v_{,x},\ v_{,y},\ v_{,xy}$

$w,\ w_{,x},\ w_{,y},\ w_{,xy}$

With the cross-derivative terms, a compatible displacement field may be obtained by using a bivariate generalization of the Hermite interpolation formula.

The results for the twist of the slit cylinder are provided in Figure 9-9. The exact solution, $r\theta = 7.8X10^{-3}$, should be maintained as a constant throughout the range of PHI. The MORRIS-24 element exhibits a rapid deterioration with increasing PHI. The hybrid and the MORRIS-48 elements give similar and much better results throughout the range of PHI.

All hybrid elements employed give identical results. This indicates that the existence of a constant twisting moment term in the stress field is a key factor for the good performance of the hybrid elements.

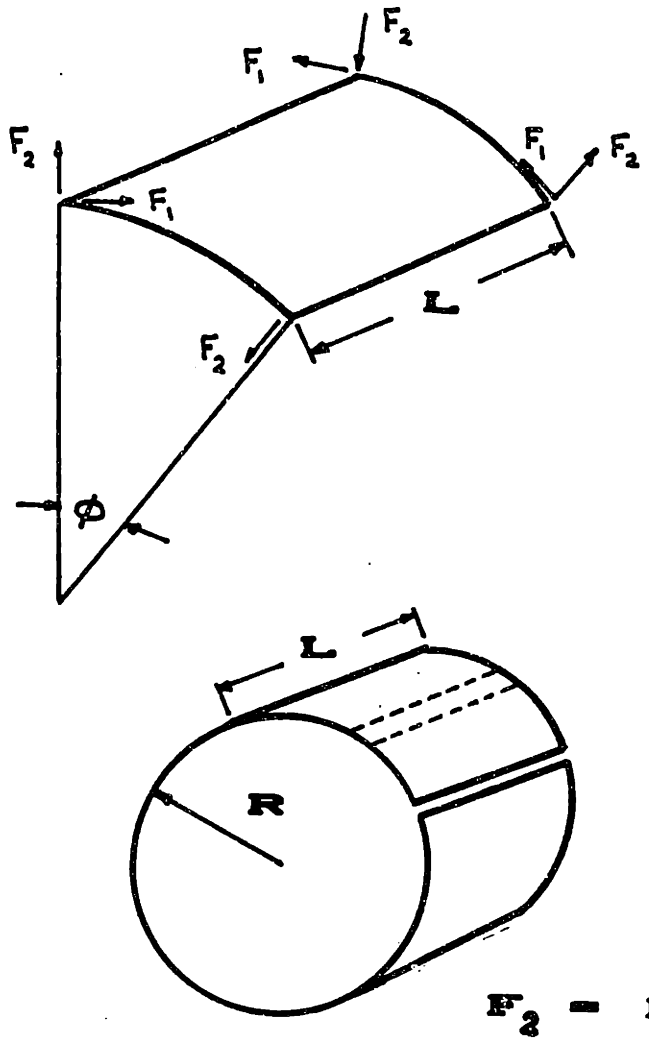

$$F_2 = F_1 \cot \frac{\Phi}{2}$$

$$\frac{L}{R} = .05$$

$$\frac{h}{R} = .01$$

$$\nu = .3$$

Figure 9-8. Torsion of Slit Cylinder.

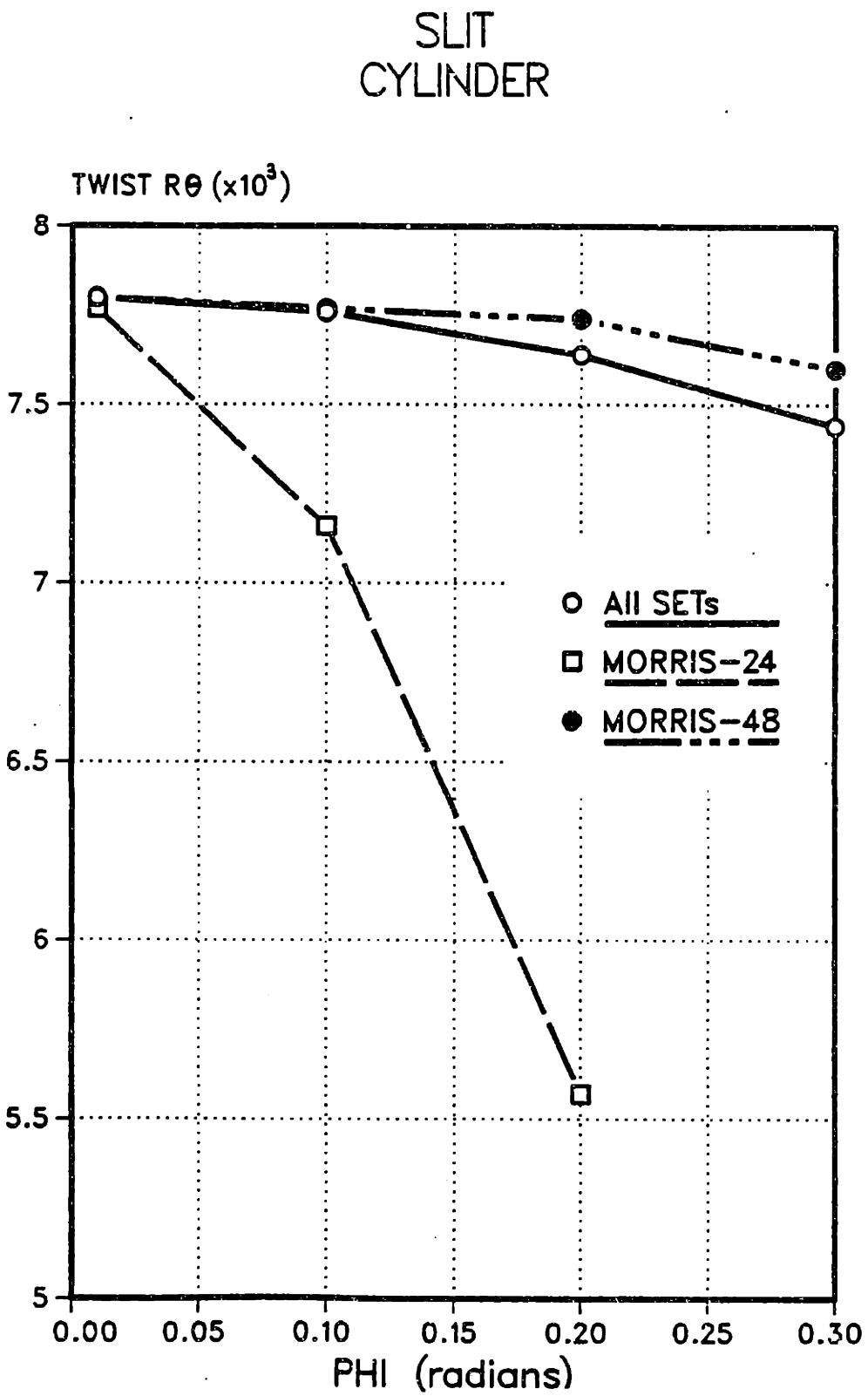

Figure 9-9. Twist of the Slit Cylinder with Increasing Element Size.

9.3.3 Pinched Open Cylinder

One of the desirable attributes for a shell element is for it to be able to represent a limiting inextensional bending behavior. Conceptually, this attribute requires that an element be able to decouple bending from membrane action.

The pinched cylinder with open ends (Figure 9-10) exemplifies a bending dominated problem. For this simple problem, a single element should provide an accurate solution if the bending-stretching actions of the element are decoupled.

The displacement results for the hybrid elements are given in Figure 9-11. The elements SET3 and SET4 give identical results to those from the element SET2. Two points merit comment. First note that the 16 β and 18 β elements provide very similar results for the respective SETs. Secondly, for a single element mesh, the SET1 element is too stiff. The results indicate an important role of the equilibrium equation for decoupling bending from membrane action.

The two elements chosen for comparison illustrate and highlight two features of the hybrid general shell. They are:

(1) 4-nodes.

(2) Bi-cubic polynomial representation of the surface.

The STANLEY element is a 4-node flat shell constructed with assumed displacement method; the element also employs the selective reduced integration. The HEPPLER element is a 16-node 80 degrees of freedom shell also constructed with assumed displacement method. However, this element utilizes full integration and does not commit a variational crime. Geometrically, the HEPPLER element can represent a bi-cubic polynomial surface.

The comparative results are provided in Figure 9-12. The flat shell element, STANLEY, converges slowly. An (8X8) mesh is required to obtain a solution comparable with one from a single hybrid element mesh. Such a large difference indicates the importance of accurately representing the shell element geometry.

The 16-node HEPPLER element also exhibits poor accuracy. Even with a better representation of the shell geometry, the C^{o} shell element constructed with the assumed displacement method does not provide a well-behaved element. Modifications that commit variational crimes must be used to "improve" the behavior of this type of element.

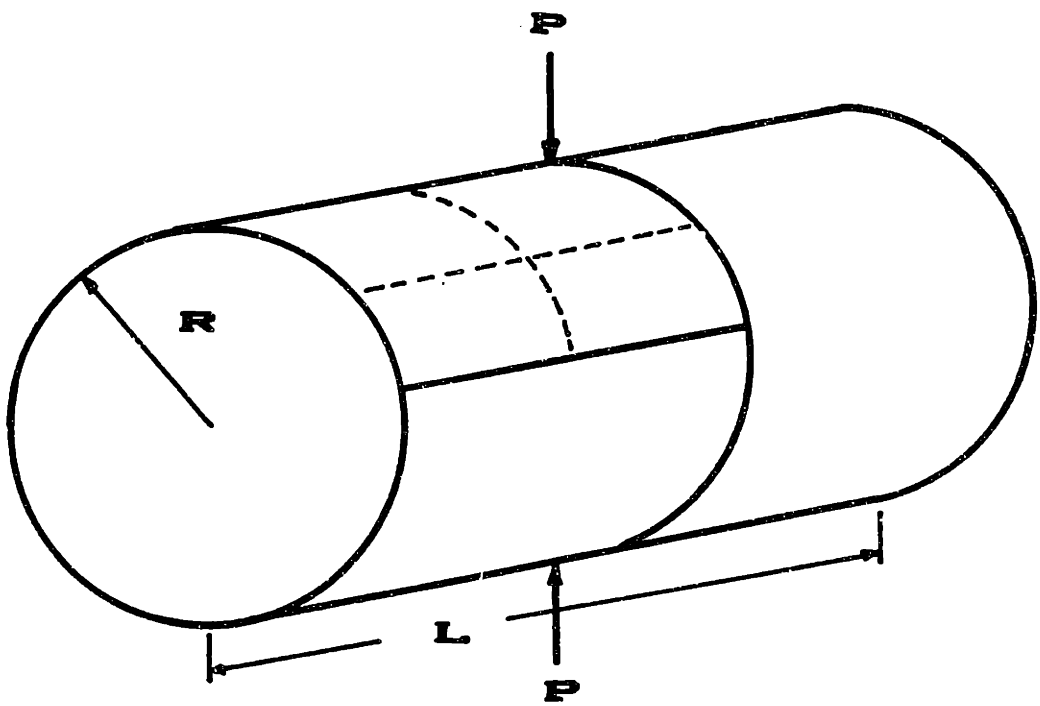

$L = 10.35$

$R = 4.953$

$h = .094$

$\nu = .3125$

$E = 10.5 \times 10^6$

Figure 9-10. Pinched Cylinder with Open Ends.

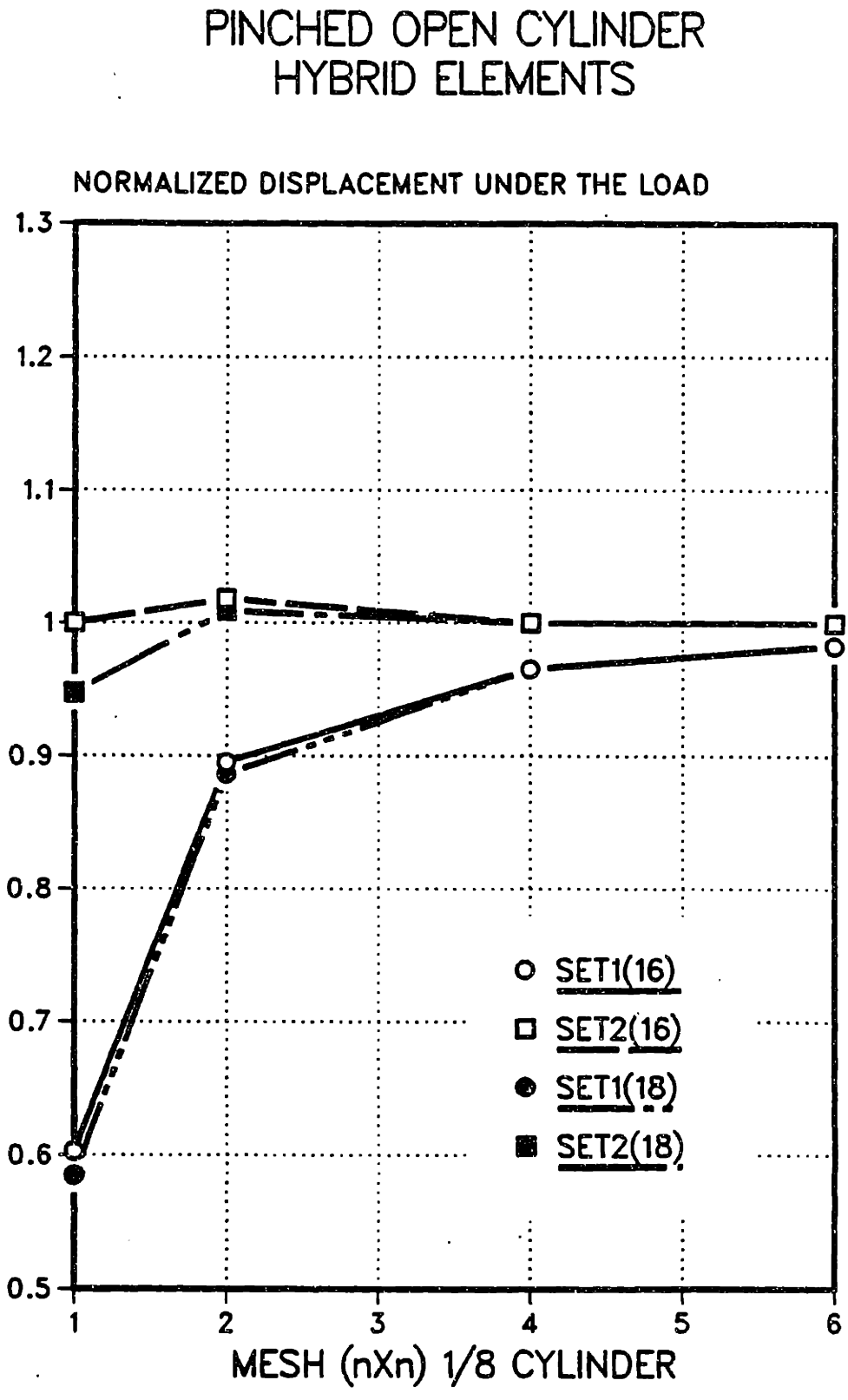

Figure 9-11. Pinched Open Cylinder Displacement Results for Hybrid Shell Elements.

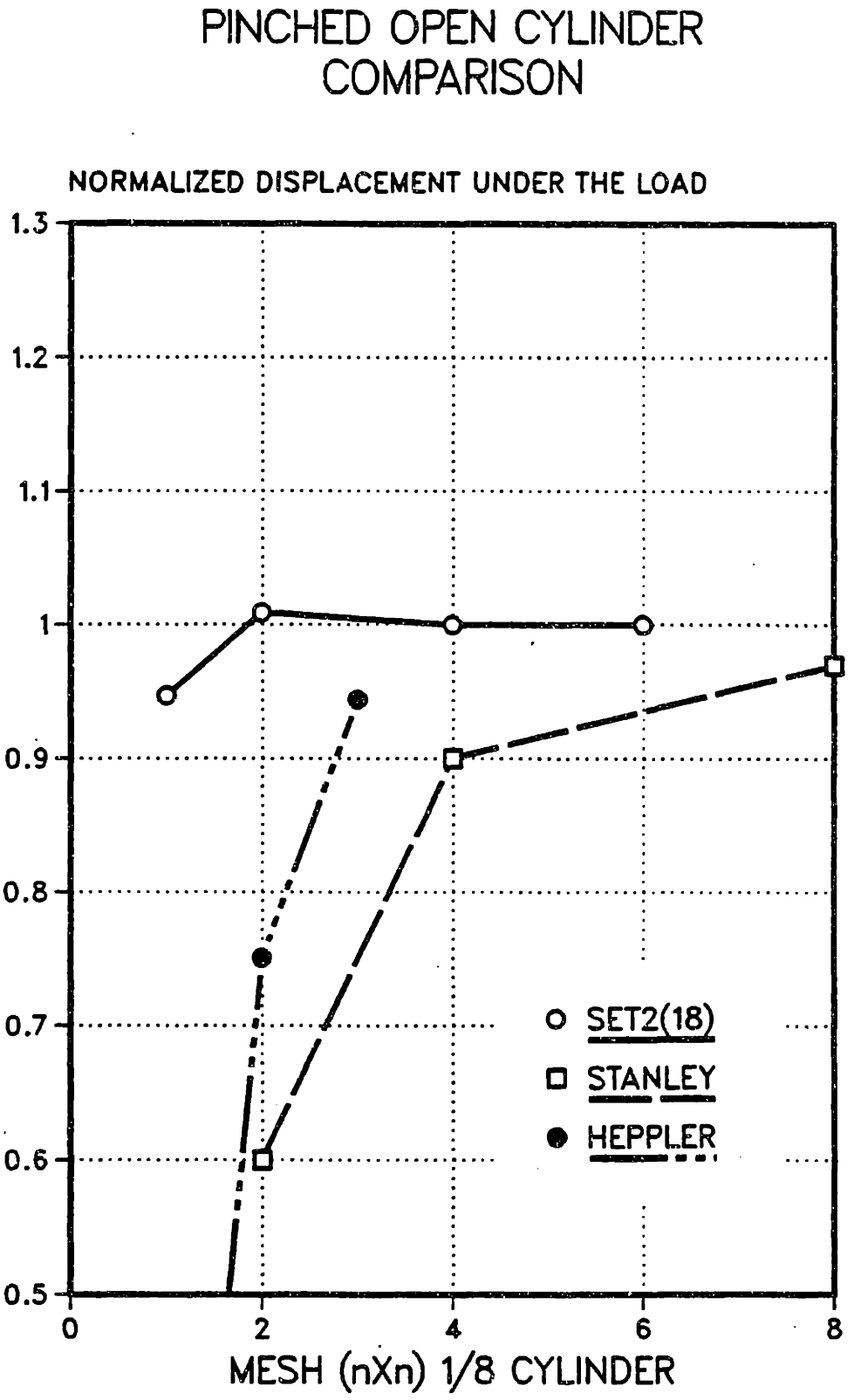

Figure 9-12. Comparison of the Pinched Open Cylinder Displacement Results.

9.3.4 Pinched Open Cylinder with Distortion

To demonstrate the effect of mesh distortion, a (2X2) mesh of elements is used to model the pinched open cylinder. Figure 9-13 defines the element distortion parameter, a. Full triangularization occurs for a=1. The element distortion results are provided in Figures 9-14 and 9-15. Generally, the rate of deterioration with mesh distortion is similar for all of the hybrid elements presented. To relate the figures for a finer mesh, note that a mesh refinement by a factor of two decreases the distortion parameter, a, by a factor of four.

Another type of distortion is characterized by rotation of the normal vector. Figure 9-16 defines the "normal distortion". A single normal is rotated circumferentially. The normal distortion results are provided in Figures 9-17 and 9-18. These results help to set a level of tolerance for the accuracy to which the normal must be represented.

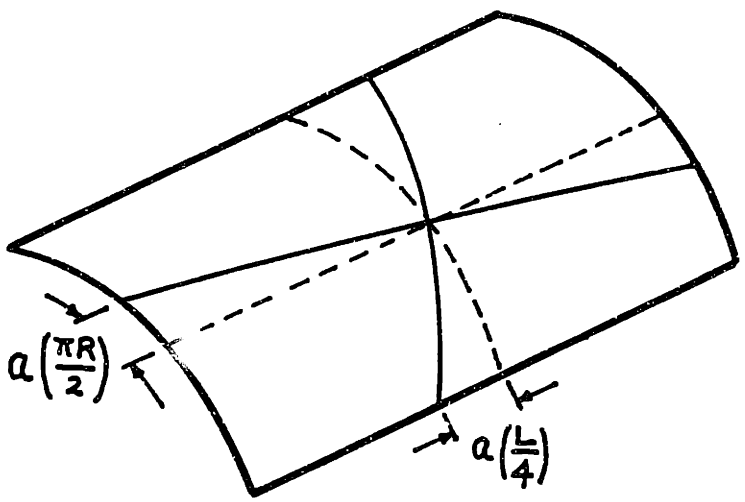

a = 1

Full Triangularization

Figure 9-13. Pinched Open Cylinder with Element Distortion.

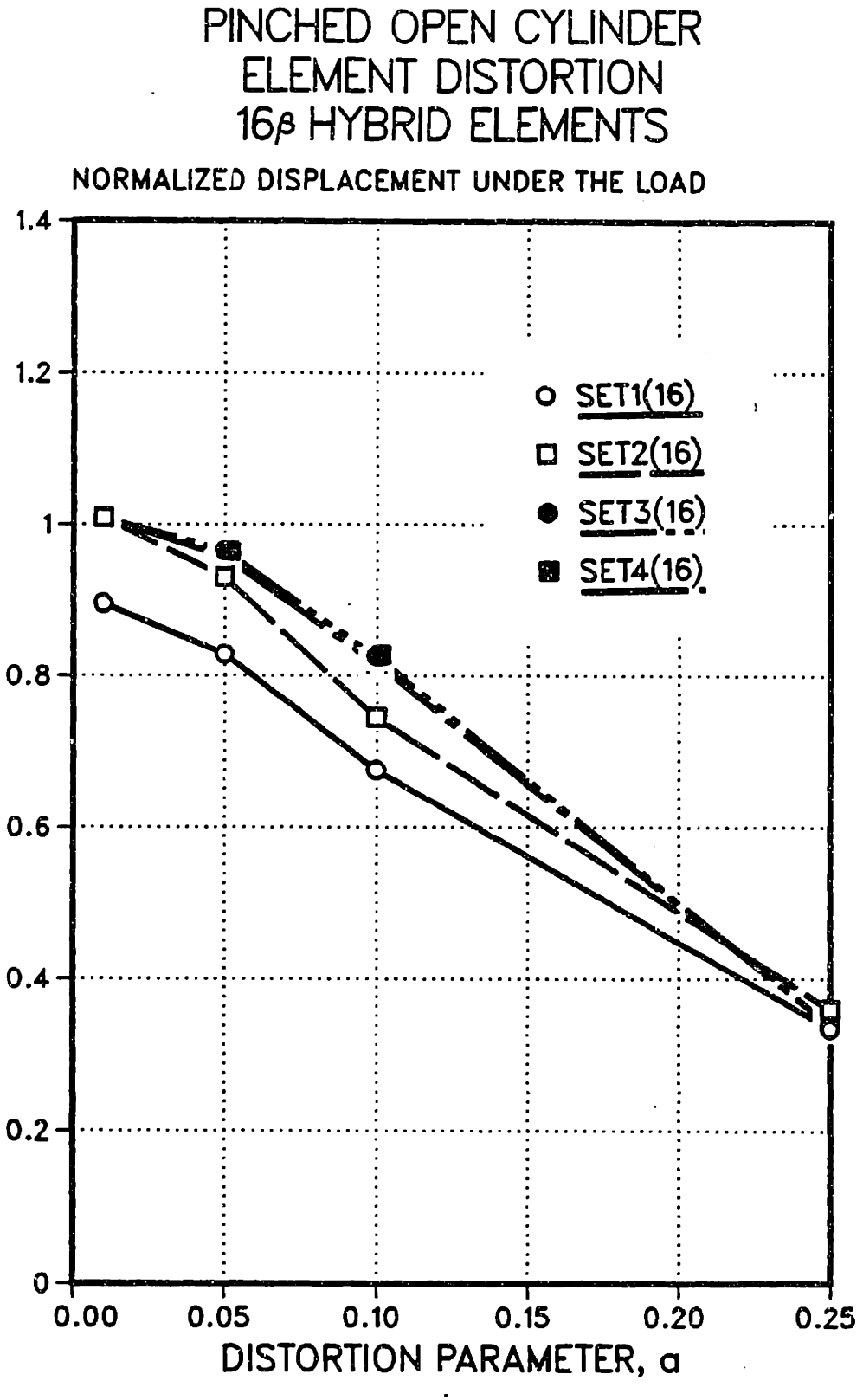

Figure 9-14. Element Distortion Results for 16 β Hybrid Elements.

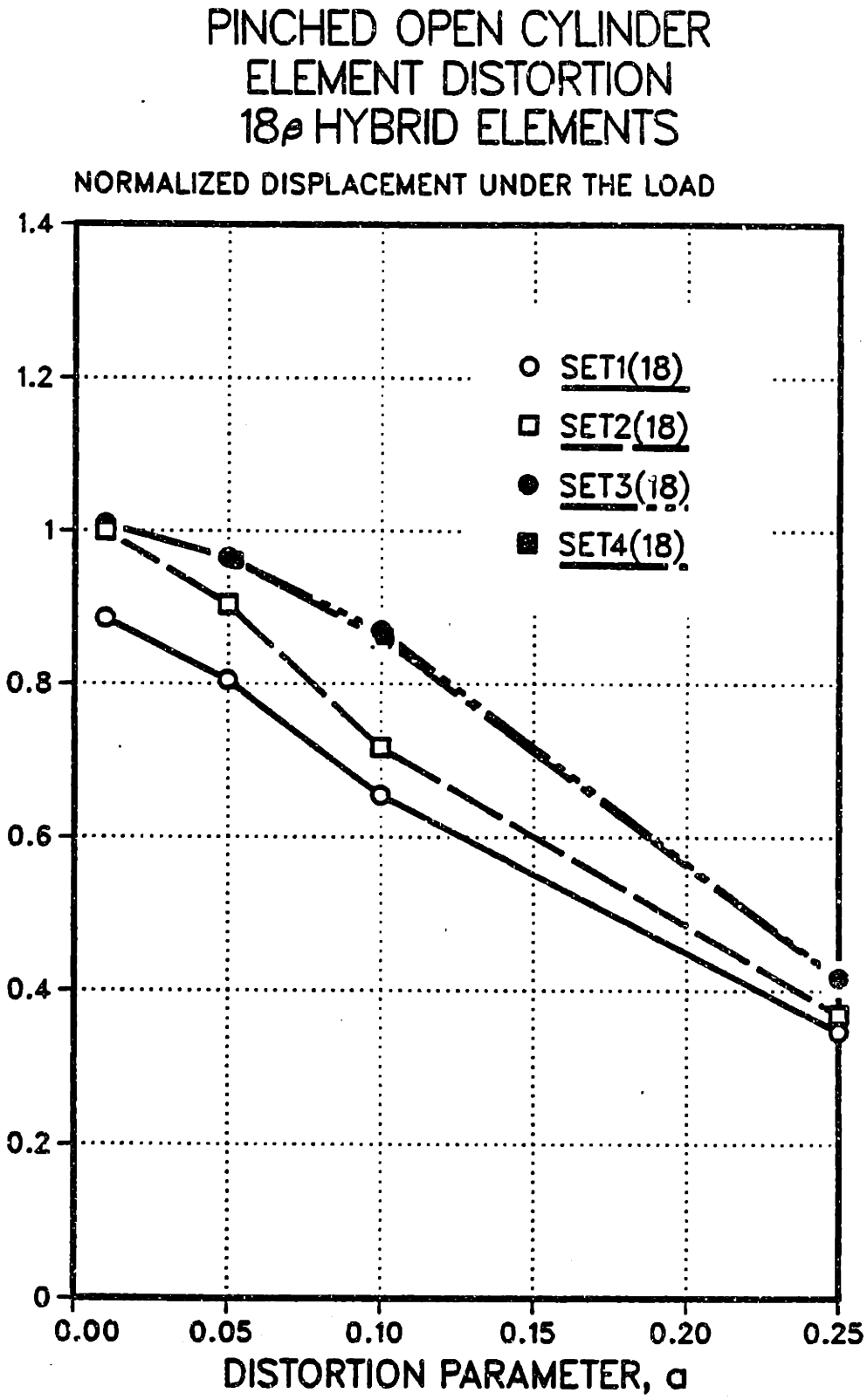

Figure 9-15. Element Distortion Results for 18 β Hybrid Elements.

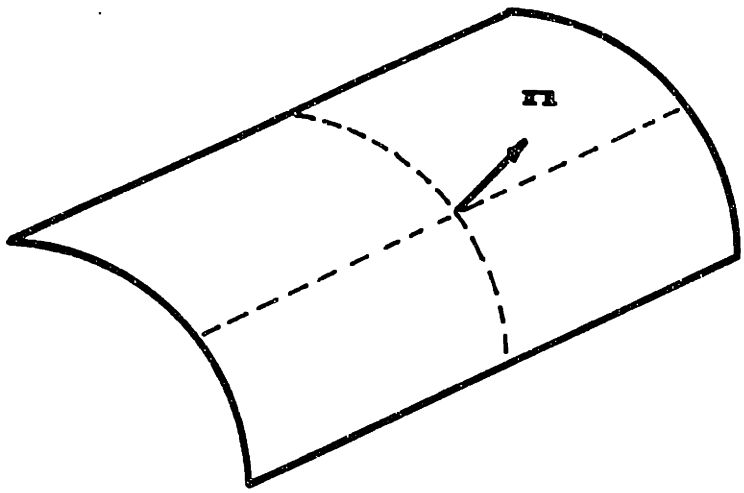

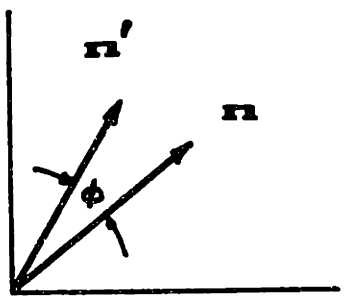

Figure 9-16. Pinched Open Cylinder with Normal Distortion.

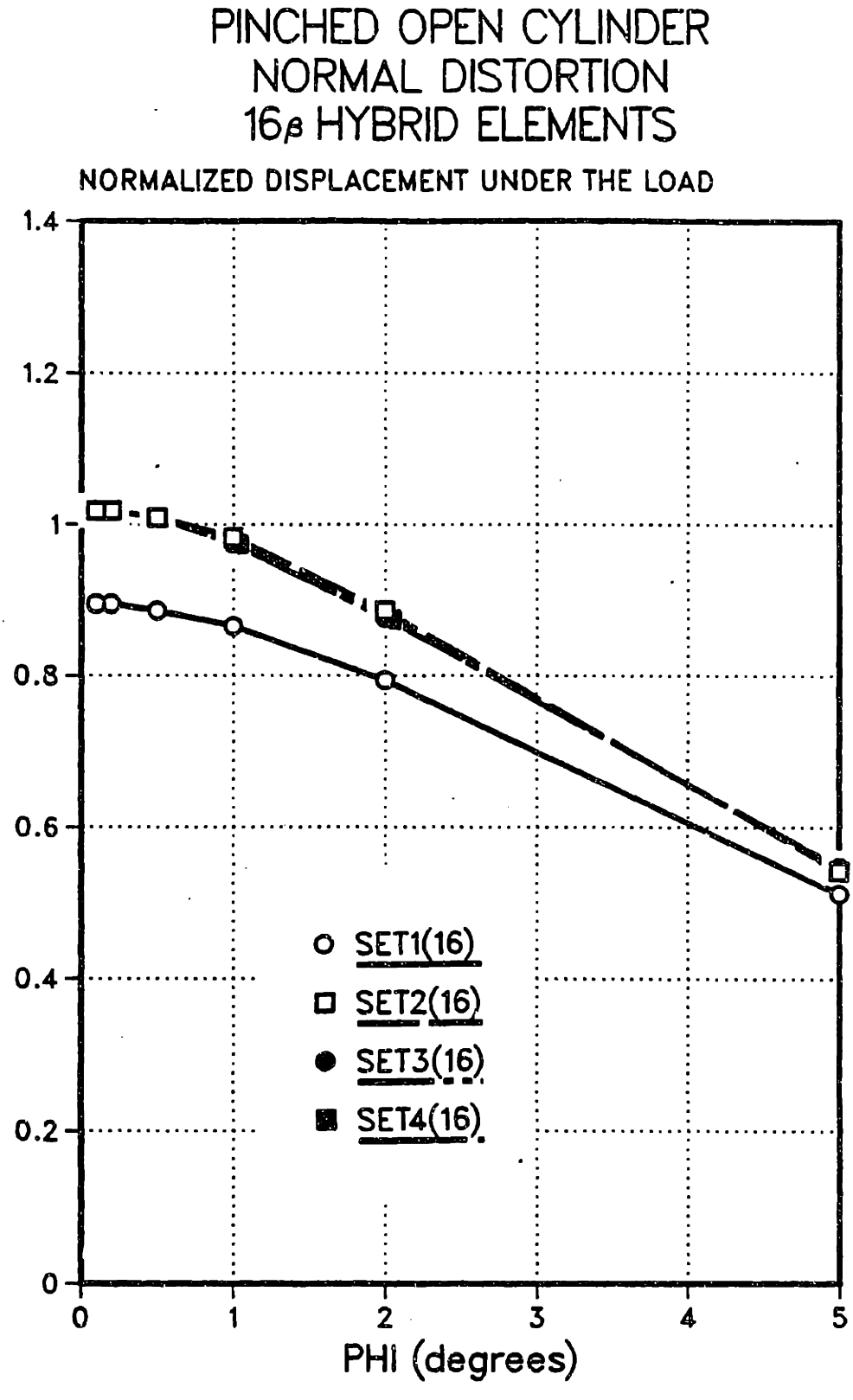

Figure 9-17. Normal Distortion Results for 16 β Hybrid Elements.

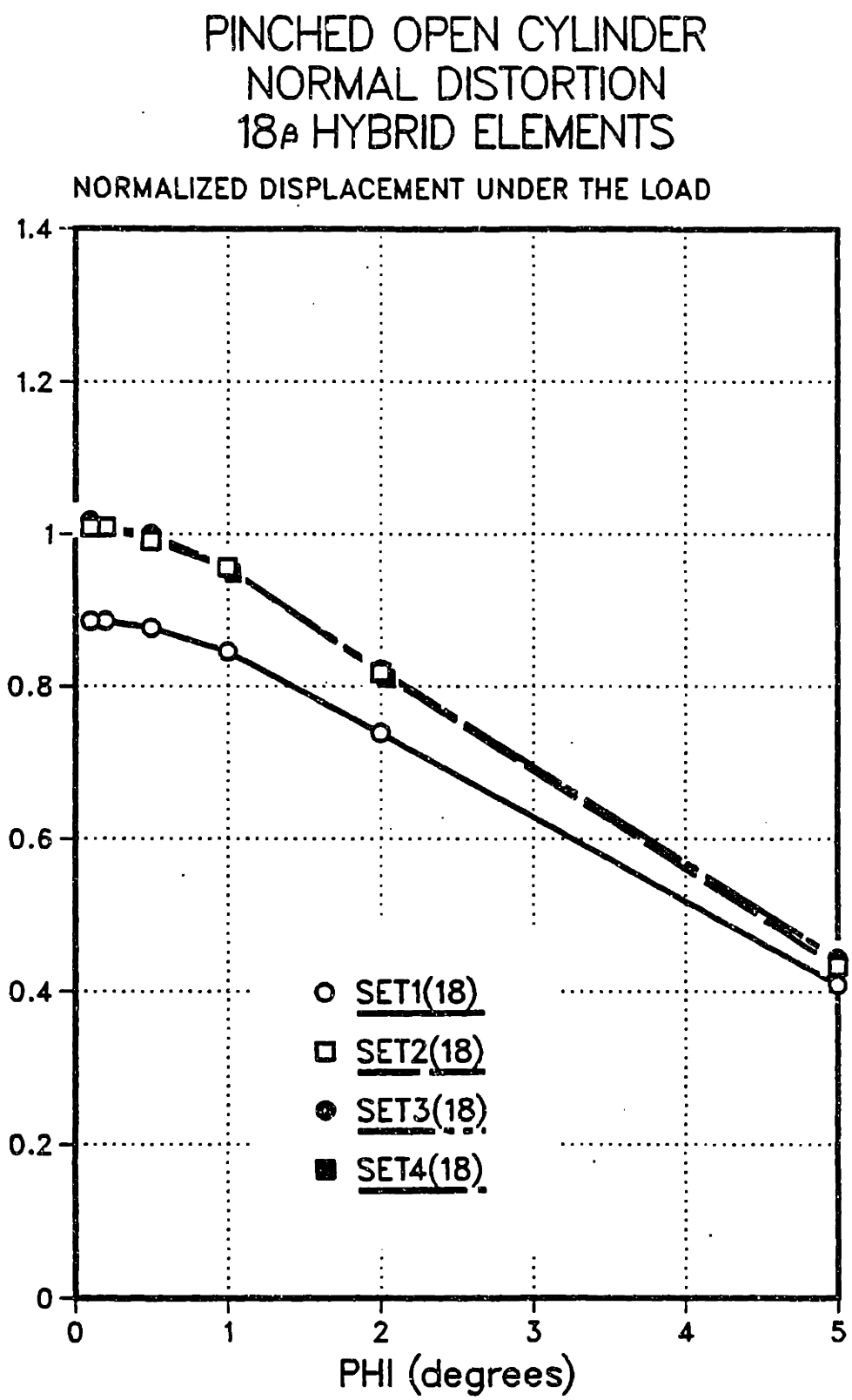

Figure 9-18. Normal Distortion Results for 18 β Hybrid Elements.

9.3.5 Pinched Cylinder with Rigid Diaphragm

A benchmark problem widely used to study the convergence behavior of shell elements is the pinched cylinder with rigid diaphragm ends (Figure 9-19) [100]. The displacement results for the hybrid elements shown in Figure 9-20, indicate a similar behavior for all relaxed equilibrium SETs for this problem.

For comparison, the results from a 4-node flat shell element, DVORKIN, and an 8-node shell element with full integration, BOLOURCHI(F), and reduced integration, BOLOURCHI(R), are plotted in Figure 9-21. The flat shell required a (20X20) mesh for a solution comparable to an (8X8) mesh of hybrid element SET2(18). The fully integrated 8-node element is much too stiff for any practical application. The reduced integrated version produced results which are comparable to the hybrid element results.

For a more complete documentation, the stress distributions obtained by using an (8X8) mesh of SET2(18) hybrid elements are provided in Figures 9-22 to 9-24. Accurate distributions are captured for all three stress resultants.

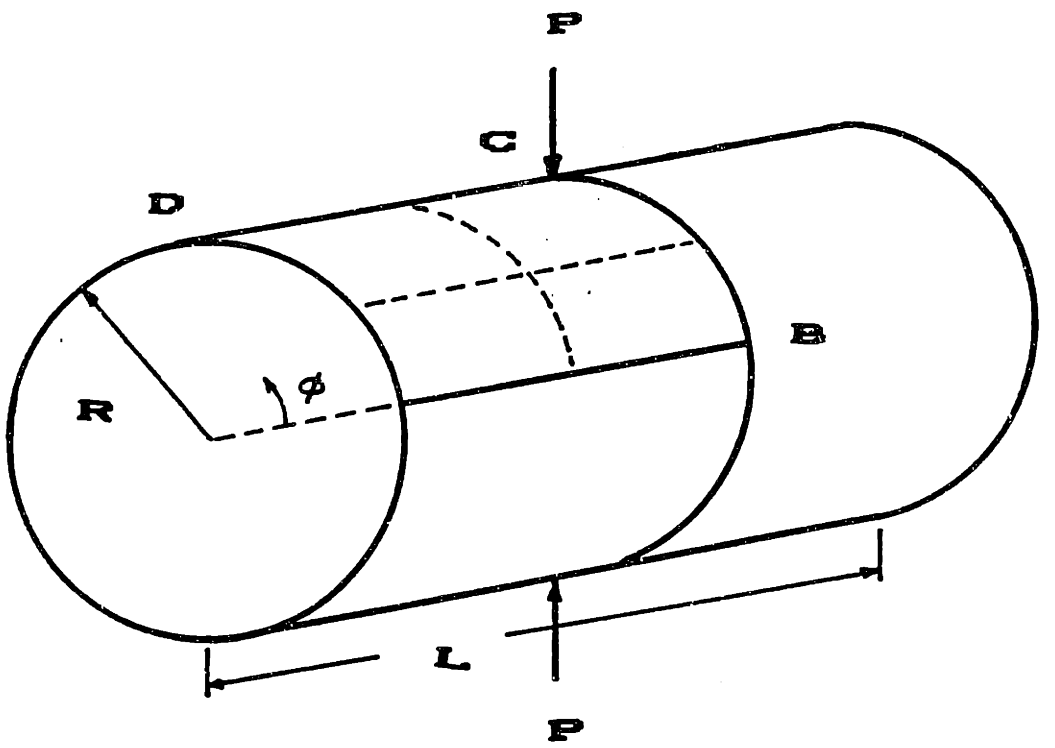

$$\frac{R}{h} = 100$$

$$\frac{L}{R} = 2$$

$$\nu = .3$$

Figure 9-19. Pinched Cylinder with Rigid Diaphragm Ends.

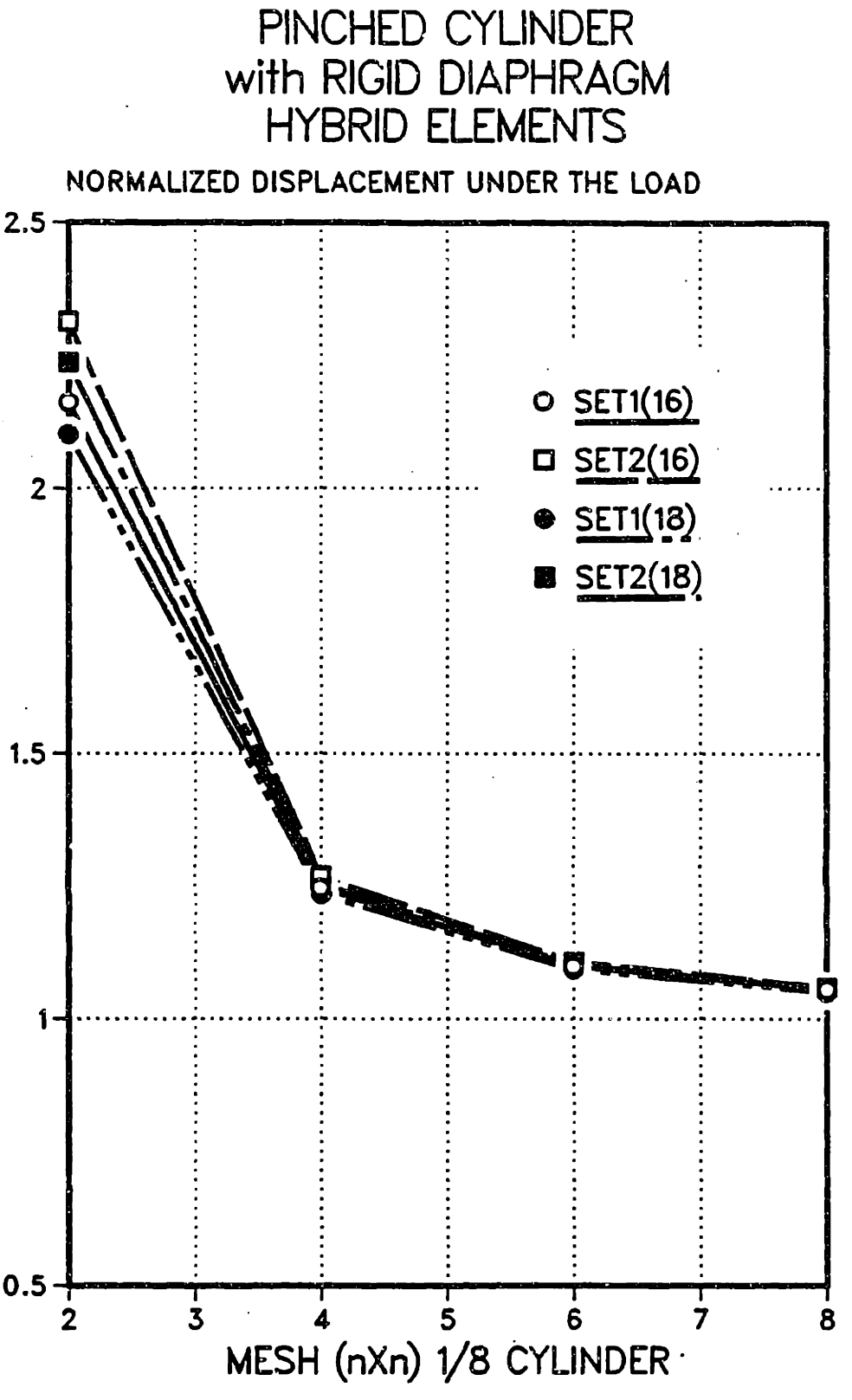

Figure 9-20. Pinched Cylinder with Rigid Diaphragm Displacement Results for Hybrid Shell Elements.

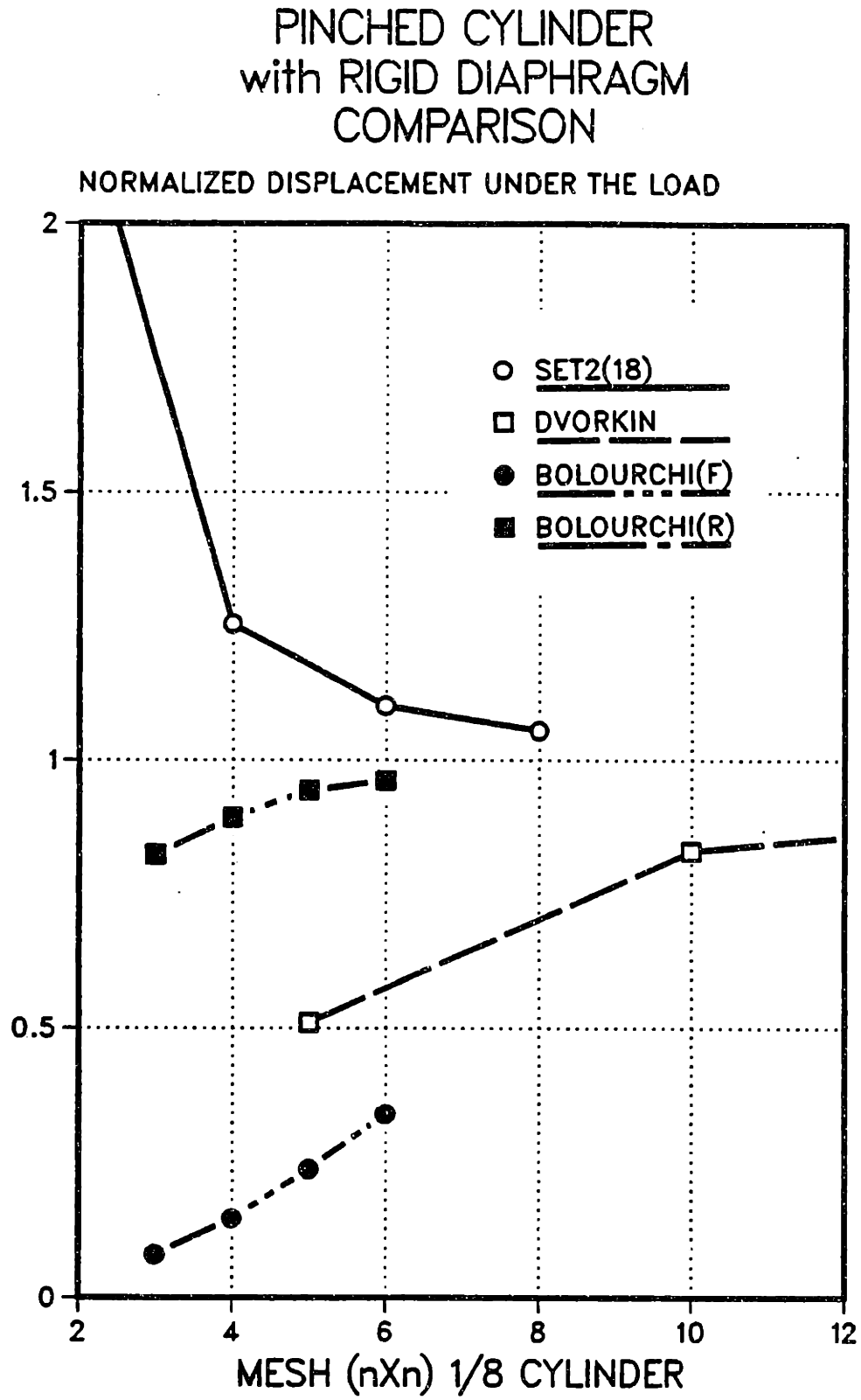

Figure 9-21. Comparison of the Pinched Cylinder with Rigid Diaphragm Displacement Results.

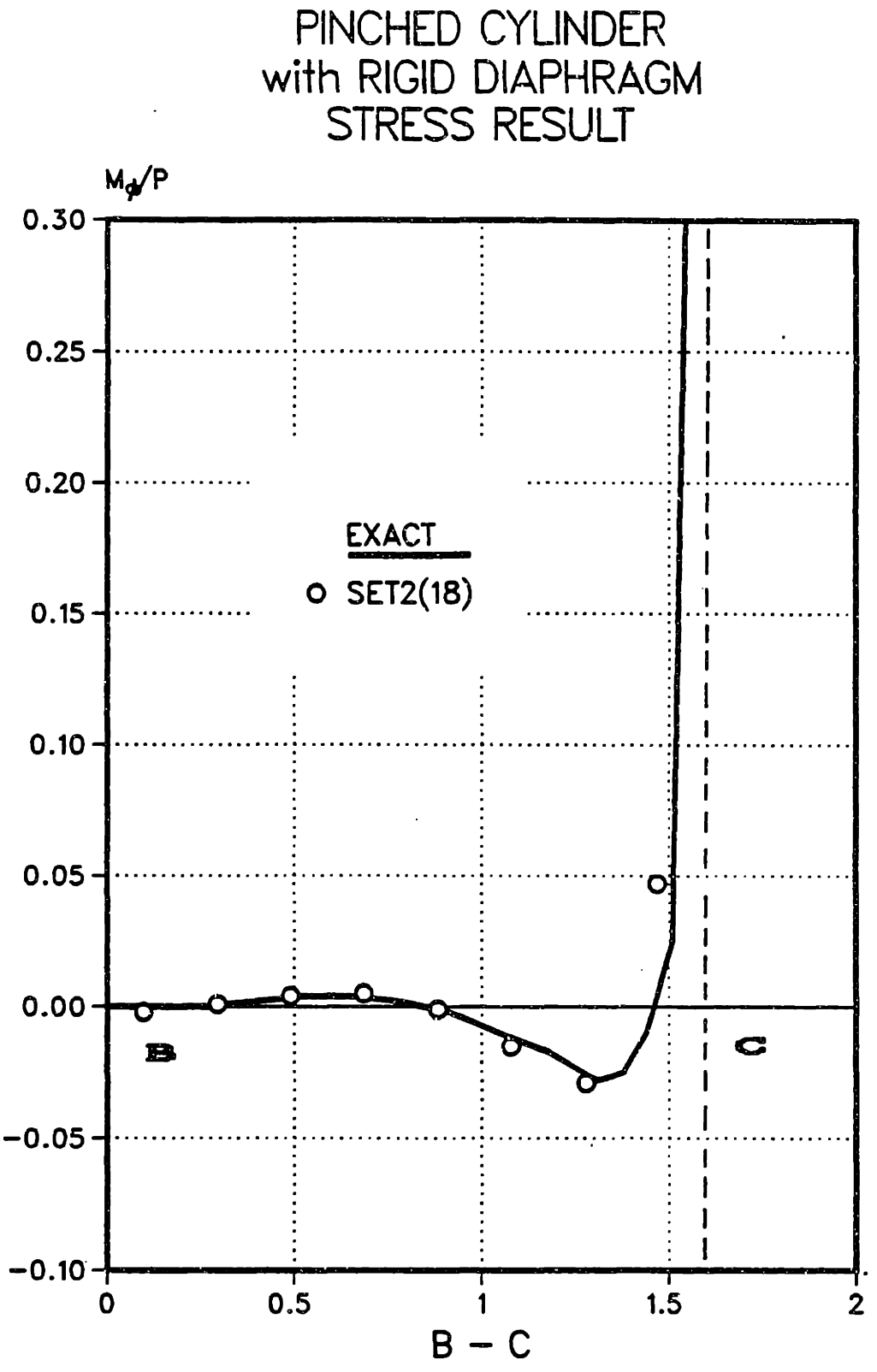

Figure 9-22. Moment Distribution for Pinched Cylinder with Rigid Diaphragm. [(8X8) Mesh]

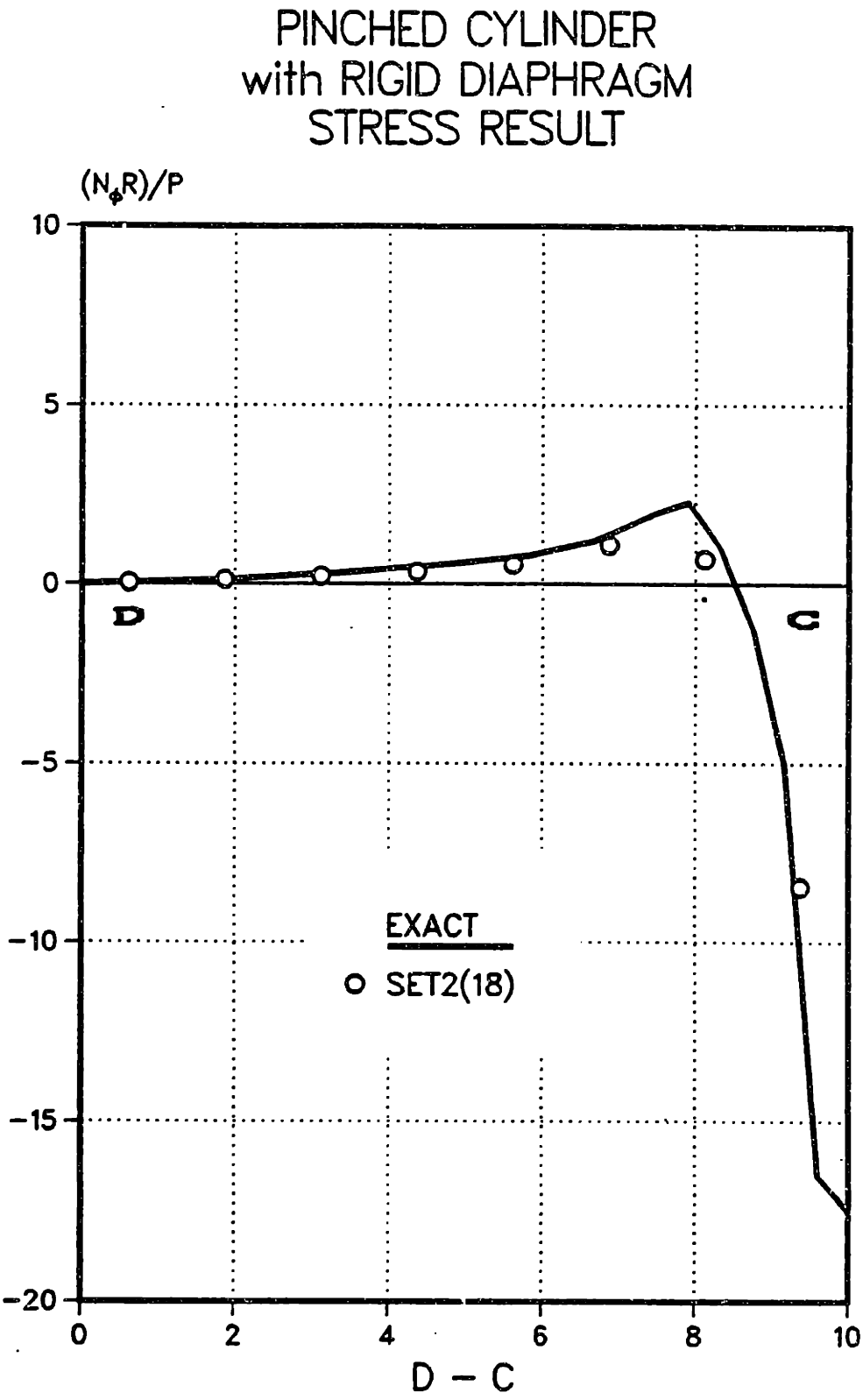

Figure 9-23. Membrane Stress Resultant Distribution for Pinched Cylinder with Rigid Diaphragm. [(8X8) Mesh]

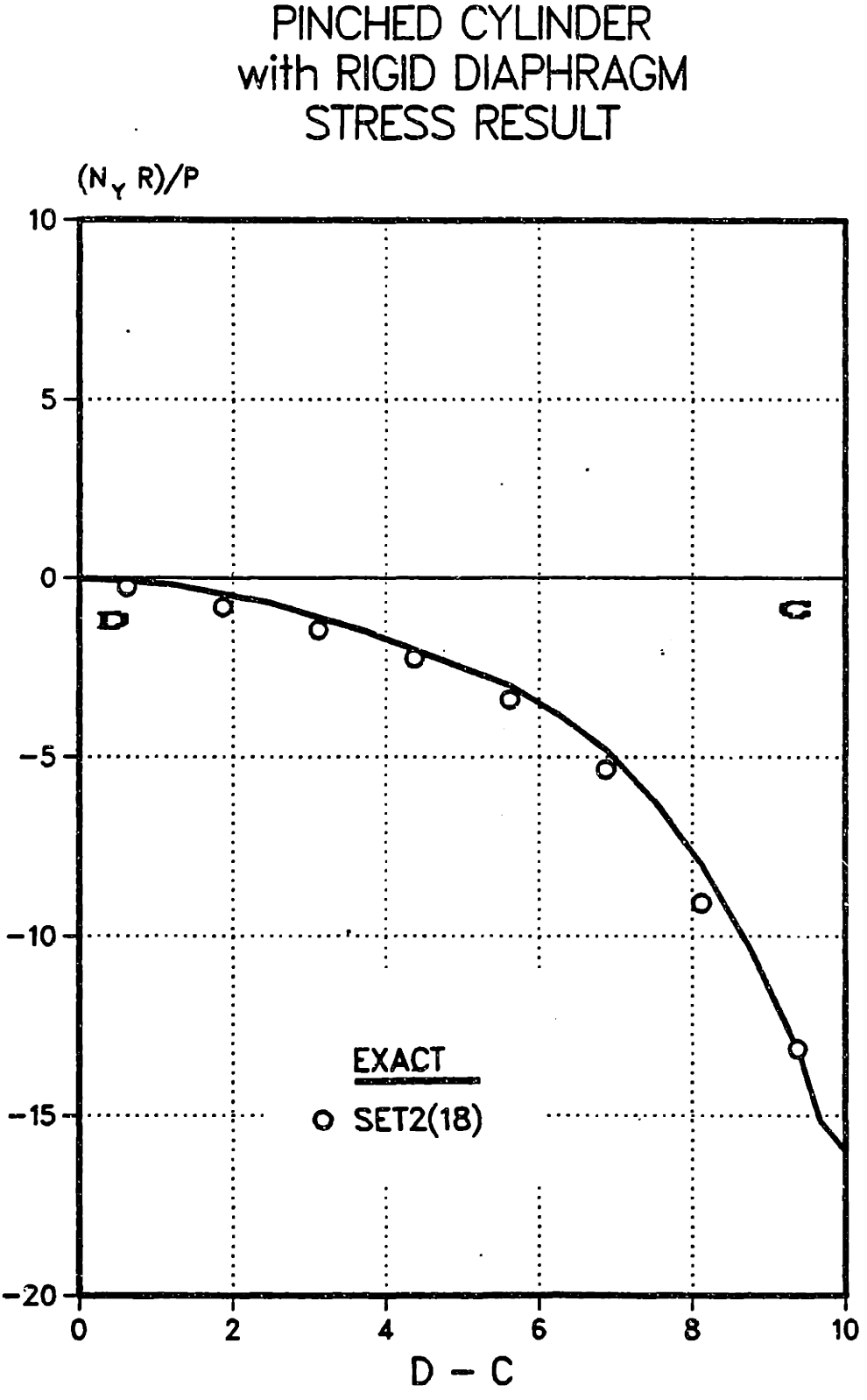

Figure 9-24. **Axial Membrane Stress Resultant Distribution for Pinched Cylinder with Rigid Diaphragm. [(8X8) Mesh]**

9.3.6 Spherical Shell Problem

As the final example, the spherical shell problem proposed by Lindberg et al. [100] was analyzed and is depicted in Figure 9-25. The force is transmitted through a rigid cap subtending an angle of β_0. The results are normalized with a converged solution. Although only a single strip of elements with symmetry conditions is required, a full 1/8 sector of the spherical shell has been modeled.

The displacement results for 16 β and 18 β hybrid elements are provided in Figures 9-26 and 9-27. For the 16 β elements, SET1 and SET2 give almost identical solutions. These elements provide slightly better results than those from the SET3 and SET4 elements. For the 18 β case, the SET1 and SET2 elements are clearly superior to the SET3 and SET4 elements. The SET2(18) element predictions are compared to those for a 3-node 36 degrees of freedom element using exact geometry. This element, denoted as LINDBERG, contains 48 degrees of freedom for a rectangular sector. The results are shown in Figure 9-28. The hybrid element provides much more accurate predictions than with LINDBERG elements which employ twice as many degrees of freedom per sector.

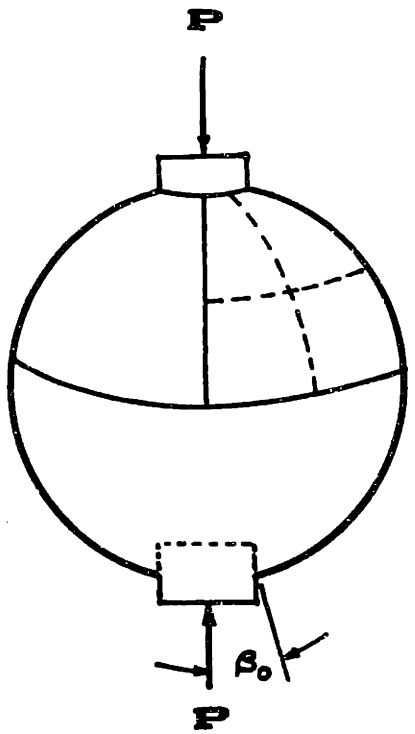

$\frac{R}{h} = 50$

$\nu = .3$

$\beta_0 = 10^\circ$

Figure 9-25. Spherical Shell Problem.

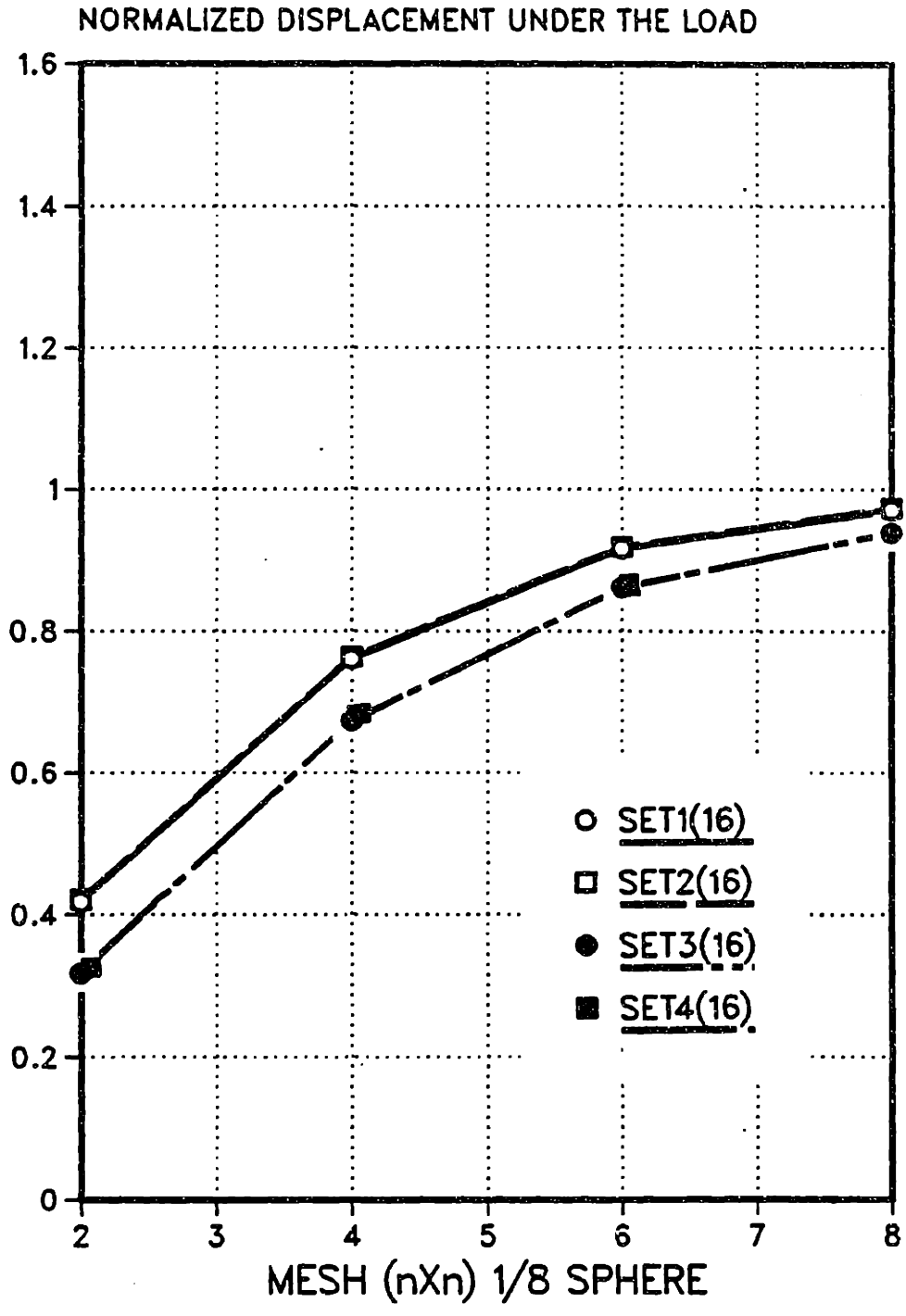

Figure 9-26. Spherical Shell Displacement Results for 16 β Hybrid Elements.

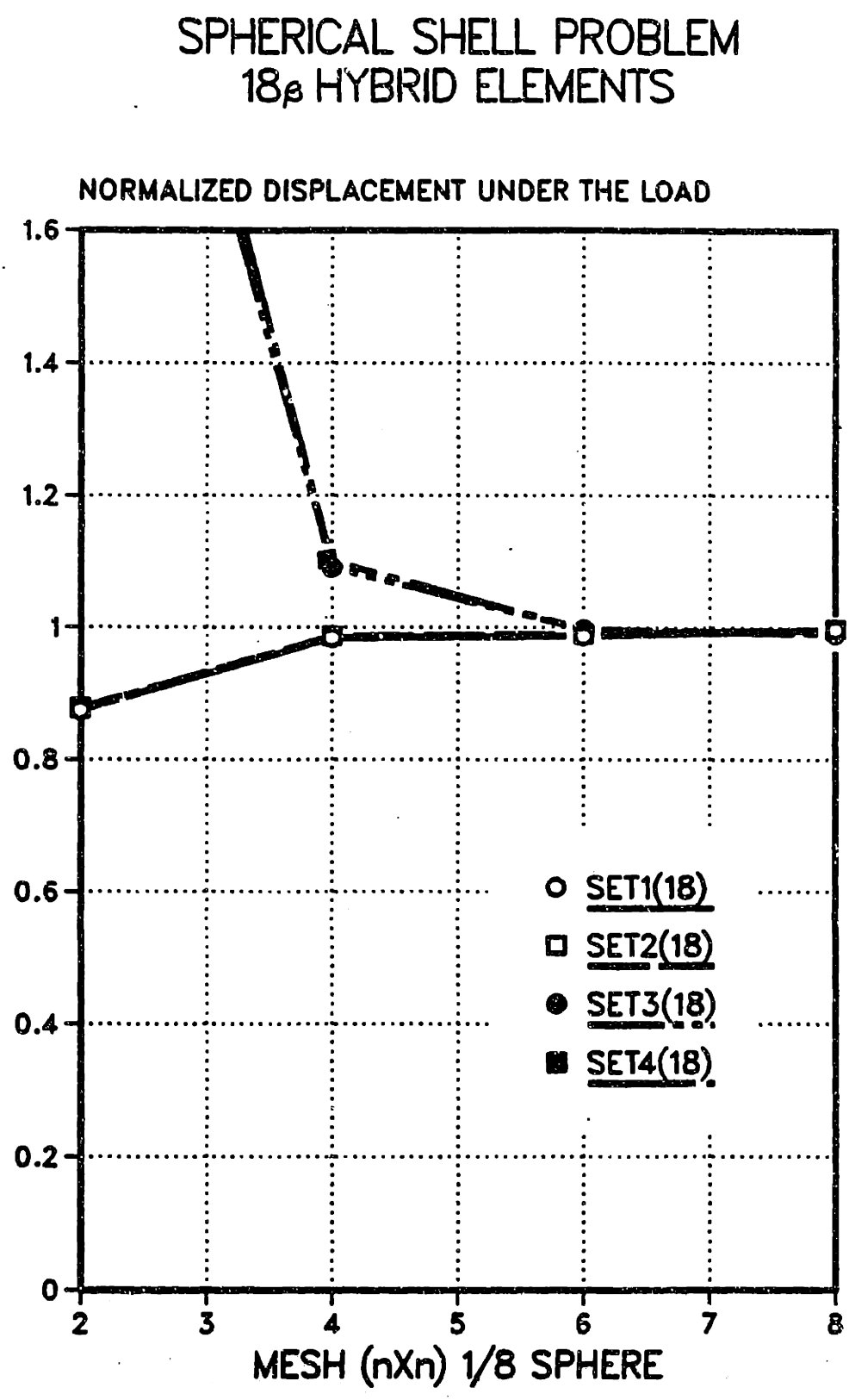

Figure 9-27. Spherical Shell Displacement Results for 18 β Hybrid Elements.

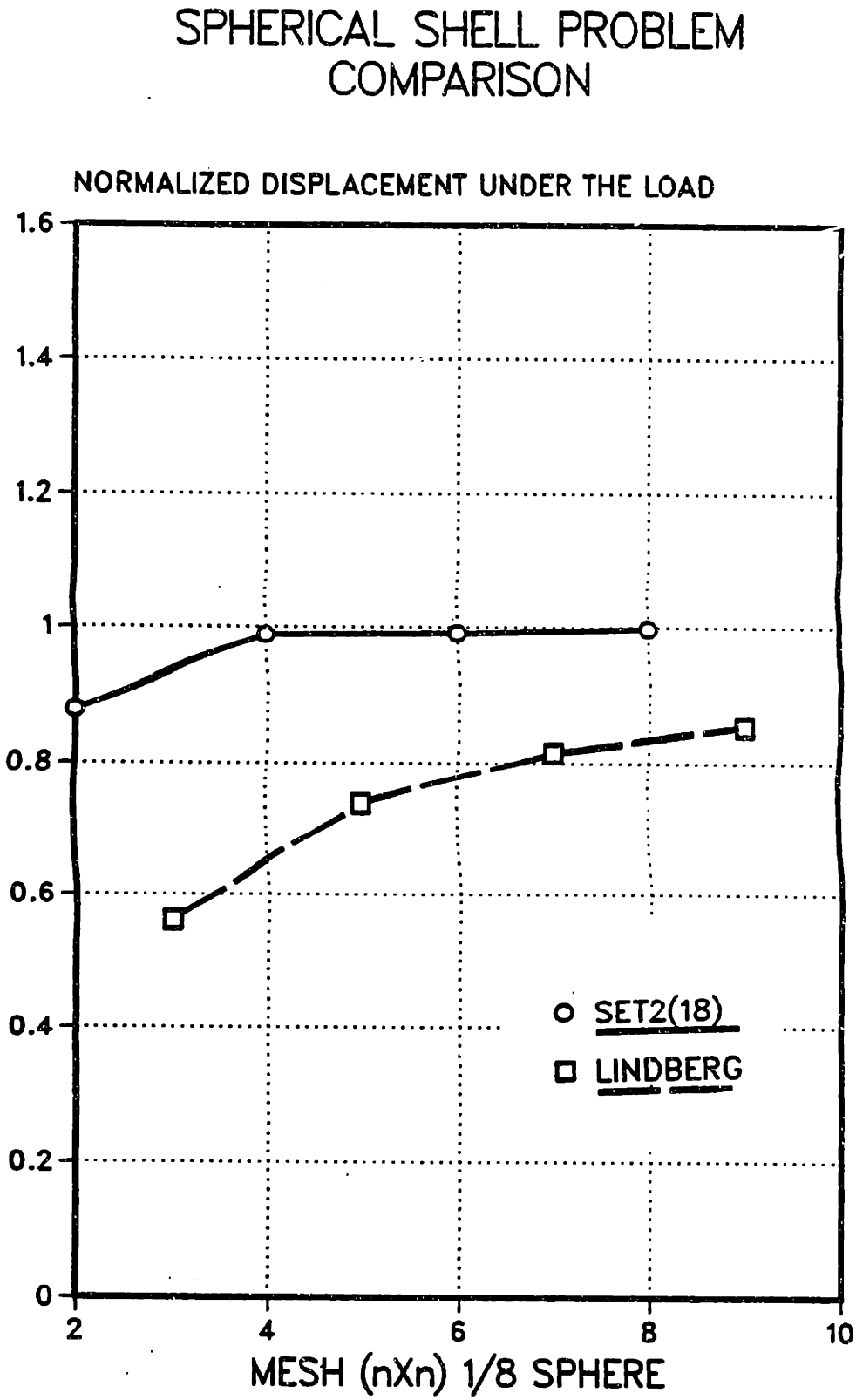

Figure 9-28. Comparison of the Spherical Shell Displacement Results.

9.3.7 Summary

Overall, the numerical examples presented demonstrate the superior performance of the SET2(18) element. The SET1 elements are eliminated because of its behavior as revealed by the pinched cylinder with open ends problem. The SET3 and SET4 elements are eliminated by their behavior shown in the analysis of the spherical shell problem. For practical applications, the SET2(16) element is recommended. The performance of this elements is quite similar to the 18β version of SET2.

The examples further illustrated the need to satisfy partially the pointwise equilibrium equations for a better representation of the rigid body motion. Furthermore, the comparative results repeatedly demonstrated that the 4-node hybrid shell elements are comparable in performance to the higher order elements which use many more degrees of freedom, constructed using the assumed displacement method.

CHAPTER 10

CONCLUSIONS AND RECOMMENDATIONS

10.1 Conclusions and Contributions

The development of the hybrid stress finite element method presented in this thesis has been extensively demonstrated through the construction of a wide range of finite elements. The family of hybrid stress elements consists of

8-Node	SOLID	(24-DOF)
4-Node	PLANE	(8-DOF)
4-Node	PLATE	(12-DOF)
2-Node	ARCH	(6-DOF)
4-Node	GENERAL SHELL	(20-DOF)

These elements are shown to be well-behaved for a large number of benchmark problems. The numerical examples, carefully chosen to assess accuracy, validate the effectiveness of these elements.

The present investigation provides following general conclusions:

1. The hybrid stress method can duplicate element

modifications, such as the reduced integration, the incompatible element formulation, and the assumed strain formulation, but in a variationally consistent manner. This is made possible through the use of the assumed stress field.

2. A direct application of the structural modelling assumptions on the three-dimensional-solid stress field provides a systematic method for selecting appropriate assumed stress fields for the various classes of hybrid elements explored.

3. The assumed stress field does not need to satisfy pointwise equilibrium equations for either distorted or curved elements. However, partial satisfaction of the equilibrium equations are necessary for performance.

Hence, the hybrid elements presented will serve as a standard of comparison for future element developments. Any further future developments in element construction should be incorporated into all five elements for comparison.

10.2 Suggestions for Further Work

The family of hybrid elements provides a basis

required to extend the research into the nonlinear applications. Incorporating these types of elements into a general finite element code would encourage wider acceptance and understanding of the hybrid elements.

From the present investigation, the following areas merit further exploration and development:

1. The hybrid method should be extended to the other field theories such as fluid and electromagnetism.

2. The special purpose elements tailored for a particular geometry should be included in a general purpose finite element codes.

REFERENCES

1. G. Dahlquist and A. Bjorck, Numerical Methods, Prentice-Hall, 1974.

2. G. Strang and G.J. Fix, An Analysis of the Finite Element Method, Prentice-Hall, 1973.

3. R. Richtmyer and K. Morton, Difference Methods for Initial-Value Problems, Interscience, 1967.

4. P.G. Hodge, Jr., Continuum Mechanics, McGraw-Hill, 1970.

5. L.E. Malvern, Introduction to the Mechanics of a Continuous Medium, Prentice-Hall, 1969.

6. H. Reismann and P.S. Pawlik, Elasticity Theory and Applications, Wiley, 1980.

7. S.P. Timoshenko and S. Woinowsky-Krieger, Theory of Plates and Shells, McGraw-Hill, 1959.

8. S.P. Timoshenko and J.N. Goodier, Theory of Elasticity, 3rd ed., McGraw-Hill, 1970.

9. K. Washizu, Variational Methods in Elasticity and Plasticity, 3rd ed., Pergamon, 1982.

10. J.T. Oden and J.N. Reddy, Variational Methods in Theoretical Mechanics, Springer-Verlag, 1983.

11. T.H.H. Pian and P. Tong, "Basis of Finite Element Methods for Solid Continua", Int.J.Num.Meth.Engng., 1, 3-28, 1969.

12. H.J. Karcher, "Finite Elements on the Basis of Continuum Mechanics", Int.J.Num.Meth.Engng., 9, 129-147, 1975.

13. S. Nemat-Nasser, ed., Variational Methods in the Mechanics of Solids, Proc. IUTAM Symp. 1978, Pergamon, 1980.

14. P.G. Ciarlet, The Finite Element Method for Elliptic Problems, North-Holland, 1980.

15. J.T. Oden and G.F. Carey, Finite Elements Mathematical Aspects IV, Prentice-Hall, 1983.

16. B. Irons and S. Ahmad, Techniques of Finite Elements, Ellis-Horwood, 1980.

17. B.M. Irons and M. Loikkanen, "An Engineers Defence of the Patch Test", Int.J.Num.Meth.Engng., 19, 1391-1401, 1983.

18. F. Stummel, "The Generalized Patch Test", Siam J.Num.Anal., 16, 449-471, 1979.

19. F. Stummel, "The Limitations of the Patch Test", Int.J.Num.Meth.Engng., 15, 177-188, 1980.

20. T.H.H. Pian, "Derivation of Element Stiffness Matrices by Assumed Stress Distribution", AIAA J., 2, 1333-1336, 1964.

21. T.H.H. Pian and P. Tong, "Rationalization in Deriving Element Stiffness Matrix by Assumed Stress Approach", AFFDL-TR-68-150, 441-469, 1968.

22. T.H.H. Pian, "Finite Element Methods by Variational Principles with Relaxed Continuity Requirement", Variational Meth. In Engng., Brebbia and Tottenham, eds., Southampton Univ. Press, 3/1-3/24, 1973.

23. T.H.H. Pian, "Variational and Finite Element Methods in Structural Analysis", Israel J.Tech., 16, 23-33, 1978.

24. T.H.H. Pian and D-P. Chen, "Alternative Ways for Formulation of Hybrid Stress Elements", Int.J.Num.Meth.Engng., 18, 1679-1684, 1982.

25. T.H.H. Pian, "Recent Advances in Hybrid/Mixed Finite Elements", Int.Conf. on Finite Element Methods, Shanghai, China, 1-19, 1982.

26. P. Tong and T.H.H. Pian, "The Convergence of Finite Element Method in Solving Linear Elastic Problems", Int.J. Solids Structures, 3, 865-879, 1967.

27. P. Tong and T.H.H. Pian, "A Variational Principle and the Convergence of a Finite Element Method Based on Assumed Stress Distribution", Int.J.Num.Meth.Engng., 1, 463-472, 1969.

28. P. Tong, "On the Construction of Three Dimensional Hybrid Stress Elements", unpublished manuscript available to the author.

29. G.M. Fix, "Hybrid Finite Element Methods", SIAM Review, 19, 460-484, 1976.

30. D.S. Kang, "C Continuity Elements by Hybrid Stress Method", M.S. Thesis, Mass. Inst. of Tech., 1982.

31. T.H.H. Pian and D. Chen, "On the Suppression of Zero Energy Deformation Modes", Int.J.Num.Meth.Engng., 19, 1741-1752, 1983.

32. C.T. Yang, R. Rubinstein, and S.N. Atluri, "On some fundamental studies into the stability of hybrid/mixed finite element methods for Navier/Stokes equations in Solid/Fluid mechanics", Proc. 6th invitational symposium on the unification of finite elements - finite difference and calculus of variations (ed. H. Kardestuncer) Univ. of Connecticut, Storrs, Conn., 25-75, 1982.

33. K-J. Bathe, Finite Element Procedures in Engineering Analysis, Prentice-Hall, 1982.

34. E.B. Becker, G.F. Carey, and J.T. Oden, Finite Elements and Introduction I, Prentice-Hall, 1981.

35. R.D. Cook, Concepts and Applications of Finite Element Analysis, 2nd ed., Wiley, 1981.

36. E. Hinton and D.R.J. Owen, Finite Element Programming, Academic Press, 1977.

37. P. Tong and J.N. Rossettos, Finite-Element Method Basic Technique and Implementation, MIT Press, 1977.

38. O.C. Zienkiewicz, The Finite Element Method, 3rd ed., McGraw-Hill, 1977.

39. J.S. Przemieniecki, Theory of Matrix Structural Analysis, McGraw-Hill, 1968.

40. W.G. Gray and M.T. Van Genuchten, "Economical Alternatives to Gaussian Quadrature over Isoparmetric Quadrilaterals", Int.J.Num.Meth.Engng., 12, 1478-1484, 1978.

41. B.M. Irons, "Quadrature Rules for Brick Based Finite Elements", Int.J.Num.Meth.Engng., 2, 293-294, 1970.

42. L. J. Hayes, "Practical Stability Test for Finite Elements with Reduced Integration", Int.J.Num.Meth.Engng., 17, 1689-1695, 1981.

43. T.J.R. Hughes, R. Taylor, and W. Kanoknukulachai, "A Simple and Efficient Finite Element for Plate Bending", Int.J.Num.Meth.Engng., 11, 1529-1543, 1977.

44. T.J.R. Hughes, M. Cohen, and M. Haroun, "Reduced and Selective Integration Techniques in the Finite Element Analysis of Plates", Nuclear Engng. and Design, 46, 203-222, 1978.

45. T.J.R. Hughes, "Generalization of Selective Integration Procedures to Anisotropic and Nonlinear Media", Int.J.Num.Meth.Engng., 15, 1413-1418, 1980.

46. C. Johnson and J. Pitkaranta, "Analysis of Some Mixed Finite Element Methods Related to Reduced Integration", Math. of Comp., 38, 375-400, 1982.

47. D.S. Malkus and T.J.R. Hughes, "Mixed Finite Element Methods - Reduced and Selective Integration Techniques: A Unification of Concepts", Comp.Meth.Appl.Mech.Engng., 15, 63-81, 1978.

48. A.K. Noor and J.M. Peters, "Mixed Models and Reduced/Selective Integration Displacement Models for Nonlinear Analysis of Curved Beams", Int.J.Num.Meth.Engng., 17, 615-631, 1981.

49. A.K. Noor and J.M. Peters, "Mixed Models and Reduced/Selective Integration Displacement Models for Vibration Analysis of Shells", Hybrid and Mixed Finite Element Methods, Atluri, Gallagher, Zienkiewicz, eds., Wiley, 1983.

50. H. Shimodaira, "Equivalence between Mixed Models and Displacement Models using Reduced Integration", Int.J.Num.Meth.Engng., 21, 89-104, 1985.

51. E. Wilson, R. Taylor, W. Doherty, and J. Ghaboussi, "Incompatible Displacement Models", in Num. and Comp. Meth. in Struct. Mech., Fenves et al., eds., Academic Press, 43-57, 1973.

52. R.L. Taylor, P.J. Beresford, and E.L. Wilson, "A Non-Conforming Element for Stress Analysis", Int.J.Num.Meth.Engng., 10, 1211-1219, 1976.

53. B.M. Irons, "An Assumed-Stress Version of the Wilson 8-Node Isoparametric Brick", Computer Report CNME/CR/56, Univ. College of Swansea, 1972.

54. R.H. MacNeal, "A Simple Quadrilateral Shell Element", Comp. and Struct., 8, 175-183, 1978.

55. R.H. MacNeal, "Derivation of Element Stiffness Matrices by Assumed Strain Distribution", Nuc. Engng. and Design, 70, 3-12, 1982.

56. E.N. Dvorkin, "On Nonlinear Finite Element Analysis of Shell Structures", Ph.D. Thesis, Mass. Inst. of Tech., 1984.

57. J. Robinson, Integrated Theory of Finite Element Methods, Wiley, 1973.

58. J. Robinson, "Automatic Extraction of Rigid Body Modes from Stress and Strain Elements", Variational Meth. in Engng., Brebbia and Tottenham, eds., 4/73-4/93, 1972.

59. J. Robinson and G.W. Haggenmacher, "LORA - An Accurate Four Node Stress Plate Bending Element", Int.J.Num.Meth.Engng., 14, 296-306, 1979.

60. M.J. Loikkanen, "Hybrid Finite Elements with Shape Function Subroutine", Ph.D. Thesis, Univ. of Calgary, 1982.

61. K.O. Friedrichs and R.F. Dressler, "A Boundary-Layer Theory for Elastic Plates", Comm. on Pure and App. Math., XIV, 1-33, 1961.

62. E.L. Reiss and S. Locke, "On The Theory of Plane Stress", Q. Appl. Math., 19, 195-203, 1961.

63. N. Laws, "A Boundary-Layer Theory for Plates with Initial Stress", Proc. Camb. Phil. Soc., 62, 313-327,1966.

64. T.H.H. Pian, D. Kang, and C. Wang, "Hybrid Plate Elements Based on Balanced Stresses and Displacements", to be published in State-of-the-Art Texts on Finite Element Methods in Plate and Shell Structural Analysis, Ed. by T.J.R. Hughes and E. Hinton, Pineridge Press, Swansea, Wales, U.K., 1986.

65. K. Sumihara, "Thin Shell and New Invariant Elements by Hybrid Stress Method", Ph.D. Thesis, Mass. Inst. of Tech., 1983.

66. T.H.H. Pian and P. Tong, "Relations Between Incompatible Displacement Model and Hybrid Stress Model", Int.J.Num.Meth.Engng., 22, 173-181, 1986.

67. T.H.H. Pian and Z.S. Tian, "Hybrid Solid Element with a Traction-Free Cylindrical Surface", Proc. Symp. on 'Hybrid and Mixed Finite Element Method'", edited by R.L. Spilker and K.W. Reed, ASME AMD, 73, 141-149, 1985.

68. R.L. Spilker and N.I. Munir, "Comparison of Hybrid-Stress Element Through-Thickness Distributions Corresponding to a High-Order Plate Theory", Comp. and Struct., 11, 579-586, 1980.

69. R.L. Spilker and N.I. Munir, "The Hybrid-Stress Model for Thin Plates", Int.J.Num.Meth.Engng., 15, 1239-1260, 1980.

70. R.L. Spilker and N.I. Munir, "A Hybrid-Stress Quadratic Serendipity Displacement Mindlin Plate Bending Element", Comp. and Struct., 12, 11-21, 1980.

71. R.L. Spilker and N.I. Munir, "A Serendipity Cubic-Displacement Hybrid-Stress Element for Thin and Moderately Thick Plates", Int.J.Num.Meth.Engng., 15, 1261-1278, 1980.

72. R.L. Spilker, "Invariant 8-Node Hybrid-Stress Elements for Thin and Moderately Thick Plates", Int.J.Num.Meth.Engng., 18, 1153-1178, 1982.

73. J.P. Wolf, Generalized Stress Models for Finite Element Analysis, Dissertation No. 5263, Swiss Federal Inst. of Tech., Zurich, 1974.

74. T.J.R. Hughes and T.E. Tezduyar, "Finite Elements Based Upon Mindlin Plate Theory with Particular References to the Four-Node Bilinear Isoparametric Element", J.Appl.Mech., 48, 587-596, 1981.

75. L.S.D. Morley, Skew Plates and Structures, Pergamon, 1963.

76. J. Robinson, "Skew-Effects - FEM user project No. 2 - Morley's simply supported skew plate problem", Finite Element News, No. 3 and 5, 1983.

77. T.H.H. Pian, P. Tong, and C.H. Luk, "Elastic Crack Analysis by a Finite Element Hybrid Method", Proc. Third Conf. on Matrix Methods in Structural Mechanics, AFFDL-TR-71-160, 661-682, 1973.

78. D.G. Ashwell and A.B. Sabir, "Limitations of Certain Curved Finite Elements when Applied to Arches", Int.J.Mech.Sci., 13, 133-139, 1971.

79. D.G. Ashwell, A.B. Sabir, and T.M. Roberts, "Further Studies in the Application of Curved Finite Elements to Circular Arches", Int.J.Mech.Sci., 13, 507-517, 1971.

80. D.G. Ashwell and A.B. Sabir, "On the Finite Element Calculation of Stress Distribution in Arches", Int.J.Mech.Sci., 16, 21-29, 1974.

81. D.G. Ashwell, "Strain Elements, with Applications to Arches, Rings, and Cylindrical Shells", in Finite Elements for Thin Shells and Curved Members, Ashwell and Gallagher, eds., Wiley, 91-112, 1976.

82. D.J. Dawe, "Curved Finite Elements for the Analysis of Shallow and Deep Arches", Computers and Structures, 4, 559-580, 1974.

83. D.J. Dawe, "Numerical Studies Using Circular Arch Finite Elements", Computers and Structures, 4, 729-740, 1974.

84. D.J. Dawe, "Some High-Order Element for Arches and Shells", in Finite Elements for Thin Shells and Curved Members, Ashwell and Gallagher, eds., Wiley, 131-154, 1976.

85. D.G. Ashwell and R.H. Gallagher, eds., Finite Elements for Thin Shells and Curved Members, Wiley, 1976.

86. L.S.D. Morley, "Polynomial Stress States in First Approximation Theory of Circular Cylindrical Shells", Q.J.Mech.Appl.Math., 25, 13-43, 1972.

87. L.S.D. Morley, "Analysis of Developable Shells With Special Reference to the Finite Element Method and Circular Cylinders", Phil.Trans.R.Soc.Lond.A., 281, 113-170, 1976.

88. L.S.D. Morley, "Inextensional Bending of a Shell Triangular Element in Quadratic Parametric Representation", Int.J.Sol.Struct., 18, 919-935, 1982.

89. L.S.D. Morley, "Approximation to Bending Trial Functions for Shell Triangular Finite Elements in Quadratic Parametric Representation", Comp. and Struct., 16, 657-668, 1983.

90. L.S.D. Morley, "Quality of Trial Functions in Quadratic Isoparametric Representation of an Arc", Int.J.Num.Meth.Engng., 19, 37-47, 1983.

91. W.E. Haisler and J.A. Stricklin, "Rigid-Body Displacements of Curved Elements in the Analysis of Shells by the Matrix-Displacement Method", AIAA J., 1525-1527, August 1967.

92. P.M. Mebane and J.A.Stricklin, "Implicit Rigid Body Motion in Curved Finite Elements", AIAA J., 9, 344-345, 1971.

93. W. Flugge, Stresses in Shells, Springer-Verlag, 1973.

94. H. Kraus, Thin Elastic Shells, Wiley, 1967.

95. H. Mollmann, Introduction to the Theory of Thin Shells, Wiley, 1981.

96. B. Budiansky and J.L. Sanders, "On the Best First-Order Linear Shell Theory", Progress in Applied Mech., The Prager Anniversary Vol., New York, 1963, 129-140.

97. W.T. Koiter, "A Consistent First Approximation in the General Theory of Thin Elastic Shells", Proc. of the Symp. in the Theory of Thin Elastic Shells, Delft, Aug. 1959, Koiter, ed., North-Holland, Delft, 12-33, 1960.

98. J.L. Sanders, "An Improved First-Approximation Theory for Thin Shells", NASA TR R-24, 1959.

99. J.L. Sanders, "Nonlinear Theories for Thin Shells", Q.Appl.Math., 21, 21-36, 1963.

100. G.M. Lindberg, M.D. Olson, and G.R. Cowper, "New Developments in the Finite Element Analysis of Shells", Q. Bull. Div. Mech. Eng. and the National Aeronautical Establishment, National Research Council of Canada, 4, 1969.

101. G.M. Stanley, Continuum-Based Shell Elements, Ph.D. Thesis, Stanford Univ., 1985.

102. G.R. Heppler and J.S. Hansen, "A Mindlin Element for Thick and Deep Shells", Comp. Meth. in Appl. Mech. and Engng., 54, 21-47, 1986.

103. S. Bolourchi, On Finite Element Nonlinear Analysis of General Shell Structures, Ph.D. Thesis, Mass. Inst. of Tech., 1979.

APPENDIX A

INCOMPRESSIBILITY

A treatment of incompressible material in the following discussion deals with standard finite elements. "standard" in the sense of element construction without resorting to specialized methods such as the penalty method. The present study is chosen to demonstrate the material-dependent accuracy inherent in using selective reduced integration.

The specific example selected for demonstration is a 4-node plane strain element. As a side note, recall that the constitutive relations for a plane strain model is an exact reduction from the three dimensional continuum. For a selectively integrated isoparametric element in an undistorted configuration, the displacement and strain fields are represented as

$$\begin{aligned} u &= \alpha_1 + \alpha_2 x + \alpha_3 y + \alpha_4 xy \\ v &= \alpha_5 + \alpha_6 x + \alpha_7 y + \alpha_8 xy \end{aligned} \tag{A.1}$$

$$\begin{aligned} \varepsilon_x &= \alpha_2 + \alpha_4 y \\ \varepsilon_y &= \alpha_7 + \alpha_8 x \\ \gamma_{xy} &= (\alpha_3 + \alpha_6) \end{aligned} \tag{A.2}$$

In the incompressible material limit

$$\varepsilon_x + \varepsilon_y = 0 \qquad (A.3)$$

Appling Eq. (A.3) to Eq. (A.2) results in

$$\begin{aligned} \alpha_2 + \alpha_7 &= 0 \\ \alpha_4 &= 0 \\ \alpha_8 &= 0 \end{aligned} \qquad (A.4)$$

As $\nu \to \frac{1}{2}$, the three constraints in Eq. (A.4) reduces the field to

$$\begin{aligned} \varepsilon_x &= \alpha_2 \\ \varepsilon_y &= \alpha_2 \\ \gamma_{xy} &= (\alpha_3 + \alpha_6) \end{aligned} \qquad (A.5)$$

With only two possible deformation modes, an element based upon the above field may lock with the application of boundary condition constraints.

For comparison, an incompatible element is formulated for the plane strain model in the following. The displacement field, with added incompatible modes, is given by

$$\begin{aligned} u &= \alpha_1 + \alpha_2 x + \alpha_3 y + \alpha_4 xy + \lambda_1(1-x^2) + \lambda_2(1-y^2) \\ v &= \alpha_5 + \alpha_6 x + \alpha_7 y + \alpha_8 xy + \lambda_3(1-x^2) + \lambda_4(1-y^2) \end{aligned} \qquad (A.6)$$

After condensation of the four incompatible modes, the resulting strain field is expressed in terms of the α's is.

$$\begin{aligned} \varepsilon_x &= \alpha_2 + \alpha_4 y - \frac{\nu}{1-\nu}\alpha_8 x \\ \varepsilon_y &= \alpha_7 + \alpha_8 x - \frac{\nu}{1-\nu}\alpha_4 y \\ \gamma_{xy} &= (\alpha_3 + \alpha_6) \end{aligned} \qquad (A.7)$$

The incompressible material limit yield

$$\varepsilon_x + \varepsilon_y = (\alpha_2 + \alpha_7) + \left(\frac{1-2\nu}{1-\nu}\right)\alpha_4 y + \left(\frac{1-2\nu}{1-\nu}\right)\alpha_8 x \to 0$$

$$\text{as} \quad \nu \to \tfrac{1}{2} \qquad (A.8)$$

Only one constraint results:

$$\alpha_2 + \alpha_7 = 0 \qquad (A.9)$$

Application of Eq. (A.7) to the constitutive relations yields

$$\begin{aligned} \sigma_x &= \beta_1 + \beta_4 y \\ \sigma_y &= \beta_2 + \beta_5 x \\ \sigma_{xy} &= \beta_3 \end{aligned} \qquad (A.10)$$

where

$$\beta_i = \beta_i(\alpha_i)$$

The above 5 β stress field is the stress assumption used

for the hybrid 4-node element.

In summary, incompatible elements and hybrid elements do not require further modification for applications in nearly incompressible material problems. Furthermore, the use of selective reduced integrated element should be avoided for nearly incompressible material, without modifications.

APPENDIX B

RIGID-BODY MOTION

The two fundamental problems concerning C^1 - shell elements with an assumed polynomial displacement field are

1) Element exhibit non-zero strain under rigid-body motion.
2) Coupling exists between membrane and bending strains.

The following discussion pertains to the first of these problems. Although an element may be constructed using polynomial assumed displacement field, the accuracy will be poor and the convergence will be in doubt.

The assumed displacement formulation, π_p , shall be modified to include a constraint on rigid-body motion so as to construct a variationally consistent functional. To begin, recall that

$$\pi_p = \int_V \tfrac{1}{2} \underset{\sim}{\varepsilon}^T \underset{\sim}{\underset{\sim}{C}} \underset{\sim}{\varepsilon} \, dV - \int_V \underset{\sim}{F}^T \underset{\sim}{u} \, dV - \int_{S_\sigma} \underset{\sim}{\bar{T}}^T \underset{\sim}{u} \, dS \qquad (B.1)$$

where

$$\underset{\sim}{\varepsilon} = \underset{\sim}{D}\,\underset{\sim}{u}$$

$$\underset{\sim}{\sigma} = \underset{\sim}{C}\,\underset{\sim}{\varepsilon}$$

Now suppose that one chooses an assumed displacement field $\underset{\sim}{u}_g$ which does not include all proper rigid-body motion. Then the actual strain, by definition, must be

$$\underset{\sim}{\varepsilon} = \underset{\sim}{D}\,\underset{\sim}{u}_g - \underset{\sim}{\varepsilon}_r = \underset{\sim}{D}\underset{\sim}{N}\,\underset{\sim}{g} - \underset{\sim}{\varepsilon}_r \qquad (B.2)$$

where

$\underset{\sim}{\varepsilon}_r$ = Rigid-body motion "strain"

$\underset{\sim}{u}_g = \underset{\sim}{N}\,\underset{\sim}{q}$

In another words, rigid-body motion "strain" must be extracted from the strain due to the $\underset{\sim}{u}_g$ field.

Although the concept illustrated by Equation (B.2) is simple, exact examples are available only for simple shell geometries. Exact application requires explicit expressions for rigid-body motion. Assuming the presence of such expressions, an element may be constructed by the following procedure. Let the rigid-body displacements be expressed by:

$$\underset{\sim}{u}_r = \underset{\sim}{u}_r(\underset{\sim}{a}_i)$$

where

a_i = arbitrary constant coefficient of the i^{th} rigid-body mode.

In finite element analysis, information is "passed through the nodes". In conjunction, evaluate $\underset{\sim}{u}_r$ at each node and construct $\underset{\sim}{A}$ with dimension of the number of dof's by the number of rigid-body modes.

$$\underset{\sim}{u}_r\Big|_{nodes} = \underset{\sim}{A} \quad \underset{\sim}{a} \qquad (B.4)$$

$$(n \times 1) = (n \times r)\ (r \times 1)$$

where

n = Number of DOF's

r = Number of Rigid-Body modes

Furthermore, the construction of an intermediate displacement field with the same interpolation function as the original displacement field, $\underset{\sim}{u}_g$, allows one to isolate the contribution from the rigid body motion. The rigid-body motion "strain" may be expressed as

$$\begin{aligned} \underset{\sim}{\varepsilon}_r &= \underset{\sim}{D}\underset{\sim}{N}\,\underset{\sim}{u}_r\Big|_{nodes} \\ &= \underset{\sim}{D}\underset{\sim}{N}\,\underset{\sim}{A}\,\underset{\sim}{a} \end{aligned} \qquad (B.5)$$

The resulting functional becomes

$$\begin{aligned} \hat{\Pi}_p = &\int_V \tfrac{1}{2}(\underset{\sim}{\varepsilon}_g - \underset{\sim}{\varepsilon}_r)^T \underset{\sim}{c}\,(\underset{\sim}{\varepsilon}_g - \underset{\sim}{\varepsilon}_r)\, dV \\ &- \int_V \underset{\sim}{F}^T \underset{\sim}{u}_g\, dV - \int_{S_G} \underset{\sim}{\bar{T}}^T \underset{\sim}{u}_g\, dS \end{aligned} \qquad (B.6)$$

The stationary condition of $\hat{\pi}_p$ yields

$$\underset{\sim}{D}^T \underset{\sim}{C} (\underset{\sim}{\varepsilon}_g - \underset{\sim}{\varepsilon}_r) + \underset{\sim}{F} = 0 \qquad \text{in } V$$

$$\underset{\sim}{n}^T \underset{\sim}{C} (\underset{\sim}{\varepsilon}_g - \underset{\sim}{\varepsilon}_r) = \underset{\sim}{T} \qquad \text{on } S_\sigma$$

$$(\underset{\sim}{\varepsilon}_g - \underset{\sim}{\varepsilon}_r) \underbrace{\delta \underset{\sim}{\varepsilon}_r} = 0 \qquad \text{in } V \qquad (B.7)$$

Non-zero only for Rigid-Body motion

The coefficients, $\underset{\sim}{a}$, of rigid-body motions are subject to variation if, and only if, the motion is pure rigid-body.

In the element domain, using standard notation

$$\hat{\pi}_p = \frac{1}{2} \underset{\sim}{g}^T \underset{\sim}{K} \underset{\sim}{g} - \underset{\sim}{a}^T \underset{\sim}{A}^T \underset{\sim}{K} \underset{\sim}{g} + \frac{1}{2} \underset{\sim}{a}^T \underset{\sim}{A}^T \underset{\sim}{K} \underset{\sim}{A} \underset{\sim}{a} - \underset{\sim}{Q}^T \underset{\sim}{g} \qquad (B.8)$$

$$\frac{\partial \hat{\pi}_p}{\partial \underset{\sim}{a}} \Rightarrow \qquad \underset{\sim}{a} = (\underset{\sim}{A}^T \underset{\sim}{K} \underset{\sim}{A})^{-1} \underset{\sim}{A}^T \underset{\sim}{K} \underset{\sim}{g} \qquad (B.9)$$

$$\frac{\partial \hat{\pi}_p}{\partial \underset{\sim}{g}} \Rightarrow \underbrace{[\underset{\sim}{K} - \underset{\sim}{K} \underset{\sim}{A} (\underset{\sim}{A}^T \underset{\sim}{K} \underset{\sim}{A})^{-1} \underset{\sim}{A} \underset{\sim}{K}]}_{\hat{\underset{\sim}{K}}} \underset{\sim}{g} = \underset{\sim}{Q} \qquad (B.10)$$

The resulting relation, Eq. (B.10), is equivalent to Cantin's work on rigid-body motion correction derived by using a discrete form of virtual work [85]. However, the derivation via a variational principle provides the

governing equations expressed as stationary condition in Eq. (B.7). The discrete form of virtual work operates on the components of the stiffness matrix.

For complex shell geometries, exact rigid-body modes are difficult to extract. An alternate viable procedure involves an inverse approach with dual field variables. The π_p functional may be modified by assuming a strain field, $\underset{\sim}{\varepsilon}$, in addition to a displacement field, $\underset{\sim}{u}_g$, which can not represent all rigid-body motion.

$$\tilde{\pi}_p = \int_V \left[\tfrac{1}{2}\,\underset{\sim}{\varepsilon}^T \underset{\sim}{C}\,\underset{\sim}{\varepsilon} - \underset{\sim}{\lambda}^T(\underset{\sim}{\varepsilon}_g - \underset{\sim}{\varepsilon})\right] dV - \int_V \underset{\sim}{F}^T \underset{\sim}{u}_g\, dV - \int_{S_\sigma} \bar{\underset{\sim}{T}}^T \underset{\sim}{u}_g\, ds \tag{B.11}$$

where

$$\underset{\sim}{\varepsilon}_g = \underset{\sim}{D}\,\underset{\sim}{u}_g \tag{B.12}$$

The first variation set equal to zero yields

$$\underset{\sim}{\lambda}^T = \underset{\sim}{\varepsilon}^T \underset{\sim}{C}$$

Substituting Eq. (B.12) into Eq. (B.11) yields

$$\tilde{\pi}_p = \int_V -\tfrac{1}{2}\,\underset{\sim}{\varepsilon}^T \underset{\sim}{C}\,\underset{\sim}{\varepsilon} + \underset{\sim}{\varepsilon}^T \underset{\sim}{C}\,\underset{\sim}{\varepsilon}_g\, dV - \int_V \underset{\sim}{F}^T \underset{\sim}{u}_g\, dV - \int_{S_\sigma} \bar{\underset{\sim}{T}}^T \underset{\sim}{u}_g\, ds \tag{B.13}$$

The functional in Eq. (B.13) bypasses the need to

define an explicit form of rigid-body motion. The assumption of a strain field implicitly includes the rigid-body motion. Furthermore, if the Lagrange multiplier, $\underset{\sim}{\lambda}$, is orthogonal to the rigid-body "strain" from $\underset{\sim}{u}_{\ell}$, then the rigid-body motion is exactly defined. Otherwise, the multiplier plays a role of a constraint in the element domain.

The functional $\tilde{\pi}_p$ may be classified as a form of the Hellinger-Reissner principle, π_R . As a result, the elements constructed by using this version of the Hellinger-Reissner principle contain implicit constraints on the rigid-body motion.

EXAMPLE: BAR ELEMENT

A two-node bar element is chosen to illustrate the two approaches in dealing with rigid-body motion. For the constant cross-sectional area considered, a linear displacement interpolation yields the exact stiffness matrix in conjunction with concentrated end loads. For the bar element, the rigid-body motion is simply a constant displacement. To establish a comparative benchmark, the stiffness matrix using a linear interpolation displacement is provided below:

$$u = \frac{1}{2}(1-\xi)\,g_1 + \frac{1}{2}(1+\xi)\,g_2$$

$$\varepsilon_x = \frac{(g_2 - g_1)}{L} \qquad (B.14)$$

$$\underset{\sim}{K}_L = \begin{bmatrix} \frac{AE}{L} & -\frac{AE}{L} \\ -\frac{AE}{L} & \frac{AE}{L} \end{bmatrix} \qquad (B.15)$$

where

A = Cross-sectional Area (constant)

E = Young's modulus

L = Bar length

Further notations and scales are provided in Figure B-1. Also, note that the rigid-body motion requires that $K_{12} = -K_{11}$ and $K_{21} = -K_{22}$ for the bar element considered.

To assess the effectiveness of rigid-body motion modification, a displacement assumption which does not satisfy rigid-body motion is purposely chosen. In cylindrical shells, the rigid-body motions are characterized by trigonometric functions while polynomials are used for displacement assumptions. In the following bar element, an inverse situation is provided.

$$u = \cos\frac{\pi}{4}(1+\xi)\,g_1 + \sin\frac{\pi}{4}(1+\xi)\,g_2$$

$$\varepsilon_x = \frac{\pi}{2L}\left[-\sin\frac{\pi}{4}(1+\xi)\,g_1 + \cos\frac{\pi}{4}(1+\xi)\,g_2\right] \qquad (B.16)$$

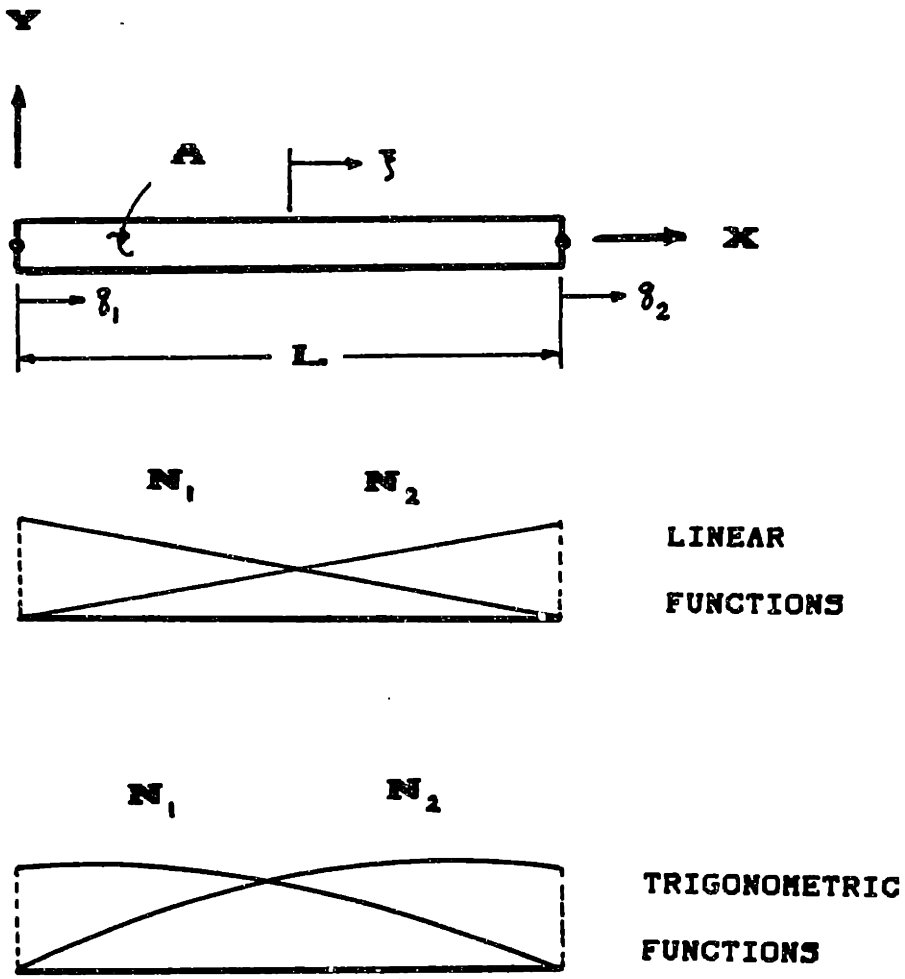

Figure B-1. Bar Element.

The stiffness matrix that results from Eq. (B.16) without any modification is denoted $\underset{\sim}{K}_T$.

$$\underset{\sim}{K}_T = \begin{bmatrix} \left(\frac{\pi^2}{8}\right)\frac{AE}{L} & -\left(\frac{\pi}{4}\right)\frac{AE}{L} \\ -\left(\frac{\pi}{4}\right)\frac{AE}{L} & \left(\frac{\pi^2}{8}\right)\frac{AE}{L} \end{bmatrix}$$

$$= \begin{bmatrix} 1.23\,\frac{AE}{L} & -.79\,\frac{AE}{L} \\ -.79\,\frac{AE}{L} & 1.23\,\frac{AE}{L} \end{bmatrix} \qquad (B.17)$$

Since an explicit expression for rigid-body motion for the bar element is available, a modified stiffness matrix may be obtained by using Eq. (B.10).

$$u_r = a$$

$$u_r/_{nodes} = \begin{bmatrix} 1 \\ 1 \end{bmatrix} \{a\} = \underset{\sim}{A}\,\underset{\sim}{a} \qquad (B.18)$$

$$\hat{\underset{\sim}{K}} = \begin{bmatrix} \left(\frac{\pi^2}{16} + \frac{\pi}{8}\right)\frac{AE}{L} & -\left(\frac{\pi^2}{16} + \frac{\pi}{8}\right)\frac{AE}{L} \\ -\left(\frac{\pi^2}{16} + \frac{\pi}{8}\right)\frac{AE}{L} & \left(\frac{\pi^2}{16} + \frac{\pi}{8}\right)\frac{AE}{L} \end{bmatrix}$$

$$= \begin{bmatrix} 1.01\,\frac{AE}{L} & -1.01\,\frac{AE}{L} \\ -1.01\,\frac{AE}{L} & 1.01\,\frac{AE}{L} \end{bmatrix} \qquad (B.19)$$

Comparing Eq. (B.19) with Eq. (B.15), the rigid-body motion is represented exactly, and the constant strain mode only has a 1% error.

The second approach assumes a strain field

separately from the displacement field. Constructing the element using Eq. (B.13) with

$$\varepsilon_x = \alpha \tag{B.20}$$

$$\varepsilon_{x_{\theta}} = \frac{\pi}{2L}\left[-\sin\frac{\pi}{4}(1+\bar{s})\theta_1 + \cos\frac{\pi}{4}(1+\bar{s})\theta_2\right]$$

the stiffness matrix becomes

$$\underset{\sim}{K}_s = \begin{bmatrix} \frac{AE}{L} & -\frac{AE}{L} \\ -\frac{AE}{L} & \frac{AE}{L} \end{bmatrix} \tag{B.21}$$

with the Euler equation reading

$$\alpha = \frac{(\theta_2 - \theta_1)}{L} \tag{B.22}$$

For this example, the assumed strain field approach provides an exact stiffness matrix.

Overall, as demonstrated with the bar element, both approaches are effective in accommodating rigid-body motion. As an added bonus, the modifications employed also improved the constant strain behavior. The same types of behavior may be observed for cylindrical shell elements [85].

APPENDIX C

ANALYTICAL SOLUTION TO CIRCULAR ARCH PROBLEM

An analytical solution to a circular arch with clamped boundary conditions is derived using Castigliano's Theorem. A full solution and an inextensional solution are provided for future reference. Refering to Figure C-1, the force equilibrium conditions may be expressed as

$$M = -\bar{P} R \cos\phi + \bar{M} - \bar{N} R (1-\sin\phi)$$
$$N = -\bar{P} \cos\phi + \bar{N} \sin\phi \qquad (C.1)$$

The constitutive relations are

$$M = EI K$$
$$N = EA \varepsilon \qquad (C.2)$$

Hence, the complementary strain energy may be obtained as:

$$U^* = \frac{1}{2} \int_0^l \left(\frac{M^2}{EI} + \frac{N^2}{EA} \right) ds \qquad (C.3a)$$

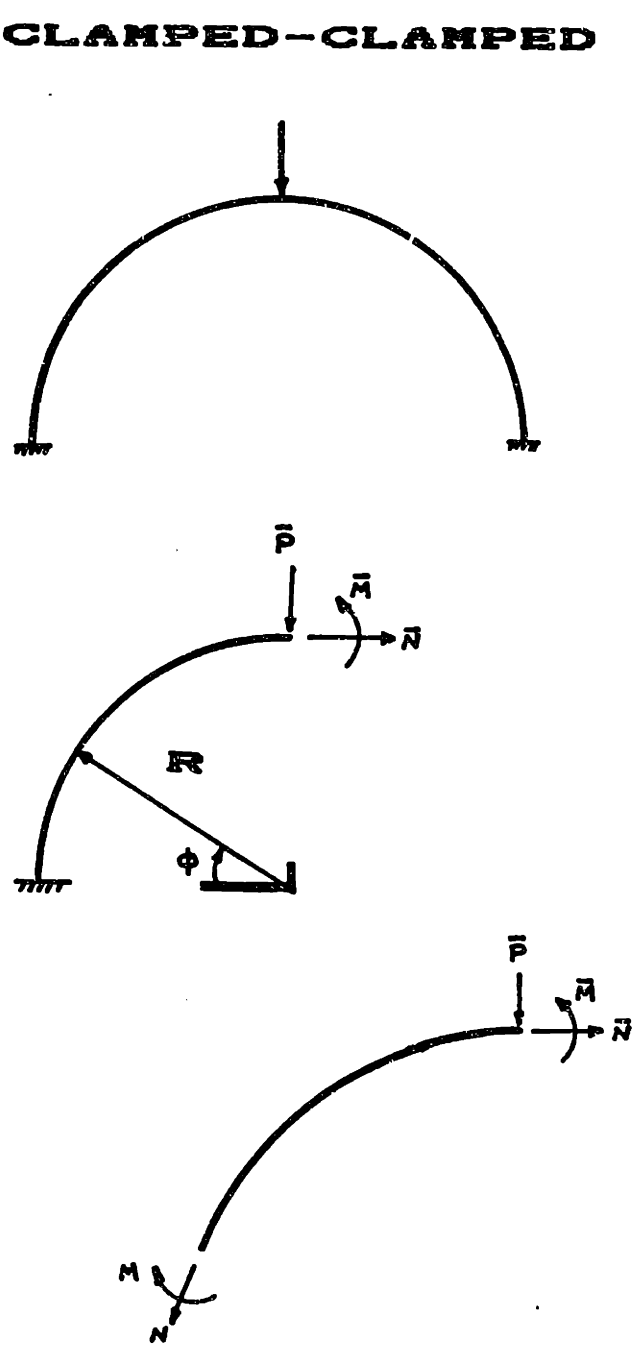

Figure C-1. Clamped Arch Problem Definition.

$$U^* = \frac{R}{2E}\int_0^{\pi/2} \frac{1}{I}\left[-\bar{P}R\cos\phi + \bar{M} - \bar{N}R(1-\sin\phi)\right]^2 + \frac{1}{A}\left[-\bar{P}\cos\phi + \bar{N}\sin\phi\right]^2 d\phi \qquad (C.3)$$

Performing the integration

$$U^* = \frac{R}{2E}\left\{\frac{1}{I}\left[\frac{\pi\bar{P}R}{4} + \frac{3\pi\bar{N}R}{4} + 2\bar{M}\left(-\bar{P}R - \frac{\pi\bar{N}R}{2}\right) + \frac{\pi\bar{M}}{2} + \bar{N}\bar{P}R^2 - 2\bar{N}^2R^2 + 2\bar{M}\bar{N}R\right] + \frac{1}{A}\left[\frac{\pi\bar{P}^2}{4} + \frac{\pi\bar{N}^2}{4} - \bar{N}\bar{P}\right]\right\} \qquad (C.4)$$

The symmetry condition imposes:

$$\frac{\partial U^*}{\partial \bar{M}} = 0$$

$$\frac{\partial U^*}{\partial \bar{N}} = 0 \qquad (C.5)$$

Solving for N and M,

$$\bar{N} = \frac{(2\pi-8)A\bar{P}R^2 + 2\pi I\bar{P}}{(\pi^2-8)AR^2 + \pi^2 I}$$

$$\bar{M} = \frac{\left[2\bar{P} + (\pi-2)\bar{N}\right]R}{\pi} \qquad (C.6)$$

Finally, the vertical displacement under the load is given by $\frac{\partial U^*}{\partial \bar{P}}$ is

$$W_c = \frac{R}{2E}\left\{\frac{1}{I}\left[\frac{\pi\bar{P}R^2}{2} - \frac{2R^2}{\pi}\left[\frac{(\pi-2)((2\pi-8)A\bar{P}R^2+2\pi I\bar{P})}{(\pi^2-8)AR^2+\pi^2 I} + 2\bar{P}\right]\right]\right.$$

$$\left. + \left[\frac{R^2}{I} - \frac{1}{A}\right]\left[\frac{(2\pi-8)A\bar{P}R^2+2\pi I\bar{P}}{(\pi^2-8)AR^2+\pi^2 I}\right] + \frac{\pi\bar{P}}{2A}\right\} \qquad (C.7)$$

For an inextensional solution, neglect the membrane contribution. The same procedure yields,

$$\bar{N} = \frac{(2\pi-8)\bar{P}}{\pi^2-8}$$

$$\bar{M} = \frac{2\bar{P}R}{\pi} + \frac{(\pi-2)R}{\pi}\bar{N} \qquad (C.8)$$

and

$$W_c = \frac{R}{2EI}\left\{\frac{(\pi^3-20\pi+32)\bar{P}R^2}{2\pi^2-16}\right\} \qquad (C.9)$$

Numerical values for

Radius = R = 10

Radius/Thickness = R/h = 100

Cross-Sectional Area = A = .1

Load = P = 1

Young's Modulus = E = 10^7

Full Solution: $w_c = 2.8012 \times 10^{-2}$

Inextensional Solution: $w_c = 2.7988 \times 10^{-2}$

For R/h=100, the difference in these solutions is less than .1%.

APPENDIX D

COMPUTATIONAL EFFICIENCY CONSIDERATIONS

The present discussion rescales the convergence results obtained for two shell examples in order to address the issue of the computational efficiency of the hybrid elements. First, the total number of the assumed parameters for various classes of hybrid elements are listed in Table D-1. The displacement parameters refer to the nodal displacement degrees of freedom and the stress parameters refer to the number of the stress terms used.

Figures D-1 and D-2 provide rescaled results for the two pinched cylinder problems. For the hybrid element SET2(18), additional 18 stress parameters, for each element, are added to the nodal displacement degrees of freedom.

By equating the stress parameters as taking on the same computational weight as the nodal displacement degrees of freedom, a very conservative estimate of the efficiency of the hybrid elements is made. Since the stress parameters are internal element parameters, they do not contribute to the bandwidth of the assembled stiffness matrix. The computational cost is strongly

dependent on the size of the bandwidth.

Even with such conservatism, the results indicate that the hybrid element is more efficient than the 4-node flat shell elements, STANLEY and DVORKIN. Within the scope of the scaling used, the 8-node BOLOURCHI element with reduced integration gives the most efficient performance. In summary, however, only fair gage to determine the computational efficiency of the hybrid elements is to optimize the hybrid element algorithm and then to implement them into an existing code.

Table D-1. Total Number of Assumed Parameters for Hybrid Elements.

ELEMENTS	DISPLACEMENT PARAMETERS	STRESS PARAMETERS
SOLID	24	18
PLANE	8	5
PLATE	12	13/11
ARCH	6	3
SHELL	20	18/16

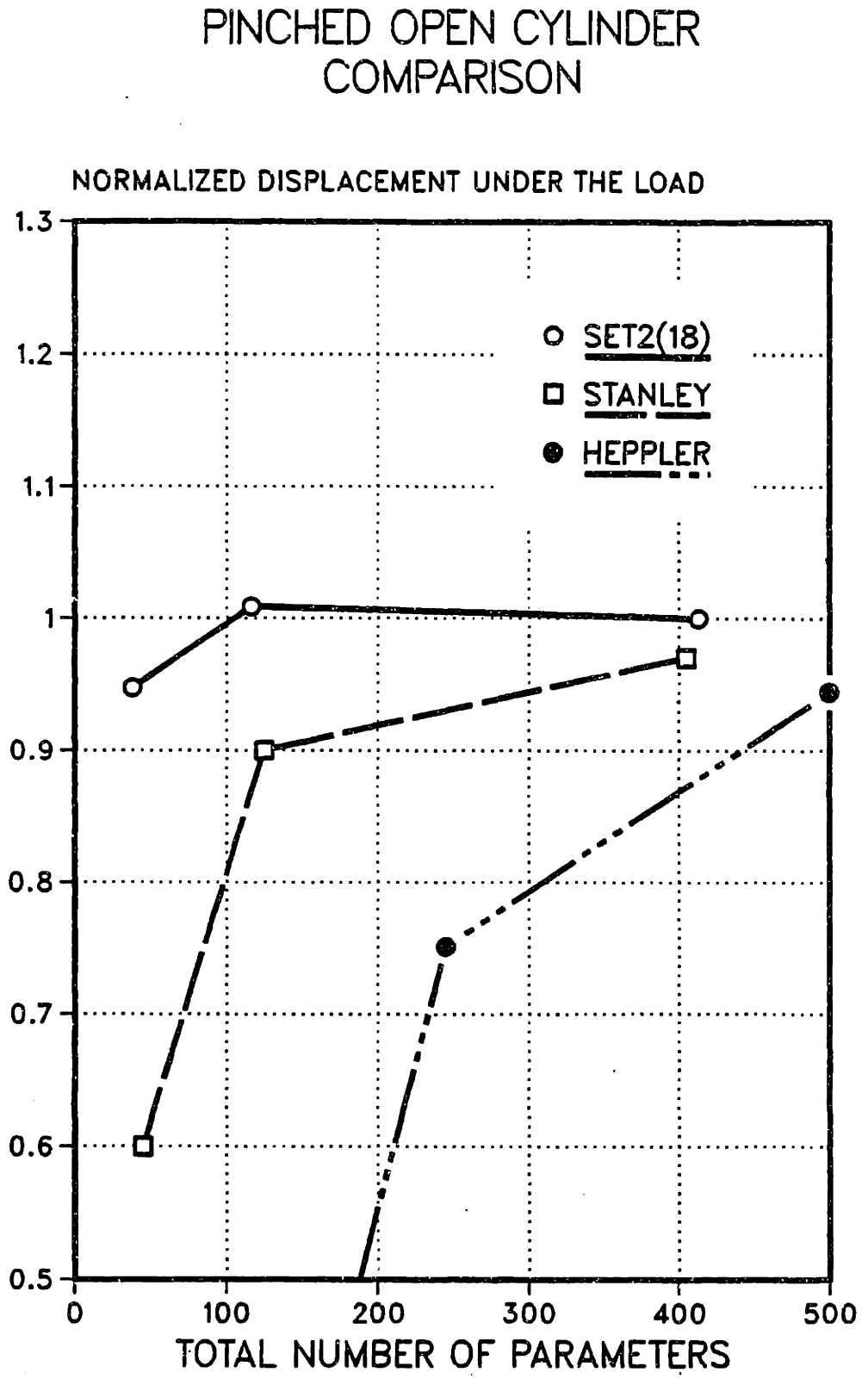

Figure D-1. Rescaled Comparison of the Pinched Open Cylinder Displacement Results.

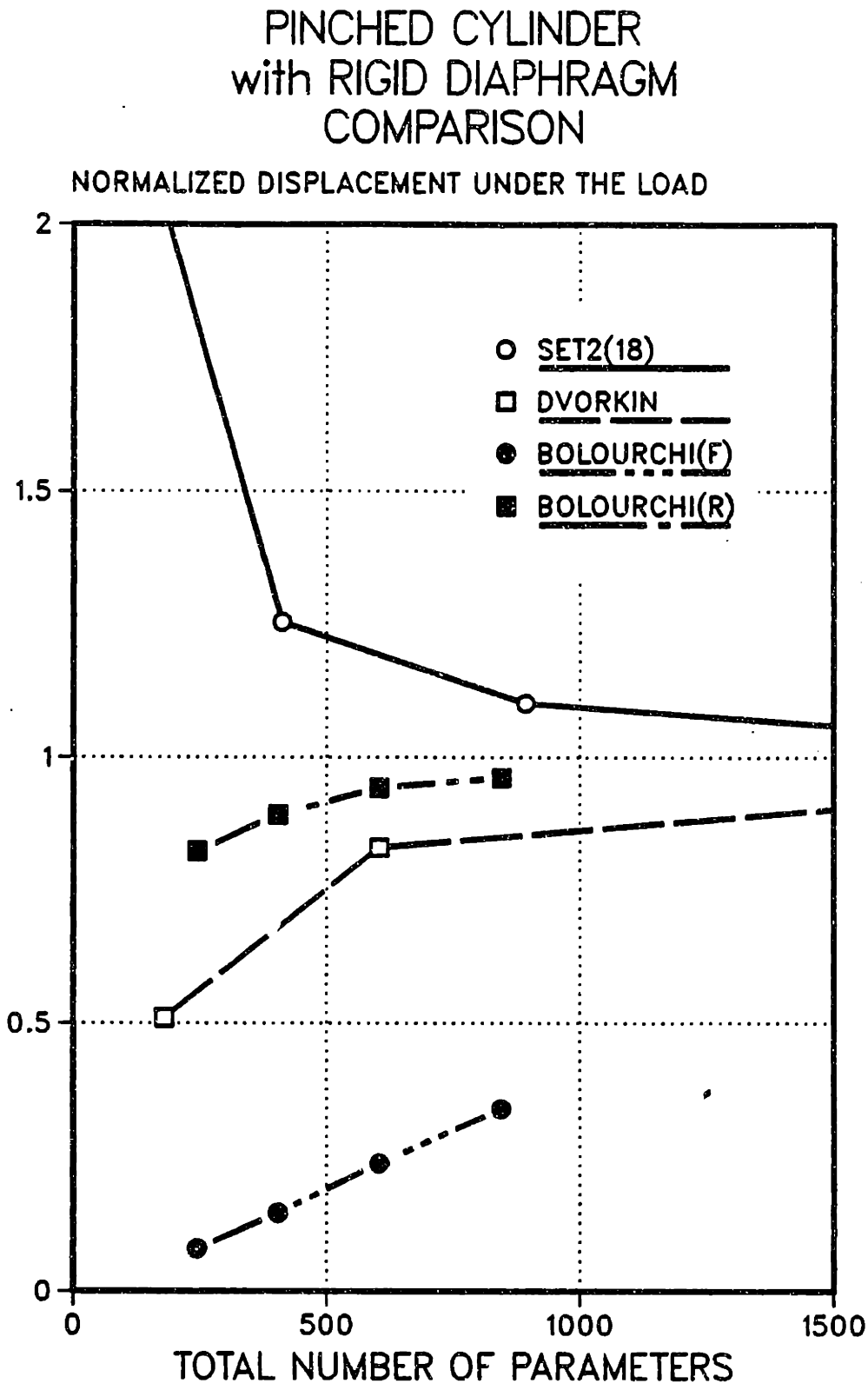

Figure D-2. Rescaled Comparison of the Pinched Cylinder with Rigid Diaphragm Displacement Results.

APPENDIX E

CONSTRUCTION OF A STIFFNESS MATRIX FOR A CYLINDRICAL SHELL

In order to further illustrate the procedure required to construct a hybrid element, consider a hybrid general shell element in a cylindrical geometry (Figure E-1). The element requires a position vector to all eight nodes and a normal vector to the first four nodes. The position vectors and the normal vectors constitute twelve pieces of information that can uniquely define a twelve parameter bi-cubic surface patch. With the geometry defined, all the geometric information is calculated numerically. Basically, a polynomial approximation of a cylindrical geometry is made. The geometric information is approximately calculated based upon this polynomial approximation.

The in-plane and the out-of-plane displacement components are interpolated as

$$\underset{\sim}{u} = \sum_m \hat{N}_m (\xi^1, \xi^2)\, \underset{\sim}{u}_m$$

$$w = \sum_m \underset{\sim}{N}_m (\xi^1, \xi^2)\, \underset{\sim}{w}_m \qquad \text{(E.1)}$$

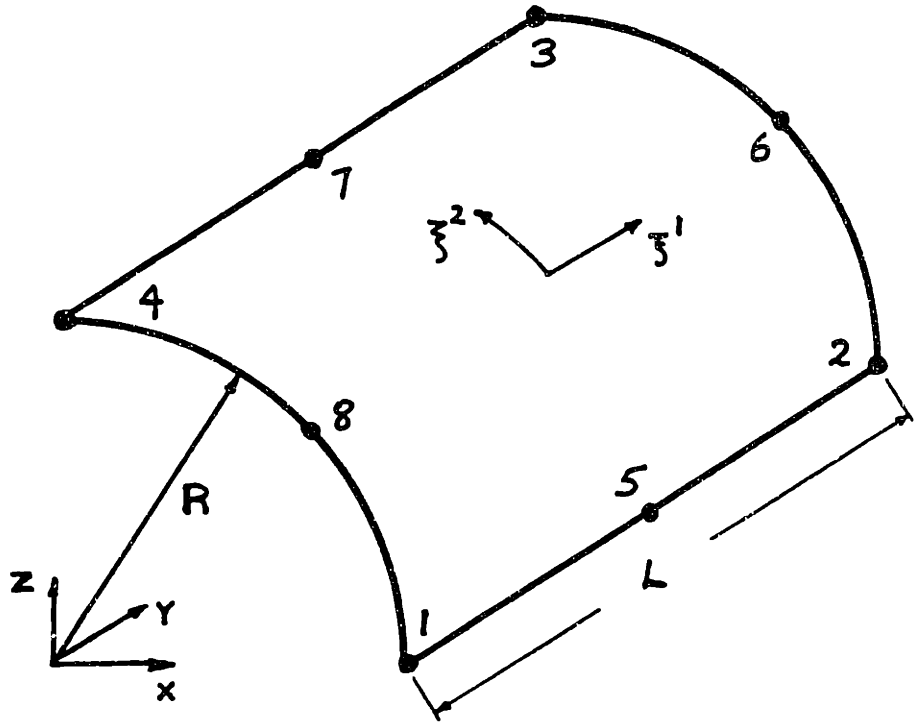

Figure E-1. Cylindrical Shell Element Geometry.

where

m = Nodes

$$\underset{\sim}{u}_m = \begin{Bmatrix} u_1\, \underset{\sim}{e}_1 \\ u_2\, \underset{\sim}{e}_2 \\ u_3\, \underset{\sim}{e}_3 \end{Bmatrix}$$

$$\underset{\sim}{w}_m = \begin{Bmatrix} w\, n \\ w_{,1}\, \underset{\sim}{a}^1 \\ w_{,2}\, \underset{\sim}{a}^2 \end{Bmatrix}$$

and

$\underset{\sim}{e}_i$ = Cartesian Base Vectors

$\underset{\sim}{n}$ = Surface Normal

$\underset{\sim}{a}^i$ = Contravariant Surface Base Vectors

The interpolation functions are explicitly defined as

$$\hat{N}_m = \tfrac{1}{4}\,(1+\xi^1_m\,\xi^1)\,(1+\xi^2_m\,\xi^2) \qquad (E.2)$$

$$\underset{\sim}{N}_m = \tfrac{1}{8}\Big[\ \Big\{(\xi^1_m\xi^1+1)(\xi^2_m\xi^2+1)(2+\xi^1_m\xi^1+\xi^2_m\xi^2-(\xi^1)^2+(\xi^2)^2)\Big\}$$

$$\Big\{\xi^1_m\,(\xi^1_m\xi^1+1)^2\,(\xi^1_m\xi^1-1)\,(\xi^2_m\xi^2+1)\Big\}$$

$$\Big\{\xi^2_m\,(\xi^1_m\xi^1+1)\,(\xi^2_m\xi^2+1)^2\,(\xi^2_m\xi^2-1)\Big\}\ \Big]$$

where

$(\xi^1_m\,,\,\xi^2_m)$ = Node m values

Using the strain-displacement relations, Eq. (9.6), the $\underset{\sim}{B}$

and $\underset{\sim}{D}$ matrices are constructed numerically.

$$\underset{\sim}{\gamma}^{0} = \underset{\sim}{B}\,\underset{\sim}{q}$$
$$\underset{\sim}{\kappa} = \underset{\sim}{D}\,\underset{\sim}{q} \qquad (E.3)$$

where

$\underset{\sim}{q}$ = 20 Global Degrees of Freedom

For example,

$$\gamma_{11}^{0} = \frac{\partial}{\partial \bar{\xi}^1}\left(\sum_m \hat{N}_m(\bar{\xi}^1,\bar{\xi}^2)\right)\underset{\sim}{u}_m - \sum_m \underset{\sim}{N}_m(\bar{\xi}^1,\bar{\xi}^2)\,\underset{\sim}{w}_m\, b_{11} \qquad (E.4)$$

For the stresses, taking the SET2(18) expression,

$$\ell^{11} = \beta_1 + \beta_4\bar{\xi}^2 + b_1^1\beta_9\bar{\xi}^1 - \tfrac{1}{2}\beta_{12}b_1^2\bar{\xi}^1$$
$$\ell^{22} = \beta_2 + \beta_5\bar{\xi}^1 + b_2^2\beta_{13}\bar{\xi}^2 - \tfrac{1}{2}\beta_{10}b_2^1\bar{\xi}^2$$
$$\ell^{12} = \beta_3 + b_2^1\beta_{11}\bar{\xi}^2 - (\tfrac{1}{2}b_2^2 - \tfrac{3}{2}b_1^1)\beta_{14}\bar{\xi}^2 - (\tfrac{1}{2}b_1^1 - \tfrac{3}{2}b_2^2)\beta_{11}\bar{\xi}^1 + b_1^2\beta_{14}\bar{\xi}^1 \qquad (E.5)$$

$$m^{11} = \beta_6 + \beta_9\bar{\xi}^1 + \beta_{12}\bar{\xi}^2 + \beta_{15}\bar{\xi}^1\bar{\xi}^2$$
$$m^{22} = \beta_7 + \beta_{10}\bar{\xi}^1 + \beta_{13}\bar{\xi}^2 + \beta_{16}\bar{\xi}^1\bar{\xi}^2$$
$$m^{12} = \beta_8 + \beta_{11}\bar{\xi}^1 + \beta_{14}\bar{\xi}^2 + \beta_{17}(\bar{\xi}^1)^2 + \beta_{18}(\bar{\xi}^2)^2$$

Organizing Eq. (E.5) into a matrix form, construct the $\underset{\sim}{P}_{\ell}$

and $\underset{\sim}{P}_m$ matrices

$$\underset{\sim}{\ell} = \underset{\sim}{P}_\ell \, \underset{\sim}{\beta}$$
$$\underset{\sim}{m} = \underset{\sim}{P}_m \, \underset{\sim}{\beta} \qquad (E.6)$$

where

$$\underset{\sim}{\beta} = \begin{Bmatrix} \beta_1 \\ \beta_2 \\ \beta_3 \\ \vdots \\ \beta_{18} \end{Bmatrix}$$

The stiffness matrix may be calculated by numerically integrating the required matrices using the matrices defined previously.

$$\underset{\sim}{K} = (\underset{\sim}{G} - \underset{\sim}{G}_v)^T \underset{\sim}{H}^{-1} (\underset{\sim}{G} - \underset{\sim}{G}_v) \qquad (E.7)$$

where

$$\underset{\sim}{H} = \int_A \frac{1}{h} \underset{\sim}{P}_\ell^T \underset{\sim}{\Sigma} \underset{\sim}{P}_\ell + \frac{12}{h^3} \underset{\sim}{P}_m^T \underset{\sim}{\Sigma} \underset{\sim}{P}_m \, dA$$

$$\underset{\sim}{G} = \int_A \underset{\sim}{P}_\ell^T \underset{\sim}{B} + \underset{\sim}{P}_m^T \underset{\sim}{D} \, dA \qquad (E.8)$$

$$\underset{\sim}{G}_v = \int_{\partial A} \underset{\sim}{P}_v^T \underset{\sim}{N}_v \, ds$$

and

$$\underset{\sim}{\nu}^T \underset{\sim}{m} \underset{\sim}{\nu} = \underset{\sim}{P}_\nu \underset{\sim}{\beta}$$

$$\tilde{w}_{,\nu} - w_{,\nu} = \underset{\sim}{N}_\nu \underset{\sim}{q}$$

$\underset{\sim}{\nu}$ = Unit Normal to the Boundary Curve

The term $\tilde{w}_{,\nu}$ is interpolated linearly along the boundary to represent a compatible displacement field. The integrals are performed numerically using a 3-point Gaussian integration rule. In summary, this presentation is a generic recipe for construction of a hybrid element.